Correlation functions and non-equilibrium dynamics in one dimensional quantum systems

PhD Thesis

Dávid Horváth

Supervisor: Dr. Gábor Takács
Professor
BME Institute of Physics
Department of Theoretical Physics

Budapest University of Technology and Economics
2019

Contents

Chapter 1

Introduction

One of the great intellectual achievements that the end of the 19th and the beginning of the 20th century witnessed is the theoretical foundation of thermodynamics and the birth of statistical mechanics. By the contributions of many outstanding physicists, in this era it had become possible to understand the phenomenological laws of thermodynamics emerging from the Hamiltonian dynamics of classical particles. Some of the most essential milestones in the history of statistical mechanics were relating micro-states of the Hamiltonian problem and macro-states of a large system expressed by Boltzmann's entropy formula and understanding the observed approach of a macroscopic system to a steady state reconciling it with the microscopic reversibility of the underlying dynamics. An aspect of similar significance is the applicability of statistical ensembles. In a generic interacting system with macroscopically many degrees of freedom, the Hamiltonian dynamics is chaotic, which ensures that the system visits all the available regions in the phase space in sufficiently large times. The ergodicity of the dynamics, however, allows to compute time averages in terms of ensemble averages and hence provide a statistical description of the observed equilibrium. The role of conserved quantities and in particular the energy was immediately understood, the latter being the only relevant conserved quantity that can be nonzero in an appropriate coordinate system.

The chaotic dynamics of the Hamiltonian system is therefore a crucial ingredient for the emergence of a statistical description, but there are numerous important examples in Hamiltonian mechanics where the dynamics is not chaotic. The most important example is classical integrable models in which, given that the system has finite $2n$ degrees of freedom, there are n independent conserved quantities. The conserved quantities impose strong constraints on the dynamics: it is restricted onto an n dimensional torus i.e. a tiny subspace in the $2n$ dimensional phase space and consequently integrable models have a rather special, unusual dynamics. Moreover, as claimed by the KAM theorem, under small integrability breaking perturbations there even remain regions in the phase space where the behaviour of the is still not chaotic. Although this is very remarkable, the fate of these regions, however, is such, that they shrink as the number of degrees of freedom is increased, and in macroscopic systems the chaotic behaviour dominates. For this reason in real world classical systems with macroscopic degrees of freedom the molecular chaos and hence ergodicity is practically always guaranteed.

In the beginning of the 20th century, quantum mechanics was born and it was soon noticed that elements that are necessary for the statistical mechanics of classical systems to work, such as indistinguishability of particles and usage of cells in phase-space to label micro-states, are of quantum mechanical origin. Apart from these quantum ingredients, however, statistical mechanics is based on classical concepts and quantum mechanics seems to have a little say in classical statistical mechanics. As a matter of fact, some of the classical concepts of statistical mechanics such as ensembles have natural quantum mechanical analogues and using quantum statistical ensembles and the principles of classical statistical mechanics in quantum systems, indeed, have a wide range of successful applicability.

Despite of its usually excellent performance, the origin of an emergent statistical description in quantum systems is far less understood than for the classical case. Notions that are essential in classical statistical

mechanics such as ergodicity and chaotic behaviour and the role of integrability and integrability breaking are highly non-trivial in the quantum context. Whereas in the classical case, chaos and ergodicity is essentially guaranteed by the non-linearity of the Hamiltonian as a consequence of the interactions, time evolution in quantum mechanics is governed by the time dependent Schrödinger equation, which is linear in time and the linearity of quantum systems manifests in the superposition principle of quantum mechanics as well. Clearly, understanding aspects such as the quantum version of ergodicity and a rigorous foundation of quantum statistical mechanics are of great importance. As most commonly believed, our universe is governed by quantum physics and classical physics and hence classical statistical mechanics are emergent descriptions of the quantum world applicable in some cases. The call for understanding whether the principles of statistical mechanics can be derived from quantum mechanics is therefore obvious and has been spurring activity over decades. As a result of these studies, a mechanism analogous to ergodicity in classical systems was proposed under the name of Eigenstate Thermalization Hypothesis (ETH) [1, 2] in the early 90' and is currently generally accepted to account for the thermalization and the emergence of a micro-canonical description in closed quantum systems with generic interactions.

In recent years, nevertheless, experimental techniques have undergone a spectacular evolution and it has become possible to study interacting quantum systems with many constituents [3–13]. In these experiments usually realized by trapped cold atoms, the interactions with the environment are so weak, that these systems can be considered isolated for times scales much longer than the ones characteristic of the dynamics of the system. Due to the large number of constituent particles and the excellent isolation from the environment, these experimental realizations have provided a wealth of information and stimulated activity in the field of out-of-equilibrium dynamics of closed quantum systems.

In most cases the experimental realization is such, that the cold atoms are confined to an elongated region of space and the dynamics of the atoms is dominated by 1D physics. The reduced dimensionality has strong effects on the dynamics. On the one hand, in 1D the role of quantum fluctuations is very important, while on the other hand the interactions are usually non-negligible as two particles with different velocities would inevitably collide which each other. Such systems are therefore usually strongly correlated and strongly interacting with pronounced quantum effects, which make them ideal test-grounds for the study of non-equilibrium phenomena and thermalization in closed quantum systems.

Perhaps the most important aspect of 1D is the existence of quantum integrable models, mostly spin chains and integrable field theories, many of which can be realized in experiments. Whereas currently there is no generally accepted definition of quantum integrability (see a summary of definitions and an appealing proposal in Ref. [14]), the most accepted one emphasizes the existence of infinitely many conserved charges in these models that are local, i.e. they are a sum or an integral of a local density. Studying and understanding thermalization in integrable models hence is motivated by real world systems and experiments and it has led to a series of unexpected behaviour and interesting surprises. Perhaps the most remarkable discovery the experiments reported is that these models do not thermalize in the usual sense [3–5, 15], and recent theoretical results show this can also occur in systems where integrability is broken, as a result of non-perturbative dynamical effects such as confinement [16]. It is important to mention that due to the special constraints on the dynamics, integrable systems admit exact solutions and analytical expressions and for such systems or their perturbed non-integrable counterparts there are often very effective numerical techniques to deal with, despite being generically strongly interacting theories. Studying the out-of-equilibrium properties of integrable systems is hence often possible by analytical means besides the experimental investigations, and analytical calculations give a direct access to studying and understanding various aspects of thermalization or testing related ideas and hypotheses in closed quantum systems. For these reasons, the study of non-equilibrium dynamics of integrable models has been attracting considerable interest not only on the experimental but also on the theoretical side.

Recent investigations of integrable models and their out-of-equilibrium properties such as the lack of thermalization due to the violation of the ETH have opened up new horizons in the foundation of quantum statistical mechanics. These investigations have also stimulated the development of efficient numerical methods such as the time-evolving block decimation [17] or truncated space approaches [18]

which are of more general applicability. Perhaps most importantly, however, a series of interesting ideas and new concepts such as the generalized Gibbs ensemble have been born, and novel and vital questions have been proposed to push forward the frontiers of our understanding in quantum statistical mechanics. In the following some of the most interesting issues are listed and briefly introduced.

Although integrable models violate the ETH and do not thermalize they do equilibrate and to describe the steady-state the generalized Gibbs ensemble was introduced [19]. This ensemble is analogous to the standard Gibbs ensemble but it includes not only the Hamiltonian but all the other local conserved charges, which form an infinite set in integrable model. Whereas the applicability of this ensemble is generally accepted, the actual set of conserved charges to be included and the their locality properties are not clear at the moment.

Another important question is related to the transition form integrable to non-integrable quantum models i.e. the integrability breaking, as according to [16], certain models even with strong integrability breaking refuse to thermalize. Whereas in the classical case in thermodynamically large systems, chaotic behaviour dominates even for broken integrability (and hence despite of the KAM theorem), in quantum system with integrability breaking the remnants of integrability can be more pronounced. This suggests a possible existence of the quantum version of KAM theorem and current and recents studies may contribute to the construction of such a theorem. Of course, the actual steady-state in such a situation is of great interest as well and the approach to the steady-state either described by a generalized Gibbs ensemble or in a situation with integrability breaking is very little known, with some case-by-case examples.

Integrable models exhibit interesting transport properties. The transfer of many physical quantities is characterized by ballistic transport, but diffusive and sub-ballistic transport phenomena were also observed in integrable models [20, 21] and it is not known what class of observables and under what conditions supports diffusive transport. Transport in integrable systems at the Euler scale can be described by the Generalized Hydrodynamic approach (GHD) [22, 23], which was recently extended to access shorter time and length scales [24]. The application of the latter approach, however, was only achieved for the XXZ spin chain and the classical hard rod gas so far and none of the two approaches was extended to integrable systems with non-diagonal scattering, such as the sine-Gordon model, whose transport properties are not known.

Last but not least it is worth mentioning the spread of correlations and entanglement in out-of-equilibrium situations, which received a lot of attention. In integrable models, where stable quasi-particles exist, a simple semiclassical picture based on these stable particles offer qualitative and often quantitative predictions for the spread of correlations and especially for the entanglement [25, 26]. In models with bounded quasi-particle velocity, the effect of a light cone can usually be observed in the spreading of correlations, but confinement can prevent light-cone-like spreading [16].

In this thesis our aim is to discuss further and review some often exotic aspects of out-of-equilibrium physics in quantum systems with a focus on integrable models and especially integrable field theories, and to contribute to better understanding some of the issues discussed above. Before presenting our own results mainly related to the so-called overlaps and the actual approach to the steady state, it is useful to introduce a more formal treatment of out-of-equilibrium physics and thermalisation in quantum systems. This allows us to phrase precisely the open questions motivating our work but also provides some room to briefly summarise existing knowledge and features of thermalisation in many body quantum systems. In the next section we discuss the Eigenstate Thermalisation Hypothesis in generic interacting quantum many-body system highlighting the role of locality in the thermalisation. This is followed by the non-equilibrium physics of integrable quantum systems, and a discussion of the motivations behind studying integrable field theories in our work.

Chapter 2

Thermalization in many-body quantum systems

In this chapter we introduce a paradigmatic setup called quantum quench to study thermalization and non-equilibrium physics in quantum systems, highlight the role of locality in equilibration and introduce the Eigenstate Thermalization Hypothesis. Then we discuss the case of integrable models where the generalized Gibbs ensemble (GGE) can be invoked to describe the steady state. Here we identify the most important open questions, which are related to the construction of, and the approach to, the steady state and the role of integrability breaking. We also motivate our preference to study integrable quantum field theories and address vital questions regarding the extension of the quench paradigm to field theories and the applicability of a field theoretical description in out-of-equilibrium situations.

2.1 Emergence of a statistical description in closed quantum systems

There are several interesting out of equilibrium scenarios in quantum systems. To name a few, one can consider Floquet systems where an external driving is applied, or inhomogeneous situations where two (half-infinite) systems prepared to different initial conditions are joined together in the most studied situation, but one can also study open quantum systems subject to a Lindbladian time evolution giving rise to interesting non-equilibrium steady states. However, perhaps the simplest and most important setting is when a closed quantum system is prepared in an initial state which not the eigenstate of the Hamiltonian governing the time evolution. Clearly, this setup is just the quantum version of the classical case studied by Boltzmann, where an isolated system is initialized to a point or a region in the phase space and the emergence of statistical distribution described by a micro-canonical ensemble is expected under general conditions. This setup has therefore a particular importance being the simplest one, where a statistical description in quantum systems emerges.

Clearly this non-equilibrium protocol is not the most general one, since the initial state is a pure state (corresponding to a single point in the phase space in classical version) but due to the superposition principle of quantum mechanics, the case of a mixed initial state described by a non-trivial density matrix (corresponding to a region in the phase space in classical version) can in general be reduced to the case a pure state. The non-equilibrium protocol we are interested in therefore consists of preparing a closed and macroscopically large quantum system in a pure state that is not the eigenstate of the Hamiltonian governing the time evolution after the preparation. This protocol is called a (global) quantum quench [27, 28], if the preparation is realized by abruptly changing some parameters in a typically translational invariant Hamiltonian and the initial state is the eigenstate, typically the ground state of the pre-quench Hamiltonian, whereas time evolution is governed by the post-quench Hamiltonian. This protocol is generally realized by a fast change in the system parameters. Depending on whether this change can be considered instantaneous or slow, the non-equilibrium scenario is either a quantum quench or a ramp.

In such a situation a very natural approach is to use the superposition principle of quantum mechanics, and write the time evolution of an operator as

$$\langle\Psi|e^{itH}\mathcal{O}e^{-itH}|\Psi\rangle = \sum_{n,m} c_n^* c_m \langle n|\mathcal{O}|m\rangle e^{it(E_n-E_m)}\,, \tag{2.1.1}$$

where $|\Psi\rangle$ is the initial state $|n\rangle$ labels the eigenstates of H with energies E_n and the c_n are the overlaps $\langle n|\Psi\rangle$. In principle, Eq. (2.1.1) encodes all the information about the steady state and time evolution and has many interesting implications. First of all, let us assume that the system reaches a steady state, which is the generally the case, and relegate the discussion under what conditions it eventually happens. If a steady state is reached, the expectation value of the operator becomes time independent and it must be equal to its time average:

$$\bar{\mathcal{O}} = \lim_{T\to\infty} \frac{1}{T}\int_0^T dt \langle\mathcal{O}(t)\rangle\,, \tag{2.1.2}$$

which under quite general assumptions is equal to the so-called diagonal ensemble average given by

$$\bar{\mathcal{O}} = \sum_n |c_n|^2 \langle n|\mathcal{O}|n\rangle\,. \tag{2.1.3}$$

This ensemble corresponds to a density matrix

$$\rho = \sum_n |c_n|^2 |n\rangle\langle n|\,, \tag{2.1.4}$$

which must be reconciled in some way with the fact that time evolution is unitary and $|\Psi(t)\rangle = e^{-itH}|\Psi\rangle$ remains a pure state at all times. The widely accepted solution is that equilibration only happens for a certain class of observables, and also involves the thermodynamic limit. The latter is necessary since in systems with a finite number of degrees of freedom partial revivals occur after a sufficiently long time (which is the quantum analogue of Poincare recurrence). This time depends on the accuracy (degree) of the revival and the number of degrees of freedom and is usually astronomically large in systems with many constituents. Therefore in the rest of this thesis we consider the quantum systems in the thermodynamic limit unless the opposite is indicated explicitly. The class of observables which are relevant for the equilibration depends heavily on the structure of the Hilbert space and the Hamiltonian governing the dynamics. In most cases the system is composed of some elementary constituents with their own Hilbert space; typical examples are provided by bosonic or fermionic gases where each constituent has an L_2 Hilbert space in coordinate representation, or spin chains, where each spin has a local, finite dimensional Hilbert space. The Hilbert space of the many-body system is then the tensor product of these 'one-body' or 'local' Hilbert spaces and due to interactions the Hamiltonian has non-zero matrix elements between these components. As a consequence when considering few-body or local operators i.e. operators that has support on only few of the one-body or local Hilbert spaces and performing a trace over the rest of the Hilbert space, the expectation value is eventually described by a mixed state, as entanglement is generated between the different parts of the Hilbert space by the dynamics governed by the Hamiltonian. For operators that are global i.e. have support on the entire Hilbert space of the many-body system, a relaxation to an expectation value dictated by a mixed state is not expected in general.

Having discussed the class of operators that can equilibrate in closed quantum systems, in the rest of this thesis we will merely refer to this class as 'local operators' for brevity. In the classical case, the ergodicity of the dynamics accounts for the actual reach of the steady state and the emergent micro-canonical description. In quantum Eq. (2.1.1) shows that in order to reach a steady-state described by (2.1.3) the spectrum of the system must be sufficiently irregular otherwise revivals can occur even in the thermodynamic limit. This corresponds with idea that a signature of quantum chaos is that distribution

of the energy level spacing follows Wigner-Dyson statistics [29]. The diagonal ensemble, however, is not suitable as a thermodynamic description since it contains all the overlap coefficients, which is a huge amount of microscopic information about the initial state, while a thermodynamic description is expected to be in terms of macroscopic state variables such as total energy, entropy, pressure etc. This is illustrated by the example of spin chains, where the entire Hilbert space and the necessary information for the DE increases exponentially with the size of the system. The observation that generic interacting closed quantum systems thermalize, in the sense discussed above, means the equilibrium expectation value $\bar{\mathcal{O}}$ can be computed by appropriate thermodynamical ensembles. In particular, the micro-canonical average of $\bar{\mathcal{O}}$ is defined as

$$\langle \mathcal{O} \rangle_{MCE} = \frac{1}{N_{MCE}} \sum{}' \langle n|\mathcal{O}|n\rangle \,, \tag{2.1.5}$$

where the primed summation means that eigenstates in the energy range $[E, E+\delta]$ are included, N_{MCE} is the number of such eigenstates and δ is chosen to be small compared to the energy E but large compared to the average level spacing. Alternatively, one can use the Gibbs ensemble i.e. the canonical average

$$\langle \mathcal{O} \rangle_{GE} = Z^{-1} \mathrm{Tr}\, \mathcal{O} e^{-\beta H} \tag{2.1.6}$$

with $Z = \mathrm{Tr}\, e^{-\beta H}$ as well. Whereas the equivalence of the micro-canonical and canonical averages are well understood in equilibrium statistical physics and depends on negligibility of the fluctuations of the energy density, to explain the equivalence of time averaging and the ensemble averages, the most widely accepted scenario is the Eigenstate Thermalization Hypothesis (ETH) originally proposed in [1, 2]. The ETH claims that in matrix elements of local operators with respect to eigenstates of a generic Hamiltonian of a large system, the off-diagonal elements are suppressed exponentially in the system size, and the diagonal elements only depend on the energy and are smooth functions of it. This can be formulated as

$$\mathcal{O}_{\alpha\beta} = \mathcal{O}(E)\delta_{\alpha\beta} + e^{-S(E)/2} f_{\mathcal{O}}(E, \omega) R_{\alpha\beta} \,, \tag{2.1.7}$$

where $\mathcal{O}_{\alpha\beta}$ denotes $\langle \alpha|\mathcal{O}|\beta\rangle$, $|\alpha\rangle$ and $\beta\rangle$ are post-quench eigenstates with energies E_α and E_β, $E = (E_\alpha + E_\beta)/2$, $\omega = E_\alpha - E_\beta$, $S(E)$ is the thermodynamic entropy, $\mathcal{O}(E)$ and $f_{\mathcal{O}}(E, \omega)$ are smooth functions and $R_{\alpha\beta}$ is a random variable with zero mean and unit variance. The ETH itself is not sufficient to guarantee the equivalence of $\bar{\mathcal{O}}$ and $\langle \mathcal{O} \rangle_{MCE}$: it is also necessary that the energy density fluctuations in the initial state become negligible int he TDL [30]. This is guaranteed if the initial state satisfies the cluster decomposition property [31], which states that for any local observable

$$\lim_{|x-y|\to\infty} \langle \Psi|\mathcal{O}(x)\mathcal{O}(y)|\Psi\rangle = \langle \Psi|\mathcal{O}(x)|\Psi\rangle \langle \Psi|\mathcal{O}(y)|\Psi\rangle \,. \tag{2.1.8}$$

As a consequence of the cluster property, the variance of the average energy density of the initial state is negligible with respect to the Hamiltonian in the thermodynamic limit, hence

$$\bar{\mathcal{O}} = \sum_n |c_n|^2 \langle n|\mathcal{O}|n\rangle = \sum{}' |c_n|^2 \langle n|\mathcal{O}|n\rangle = \frac{1}{N_{MCE}} \sum{}' \langle n|\mathcal{O}|n\rangle \,, \tag{2.1.9}$$

since $\sum' |c_n|^2 \approx 1$ and $\mathcal{O}(E)$ is a smooth function. The behaviour of the off-diagonal elements in Eq. (2.1.7) is also important. Even if the spectrum is highly irregular, eigenvalues can be close to each other exponentially in system size, hence the approach to the steady state can be exponentially slow. This is in marked contrast with experimental and numerical observation reporting usually fast relaxation. The 2nd term in Eq. (2.1.7) and in particular the exponential suppression accounts for realistic relaxation times which are much shorter than the astronomically large time scales implied by the energy spacings, and this formulation of the ETH results in ergodicity in a strong sense.

The ETH can therefore be regarded as the quantum version of the ergodic hypothesis explaining thermalization in closed quantum systems and has been tested in various setups [2,32–47] including models of hard- and soft-core bosons, interacting spin chains, spinless and spinful fermions and the transverse field Ising model in two dimensions.

For generic interacting many-body quantum systems the ETH holds, but there are interesting examples where this hypothesis is violated. In finite systems, there may exist rare state that violate (2.1.7) and which are expected vanish in the TDL. This requirement is usually difficult to check and there are known cases where such (usually low energy) states persist [48, 49]. These states are usually at the edges of the spectrum and often related to an emergent low-energy integrability [50].

In fact, integrable models provide the most important example when ETH is violated and as a consequence, integrable models do not thermalize in the usual sense. The discussion of integrable models is carried out in the following section but before that, we briefly discuss the effects of breaking integrability which holds many surprises as well. As discussed in the Introduction, in the classical case the region in phase space where the dynamics remains not chaotic shrinks with the number of degrees of freedom and as a consequence in thermodynamically large systems the chaotic behaviour dominates and remnants of integrability are absent. In contrast, in quantum systems with broken integrability, the remnants of integrability are more pronounced. A typical scenario is that, following a quench in such a system, local operators undergo a fast relaxation to a quasi-stationary state [51], which is called pre-thermalization. Observables eventually thermalize, but this happens as a slow drift from the pre-thermalization plateaux and the typical time scale of the transition behaves as $1/\lambda^2$ for small λ, if λ denotes the coupling constant of the non-integrable part of the Hamiltonian [52,53]. This plateaux is influenced by the integrable part of the Hamiltonian which includes integrability breaking terms as well and can be very robust against varying the magnitude of integrability breaking [52]. Such plateaux was also observed in a strongly non-integrable model with long range order in the initial state [54].

Whereas currently there is no complete description of this phenomenon, most models exhibiting these behaviours eventually thermalize. There is however an important case of integrability breaking where this scenario does not seem to apply. An example is provided by the longitudinal perturbation of the transverse field quantum Ising model, where the longitudinal field results in the confinement of the domain wall excitations, which are the quasi-particles in the ordered phase. In this non-integrable model, the confined meson-like excitations cause an anomalous spreading in the correlations and prevent the system from thermalizing up to very long times [16]. The field theory version of this model was studied in Ref. [55], where ETH was found to be violated due to the persistent rare states made up by the mesons. There are a series of interesting question related to this problem. Whereas the non-integrable continuum model does not thermalize for various initial states, the observed lack of thermalization in the lattice model can be actually a very long transient. The role of integrability is also unclear in this situation as similar rare states were found in the 2D Ising model as well [55]. Confinement has an important role in high energy physics and could have important implications for heavy ion collisions and the early Universe, if confinement prevented thermalization.

2.2 Thermalization in integrable models

Integrable models together with the phenomenon of many-body localization (MBL) offer probably the best known example where ETH is violated, though equilibration usually occurs at least in integrable models as well. The violation of ETH is not surprising in view of the experimental results reporting the lack of thermalization in integrable models [3–5, 15], which, as a matter of fact, was already observed in the seminal work of Fermi, Pasta, Ulam and Tsingou [56]. The anomalous behaviour of integrable systems is related to the presence of infinitely many local conserved charges and can be easily understood. In translational invariant situations. i.e. global quantum quenches, the expectation value of densities of the charges equals the expectation value of the charge divided by the size of the system. If these charges are conserved, however, their initial expectation value must equal the equilibrated one. Therefore the steady-

state must retain much more information about the initial state to correctly describe the expectation values of the charges as well. Thus models with infinitely many local conserved charges such as integrable systems generally do not thermalize and do not satisfy the conventional ETH [1,2], in which the diagonal matrix elements depend only on the energy. For brevity, we refuse to enter the discussion of MBL and related concepts and thermalization is systems with MBL and recommend the review [57] instead for the interested reader. It is important to note, that the construction of infinitely many conserved charges is possible in systems with MBL as well (at least in principle), and the conserved charges are the projectors of localized eigenstates of the model. MBL can hence be regarded as a localized integrability, which hinders not only thermalization but equilibration as well.

Although integrable models do not thermalise in the usual sense, they do equilibrate and to explain the stationary state of integrable quantum systems, the idea of the generalised Gibbs ensemble (GGE) was proposed [19] using the maximum entropy principle [58] and later experimentally confirmed [6]. The GGE invokes the inclusion of all local conserved charges and accordingly expectation values of local operators in the stationary state can be calculated as

$$\langle \mathcal{O} \rangle_{GGE} = Z^{-1} \mathrm{Tr}\, \mathcal{O} e^{-\sum \lambda_i Q_i}\,, \tag{2.2.1}$$

where $Z = \mathrm{Tr}\, e^{-\sum \lambda_i Q_i}$, Q_i are the local conserved charges and β_i are Lagrange multiplies often called generalized chemical potentials or inverse temperatures. The generalized chemical potentials are determined the expectation values of the corresponding charges in the initial state. It is now a widely accepted scenario that isolated integrable systems equilibrate in the TDL to the steady state in the same sense as non-integrable ones do, and the stationary state can be characterized by the GGE. While it is an unconventional ensemble, the GGE can be argued to provide a statistical description, since in the TDL the number of local conserved charges scale polynomially with the system size instead of the exponential scaling which is the case for the diagonal ensemble.

This scaling, or more precisely, the actual set of conserved charges necessary to include in the GGE turned out to be a rather non-trivial problem [59–66]. Whereas integrable models possess infinitely many local conserved charges, the inclusion of the local ones proved to be insufficient for the GGE to offer correct predictions in the XXZ model [59,60] and it is necessary to extend the set of charges with class of quasi-local ones, which are charges corresponding to densities which, instead of compact supports decrease sufficiently fast with distance [65,66]. The necessary inclusion of quasi-local charges is much less intuitive than the role played by the local, or for a more precise terminology, ultra-local charges. In addition the eventual construction of the GGE may requires a careful limiting procedure [67], nevertheless the statistical description of the steady state is retained as the number of ultra-local and quasi-local conserved charges scale still polynomially with the system size [62]. However, it is not clear at present what are the conditions that identify the full set of quasi-local charges necessary to describe the equilibrium state, and how this set depends on the specific models under consideration or on the initial state. For this very important open question, the representative state approaches discussed later and a particle-based perspective [68] may provide some hints.

In fact, the use of the generalized Gibbs ensemble for the steady-state can be circumvented as the GGE is not the only statistical ensemble that can describe the steady-state of an integrable system. Similarly to the case of non-integrable models, one can use a generalized micro-canonical ensemble and declare the generalized ETH (GETH) to account for the generalized thermalization[1], i.e. the approach to a steady state that can be described by the generalized statistical ensembles. Expectation values in a generalized micro-canonical ensemble can be defined as

$$\langle \mathcal{O} \rangle_{GMCE} = \frac{1}{N_{GMCE}} \tilde{\sum} \langle n | \mathcal{O} | n \rangle\,, \tag{2.2.2}$$

[1]We stress, it is a generalized thermalization as in the steady state or in the GGE all the conserved charges appear, whereas the unitary time evolution is governed by only the Hamiltonian.

where the tilde over the sum means that it runs over eigenstates satisfying the conditions

$$|\langle n|Q_i|n\rangle - \langle \Psi_0|Q_i|n\Psi_0\rangle| \leq \delta_i \tag{2.2.3}$$

for the relevant ultra- and quasi-local charges. In the same spirit, the GETH can be formulated by postulating that the diagonal matrix elements of local observables are smooth functions not only of the energy, but of the eigenvalues of the higher conserved charges as well. The GETH, formulated first in Ref. [69] and verified in Ref. [65] hence ensures that the time averaged expectation values coincide with those computed using the generalized micro-canonical ensemble if the initial state satisfies the cluster property (2.1.8). It is perhaps surprising that the equivalence of the GMCE and GGE is not automatic and the GGE itself is not always well-defined [65]. Whereas this problem was overcome in Ref. [67] by taking an appropriate truncation of the set of charges and performing a limit on the truncation parameter, the generalized micro-canonical ensemble often provides a more well-behaved description of the steady state. This fact is also reflected in that the GGE itself is often understood as a GMCE. In the next section we briefly discuss some ideas behind the construction of the GMCE or equivalent representative states in integrable models. A great advantage of the representative state approaches is that in most cases they can be constructed without knowing the necessary set of charges and their explicit expressions.

2.3 Overlaps, time evolution and representative state approaches in integrable models

Compared to the ensemble description there are alternative ways of computing the equilibrium expectation values of observables. The idea of the representative state approaches is that equilibrium expectation values can be computed by merely a single post-quench eigenstate from Eq. (2.2.2) as a consequence of the GETH and the actual construction of the ensemble (2.2.2) is unnecessary. In most integrable models there exist stable quasiparticles, which can be used to obtain all eigenstates of the Hamiltonian. A representative state is a pure state, which can be characterized in integrable models by continuous densities instead of giving the possible quantum numbers of the quasiparticles making up a state (such as the set of momenta). In particular for the root density denoted by $\rho(\vartheta)$ the number of quasiparticles in the range $[\vartheta, \vartheta + \Delta\vartheta]$ is proportional to $L\rho(\vartheta)\Delta\vartheta$, if L is the system size and ϑ is a spectral parameter, which is usually the function of the energy or the momentum. When there are additional quantum numbers in the system related to discrete symmetries or more species of quasiparticles, then more than one densities are to be used, which are labeled by the discrete quantum numbers. Strictly speaking these densities represent a density matrix rather than a single state and always possess finite entropy density. However, any microscopic realization of the occupied quantum numbers corresponds to the same macro-state and the same equilibrium averages, since the root densities uniquely determine the expectation values of local observables in the TDL [70].

A representative state with density $\rho(\vartheta)$ offers a natural way to construct the GMCE as well after a quantum quench by requiring that

$$\langle \rho|Q_i|\rho\rangle = \langle \Psi_0|Q_i|\Psi_0\rangle \tag{2.3.1}$$

for all i(i.e. all ultra-local charges) where $|\rho\rangle$ denotes the representative state or more precisely, one of its microscopic realizations. Besides free fermion systems, this approach was successfully applied to quenches in the XXZ spin chain, where it was found that the quasi-local charges and their initial state expectation values are indeed necessary for the unique determination of $|\rho\rangle$ [71] contrary to the free fermion case, where the expectation values of the ultra-local charges are sufficient. Note that in these constructions there is no explicit entropy maximalization involved which suggests that the sufficient set of quasi-local charges uniquely determines the root density without the need for explicit entropy maximalization.

As already discussed, the lack of the knowledge of the necessary class of charges prevents the use of the charges to determine $|\rho\rangle$ in most cases. In contrast, the idea of the Quench Action (QA) approach

relies on the knowledge of the overlaps instead of the charges in a quantum quench. In many cases we have a better access to the overlaps than to the charges and their action. Starting from the overlaps of the initial state has the additional advantage of being able to describe the time evolution as well. For the case of integrable models, this approach leads to a number of exact results, although its drawback is that the construction of the overlaps is a hard issue that has only been resolved for a restricted set of initial states in a few interacting models. It is important to mention that recently the Quantum Transfer Matrix Approach [72] has been successfully applied for quantum quenches [73–76] and in particular this approach can provide directly the root densities of the representative state for particular 'few-site' initial states. This approach bypasses the usage of overlaps, nevertheless its applicability is restricted to initial states in lattice systems without a sensible analog in field theories. In integrable field theories, also the set of charges necessary to describe the equilibrium state is essentially unknown apart from the case of free field theories and there are also additional complications regarding the locality properties of the charges, which are necessary for the GGE [77, 78]. In this case the approach based on overlaps works much better especially if a special factorized structure (to be discussed later) is assumed. In fact, the knowledge of the overlaps [59–61, 79–86] made it possible to calculate steady-state expectation values of one-point functions and correlation functions in several examples [59–61, 85, 86] and in integrable field theories assuming the factorized structure for the overlaps, steady-state expectation values of one-point functions can be computed generally [70, 87]. The expectation values in IQFTs with factorized overlaps can be written in terms of an infinite series, but for certain operators simpler expression can be obtained in the sinh-Gordon model [88] and in its non-relativistic limit, i.e. the Lieb-Liniger model [89]. In addition, the overlaps offer a relatively direct access to the time evolution after a quench as well via (2.1.1). However, analytical results have mainly been obtained in systems that can be mapped to free particles [86,87,90–102] and in conformal field theory [27, 28] and only in a few cases in interacting integrable systems [73, 74, 83, 103–106] so far. In the context of integrable quantum field theory, more general approaches to describe the evolutions were used in [107–113], which are either perturbative [111, 112] or based on form factors of the theory and the overlaps of the quench [107–110] and there is also a semi-classical treatment [113] whose input is the again the overlaps. Our aim here is rather to demonstrate the role of overlaps in the study of time-evolution as well, and we return to a more detailed discussion of time evolution in Chapter 8.

The starting point of the QA approach is to write the time dependent expectation value of a local operator as

$$\langle\Psi_0|\mathcal{O}(t)|\Psi_0\rangle = \frac{1}{\langle\Psi_0|\Psi_0\rangle}\sum_{\Phi,\Phi'} e^{-\varepsilon_\Phi^*-\varepsilon_{\Phi'}} e^{i(\omega_\Phi-\omega_{\Phi'})t}\langle\Phi|\mathcal{O}(t)|\Phi'\rangle\,, \tag{2.3.2}$$

where Φ and Φ' labels the eigenstates of the Hamiltonian with energies ω_Φ and $\omega_{\Phi'}$ respectively and ε_Φ is the logarithmic overlap

$$\varepsilon_\Phi = -\ln\langle\Phi|\Psi_0\rangle\,. \tag{2.3.3}$$

The main idea is to switch from a summation on eigenstates to a functional integral over the root densities in the TDL yielding

$$\langle\mathcal{O}(t)\rangle_{\Psi_0} = \frac{1}{\langle\Psi_0|\Psi_0\rangle}\int\mathcal{D}[\rho]e^{S[\rho]}\sum_{\Phi}\left[e^{-\varepsilon_\Phi^*-\varepsilon_\rho}e^{i(\omega_\Phi-\omega_\rho)t}\langle\Phi|\mathcal{O}(t)|\rho\rangle + \Phi\leftrightarrow\rho\right], \tag{2.3.4}$$

where $S[\rho]$ is the Yang-Yang entropy, which is equal to the logarithm of the number of micro-states corresponding to a given macro-state. If $\mathcal{O}$ is a local operator, the matrix element $\langle\Phi|\mathcal{O}(t)|\Phi'\rangle$ is non zero if Φ and Φ' corresponds to the same macro-state in the TDL up to microscopic differences or in other words a finite number of excitations. Another key assumption is that the functional integral on root densities is dominated by a single saddle-point root density ρ_{sp}. This saddle-point density can be determined by an effective free energy functional

$$\langle \Psi_0 | \Psi_0 \rangle = \int \mathcal{D}[\rho] e^{-2\Re e(\varepsilon_\rho)+S[\rho]} \tag{2.3.5}$$

which ensures the normalization of $\langle \mathcal{O}(t) \rangle$ by the condition

$$\frac{\delta \mathcal{F}[\rho]}{\delta \rho} = 0\,, \tag{2.3.6}$$

where

$$\mathcal{F}[\rho] = 2\Re e\left(\varepsilon_\rho\right) - S[\rho]\,. \tag{2.3.7}$$

It is important to mention that in order to shift the saddle point (2.3.5) by the operator insertion (2.3.4), the operator $\mathcal{O}$ needs to have matrix elements exponentially large in the system size. As the matrix elements of local operators are usually $\mathcal{O}(1)$, the insertion of a local operator does not shift the saddle point of (2.3.5)[2]. To calculate the saddle-point density ρ_{sp} by Eq. (2.3.6), the necessary ingredient is the knowledge of the overlaps, or more precisely, the extensive part of the logarithm of the overlaps. Once the overlaps are known, the construction of the root density is relatively straightforward. The calculation of steady-state expectation values of local operators, i.e.

$$\langle \rho_{sp} | \mathcal{O} | \rho_{sp} \rangle\,, \tag{2.3.8}$$

has been carried out in the XXZ [59,60], and in the Lieb-Liniger model for particular quench protocols [85]. As already mentioned these expectation value of local operators in interacting integrable field theories after particular quenches can be expressed in terms of an infinite series [70,87], with the exception of some operators in the sinh-Gordon model [88] and the Lieb-Liniger model [89], where they can be calculated by integral equations.

An advantage of the QA framework is that it shall, in principle, be able to describe the late time evolution after a quench, which is determined by the excitations atop the representative state $|\rho_{sp}\rangle$. The the time dependence of a one-point function for late times is given formally as [83, 114, 115]

$$\langle \mathcal{O}(t) \rangle = \frac{1}{2} \sum_{m=0}^{\infty} \int \mathrm{d}[h,p]_m \left[e^{-it\omega[\rho_{sp},\{h_i,p_i\}]} e^{-\delta s[\rho_{sp},\{h_i,p_i\}]} \langle \rho_{sp} | \mathcal{O} | \rho_{sp}, \{h_i,p_i\} \rangle + \text{mirr.} \right]\,, \tag{2.3.9}$$

where h and p denotes quasi-particle and hole excitation on top of the reference state, with energy $\omega[\rho_{sp},\{h_i,p_i\}]$ and a differential overlap coefficient $\delta s[\rho_{sp},\{h_i,p_i\}]$. For the infinite time limit, this expression is dominated by the minimum number of particles and holes the operator has non-vanishing matrix elements with.

This interpretation of the late time dependence by (2.3.9) in terms of quasi-particles and quasi-holes is very suggestive, nevertheless, for concrete predictions matrix elements such as $\langle \rho_{sp} | \mathcal{O} | \rho_{sp} \rangle$ and $\langle \rho_{sp} | \mathcal{O} | \rho_{sp}, \{h_i,p_i\} \rangle$ are inevitable. Unfortunately, there is currently no general recipe even for the calculation of $\langle \rho_{sp} | \mathcal{O} | \rho_{sp} \rangle$ and the field theory results [70, 87] admit only an infinite series representation in general. Matrix elements of highly excited states such as representative states are an extremely challenging problem [70, 87, 116–120] with some effort being made [119–121] recently, which may spur activity in this direction. Whereas currently it is not known how to construct matrix elements of highly excited states practically (with some important exceptions already discussed [88, 89] and some cases in the XXZ chain [119]), the role of the overlaps is of great importance within the QA approach and, as demonstrated later in this thesis, the direct way to obtain the time evolution via (2.1.1) and hence by the overlaps can be, though rather technical, but relatively straightforward in many cases. Therefore the main focus of this

[2]This is not true for the Rényi entropies of the diagonal ensemble.

thesis is on the determination of overlaps and the time-evolution after quantum quenches. Before presenting our own results it is important to make a few comments on the quench paradigm in field theories and to motivate our preference for continuum models for the rest of the thesis.

2.4 Quenches in field theories

Quantum field theories (QFTs) are known to provide a universal description of quantum systems near quantum critical points and so offer an ideal starting point to identify and describe universal features of out-of-equilibrium physics in the vicinity of the critical point. Furthermore, non-equilibrium physics in quantum field theories is directly relevant to certain experiments as well, e.g. the emergent description provided by the quantum sine-Gordon model in trapped Bose gases [12, 13]. It is also interesting also in its own right especially in the context of high energy physics and cosmology.

Many 1+1 dimensional quantum field theories are integrable, and a paradigmatic example is given by the already mentioned sine-Gordon theory. In most explicitly known integrable quantum field theories (IQFTs), the S-matrices of the model and form factors i.e. matrix elements of (local) operators are known and in the next chapter we provide the details necessary for the present work. Therefore in these models it is natural to rely on Eq. (2.1.1) for the study of both the time evolution and the steady-state resulting after quantum quenches. In addition, there are powerful numerical methods available for 1+1 dimensional quantum field theories, which are independent of integrability and so apply to non-integrable models as well. In particular, truncated Hamiltonian methods can be extended to describe the non-equilibrium physics as well, giving access to the overlaps and time evolution. As discussed in Section 2.3, steady-state expectation values can be computed in terms of an infinite series involving form factors and the overlaps; however there are no analogous and general result for the time dependence. Our aim in this thesis is to fill in this gap by studying time evolution in IQFTs including the construction of the overlaps, which are input for both the steady-state and time-dependent quantities.

Out-of-equilibrium physics and the applicability or the emergence of a statistical description in a QFT is even less trivial than for the case of countably infinite degrees of freedom and additional questions and unexpected behavoiur may be encountered. We already discussed the case of confinement and the absence of thermalisation in confining and non-integrable QFTs. Moreover, the question of what class of operators can relax in a relativistic QFT is more subtle than in the case of spin chains or atomic gases. In relativistic QFTs, local operators and the locality principle play a central role, the structure of a Hilbert space in a QFT is essentially different from what we discussed in Section 2.1 due to the lack of elementary components. It is currently not known which operators in a QFT can equilibrate, but is generally believed that local operators do relax. Another fundamental question concerns the applicability of the quench paradigm in a QFT. In most cases QFT provides a universal effective description of a physical system, which is only valid at long distances and hence involves a certain (short distance or equivalently high-energy) cut-off. After a quantum quench an infinite amount of energy is injected to the system and it is a priori not obvious whether it is possible to obtain a universal i.e. cut-off independent description of the post-quench dynamics. In this work we demonstrate that the quench overlaps generically decrease with the energy of the eigenstate, and consequently the effects of the cut-off can be neglected if the quench is not too large.

The structure of the thesis is the following. In Chapter 3 we review the scattering theory of massive IQFTs and introduce their S-matrices and form factors and their finite volume regularization. Chapter 4 is devoted to the study of integrable quenches, in which the expansion of initial state in the post-quench basis possesses a factorized structure. Due to their resemblance to the Ghoshal-Zamolodchikov boundary states [122] corresponding to integrable boundary conditions, we provide a brief introduction to integrable boundary states followed by a detailed discussion of integrable quenches and the finite volume regularization of such initial states. In Chapter 5, the regularity properties of the overlaps are analyzed and it is demonstrated that they possess poles if zero-momentum particles are present in the initial state. For particular quench protocols, the overlaps are analytically calculated in the sinh-Gordon model in Chapter

6 and by the truncated conformal space approach in the sine-Gordon theory in Chapter 7. The two results are compared using a well-known correspondence between the two models by an analytic continuation of the coupling constant. Finally, in Chapter 8, the time evolution of one-point functions is studied and calculated up to a certain order in the number of particles in the post-quench expansion of the initial state. We present our conclusions and outlook in Chapter 9. Tedious calculations or more technical details of some calculations as well as numerical checks and tables can be found in the appendices after the main part.

Chapter 3

Some elements of Integrable Quantum Field Theory

Integrable quantum quantum field theories are most conveniently formulated in terms of their scattering theory, which we review in this chapter in order to introduce the formalism for use in the rest of thesis. For the specific examples of the sinh- and sine-Gordon theories, the Lagrangian definitions together with some relevant S-matrices and form factors can be found in Section 3.4, where the formulation of the sine-Gordon model as a perturbed conformal field theory is also discussed. We also introduce the important example of Ising field theory, which describes the continuum limit of the quantum Ising spin chain.

3.1 Asymptotic states, factorized scattering and the Zamolodchikov-Faddeev algebra

In massive, relativistic quantum field theories one can consider initial and final scattering states corresponding to free particles if they are well-separated from each other. Therefore, the initial and final states can be described as multi-particle states labeled by the momenta and quantum numbers of the particles. In the usual terminology, the initial states are made up by incoming, and the final states by outgoing particles reflected by the in/out subscripts in the notation as

$$|p_1, p_2, ...p_n, \{i_1, i_2, ..., i_n\}\rangle_{in}$$

$$|q_1, q_2, ...q_m, \{j_1, j_2, ..., j_m\}\rangle_{out.}$$

In view of the asymptotic completeness, both the in and out states form a complete basis, hence the scattering matrix (S-matrix) connecting the initial and final states written in terms of the in and out states as

$$_{out}\langle \text{final}|\text{initial}\rangle_{in} = S_{f,i}$$

is a unitary operator. The dependence of the matrix elements of S on the momenta and quantum numbers are constrained by symmetry. Clearly, a scattering process must fulfill the conservation of energy and momenta and the scattering amplitude can depend only on Lorentz invariant combinations of the four-momenta of the particles. The general structure of the S-matrix respecting the constraints of a relativistic quantum field theory was analyzed in the 70's under the program called analytic S-matrix theory [123]. Instead of going into details, we only discuss the case of $1+1D$ integrable quantum field theories, where the analytic structure of the S-matrix greatly simplifies. In such theories, due to the presence of the infinitely many local conserved charges, the following additional restrictions emerge for the scattering:

- the scattering is purely elastic, i.e., the number of incoming and outgoing particles is the same;
- any scattering factorizes to the consecutive scattering of two particles.

Therefore to describe scattering in integrable QFTs, the only necessary object is the two-particle S-matrix S_{ab}^{cd}, where Latin indices refer to particle species. We parametrize the particles in terms of the rapidity variables as

$$(E_a, p_a) = m_a \left(\cosh\vartheta, \sinh\vartheta\right)$$

and exploit Lorentz invariance which implies that the amplitude S_{ab}^{cd} only depends on the difference of the rapidities. As an important consequence of the factorization property, the two particle S-matrix satisfies the Yang-Baxter equation [124–126]

$$S_{a_1a_2}^{c_1c_2}(\vartheta_{12})S_{c_1c_3}^{b_1b_3}(\vartheta_{13})S_{c_2a_3}^{b_2c_3}(\vartheta_{23}) = S_{a_1a_3}^{c_1c_3}(\vartheta_{13})S_{c_1c_2}^{b_1b_2}(\vartheta_{12})S_{a_3c_3}^{c_2b_3}(\vartheta_{23})\,, \tag{3.1.1}$$

where $\vartheta_{ij} = \vartheta_i - \vartheta_j$. For particles with non-degenerate mass spectrum or more generally, with a difference in the eigenvalues of some of the conserved charges, the two particle S-matrix simplifies as

$$S_{ab}^{cd}(\vartheta) = S_{ab}(\vartheta)\delta_{ac}\delta_{bd}$$

in which case the scattering is called diagonal and the Yang-Baxter equation is trivially satisfied.

To keep our exposition simple, in the following we restrict ourselves to the case of diagonal scattering. The analytic properties of the two-particle S matrix involve unitarity and crossing symmetry which have the form

$$\begin{aligned} S_{ab}(\vartheta)S_{ab}^*(\vartheta) &= 1 \\ S_{ab}(i\pi - \vartheta) &= S_{a\bar{b}}(\vartheta) \end{aligned} \tag{3.1.2}$$

corresponding to the unitarity and crossing symmetry, where $\bar{b}$ denotes the anti-particle of b. It is generally true in QFT with time reversal symmetry [127] that the S-matrix is real analytic in terms of the Mandelstam variable $s = (p_a + p_b)^2$. As a consequence one can write

$$S_{ab}(\vartheta) = S_{ab}(-\vartheta^*) = S_{ab}^*(-\vartheta)\,, \tag{3.1.3}$$

and the unitarity condition can also be written as

$$S_{ab}(\vartheta)S_{ab}(-\vartheta) = 1\,. \tag{3.1.4}$$

The relations (3.1.2), (3.1.3) and (3.1.4) impose strong restrictions on the functional form of S_{ab} whose most general expression reads

$$S_{ab}(\vartheta) = \prod_{\alpha\in\mathcal{K}_{ab}} s_\alpha(\vartheta) \tag{3.1.5}$$

with

$$s_\alpha(\vartheta) = \frac{\sinh(\vartheta) + i\sin(\pi\alpha)}{\sinh(\vartheta) - i\sin(\pi\alpha)} \tag{3.1.6}$$

and a finite set of parameters $\mathcal{K}_{ab}$. The S-matrix (3.1.5) possesses a series of poles and zeros on the complex plane specified by α. The simple poles are associated with particles a and b forming a bound state. The S-matrix bootstrap approach consists of finding solutions for the S-matrices in which the pole structure is consistent with a theory with a set of particles. In many integrable models consistent solutions

for the S-matrices can be obtained by the bootstrap, which results in exact expressions for the scattering amplitudes within a finite set of particles.

Given the S-matrix, is is convenient to introduce particle creation and annihilation operators satisfying the Zamolodchikov-Faddeev algebra [128–130]

$$\begin{aligned} Z^\dagger(\vartheta_1)Z^\dagger(\vartheta_2) &= S(\vartheta_1-\vartheta_2)Z^\dagger(\vartheta_2)Z^\dagger(\vartheta_1)\,, \\ Z(\vartheta_1)Z(\vartheta_2) &= S(\vartheta_1-\vartheta_2)Z(\vartheta_2)Z(\vartheta_1)\,, \\ Z(\vartheta_1)Z^\dagger(\vartheta_2) &= S(\vartheta_2-\vartheta_1)Z^\dagger(\vartheta_2)Z(\vartheta_1)+2\pi\delta(\vartheta_1-\vartheta_2)\mathbf{1}\,, \end{aligned} \tag{3.1.7}$$

where the operator $Z^\dagger(\vartheta)$ creates a particle excitation with rapidity ϑ. With these operators, asymptotic states can be obtained by their repeated action on the vacuum $|0\rangle$. In particular, the in- and out-states can be obtained as

$$\begin{aligned} |\vartheta_1,\vartheta_2,...,\vartheta_n\rangle_{in} &= Z^\dagger(\vartheta_1)Z^\dagger(\vartheta_2)...Z^\dagger(\vartheta_n)|0\rangle, \qquad \vartheta_1>\vartheta_2>...>\vartheta_n \\ |\vartheta_n,\vartheta_{n-1},...\vartheta_1\rangle_{out} &= Z^\dagger(\vartheta_n)Z^\dagger(\vartheta_{n-1})...Z^\dagger(\vartheta_1)|0\rangle, \qquad \vartheta_1>\vartheta_2>...>\vartheta_n \end{aligned} \tag{3.1.8}$$

where the particular ordering in the rapidities ensures

$$S_{f,i} = {}_{out}\langle\vartheta_1',\vartheta_2'|\vartheta_1,\vartheta_2\rangle_{in} = S(\vartheta_1-\vartheta_2)2\pi\delta(\vartheta_1-\vartheta_1')2\pi\delta(\vartheta_2-\vartheta_2')$$

for $\vartheta_1>\vartheta_2$ and $\vartheta_1'>\vartheta_2'$.

3.2 Form factors bootstrap

For the sake of brevity, in the following we focus on theories without bound states and with a single particle species only. Form factors are matrix elements of local operators between asymptotic states. In particular, we define the n-particle elementary form factor of some local operator $\mathcal{O}$ as

$$F_n^{\mathcal{O}}(\vartheta_1,\vartheta_2,...\vartheta_n) = \langle 0|\mathcal{O}(0)|\vartheta_1,\vartheta_2,...\vartheta_n\rangle\,. \tag{3.2.1}$$

By means of the elementary form factors, generic matrix elements

$$F_{n,m}^{\mathcal{O}}(\vartheta_1',\vartheta_2',...\vartheta_m'|\vartheta_1,\vartheta_2,...\vartheta_n) = \langle\vartheta_1',\vartheta_2',...\vartheta_m'|\mathcal{O}(0)|\vartheta_1,\vartheta_2,...\vartheta_n\rangle\,. \tag{3.2.2}$$

can be reconstructed by repeated use of the crossing relations [131]

$$\begin{aligned} F_{n,m}^{\mathcal{O}}(\vartheta_1',...\vartheta_m'|\vartheta_1,...\vartheta_n) =& F_{n-1,m+1}^{\mathcal{O}}(\vartheta_1',...\vartheta_{m-1}'|\vartheta_m'+i\pi,\vartheta_1,...\vartheta_n) \\ &+\sum_{k=1}^{n}2\pi\delta(\vartheta_m'-\vartheta_k)\prod_{l=1}^{k-1}S(\vartheta_l-\vartheta_k)\times \\ &F_{n-1,m-1}^{\mathcal{O}}(\vartheta_1',...\vartheta_{m-1}'|\vartheta_1,...,\vartheta_{k-1},\vartheta_{k+1},...\vartheta_n) \end{aligned} \tag{3.2.3}$$

The analytic properties of elementary form factors, which are called form factor equations are the consequences of the factorized and elastic scattering of the integrable theory, the locality and unitarity principles and Lorentz symmetry of relativistic quantum field theory and are summarized as follows [131]:

1. Exchange
$$F_n^{\mathcal{O}}(\vartheta_1,...,\vartheta_k,\vartheta_{k+1},...\vartheta_n) = S(\vartheta_k-\vartheta_{k+1})F_n^{\mathcal{O}}(\vartheta_1,...,\vartheta_{k+1},\vartheta_k,...\vartheta_n) \tag{3.2.4}$$

2. Cyclic permutation
$$F_n^{\mathcal{O}}(\vartheta_1 + 2\pi i, \vartheta_2, ...\vartheta_n) = e^{2\pi i\gamma} F_n^{\mathcal{O}}(\vartheta_2, ...\vartheta_n, \vartheta_1) \tag{3.2.5}$$

3. Kinematical singularity
$$-i \operatorname*{Res}_{\vartheta=\vartheta'} F_{n+2}^{\mathcal{O}}(\vartheta' + i\pi, \vartheta, \vartheta_1, \vartheta_2, ...\vartheta_n) = \left(1 - e^{2\pi i\gamma} \prod_{i=1}^{n} S(\vartheta - \vartheta_i)\right) F_n^{\mathcal{O}}(\vartheta_1, \vartheta_2, ...\vartheta_n) \tag{3.2.6}$$

The $e^{2\pi i\gamma}$ factor in (3.2.5) and (3.2.6) is called the semi-local or mutual locality index of the operator $\mathcal{O}$ with respect to the interpolating field ϕ, i.e. the field with non-zero matrix element between the vacuum and a one-particle state as

$$\langle 0|\phi|\vartheta\rangle = e^{-ixm\sinh\vartheta} \frac{Z_\phi^{1/2}}{(2\pi)^{d/2}} .$$

The locality index is defined via the condition

$$\mathcal{O}(x,t)\phi(y,t') = e^{2\pi i\gamma}\phi(y,t')\mathcal{O}(x,t) \tag{3.2.7}$$

for space-like separated space-time points. Local operators correspond to $e^{2\pi i\gamma} = 1$, while fields with $e^{2\pi i\gamma} \neq 1$ are called semi-local.

4. Lorentz symmetry
$$F_n^{\mathcal{O}}(\vartheta_1 + \Lambda, \vartheta_2 + \Lambda, ...\vartheta_n + \Lambda) = e^{s\Lambda} F_n^{\mathcal{O}}(\vartheta_1, \vartheta_2, ...\vartheta_n) , \tag{3.2.8}$$

where s is the Lorentz spin of the operator.

5. Cluster property
$$\lim_{\Lambda\to\infty} F_{n+m}^{\mathcal{O}}(\vartheta_1 + \Lambda, \vartheta_2 + \Lambda, ...\vartheta_n + \Lambda, \beta_1, ...\beta_m) = \frac{1}{\langle 0|\mathcal{O}|0\rangle} F_n^{\mathcal{O}}(\vartheta_1, ...\vartheta_n) F_m^{\mathcal{O}}(\beta_1, ...\beta_m) , \tag{3.2.9}$$

which is satisfied if the field $\mathcal{O}$ corresponds to a relevant scaling field in the ultra-violet (UV) limiting conformal field theory [132] describing the high-energy behaviour of the IQFT.

The properties Eqs. (3.2.4)-(3.2.9) allow the exact construction of form factors of various operators in many integrable models. This is called the form factor bootstrap program [133–136] and involves the assumption of maximal analyticity, which means that the form factors as functions of complex variables cannot possess additional poles or branch cuts than those required and dictated by the equations above, In the bootstrap approach it is customary to consider the following Ansatz for the form factors involving n particles

$$F_n^{\mathcal{O}}(\vartheta_1, \ldots, \vartheta_n) \quad = \langle 0|\, \mathcal{O}(0) |\vartheta_1, \ldots, \vartheta_n\rangle = \quad \mathcal{N}_n \frac{Q_n^{\mathcal{O}}(x_1, \ldots, x_n)}{\prod_{i<j}(x_i + x_j)} \prod_{i<j} f_{min}(\vartheta_i - \vartheta_j) , \tag{3.2.10}$$

where $x_i = e^{\vartheta_i}$ and $\mathcal{N}_n$ is a normalisation. The minimal form factors f_{min} satisfying

$$f_{min}(-\vartheta) = S(\vartheta) f_{min}(\vartheta) \quad \text{and} \quad f_{min}(i\pi - \vartheta) = f_{min}(i\pi + \vartheta)$$

ensure (3.2.4). The dependence of the rest only on x_i guarantees (3.2.5), the product in the denominators ensures the presence of poles prescribed by (3.2.6), and the dependence of the particular operator is encoded in $Q_n^{\mathcal{O}}$, which is a symmetric polynomial of the variables and apart from an overall factor $(\prod x_i)^{min(\gamma,1-\gamma)}$ which is present when the locality index gamma is nontrivial. The minimal form factor can be expressed as

$$f_{min}(\vartheta) = \exp\left(-\frac{1}{4}\int_{-\infty}^{\infty}\frac{\mathrm{d}t}{t}\frac{B(t)}{\sinh t}\exp\left[\frac{t(\vartheta - i\pi)}{i\pi}\right]\right), \tag{3.2.11}$$

where $B(\mathrm{t})$ is defined by

$$S(\vartheta) = \exp\left(\frac{1}{2}\int_{-\infty}^{\infty}\frac{\mathrm{d}t}{t}B(t)\exp\left[\frac{t\vartheta}{i\pi}\right]\right). \tag{3.2.12}$$

By means of the form factors, observable operators can be written as an expansion [137] in terms of the Zamolodchikov-Faddeev operators (3.1.7)

$$\mathcal{O} = \sum_{m,n=0}^{\infty}\frac{1}{m!n!}\int\prod_{i=1}^{m}\frac{\mathrm{d}\vartheta_i}{2\pi}\int\prod_{j=1}^{n}\frac{\mathrm{d}\eta_j}{2\pi}f^{\mathcal{O}}_{m,n}(\vartheta_1,\dots,\vartheta_m|\eta_1,\dots\eta_n)Z^\dagger(\vartheta_1)\dots Z^\dagger(\vartheta_m)Z(\eta_1)\dots Z(\eta_n)\,, \tag{3.2.13}$$

where the functions f can be expressed in terms of the elementary form factors

$$f^{\mathcal{O}}_{m,n}(\vartheta_1,\dots,\vartheta_m|\eta_1,\dots,\eta_n) = F^{\mathcal{O}}_{m+n}(\vartheta_m + i\pi + i0,\dots,\vartheta_1 + i\pi + i0,\eta_n - i0,\dots,\eta_1 - i0)\,. \tag{3.2.14}$$

It is easy to verify that (3.2.13) reproduces correctly the form factors of the local field $\mathcal{O}$

$$\begin{aligned} F^{\mathcal{O}}_{m+n}(\vartheta_m + i\pi + i0,\dots,\vartheta_1 + i\pi + i0,\eta_n - i0,\dots,\eta_1 - i0) &= \langle\vartheta_m + i0,...,\vartheta_1 + i0|\mathcal{O}|\eta_n - i0,\dots,\eta_1 - i0\rangle \\ &= f^{\mathcal{O}}_{m,n}(\vartheta_1,\dots,\vartheta_m|\eta_1,\dots,\eta_n)\,, \end{aligned} \tag{3.2.15}$$

where the opposite imaginary shifts of left and right rapidities serve to regularize the terms that are disconnected from the operator $\mathcal{O}$.

From (3.2.4) the functions $f^{\mathcal{O}}_{m,n}$ satisfy the permutation relations

$$\begin{aligned} f^{\mathcal{O}}_{m,n}(\dots\vartheta_i,\vartheta_{i+1}\dots|\dots) &= S(\vartheta_{i+1} - \vartheta_i)f^{\mathcal{O}}_{m,n}(\dots\vartheta_{i+1},\vartheta_i\dots|\dots)\,, \\ f^{\mathcal{O}}_{m,n}(\dots|\dots,\eta_i,\eta_{i+1}\dots) &= S(\eta_{i+1} - \eta_i)f^{\mathcal{O}}_{m,n}(\dots|\dots,\eta_{i+1},\eta_i\dots)\,. \end{aligned} \tag{3.2.16}$$

3.3 IQFT in finite volume, Bethe states and finite volume FF

It is often useful to restrict IQFTs to a finite segment of space hence in this section we discuss some features of IQFTs in a finite volume L and introduce our notations used throughout this thesis. For simplicity we restrict our attention again to the case of a theory with one particle species without a bound state.

In finite volume it is possible to construct eigenstates of the finite volume Hamiltonian analogous to the scattering states in the infinity volume theory [138, 139]. Imposing periodic boundary conditions (PBC) the excited states of a massive integrable quantum field theory in a large, but finite volume can be described as scattering states consisting of n particles with rapidities ϑ_n, where these rapidities are now given by the solution of the Bethe–Yang equations

$$Q_k = mL\sinh\vartheta_k + \sum_{j\neq k}\delta(\vartheta_k - \vartheta_j) = 2\pi I_k\,, \qquad k = 1,\dots,n\,. \tag{3.3.1}$$

In contrast to the Bethe Ansatz solution on spin chains [140], this scattering state is just an approximate solution of the model neglecting finite site effects that decay exponentially in the volume [138].

Using the fact that the effective statistics is fermionic, i.e. $S(0) = -1$ in all known interacting theories with one species the two-particle phase shift function $\delta(\vartheta)$ is defined as

$$S(\vartheta) = -e^{i\delta(\vartheta)}\,, \qquad \delta(-\vartheta) = -\delta(\vartheta)\,, \tag{3.3.2}$$

and the following prescription is obtained for the quantum numbers of the particles:

$$I_k \in \mathbb{Z} \qquad \text{for odd } n\ , \qquad\qquad I_k \in \mathbb{Z} + \frac{1}{2} \qquad \text{for even } n\ .$$

The state corresponding to quantum numbers $\{I_1, \dots, I_n\}$ is denoted as

$$|\{I_1 \dots I_n\}\rangle_L\ ,$$

and it is independent (up to a possible phase ambiguity) of the ordering of the I_k. They are normalised so that their scalar products are

$${}_L\langle\{I_1 \dots I_n\}|\{I'_1 \dots I'_m\}\rangle_L = \delta_{nm}\delta_{I_1,I'_1} \dots \delta_{I_n,I'_n}\ ,$$

with the quantum numbers ordered by convention as $I_1 < \dots < I_n$ and $I'_1 < \dots < I'_m$. The total energy and momentum can be expressed as

$$E = \sum_{i=1}^{n} m \cosh\vartheta_i + O(e^{-\mu L})\ , \qquad\qquad P = \sum_{i=1}^{n} m \sinh\vartheta_i + O(e^{-\mu L})$$

up to exponential corrections governed by some mass scale μ. The systematic treatment of exponential corrections to excitation energies can be found in [138, 141–143].

It is useful to introduce the rapidity space density of n-particle states, which is given by the Jacobian

$$\rho_n(\vartheta_1, \dots, \vartheta_n) = \det J_{kl}\ , \qquad J_{kl} = \frac{\partial Q_k}{\partial \vartheta_l}\ . \tag{3.3.3}$$

In finite volume one can consider finite volume form factors, which are now matrix elements of local operators with the Bethe states

$${}_L\langle\{I'_1 \dots I'_k\}|\mathcal{O}|\{I_1 \dots I_l\}\rangle_L\ .$$

When the sets of rapidities in the bra and ket states are disjoint, the finite and infinite volume form factors can be related [144] as

$${}_L\langle\{I'_1 \dots I'_k\}|\mathcal{O}|\{I_1 \dots I_l\}\rangle_L = \frac{F^{\mathcal{O}}_{k+l}\left(\vartheta'_1 + i\pi, \dots \vartheta'_k, +i\pi, \vartheta_1 \dots \vartheta_l\right)}{\sqrt{\rho_k(\vartheta'_1, \dots, \vartheta'_k)\rho_l(\vartheta_1, \dots, \vartheta_l)}} + O(e^{-\mu L})\ . \tag{3.3.4}$$

For the case of coinciding rapidities this relation must be modified to account for disconnected contributions [144], but we do not need the corresponding expressions in this work. Note that the equality (3.3.4) is valid up to a suitably chosen phase factor which can be changed by redefining the phases of the finite volume eigenstates $|\{I_1, \dots, I_n\}\rangle_L$. This accounts for the fact that the ordering of the particles is not determined by first principles and any exchange leads to an S-matrix factor according to (3.2.4). It is clear that all such ambiguities cancel in expectation values of physical observables and correlation functions; however, for a practical calculation one must fix the phases of the multi-particle contributions to the matrix elements consistently.

3.4 The sinh- and sine-Gordon models and the Ising field theory

3.4.1 The sinh-Gordon model

The sinh-Gordon model is defined by the Hamiltonian

$$\begin{aligned} H &= \int \mathrm{d}x \left[\frac{1}{2}\pi^2 + \frac{1}{2}(\partial_x\phi)^2 + \frac{m_0^2}{g^2} : \cosh g\phi :\right]\ , \\ &\quad [\phi(t,x), \pi(t,y)] = i\delta(x-y) \end{aligned} \tag{3.4.1}$$

where m_0 is the classical particle mass and g is the coupling constant. The model is one of the simplest examples of an IQFT, which is invariant under the Z_2 symmetry $\phi \to -\phi$ and its spectrum consists of multi-particle states of a single massive bosonic particle with exact mass m. The two-particle S-matrix is [145]

$$S(\vartheta) = \frac{\sinh(\vartheta) - (\omega - \omega^{-1})/2}{\sinh(\vartheta) + (\omega - \omega^{-1})/2} = \frac{\tanh\frac{1}{2}(\vartheta - i\frac{\pi B}{2})}{\tanh\frac{1}{2}(\vartheta + i\frac{\pi B}{2})}, \tag{3.4.2}$$

where $\vartheta = \vartheta_1 - \vartheta_2$ is the relative rapidity of the particles and we introduced the notation

$$\omega = e^{i\frac{\pi B}{2}}, \tag{3.4.3}$$

where B is related to the coupling g in (3.4.1) by

$$B \;=\; \frac{2g^2}{8\pi + g^2}\,. \tag{3.4.4}$$

For the sinh-Gordon form factors, solutions of the system (3.2.4)-(3.2.9) were first constructed in Ref. [146]. In Ref. [147], form factors of the exponential operators

$$: e^{\kappa g \phi} : \tag{3.4.5}$$

with locality index $\gamma = 0$ were obtained, where $\kappa \in \mathbb{R}$. The form factors of exponential operators take the following form [147]

$$F_n^{\kappa}(\vartheta_1, \ldots, \vartheta_n) = \langle 0| : e^{\kappa g \phi} : |\vartheta_1, \ldots, \vartheta_n\rangle = G_{\kappa}^{shG} \left(\frac{4\sin\frac{\pi B}{2}}{\mathcal{N}}\right)^{n/2} \frac{Q_n^{\kappa}(x_1, \ldots, x_n)}{\prod_{i<j}(x_i + x_j)} \prod_{i<j} f_{min}(\vartheta_i - \vartheta_j)\,, \tag{3.4.6}$$

where $x_i = e^{\vartheta_i}$. The minimal form factor f_{min} for the sinh-Gordon model reads

$$\begin{aligned} f_{min}(\vartheta, B) \;&=\; \mathcal{N}\, \tilde{f}_{min}(\vartheta, B)\,, \qquad (3.4.7)\\ \tilde{f}_{min}(\vartheta, B) &= \exp\left[8\int_0^{\infty} \frac{\mathrm{d}t}{t} \frac{\sinh\frac{Bt}{4}\sinh\frac{t}{2}\left(1 - \frac{B}{2}\right)\sinh\frac{t}{2}}{\sinh^2 t} \sin^2\left[\frac{t(i\pi - \vartheta)}{2\pi}\right]\right]\,, \end{aligned}$$

which is a complex valued meromorphic function without singularities for real rapidities. This function tends to unity for large rapidities, i.e., $\lim_{\vartheta \to \pm\infty} f_{min}(\vartheta) = 1$, so long as the normalisation is chosen to be

$$\mathcal{N} = f_{min}(i\pi, B) = \exp\left[-4\int_0^{\infty} \frac{\mathrm{d}t}{t} \frac{\sinh\frac{Bt}{4}\sinh\frac{t}{2}\left(1 - \frac{B}{2}\right)\sinh\frac{t}{2}}{\sinh^2 t}\right]\,. \tag{3.4.8}$$

The functions Q_n appearing in (3.4.6) are entire functions and completely symmetric in the variables x_i; for an operator with a power-like short distance singularity they can only grow exponentially for large values of the rapidities and are therefore restricted to be polynomials [136]. These functions are called *form factor polynomials*; their growth at infinity is related to the ultraviolet scaling dimension of the operator, and solutions with the lowest possible growth at infinity, called minimal solutions, correspond to operators with the lowest possible conformal dimensions.

For the exponential operators discussed here, the form factor polynomials can be written as

$$Q_n^{\kappa} = \det M_{ij}(\kappa) \tag{3.4.9}$$

where M is an $(n-1) \times (n-1)$ matrix with elements

$$M_{ij}(\kappa) = [\kappa + i - j]\, \sigma_{2i-j}^{(n)}\,, \tag{3.4.10}$$

where

$$[n] = \frac{\sin n\frac{\pi B}{2}}{\sin \frac{\pi B}{2}} \,, \tag{3.4.11}$$

and $\sigma_i^{(n)}$ denotes the ith symmetric polynomial of n variables $x_1, \ldots, x_n$ defined by the generating function

$$\prod_{i=1}^{n}(x + x_i) = \sum_{k=0}^{n} x^{n-k}\sigma_k^{(n)}(x_1, \ldots, x_n) \,.$$

The exponential operators are spinless (3.2.8), hence the total degree of the polynomials (3.4.9) must be the same as that of the denominator in (3.4.6); since the total degree of Q_n^κ is $n(n-1)/2$ this is indeed satisfied. The partial degree of the polynomials is at most $n-1$, which ensures that $\lim_{\theta_i\to\infty} F_n^\kappa(\theta_1, \ldots, \theta_n)$ is bounded by a constant.

Finally, G_κ^{shG} are the exact vacuum expectation values of these operators whose exact expressions were found in [148]:

$$G_\kappa^{shG} = \langle 0| : e^{\kappa g\phi} : |0\rangle \,. \tag{3.4.12}$$

For later use we note that the form factors of the elementary field ϕ in the sinh-Gordon model are proportional to

$$\frac{dF_n^\kappa}{d\kappa}|_{\kappa=0} \,,$$

in which the polynomial part reads $Q_n^0 = \det M_{ij}(0)$. These form factors are only non-zero when n is odd in accordance with the symmetry $\phi \to -\phi$, and satisfy the cluster property as well with the modification that the r.h.s in (3.2.9) is divided by F_1^ϕ instead of $\langle 0|\phi|0\rangle$, which is zero.

3.4.2 The sine-Gordon model

The sine-Gordon theory is defined by the Hamiltonian

$$\begin{aligned} H &= \int \mathrm{d}x \left[\frac{1}{2}\pi^2 + \frac{1}{2}(\partial_x\phi)^2 - \frac{\mu^2}{\beta^2} : \cos\beta\phi :\right] \,, \\ &\quad [\phi(t,x), \pi(t,y)] = i\delta(x-y). \end{aligned} \tag{3.4.13}$$

To describe the interaction strength it is useful to introduce the quantity

$$\xi = \frac{\beta^2}{8\pi - \beta^2} \,. \tag{3.4.14}$$

The fundamental excitations are a doublet of soliton/anti-soliton of mass M, but in the attractive regime of the model, where $\xi < 1$ the spectrum also contains breathers B_r (soliton–anti-soliton bound states) with masses

$$m_r = 2M \sin\frac{r\pi\xi}{2}$$

with r a positive integer less than ξ^{-1}. The sine-Gordon theory is integrable, and its exact factorised S matrix is known [126]. The scattering amongst the breathers and between breathers and solitons is diagonal, whereas for soliton--anti-soliton scattering, the S-matrix has a real matrix structure in space of the soliton–anti-soliton doublet.

In this work we mainly focus on states made up exclusively by first breather excitations. Under the analytic continuation to imaginary couplings $g \to i\beta$, the sinh-Gordon particle corresponds to the first breather B_1, which can be supported both by perturbation theory and the correspondence between the

respective S matrix amplitudes. As a result, the S-matrix for B_1 can be rewritten with that of the sinh-Gordon model (3.4.2) as

$$S_{B_1B_1}(\vartheta,\xi) = S_{shG}(\vartheta, B)\mid_{B=-2\xi} \tag{3.4.15}$$

and form factors of local operators containing only the first breather B_1 are also identical to the corresponding sinh-Gordon quantities under the same analytic continuation, which are all known in the model. In particular for the vertex operators in the sine-Gordon theory

$$V_\alpha =: e^{i\alpha\beta\phi} : \tag{3.4.16}$$

its form factors involving first breathers can be obtained from the sinh-Gordon form factors for the exponential fields, i.e.,

$$F^\alpha_{n,B_1}(\vartheta_1,\ldots,\vartheta_n) = \langle 0|: e^{i\alpha\beta\phi} : |\vartheta_1,\ldots,\vartheta_n\rangle_{B_1} = G^{sG}_\alpha[\alpha]_\xi \left(i\bar\lambda(\xi)\right)^n Q^\alpha_n(x_1,\ldots,x_n)_\xi \prod_{i<j}\frac{f_\xi(\vartheta_j-\vartheta_i)}{x_i+x_j}, \tag{3.4.17}$$

where

$$[n]_\xi = [n]\mid_{B=-2\xi},$$

$$Q^\alpha_n(x_1,\ldots,x_n)_\xi = Q^\alpha_n(x_1,\ldots,x_n)\mid_{B=-2\xi}.$$

(See (3.4.9), (3.4.10) and (3.4.11) for definition). The quantities entering Eq. (3.4.17) are defined as follows:

$$\bar\lambda(\xi) = 2\cos\frac{\pi\xi}{2}\sqrt{2\sin\frac{\pi\xi}{2}}\exp\left(-\int_0^{\pi\xi}\frac{dt}{2\pi}\frac{t}{\sin t}\right), \tag{3.4.18}$$

and

$$f_\xi(\vartheta) = v(i\pi+\vartheta,-1)v(i\pi+\vartheta,-\xi)v(i\pi+\vartheta,1+\xi)v(-i\pi-\vartheta,-1)v(-i\pi-\vartheta,-\xi)v(-i\pi-\vartheta,1+\xi), \tag{3.4.19}$$

with

$$\begin{aligned} v(\vartheta,\sigma) = &\prod_{k=1}^N\left(\frac{\vartheta+i\pi(2k+\sigma)}{\vartheta+i\pi(2k-\sigma)}\right)^k \times \\ &\exp\left\{\int_0^\infty\frac{\mathrm{d}t}{t}\left(-\frac{\sigma}{4\sinh\frac{t}{2}}-\frac{i\sigma\vartheta}{2\pi\cosh\frac{t}{2}}+\left(N+1-Ne^{-2t}\right)e^{-2Nt+\frac{it\vartheta}{\pi}}\frac{\sinh(\sigma t)}{2\sinh^2 t}\right)\right\}. \end{aligned} \tag{3.4.20}$$

For the vacuum expectation value G^{sG}_α, we have [149]

$$\begin{aligned} G^{sG}_\alpha = &\left[\frac{M\sqrt{\pi}\,\Gamma\left(\frac{4\pi}{8\pi-\beta^2}\right)}{2\Gamma\left(\frac{\beta^2}{8\pi-\beta^2}\right)}\right]^{\frac{\alpha^2\beta^2}{4\pi}} \times \\ &\exp\left\{\int_0^\infty\frac{\mathrm{d}t}{t}\left[\frac{\sinh^2\left(\frac{\alpha}{4\pi}t\right)}{2\sinh\left(\frac{\beta^2}{8\pi}t\right)\cosh\left(\left(1-\frac{\beta^2}{8\pi}\right)t\right)\sinh t}-\frac{\alpha^2\beta^2}{4\pi}e^{-2t}\right]\right\}. \end{aligned} \tag{3.4.21}$$

Similarly to the sinh-Gordon case, the B_1 form factors of the field ϕ can be obtained by differentiating the form factors for the vertex operators with respect to α.

For the sine-Gordon theory another useful approach is provided by considering it as a perturbed conformal field theory (PCFT) as well, which is a paradigmatic approach to a massive quantum field theory regarding it as a perturbation of an ultra-violet (UV) conformal field theory (CFT) [150] with appropriate relevant operators. In this terminology perturbation is understood as a deformation of the conformal field theory and does not signify a commitment to smallness of any parameter. In models with one space dimension, there exist powerful non-perturbative methods which allow to treat these models for strong couplings as well.

For the sine-Gordon model the corresponding description treats (3.4.13) as a compactified massless bosonic conformal field theory in finite volume L, perturbed by the operator $\int dx \ :\cos\beta\phi:$, which is relevant if $\beta^2 < 8\pi$. $\beta^2 = 8\pi$ is known as the Kosterlitz-Thouless point, above which the perturbation is irrelevant. The compactification of the bosonic field ϕ means that it takes values on a circle with the identification $\phi \equiv \phi + m\frac{2\pi}{\beta}$, and space-time has a cylindrical geometry due to periodic boundary conditions (PBC) $x \equiv x + L$. Then the perturbed conformal Hamiltonian H_{PCFT} reads

$$H_{PCFT} = \int_0^L \mathrm{d}x \, \frac{1}{2} : (\partial_t\phi)^2 + (\partial_x\phi)^2 : - \frac{\lambda}{2}\int_0^L \mathrm{d}x \, \left(V_1^{cyl} + V_{-1}^{cyl}\right) , \tag{3.4.22}$$

where the semicolon denotes normal ordering with respect to the massless scalar field modes. The upper index "cyl" of the normal ordering indicates that these vertex operators have a canonical CFT normalisation specified as

$$\langle 0|V_n^{cyl}(w_1,\bar{w}_1)V_m^{cyl}(w_2,\bar{w}_2)|0\rangle \sim \frac{\delta_{n,-m}}{(w_1-w_2)^{4n^2\Delta}} . \tag{3.4.23}$$

with $w = \tau - ix$,$w = \bar{\tau} + ix$ complex coordinates on the resulting Euclidean space-time cylinder. As a result, the coupling λ has a nontrivial dimension related to the scaling exponent Δ. Integrability allows to determine the exact relation between the coupling and the mass scale of excitations [151]:

$$\lambda = \frac{2\Gamma(\Delta)}{\pi\Gamma(1-\Delta)} \left(\frac{\sqrt{\pi}\Gamma\left(\frac{1}{2-2\Delta}\right) M}{2\Gamma\left(\frac{\Delta}{2-2\Delta}\right)} \right)^{2-2\Delta} \qquad \text{with} \qquad \Delta = \frac{\beta^2}{8\pi} , \tag{3.4.24}$$

where M is the mass of the soliton (note that the soliton mass M is not the gap, at least not for all values of β). Relation (3.4.24) allows to express all physical quantities in units of appropriate powers of the soliton mass M.

Mapping the cylinder to the complex plane using the exponential mapping

$$z = \exp\frac{2\pi}{L}w$$

the exponential operator transforms as [150]

$$V_{\pm1}^{pl}(z,\bar{z}) \left(|z|\,\frac{2\pi}{L}\right)^{2\Delta} = V_{\pm1}^{cyl}(w,\bar{w}) . \tag{3.4.25}$$

V_α^{pl} is a dimensionless operator and is often more convenient to use than the one defined on the cylinder. For example, the Hamiltonian (3.4.22) can be expressed as

$$H_{PCFT} = \frac{2\pi}{L}\left(L_0 + \bar{L}_0 - \frac{1}{12}\right) - \lambda\left(\frac{2\pi}{L}\right)^{2\Delta}\frac{L}{2}\int_0^{2\pi}\frac{\mathrm{d}\varphi}{2\pi}\left[V_{+1}^{pl}(e^{i\varphi},e^{-i\varphi}) + V_{-1}^{pl}(e^{i\varphi},e^{-i\varphi})\right] , \tag{3.4.26}$$

where the first part of the Hamiltonian (3.4.26) involves the generators L_0 and $\bar{L}_0$ of the Virasoro algebra and is just the free massless boson Hamiltonian in finite volume, which can be rewritten in terms of the usual bosonic operators as

$$H_{CFT} = \frac{2\pi}{L}\left(\pi_0^2 + \sum_{k>0} a_{-k}a_k + \sum_{k>0}\bar{a}_{-k}\bar{a}_k - \frac{1}{12}\right) , \tag{3.4.27}$$

with

$$\begin{aligned} &[\phi_0, \pi_0] = i \qquad [a_k, a_l] = k\delta_{k+l} \\ &[\bar{a}_k, \bar{a}_l] = k\delta_{k+l} \, , \end{aligned} \tag{3.4.28}$$

where ϕ_0 and π_0 are the zero mode of the canonical field and its conjugate momentum. The operators a_k and $\bar{a}_k$ correspond to right and left oscillator modes creating/annihilating particles with momentum indexed by the quantum numbers k in units of $2\pi/L$.

The Hilbert space $\mathcal{H}$ is composed of Fock modules $\mathcal{F}_n$, built upon Fock vacua

$$|n\rangle = V_n(z=0)|0\rangle$$

using the oscillator modes, and its basis is given as

$$a_{-k_1}...a_{-k_r}\bar{a}_{-p_1}...\bar{a}_{-p_l}|n\rangle : \, n \subset \mathbb{Z} \, , \, r, \, l \subset \mathbb{N} \, , k_i \, , \, p_j \subset \frac{2\pi}{L}\mathbb{N} \, , \tag{3.4.29}$$

which are eigenstates of H_{CFT} with energy

$$E = \frac{2\pi}{L}\left(\frac{(n\beta)^2}{4\pi} + \sum_{i=1}^{r} k_i + \sum_{j=1}^{l} p_j - \frac{1}{12}\right) . \tag{3.4.30}$$

The ground state of the conformal field theory is the Fock vacuum with $n = 0$, i.e. $|0\rangle$.

This formulation of the theory enables the use of the truncated conformal space approach (TCSA), which is an efficient numerical method [18]. As discussed in Section 7.1 in more details, it is possible to compute matrix elements of vertex operators and in particular the cosine operator in the conformal basis. Truncating the basis of the free model, which is discrete due to the finite volume L, the diagonalization of the Hamiltonian or calculating expectation values becomes possible via manipulations with finite dimensional matrices.

3.4.3 The Ising field theory

Before the discussion of the Ising field theory, it is instructive to introduce briefly the lattice model and its continuum limit resulting in the field theory. The transverse field quantum Ising model (TQIM) is defined by the Hamiltonian

$$H = -J\sum_{i=1}^{N}\left(\sigma_i^x\sigma_{i+1}^x + h\sigma_i^z\right) , \tag{3.4.31}$$

where σ_i^α denotes the Pauli matrices at site i, $J > 0$, h is the transverse field and the boundary conditions are assumed to be periodic. Applying the Jordan-Wigner transformation, the Hamiltonian (3.4.31) can be mapped to spinless Majorana fermions with dispersion relation [152, 153]

$$\varepsilon_h(k) = 2J\sqrt{1 + h^2 - 2h\cos k} \tag{3.4.32}$$

which has an energy gap $\Delta = 2J|1-h|$. The model possesses a quantum critical point at $h = 1$ separating the disordered or paramagnetic phase (PM) for $h > 1$ and the ordered, ferromagnetic phase (FM) for $h < 1$. In the disordered phase, the expectation value of the magnetisation operator vanishes, while in the ferromagnetic phase its value is given by [153]

$$\langle \sigma_i^x \rangle = \left(1 - h^2\right)^{1/8} . \tag{3.4.33}$$

The Hilbert space of the model consists of two sectors with respect to fermion number parity. In the Neveu–Schwarz and Ramond sectors states with even and odd number of fermions are present, respectively, resulting in the following quantisation conditions for the wave numbers

$$\begin{aligned} k_n =& \frac{2\pi}{N}\left(n + \frac{1}{2}\right) \quad \text{Neveu-Schwarz} \\ p_n =& \frac{2\pi}{N} n \qquad\qquad\quad \text{Ramond} , \end{aligned} \tag{3.4.34}$$

where n is a positive integer. In particular, the Fock space of the model in the paramagnetic phase can be written as

$$\begin{aligned} |p_1, ..., p_{2m+1}\rangle =& \prod_{i=1}^{2m+1} a^\dagger_{p_i} |0\rangle_R^{PM} \quad p_i \subset \mathrm{R} , \\ |k_1, ..., k_{2n}\rangle =& \prod_{i=1}^{2n} a^\dagger_{k_i} |0\rangle_{NS}^{PM} \qquad k_i \subset \mathrm{NS} , \end{aligned} \tag{3.4.35}$$

and the ground state is the Neveu–Schwarz vacuum $|0\rangle_{NS}^{PM}$. In the ferromagnetic phase, the zero momentum excitation has negative energy, therefore the Ramond vacuum is redefined as $|0\rangle_R \to a_0^\dagger |0\rangle_R$ after which a particle-hole transformation is implemented by exchanging $a_0^\dagger$ with a_0. The Fock space of the model in the FM regime is therefore

$$\begin{aligned} |p_1, ..., p_{2m}\rangle =& \prod_{i=1}^{2m} a^\dagger_{p_i} |0\rangle_R^{FM} \qquad p_i \subset \mathrm{R} , \\ |k_1, ..., k_{2n}\rangle =& \prod_{i=1}^{2n} a^\dagger_{k_i} |0\rangle_{NS}^{FM} \qquad k_i \subset \mathrm{NS} , \end{aligned} \tag{3.4.36}$$

where the ground state becomes degenerate in the thermodynamic limit and the finite volume states corresponding to fixed orientations of the macroscopic magnetisation are $\frac{1}{\sqrt{2}}(|0\rangle_{NS}^{FM} \pm |0\rangle_R^{FM})$.

The scaling limit of the TQIM results in the Ising field theory. In the limiting procedure J is sent to infinity together with $h \to 1$ such that the gap associated with the fermion mass remains finite

$$M = 2J|1-h| . \tag{3.4.37}$$

In addition, the lattice spacing is sent to zero as

$$a = \frac{c}{2J} , \tag{3.4.38}$$

where c is the speed of light that can be set to 1 with an appropriate choice of units.. It is easy to see that the dispersion relation (3.4.32) under scaling limit transforms as

$$\varepsilon_h(ka) \to E(p) = \sqrt{M^2 + p^2}\,. \tag{3.4.39}$$

The Hamiltonian (3.4.31) scales to the Hamiltonian of a massive Majorana fermion field theory

$$H = \frac{1}{2\pi}\int dx \frac{i}{2}\left(\psi(x)\partial_x\psi(x) - \bar{\psi}(x)\partial_x\bar{\psi}(x)\right) - iM\bar{\psi}(x)\psi(x)\,, \tag{3.4.40}$$

with

$$\{\psi(x,t), \bar{\psi}(y,t)\} = 2\pi\delta(x-y)\,. \tag{3.4.41}$$

The lattice magnetisation operator σ_i^x is related to the continuum field σ with the conformal normalisation via

$$\sigma(na) = \bar{s}J^{\frac{1}{8}}\sigma_n^x\,, \tag{3.4.42}$$

with

$$\bar{s} = 2^{\frac{1}{12}}e^{-\frac{1}{8}}\mathcal{A}^{\frac{3}{2}}\,, \tag{3.4.43}$$

where $\mathcal{A}$=1.282427129... is Glaisher's constant.

Since the Hamiltonian (3.4.40) of the Ising field theory is the Hamiltonian of a free Majorana fermion field, the two-particle S-matrix describing the scattering of the free fermionic particles is simply

$$S = -1\,. \tag{3.4.44}$$

However, the form factors of local operators are not necessarily trivial due to the Jordan-Wigner transformation connecting the spin and fermion operators. In particular the form factors of the spin field are

$$F_n^\sigma(\vartheta_1, ...\vartheta_n) = \bar{s}i^{\frac{n-1}{2}}\prod_{i<j}\tanh\frac{\vartheta_i - \vartheta_j}{2}\,, \tag{3.4.45}$$

and F^σ is only non-zero between Neveu-Schwatz and Ramond states. Of course, F^σ satisfies (3.2.4)-(3.2.9) with $S = -1$.

Chapter 4

Integrable quenches

The following four chapters of this thesis are devoted to the overlaps after quantum quenches in massive IQFTs. As discussed in Chapter 2, knowledge of the overlaps allows (at least in principle) the construction of a representative state for the steady-state and Eq. (2.1.1) allows a direct treatment of the time evolution as well, since in integrable models both the spectrum and form factors are known. In this chapter the so-called integrable quenches are discussed, which have a distinctive property that the initial state expanded in the post-quench basis possesses a particular structure corresponding to a factorized structure of the overlaps with the post-quench multi-particle basis. Integrable quenches play a central role in the study of quantum quenches: all exactly solved quenches fall into this category.

Due to the close relation between integrable quenches in massive IQFTs and integrable boundaries, we first review some basic aspects of integrable boundary field theories in Section 4.1. This is followed by a discussion of the general definition of integrable quenches and their relation to the squeezed-coherent structure of the initial state in Section 4.2. The discussion illuminates important properties of integrable quenches and also help us find conditions when a given quench protocol can be considered or approximated by an integrable quench. Finally the finite volume approach to integrable quenches is reviewed in Section 4.3.

4.1 Integrable boundary field theories

In Chapter 3 we briefly discussed some important features of integrable field theories. It is possible to restrict these models to a half infinite segment of space $x \in (-\infty, 0]$ with some prescribed boundary condition at $x = 0$ while preserving integrability at the same time. For integrable theories, i.e. models that are integrable in the bulk, there exist special boundary conditions that preserve the integrability of the model, i.e. the existence of infinitely many local conserved charges [122]. As an important consequence one can retain the concept of factorized scattering for massive models. The new ingredient is that when a particle with rapidity ϑ hits the boundary it undergoes a perfect reflection with reflection amplitude $R_B(\vartheta)$. (For one type of particle species, we can neglect additional indices.) This can be written formally as

$$|\vartheta\rangle_B = R_B(\vartheta)|-\vartheta\rangle_B\,, \tag{4.1.1}$$

where $|\vartheta\rangle = Z^\dagger(\vartheta)|0\rangle_B$ with $|0\rangle_B$ denoting the vacuum of the boundary theory. The definition of *in* and *out* state is analogous to the bulk case with following ordering convention

$$Z^\dagger(\vartheta_1)Z^\dagger(\vartheta_2)...Z^\dagger(\vartheta_n)|0\rangle_B, \qquad \vartheta_1 > \vartheta_2 > ... > \vartheta_n > 0 \tag{4.1.2}$$

for *in* states and

$$|Z(-\vartheta_1)Z^\dagger(-\vartheta_2)...Z^\dagger(-\vartheta_n)|0\rangle_B, \qquad \vartheta_1 > \vartheta_2 > ... > \vartheta_n > 0 \tag{4.1.3}$$

for *out* states. The expansion of the *in* states in terms of the *out* states now involves not only the bulk two-particle S-matrices but also the reflection amplitudes, e.g.

$$Z^\dagger(\vartheta_1)Z^\dagger(\vartheta_2)|0\rangle_B = S(\vartheta_1-\vartheta_2)R(\vartheta_1)S(\vartheta_1+\vartheta_2)R_B(\vartheta_2)Z^\dagger(-\vartheta_1)Z^\dagger(-\vartheta_2)|0\rangle_B\,, \tag{4.1.4}$$

with $\vartheta_1 > \vartheta_2 > 0$.

Similarly to the S-matrix, the reflection amplitude must fulfill some constraints which can be viewed as the boundary analogues of the properties of the bulk S-matrix. These include the boundary Yang-Baxter relation [154], which is automatically satisfied for one species of particles similarly to its bulk counterpart, the boundary unitarity condition [154]

$$R_B(\vartheta)R_B(-\vartheta) = 1\,, \tag{4.1.5}$$

and the boundary crossing property [122]

$$K_B(\vartheta) = S(2\vartheta)K_B(-\vartheta)\,, \tag{4.1.6}$$

where

$$K_B(\vartheta) = R_B\left(\frac{i\pi}{2}-\vartheta\right) \tag{4.1.7}$$

is called the boundary K-function. Given the bulk S-matrix of the theory, it is often possible to find solutions for R_B satisfying (4.1.5) and (4.1.6). As a result of the boundary bootstrap program [122, 155], i.e. finding and classifying solution for the reflection amplitude, for many theories the integrable boundaries are explicitly known, and they are often labeled by so-called boundary parameters which arise in addition to the parameters of the bulk.

Extending the notion of crossing symmetry to the boundary situation results in the concept of the boundary state, which also plays an important role in the study of quantum quenches. Applying a Euclidean rotation the x-coordinate in the original theory becomes $i\tau$, where τ is the Euclidean time variable, and the t-coordinate becomes the space coordinate y of the Euclidean theory. After this procedure the boundary in the Minkowski picture can be interpreted as an initial (or final) state in the Hilbert space of the infinite volume Hamiltonian without a boundary, which is called a boundary state. For integrable boundaries, the corresponding boundary state is called an integrable boundary state and can be written as [122]

$$|B\rangle = \mathcal{N}\exp\left(\frac{1}{2}\int\frac{d\vartheta}{2\pi}K_B(\vartheta)Z^\dagger(-\vartheta)Z^\dagger(\vartheta)\right)|0\rangle\,, \tag{4.1.8}$$

which has a peculiar structure composed of a coherent superposition of pairs of particles with opposite momenta and where $\mathcal{N}$ is a normalisation constant. However these states are not normalisable in a strict sense since K_B does not decrease for large ϑ. In theories with diagonal scattering, K_B can be expressed as a product of blocks

$$\frac{\sinh\left(\frac{\vartheta}{2}+i\pi x\right)}{\sinh\left(\frac{\vartheta}{2}-i\pi x\right)}\,,$$

whose $\vartheta\to\pm\infty$ limit is a pure phase. To provide a concrete example, in the sine-Gordon theory with a Dirichlet boundary condition $\phi\,|_{x=0}= 0$, the corresponding boundary K-function reads

$$K_D(\vartheta) = i\tanh(\vartheta/2)\frac{\cosh\left(\frac{\vartheta}{2}-\frac{i\pi B}{8}\right)\sinh\left(\frac{\vartheta}{2}+\frac{i\pi(B+2)}{8}\right)}{\sinh\left(\frac{\vartheta}{2}+\frac{i\pi B}{8}\right)\cosh\left(\frac{\vartheta}{2}-\frac{i\pi(B+2)}{8}\right)}\,, \tag{4.1.9}$$

where B is related wit the coupling in the sinh-Gordon model in (3.4.4) and boundary state is denoted by $|D\rangle$. It satisfies

$$\phi(\tau = 0, y)|D\rangle = 0\,, \tag{4.1.10}$$

i.e. $|D\rangle$ is a state annihilated by the sinh-Gordon field ϕ, which is consistent with its identification as the boundary state corresponding to the Dirichlet boundary condition.

The form of the boundary state (4.1.8) is not the most general one, as it is possible to find integrable boundary conditions, where the boundary state contains zero momentum particles as well:

$$|B\rangle = \mathcal{N} \exp\left(\bar{g}_B Z^\dagger(0) + \frac{1}{2}\int \frac{d\vartheta}{2\pi} K_B(\vartheta) Z^\dagger(-\vartheta) Z^\dagger(\vartheta)\right)|0\rangle\,. \tag{4.1.11}$$

The one-particle coupling implies a pole for the reflection factor

$$R_B(\vartheta) \sim \frac{i}{2}\frac{g_B^2}{\vartheta - i\pi/2}\,,$$

which then yields a pole at the origin

$$K_B(\vartheta) \sim -\frac{i}{2}\frac{g_B^2}{\vartheta}\,, \tag{4.1.12}$$

for the boundary K-function. Whereas it was argued that $\bar{g}_B = g_B$ in [122], it was later demonstrated in [156, 157] that the correct relation is $\bar{g}_B = g_B/2$, with a general proof given in [158]. This behaviour is of course compatible with (4.1.6) as in all interacting integrable models $S(0) = -1$, which results in a $K_B(\vartheta) \sim \vartheta$ behaviour when there is no one-particle coupling. As discussed in Section 5 and in Chapter 8, the pole is also present in the two-particle overlaps for quenches with non-zero overlaps for a standing particle and this structure has notable consequences for the the time evolution of one-point functions followed by a quench.

4.2 Integrable quenches: definition, their structure and examples

As discussed in the introduction, describing quantitatively a system after a quantum quench is an extremely difficult problem even for integrable systems. However there exist special quenches or equivalently, special initial states in integrable models which are possible to treat analytically to a certain extent, and in many cases exact expressions for the steady state or time-dependent quantities are available. These are called integrable quenches and in the following we give their most general definition, discuss some of their properties and establish connection with the integrable boundary states introduced in the previous section. The definition for integrable quenches we present here can be formulated with the action of parity odd operators of the local conserved charges on the initial state $|\Omega\rangle$ as [75]

$$Q_s^o|\Omega\rangle = 0. \tag{4.2.1}$$

In massive relativistic IQFT, the action of the conserved charges on the asymptotic state is the sum of the one-particle contributions

$$Q_s^e|\vartheta_1, ...\vartheta_n\rangle = \sum_{i=1}^n q_s \cosh(s\vartheta_i)\,|\vartheta_1, ...\vartheta_n\rangle \tag{4.2.2}$$

for even charges and

$$Q_s^o|\vartheta_1, ...\vartheta_n\rangle = \sum_{i=1}^n q_s \sinh(s\vartheta_i)\,|\vartheta_1, ...\vartheta_n\rangle \tag{4.2.3}$$

for odd charges, where s is the Lorentz-spin and q_s is the one-particle eigenvalue of the charge and the charges themselves can be written as

$$Q_s^e = \int \frac{d\vartheta}{2\pi}\, q_s \cosh\left(s\vartheta_i\right) Z^\dagger(\vartheta) Z(\vartheta) \tag{4.2.4}$$

and

$$Q_s^o = \int \frac{d\vartheta}{2\pi}\, q_s \sinh\left(s\vartheta_i\right) Z^\dagger(\vartheta) Z(\vartheta)\,. \tag{4.2.5}$$

As an immediate consequence of (4.2.1) and (4.2.3), quenches sharing the structure of the boundary states (4.1.8) and (4.1.11) are integrable so if the initial state can be cast in the form

$$|\Omega\rangle = \mathcal{N} \exp\left(\frac{1}{2}\int \frac{d\vartheta}{2\pi} K(\vartheta) Z^\dagger(-\vartheta) Z^\dagger(\vartheta)\right)|0\rangle \tag{4.2.6}$$

or

$$|\Omega\rangle = \mathcal{N} \exp\left(\frac{g}{2} Z^\dagger(0) + \frac{1}{2}\int \frac{d\vartheta}{2\pi} K(\vartheta) Z^\dagger(-\vartheta) Z^\dagger(\vartheta)\right)|0\rangle \tag{4.2.7}$$

then the quench is integrable. In this case, the name integrable quench is also motivated by the fact that the amplitudes of states with larger number of particles factorise into the product of two-particle states, which is reminiscent of the factorisation of the many-body scattering matrix into two-particle scattering amplitudes. Similarly to the boundary states, the K-function entering (4.2.6) and (4.2.7) satisfies the boundary crossing relation (4.1.6) which in the quench context ensures that the initial state is insensitive to a reordering of the creation operators. However the boundary unitarity condition (4.1.5) is usually violated and the K functions decrease for large rapidities sufficiently fast so that the state remains normalisable.

It is worth discussing the conditions under which the squeezed coherent form (4.2.6) (or (4.2.7)) follows from the property of integrability stated in (4.2.1) and to avoid confusions, integrable states with the exponential structure will be referred to as (integrable) squeezed coherent states in the following. Instead of giving a rigorous proof, our aim here is to shed more light on the properties of integrable quenches and on how these properties are related to each other. The core of the argument we present here can be found in Ref. [159] and an analogous and more complete version of the argument valid for spin chains was presented in Ref. [75].

4.2.1 Connection between the integrability of the quench and the squeezed-coherent initial state

The first step in the line of arguments is to show that if the initial state consists of pairs of particles with opposite momenta then the initial state must be a squeezed coherent state. In order to show this, it is assumed that the initial state satisfies the cluster property (2.1.8), which is generally true for ground or thermal states of quantum systems with local interactions. To make some simplifications, consider first the case of a single massive excitation and the absence of zero-momentum particles in $|\Psi\rangle$ that contains only excitations with zero total momentum and even number of particles. Without loss of generality we can write such a state in the form of a cumulant expansion

$$|\Psi\rangle = \exp\left(\sum_{m=1}^{\infty}\int K_m^\Psi(\vartheta_1,\vartheta_2,\ldots,\vartheta_m)\prod_{i=1}^{m} Z^\dagger(\vartheta_i)\frac{d\vartheta_i}{2\pi}\right)|0\rangle\,, \tag{4.2.8}$$

where the amplitudes $K_m^\Psi(\vartheta_1,...,\vartheta_m)$ contain a δ-factor $2\pi\delta(\sum_i p(\theta_i))$ due to the conservation of total momentum and all odd amplitudes $K_{2n+1}^\Psi(\theta_1,...,\theta_{2n+1})$ are zero. In the context of global quantum quenches when a finite energy density and therefore infinite energy is injected into the system, the charges Q_s which are spatial integrals of local operators are also extensive thermodynamic quantities.

We show that the expectation values of the local charges Q_s in the above state are extensive quantities i.e. they increase linearly with the system size L only if the amplitudes K_{2n} do not contain any other δ-function factor except of the one that accounts for the zero total momentum, $\delta(\sum_i p(\theta_i))$. The expectation values of Q_s^e in the state $|\Psi\rangle$ are

$$\frac{\langle\Psi|Q_s^e|\Psi\rangle}{\langle\Psi|\Psi\rangle} \equiv \langle\Psi|Q_s^e|\Psi\rangle_{conn} \,, \tag{4.2.9}$$

and correspond to the sum of all possible ways to contract left and right excitations in the expansion of (4.2.8) with the charge operator (4.2.4), which has two legs and with each other, in such a way that no part is disconnected from the rest. Diagrammatically this is represented by fully connected graphs as in Fig. 4.2.1.

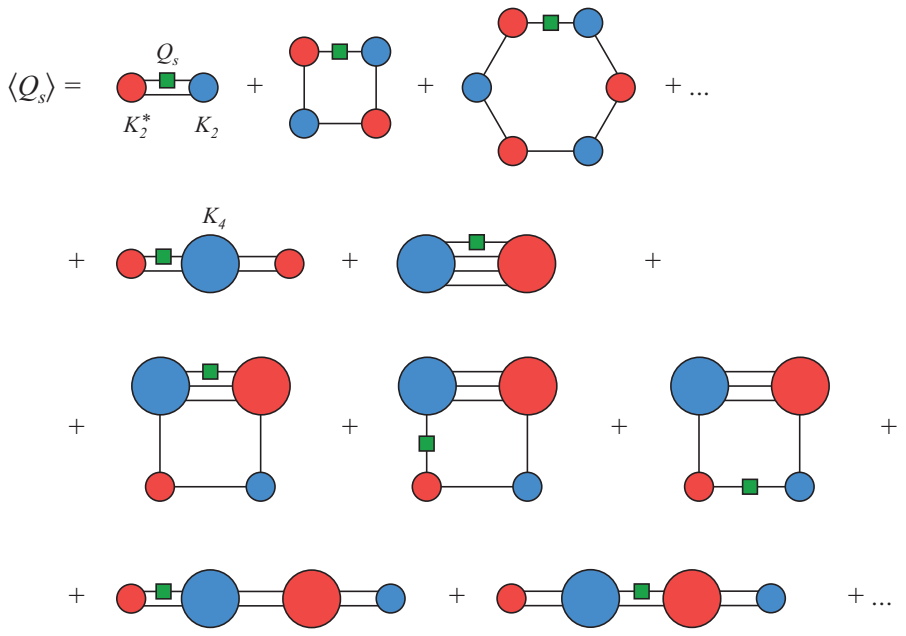

Figure 4.2.1: Diagrammatic expansion of the expectation value of a local charge in the state $|\Omega\rangle$. The bra-excitations (red circles) and the ket-excitations (blue circles) must be contracted with each other and with the charge operator (green square) in all possible fully connected ways. Contractions are denoted by lines, each of which connects two circles of different colours. The green square can be inserted on any of these lines. Small circles correspond to pair excitations and have two legs, larger circles correspond to 4-particle excitations and have four legs, and so on (the full equation contains red and blue circles with any even number of legs).

In order to determine the scaling of thermodynamic quantities with L we should simply count the number of redundant δ-function factors of momentum variables in the expectation values of the corresponding operator since $\delta(0)$ can be interpreted as the volume L. As mentioned above, the amplitudes K_{2n}^{Ψ} contain a factor $\delta(\sum_i p(\theta_i))$ due to the translation invariance. Taking into account all of those δ-function factors involved in each connected graph and assuming that the K_{2n}^{Ψ} do not contain any other δ-function factors, we can easily see that each graph has exactly one left over factor of $\delta(0)$, which is nothing but a factor equal to the system size L. This means that the contribution of such graphs is linear in L i.e. extensive. If however some K_{2n}^{Ψ} contains two δ-function singularities in the momentum variables, then the corresponding graphs contain one extra $\delta(0) \sim L$ factor i.e. scale more than linearly with L and are not extensive. Supposing that the charges Q_s are functionally independent and complete, extensivity of the charges requires that contributions of all graphs are separately extensive, which is only true if there is no amplitude K_{2n}^{Ψ} with more than one δ-function. The same condition ensures the extensivity of the

generating function $\log Z = \log\langle\Psi|\Psi\rangle$ (analogous to the free energy) from which other thermodynamic quantities can be derived.

Note that the argument requires the functional completeness of the charges, which may require taking into consideration quasi-local charges [65]. However, as long as these additional charges are extensive for large system sizes, such as the case e.g. for the charges used in completing the GGE for the XXZ spin chain [65], the argument is left unchanged.

Given the completeness of charges, the operator condition (4.2.1) is only satisfied if the state exclusively consists of pairs of particles with opposite momenta. We have thus shown that if $|\Omega\rangle$ satisfies the cluster decomposition principle and the conserved charges form a complete set, then from (4.2.1) it follows that $|\Omega\rangle$ can be cast in the form (4.1.8).

The above argument assumed that there is only a single species of particles, but it can be easily extended to the case of multiple species. If the eigenvalues of the charges are not degenerate with respect to the particle species, which is the general situation, than the argument remains valid, and (4.2.1) together with the completeness of the charges and the cluster decomposition principle imply

$$|\Omega\rangle = \mathcal{N}\exp\left(\frac{1}{2}\int\frac{d\vartheta}{2\pi}K_a(\vartheta)Z_a^\dagger(-\vartheta)Z_a^\dagger(\vartheta)\right)|0\rangle\,, \tag{4.2.10}$$

where the subscript $a$indexes the particle species. In this case it may be necessary to consider further global charges as exemplified by the soliton excitations in the sine-Gordon model. The solitons and anti-solitions labeled by s and $\bar{s}$ have the same eigenvalues q_s but have a different topological charge. In such a case, however, prescribing that

$$Q_{top}|\Omega\rangle = 0 \tag{4.2.11}$$

forces the state to be composed of soliton–anti-soliton pairs and hence the initial state to be

$$|\Omega\rangle = \mathcal{N}\exp\left(\frac{1}{2}\int\frac{d\vartheta}{2\pi}K_{a,b}(\vartheta)Z_a^\dagger(-\vartheta)Z_b^\dagger(\vartheta)\right)|0\rangle\,, \tag{4.2.12}$$

where a and b can be either s or $\bar{s}$ and K_{ab} vanishes for $a = b$.

It is important to note that the case of initial states with zero-momentum particles can also be treated. When the initial state has contributions of odd-particle number states as well, then the annihilation of the initial state by the parity odd charges again force $|\Omega\rangle$ to have either pairs of particles with opposite momenta or the same pairs with one stationary particle. But then counting the redundant δ-functions and the requirement for extensivity imply that the $|\Omega\rangle$ must obey (4.2.7). However, there is a subtlety in this case: as will be discussed in Subsection 5, the presence of zero-momentum particles implies the existence of a pole in K at the origin, hence besides the δ-functions, additional singularities can emerge.

Finally, it is worth mentioning that our statement presented here can be proven referring to the Quench Action formalism too. The extensivity of the generating function $\log Z = \log\langle\Psi|\Psi\rangle$ is only guaranteed if the overlaps factorize once the their pair structure is assumed. As a consequence, the overlap term and the entropy contribution in the functional $\mathcal{F}$ in Eq. (2.3.7) scale with same power of L and hence result in sensible Quench Action equations only if the factorized structure holds. This is an important observation since arguing with the scaling of $\log Z$ and eventually the solvability of the quench action is likely to have a non-field theory specific form valid for lattice systems too, which would be interesting to work out.

In summary Eq. (4.2.1) with the functional completeness of the conserved charges imply that integrable initial states can be written in the form (4.2.6) or (4.2.7) in massive IQFTs. In massless theories this statement is not necessarily true and a counter-example is provided the XX spin chain, which corresponds to a Luttinger-liquid in the continuum limit, i.e. a massless bosonic CFT. In this case (4.2.1) does not guarantees the pair structure of the excitations and hence the analogous form of (4.2.6) [160].

4.2.2 Integrable initial states for small quenches

So far we have only defined a class of special quenches and discussed their distinctive properties. However, a typical realisation of a quantum quench is provided by preparing the initial state in the ground state of a local Hamiltonian and then letting it evolve with a different post-quench Hamiltonian. The natural questions are whether we can tell if a given quench protocol corresponds an integrable quench and if we can determine the overlaps. In the literature, several quench protocols are known to be integrable. In fact, these are the sole examples of quenches that can be solved exactly, i.e. such that their overlaps are known and/or the stationary state the system reaches can be constructed. These cases include spin chains and the Lieb-Liniger model [79–82, 85, 161, 162] and models that can be mapped to non-interacting theories. However, in massive IQFTs no exact results have been obtained until now apart from the free theories and the continuum limit of the transverse field Ising model [107] (again equivalent to a free theory). In free systems it is possible to relate the pre- and post-quench model operators via a Bogolyubov transformation which results in the squeezed-coherent structure of the initial state expanded in the post-quench basis.

We would also like to note that factorization of the overlap is tied very closely to certain algebraic structures, for example fusion hierarchy and Y -system in the XXZ spin chain [163]. Although in QFT there is less control over the underlying algabraic structures and the only known initial states satisfying the Y system are 'few-site' states [163] and have hence no sensible analogs in QFT, this perspective may spur activity on the field theory side in the future.

Despite the lack of exact overlaps and the inability of deciding if a given quench protocol gives rise to an integrable quench in an IQFT, integrable initial states and in particular the squeezed-coherent states are an ideal starting point for analytic considerations in field theory. For such initial states it is possible (at least in principle) to construct the GGE expectation values of local operators [70, 87, 88] and calculate time dependence for local operators [107–109, 113].

Now we present a simple argument stating that for small enough quenches the squeezed-coherent form of the initial state is a very good approximation irrespectively of the integrability of the model, hence in the small-quench limit the approximate integrability of the quench is guaranteed as long as the model is massive [159]. We assume translation invariance of the initial state, which holds for ground states of local Hamiltonians. A quench is considered small when the post-quench energy density is small compared to the natural scale m^2 where m is the mass gap in the post-quench system. In this case the density of particles created after a quench is small and the average distance d between particles is much larger than the correlation length m^{-1}. Since the interactions are suppressed by the distance d as $e^{-m_1 d}$, the creation of particles is dominated by pairs separated by a distance larger than the correlation length $\xi = m^{-1}$. One expects that the amplitude for the creation of higher number of particles is well-approximated by the product of amplitudes corresponding to independent pairs, leading to an initial state (4.2.8) having the form (4.2.6). If the quench allows production of odd number of particles, then instead the initial state is expected to have the form (4.2.7).

There exist some exceptions to this scenario, for example a quench in a ϕ^4 coupling when perturbatively the leading process is the creation of a quartet. A further limitation of the above scenario is that for more than one species of particles even the smallness of the quench is insufficient to guarantee the integrability of the quench as demonstrated in [164]. However, for models with one particle species, and in particular for the sine-Gordon model in its repulsive regime where the spectrum consists of only solitons and anti-solitons our argument can be safely applied. Moreover, even in the case of more than one particle species, for states composed exclusively of a single particle species the factorization of overlaps into products of pair amplitudes is expected to hold.

4.3 Overlaps in finite volume

Here we review the formulation of squeezed coherent states in finite volume, as this is needed to regulate divergences related to disconnected contributions and is used later in Section 8. This formalism was

developed in [165] for integrable boundary states. Whereas here we focus only on the case of integrable initial states, it is easy to write down the finite volume counterpart of any initial state as long as they are translationally invariant.

The integrable initial state (4.2.7) can be written in finite volume as

$$|\Omega\rangle_L = \mathcal{N}(L)\Big(|0\rangle_L + \frac{g}{2}\sqrt{mL}|\{0\}\rangle_L + \sum_{I>0} K(\vartheta)N_2(\vartheta,L)|\{-I,I\}\rangle_L$$
$$+ \sum_I \frac{g}{2}K(\vartheta)N_3(\vartheta,L)|\{-I,I,0\}\rangle_L + \frac{1}{2}\sum_{I\neq J} K(\vartheta_1)K_j(\vartheta_2)N_4(\vartheta_1,\vartheta_2,L)|\{-I,I,-J,J,0\}\rangle_L\Big) + \dots , \quad (4.3.1)$$

where the rapidities ϑ are the solutions of the appropriate Bethe–Yang equations with a constraint of zero overall momentum. For the two-particle states the constrained Bethe-Yang equation is

$$\bar{Q}_2(\vartheta) = mL\sinh\vartheta + \delta(2\vartheta) = 2\pi I \ , \quad (4.3.2)$$

with $\delta(\varphi)$ defined in (3.3.2), and the sum in (4.3.1) only runs over $I > 0$ because the states $|-I,I\rangle_L$ and $|-I,I\rangle_L$ are identical. As $\delta(\vartheta)$ is defined as $S(\vartheta) = e^{-i\delta(\vartheta)}$, he allowed values for I are the positive half-integers. The three-particle sector consists of states with rapidities $\{-\vartheta, 0, \vartheta\}$ where ϑ is determined by the corresponding quantisation condition

$$\bar{Q}_3(\vartheta) = mL\sinh\vartheta + \delta(\vartheta) + \delta(2\vartheta) = 2\pi J \ , \quad (4.3.3)$$

where J can be an arbitrary positive integer and for the four-particle case the quantisation condition for the rapidities $\{-\vartheta_1, \vartheta_1, -\vartheta_2, \vartheta_2\}$ is given by the system of equations

$$\bar{Q}_{4,1} = mL\sinh\vartheta_1 + \delta(\vartheta_1-\vartheta_2) + \delta(\vartheta_1+\vartheta_2) + \delta(2\vartheta_1) = 2\pi I_1 \ ,$$
$$\bar{Q}_{4,2} = mL\sinh\vartheta_2 + \delta(\vartheta_2-\vartheta_1) + \delta(\vartheta_1+\vartheta_2) + \delta(2\vartheta_2) = 2\pi I_2 \ ,$$

with I_1 and I_2 being half-integers. The normalisation factors $N_1(L)$, $N_2(\theta,L)$, $N_3(\vartheta,L)$ and $N_4(\vartheta_1,\vartheta_2,L)$ in (4.3.1) were calculated in [165] up to finite size effects with exponential decay. For the one and two-particle states one finds

$$N_1(L) = \sqrt{mL} + \mathcal{O}(e^{-\mu L}) \ , \qquad N_2(\vartheta,L) = \frac{\sqrt{\rho_2(\vartheta,-\vartheta)}}{\bar{\rho}_2(\vartheta)} + \mathcal{O}(e^{-\mu L}) \ , \quad (4.3.4)$$

where

$$\bar{\rho}_2(\vartheta) = \frac{d\bar{Q}_2}{d\vartheta} = mL\cosh\vartheta + 2\varphi(2\vartheta)$$

can be interpreted as a constrained density of state. Note that the total two-particle density ρ_2 satisfies

$$\rho_2(\vartheta,-\vartheta) = \rho_1(\vartheta)\bar{\rho}_2(\vartheta) \ ,$$

and so

$$N_2(\vartheta,L) = \sqrt{\frac{\rho_1(\vartheta)}{\bar{\rho}_2(\vartheta)}} = 1 - \frac{\varphi(2\vartheta)}{mL\cosh\vartheta} + \mathcal{O}(1/L^2) \ . \quad (4.3.5)$$

For the three-particle state the normalisation of the three-particle states is given by

$$N_3(\vartheta,L) = \frac{\sqrt{\rho_3(\vartheta,0,-\vartheta)}}{\bar{\rho}_3(\vartheta)} \ ,$$

where

$$\bar{\rho}_3(\vartheta) = \frac{d\bar{Q}_3}{d\vartheta} \ , \tag{4.3.6}$$

and in the four-particle case the normalisation reads

$$N_4(\vartheta_1, \vartheta_2, L) = \frac{\sqrt{\rho_4(\vartheta_1, -\vartheta_1, \vartheta_2, -\vartheta_2)}}{\bar{\rho}_4(\vartheta_1, \vartheta_2)} \ ,$$

with

$$\bar{\rho}_4(\vartheta_1, \vartheta_2) = \det J \qquad \text{with} \qquad J_{ik} = \frac{\partial \bar{Q}_{4,i}}{\partial \vartheta_k} \ , \qquad i, k = 1, 2 \ .$$

It is easy to continue the finite volume expansion of the integrable state (4.3.1) to higher orders, and also to write down the finite volume expression for non-integrable states, where the only constraint on the contributing states is the vanishing of their total momentum instead of the detailed pair structure.

4.4 Summary

In this chapter we investigated integrable quenches in massive IQFTs, which are a very important starting point in the study of quantum quenches. These quenches are defined by the condition that the initial state $|\Omega\rangle$ is annihilated by all the odd conserved charges i.e. $Q_s^o|\Omega\rangle = 0$. We showed that if the initial state satisfies the cluster decomposition principle then this operator condition implies that the integrable initial state in a generic integrable model can be written in a squeezed-coherent form (4.2.6), (4.2.7) resembling integrable boundary states that are relevant in the context of boundary field theory.

Integrable quenches are important since they include all cases in which it is possible to find exact analytic results for the steady state expectation values and/or the time evolution of observables. On the other hand, a given quench protocol is not guaranteed to yield an integrable initial state even if both the pre- and post-quench Hamiltonians are integrable. However, we argued that in massive IQFTs with one particle species or in the attractive regime of the sine-Gordon model, for quenches with sufficiently low energy density the integrable structure of the quench holds to a good accuracy and thus the integrable quench assumption can apply in various situations. Interestingly, in the small quench limit, the integrable structure of the initial state is ensured in any massive QFTs with one particle species.

Although we have not discussed the problem of determining the overlaps after a particular quantum quench, clearly, if the integrable structure of the quench is known, the problem reduces to determining the pair overlaps only. As demonstrated in Chapters 6 and 7 in many cases, the pair overlaps can be calculated or at least approximated efficiently, whereas determination of overlaps in general remains a difficult and unsolved problem.

Chapter 5

Quenches with one-particle coupling and singular overlaps

In this chapter we consider quantum quenches with initial states containing odd number of particles. Such a situation can naturally emerge when the quench breaks particle number parity as discussed in Section 5.3 via a particular example. Focusing on translation invariant initial states, we demonstrate that if there is a one-particle zero-momentum term in the expansion of the initial state, then the pair amplitude possesses a first order pole at the origin. The presence of the pole has important consequences for the time evolution (c.f. Chapter 8) of one- or multipoint functions with Eq. (2.1.1) and failing to realize its presence led to some incorrect results in previous literature.

For integrable squeezed-coherent states (4.2.7) the coupling of the one-particle term g is related to the pole strength of the K-function:

$$K(\vartheta) \sim -\frac{i}{2}\frac{g^2}{\vartheta} \ . \tag{5.0.1}$$

This relation is also valid for non-integrable states, as long as the one particle term is present and its coefficient is $g/2$ like in the integrable case:

$$\mathcal{N}\left(|0\rangle + \frac{g}{2}|\{0\}\rangle + \frac{1}{2}\int \frac{d\vartheta}{2\pi} K(\vartheta)|-\vartheta,\vartheta\rangle + ...\right), \tag{5.0.2}$$

since that up to the two-particle term, the expansions of the integrable and non-integrable initial states are the same due to momentum conservation. Here we demonstrate the validity of our statement regarding the singularity of overlaps and support our claim by a more rigorous argument using a linked-cluster expansion for time dependent one-point functions in Chapter 8. For simplicity we focus on models with one particle species but the argument carries over to systems with several particle species.

First we present the general argument based on an analogy with the one-point functions of bulk operators in the presence of boundaries discussed in [165]. The core of the argument is based on the cancellation of divergent terms in the expectation value which is evaluated using finite volume as a regulator. At first, this analogy only supports our statement for the integrable quench case, but as shown in Section 8.2 it can also be extended to non-integrable with one-particle coupling. We then proceed to a concrete example of a quench in the Ising field theory crossing the phase boundary, i.e. from the ferromagnetic to the paramagnetic phase, and also discuss an interesting quench in the sine–Gordon model, for which the one-particle coupling and the singular part of the K function can be calculated to lowest order in the quench parameter and the presence of the singularity in K and the relation of its residue to g can be verified explicitly. As discussed in Section 8.2 many important features of the sine-Gordon calculation turn out to be general, and so the perturbative argument for the presence of the overlap singularity can be extended to the non-integrable case as well.

5.1 Analogy between integrable quenches and integrable boundaries

In the following we briefly review the boundary problem discussed in [165]. We consider an integrable field theory with a single massive particle constrained on a finite line $x \in [0, \mathcal{R}]$ with integrable boundary conditions α and β at the two ends; for simplicity we focus on the case when the left/right boundary conditions are identical i.e. $\alpha = \beta = B$. The vacuum expectation value

$$\langle \mathcal{O}(x) \rangle^B \tag{5.1.1}$$

taken with respect to the ground state of the finite volume Hamiltonian $H^B_{\mathcal{R}}$ can be rewritten using an Euclidean rotation

$$\langle \mathcal{O}(x) \rangle^B = \frac{\langle B|\ e^{-Hx}\mathcal{O}(0)\ e^{-H(\mathcal{R}-x)}\ |B\rangle}{\langle B|e^{-H\mathcal{R}}|B\rangle}\ , \tag{5.1.2}$$

where the coordinate x plays the role of the Euclidean time variable, H is the infinite volume Hamiltonian in the crossed channel and $|B\rangle$ is the boundary state corresponding to the boundary condition B. As discussed at the end of Section 4.1, in the case when the boundary state contains zero-momentum particles associated with a non-zero coupling of a single particle state to the boundary in the original channel, the boundary K-function has a pole in the expansion of $|B\rangle$ (4.1.11):

$$K_B(\vartheta) \sim -\frac{i}{2}\frac{g_B^2}{\vartheta}\ . \tag{5.1.3}$$

The proper relation (5.1.3) between the residue of K and the boundary one-particle coupling [156–158] is crucial for the consistency of a number of theoretical constructs, such as the boundary form factor bootstrap considered in [166].

In particular following [165] consider the one-point function of a bulk operator $\mathcal{O}$ by putting the theory in a finite volume L in the crossed channel (with periodic boundary conditions) and take the limit

$$\langle \mathcal{O}(x) \rangle^B = \lim_{L\to\infty} \langle \mathcal{O}(x) \rangle^B_L = \lim_{L\to\infty} \frac{\langle B_L|\ e^{-H_L x}\mathcal{O}(0)\ e^{-H_L(\mathcal{R}-x)}\ |B_L\rangle}{\langle B_L|e^{-H_L\mathcal{R}}|B_L\rangle}\ , \tag{5.1.4}$$

where H_L is the finite volume Hamiltonian with periodic boundary conditions and $|B_L\rangle$ represents the boundary state in finite volume. The finite volume is introduced here as a regulator for disconnected contributions arising from the matrix elements of the operator $\mathcal{O}$ which appear once $|B_L\rangle$ is expanded in terms of the corresponding finite volume multi-particle eigenstates of H_L. The disconnected terms lead to positive powers of the dimensionless volume variable mL which only cancel if the singularity of K_B is exactly given by the expression (5.1.3). Therefore the singularity of K_B and the relation of its residue to the one-particle coupling are consistency criteria for the existence of well-defined one-point functions in the infinite volume limit.

The time evolution of the expectation value of a local operator $\mathcal{O}$ after a quantum quench with initial state (4.2.7) and post-quench Hamiltonian H is given by the expression

$$\langle \mathcal{O}(t) \rangle = \frac{\langle \Omega|\ e^{itH}\mathcal{O}(0)\ e^{-itH}|\Omega\rangle}{\langle \Omega|\Omega\rangle}\ ,$$

which is just a real time analogue of the boundary expectation value. The only difference is that the K function appearing in $|\Omega\rangle$ is not related to any reflection factor; in fact, Ghoshal–Zamolodchikov boundary states are not normalisable, while for quench initial states the factor $\mathcal{N}$ is chosen to ensure $\langle\Omega|\Omega\rangle = 1$. However, it is clear from the calculations performed in [165] that the condition for the cancellation of singularities is unaffected by these details, therefore in order to have a well-defined expectation value $\langle \mathcal{O}(t) \rangle$ after an integrable quench with one-particle coupling $g/2$, the K function must have a first order pole at the origin with a residue equal to $-ig^2/2$.

In the following two subsections we discuss two examples where this relation can be verified explicitly, while in Chapter 8 we consider the real time evolution and show directly that this condition must indeed hold for consistency.

5.2 Quench in the Ising field theory from the ferromagnetic to the paramagnetic phase

Quenches in the Ising quantum spin chain were discussed in [94–96] and for particular quenches within the ferromagnetic phase, calculations also in the continuum model [107] were performed and numerically checked [167]. Although for the $FM \to PM$ quench such calculations in the QFT were not carried out, the scaling limit of the analogous quantities in the lattice model make perfect sense.

Let us recall the relevant features of this model which were already introduced in Section 3.4.3. The lattice Hamiltonian is

$$H = -J\sum_{i=1}^{N}\left(\sigma_i^x\sigma_{i+1}^x + h\sigma_i^z\right) \,, \tag{5.2.1}$$

where σ_i^α denotes the Pauli matrices at site i, $J > 0$, h is the transverse field and the boundary conditions are assumed to be periodic. By applying the Jordan–Wigner transformation, the Hamiltonian (5.2.1) can be mapped to spinless Majorana fermions with dispersion relation [152, 153]

$$\varepsilon_h(k) = 2J\sqrt{1 + h^2 - 2h\cos k} \,, \tag{5.2.2}$$

and with an energy gap $\Delta = 2J|1-h|$. The model possesses a quantum critical point at $h = 1$ separating the paramagnetic or disordered phase for $h > 1$ and the ferromagnetic, ordered phase for $h < 1$. In the disordered phase, the expectation value of σ_i^x, i.e. that of the magnetisation operator vanishes, while in the ferromagnetic phase its value is non-zero. The Hilbert space of the model consists of two sectors with respect to fermion number parity. In the Neveu–Schwarz and Ramond sectors states with even and odd number of fermions are present, respectively, resulting in the quantisation condition for the wave numbers

$$\begin{aligned} k_n =& \frac{2\pi}{N}\left(n + \frac{1}{2}\right) \quad \text{Neveu–Schwarz} \\ p_n =& \frac{2\pi}{N} n \qquad\qquad\quad \text{Ramond} \,, \end{aligned} \tag{5.2.3}$$

where n is a positive integer.

Performing a quench in the transverse field h, the pre- and post-quench excitations can be related via a Bogoliubov transformation. As a consequence, if the initial state is the ground state of the pre-quench Hamiltonian the squeezed-coherent form of the initial state in the post quench basis (4.2.6) (or as will turn out, eventually (4.2.7)) is guaranteed. Focusing on the quench from the ground state of the FM phase to the PM phase ($h_0 \to h$ with $h_0 < 1$ and $h > 1$) one can write [94–96]

$$\begin{aligned} \frac{|0,h_0\rangle_{NS}^{FM} \pm |0,h_0\rangle_{R}^{FM}}{\sqrt{2}} =& \frac{1}{\sqrt{2}N_{NS}} \exp\left(i\sum_{k\in NS} K(k)a_{-k}^\dagger a_k^\dagger\right)|0,h\rangle_{NS}^{PM} \\ & \pm \frac{1}{\sqrt{2}N_R} \exp\left(i\sum_{p\in R\setminus\{0\}} K(p)a_{-p}^\dagger a_p^\dagger\right) a_0^\dagger |0,h\rangle_R^{PM}, \end{aligned} \tag{5.2.4}$$

where N_{NS} and N_R are normalisation constants and

$$|K(k)|^2 = \frac{1-\cos\Delta_k}{1+\cos\Delta_k} \,, \tag{5.2.5}$$

with

$$\cos\Delta_k = (2J)^2 \frac{h_0 h - (h+h_0)\cos k + 1}{\varepsilon_h(k)\varepsilon_{h_0}(k)} \ . \tag{5.2.6}$$

For later use we also quote the late time evolution of the magnetisation operator, which is given by the expression [95]:

$$|\langle\sigma_i^x(t)\rangle| = (\mathcal{C}_{FP}^x)^{\frac{1}{2}} \left[1+\cos\left(2\varepsilon_h(k_0)t+\alpha\right)+...\right]^{\frac{1}{2}} \exp\left[t\int_0^\pi \frac{dk}{\pi}\varepsilon_h'(k)\ln|\cos\Delta_k|\right] \ , \tag{5.2.7}$$

where k_0 is a solution of the equation $\cos\Delta_k = 0$, $\alpha(h,h_0)$ is an unknown constant and

$$\mathcal{C}_{FP}^x = \left[\frac{h\sqrt{1-h_0^2}}{h+h_0}\right]^{\frac{1}{2}} \ . \tag{5.2.8}$$

In the scaling limit of the TQIM, J is sent to infinity together with $h \to 1$ such that the gap associated with the fermion mass remains finite

$$M = 2J|1-h| \ . \tag{5.2.9}$$

In addition, the lattice spacing is sent to zero as $a = \frac{c}{2J}$, where c is the speed of light that we set to 1. It is easy to see that the dispersion relation (3.4.32) under scaling limit transforms as

$$\varepsilon_h(ka) \to E(p) = \sqrt{M^2+p^2} \ , \tag{5.2.10}$$

and the Hamiltonian (3.4.31) scales to the Hamiltonian of a massive Majorana fermion field theory (3.4.40).

In the following we perform the continuum limit for quantities relevant for the $FM \to PM$ quench. It is important to note, however, that unlike for quenches within the ferromagnetic phase, where explicit calculations in the field theory framework [107] and numerical studies [167] were carried out, for the $FM \to PM$ quench no results are available. However, the naive scaling limit of the lattice results makes perfect sense and therefore it is expected to reproduce the quench dynamics in the continuum field theory. In the scaling limit we can write

$$\begin{aligned} h = 1+\delta h \ , \quad h_0 = 1 - \frac{M_0}{M}\delta h \ , \\ J = \frac{M}{2\delta h} \ , \quad a = \frac{\delta h}{M} \ , \end{aligned} \tag{5.2.11}$$

which ensures that the dispersion relation in the post- and pre-quench model is $\sqrt{M^2+p^2}$ and $\sqrt{M_0^2+p^2}$ respectively. Upon the substitution $k = pa$, the continuum limit of 41 and (5.2.6) are

$$|K(p)|^2 = \frac{\sqrt{p^2+M^2}\sqrt{p^2+M_0^2} - p^2 + MM_0}{\sqrt{p^2+M^2}\sqrt{p^2+M_0^2} + p^2 - MM_0} \, , \tag{5.2.12}$$

and

$$\cos\Delta(p) = \frac{p^2 - MM_0}{\sqrt{p^2+M^2}\sqrt{p^2+M_0^2}} \ . \tag{5.2.13}$$

Introducing $\bar\sigma = \bar s M_0^{\frac{1}{8}}$, which is just the pre-quench spontaneous magnetisation in the continuum theory obtained from (3.4.33), the scaling limit of (5.2.7) reads

$$|\langle\sigma(t)\rangle| = \bar\sigma \frac{1}{2^{1/4}} \left[1+\cos\left(2\sqrt{M^2+MM_0}t+\alpha\right)+...\right]^{\frac{1}{2}} \exp\left[-M\, t\zeta\right] \ , \tag{5.2.14}$$

where

$$-M\,\zeta = \frac{1}{\pi}\left\{\frac{1}{2}\sqrt{M^2-M_0^2}\ln\left(\frac{M+\sqrt{M^2-M_0^2}}{M-\sqrt{M^2-M_0^2}}\right) - \sqrt{M^2+M\,M_0}\ln\left(\frac{\sqrt{M^2+M\,M_0}+M}{\sqrt{M^2+M\,M_0}-M}\right)\right\} \tag{5.2.15}$$

for $M > M_0$ and

$$-M\,\zeta = \frac{1}{\pi}\left\{\sqrt{M_0^2-M^2}\left(\tan^{-1}\left(\frac{M}{\sqrt{M_0^2-M^2}}\right)-\frac{\pi}{2}\right) - \sqrt{M^2+M\,M_0}\ln\left(\frac{\sqrt{M^2+M\,M_0}+M}{\sqrt{M^2+M\,M_0}-M}\right)\right\} \tag{5.2.16}$$

for $M < M_0$. Note that ζ has a finite limit $-\ln 2$ when $M_0 = 0$, but its derivative is infinite at the origin as $M_0 \to 0$, hence ζ is not an analytic expression for small values of M_0.

From (5.2.12) it is easily to see that this function has a $1/p^2$ singularity at the origin with the coefficient

$$\frac{4M_0^2M^2}{(M+M_0)^2}\,.$$

This singularity corresponds to the presence of a zero-momentum particle in the Ramond contribution to the initial state (5.2.4). As $p = M\sinh\vartheta$, the coefficient of the singularity of $|K(p)|^2$ equals $\frac{g^4}{4}M^2$, therefore $K(\vartheta)$ can be written in the form (5.0.1) with

$$g = 2\sqrt{\frac{M_0}{M+M_0}}\,. \tag{5.2.17}$$

Now we show that the one-particle coupling expressed with M and M_0 in (5.2.4) equals g. To calculate the latter, we put the theory into finite volume, where the first terms of the finite volume expansion of the integrable initial state (4.3.1) reads

$$|\Omega\rangle_L = \mathcal{N}(L)\left(|0\rangle_L + \frac{g}{2}\sqrt{ML}|\{0\}\rangle_L + \sum_I K(\vartheta)N_2(\vartheta,L)|\{-I,I\}\rangle_L. + ...\right)\,, \tag{5.2.18}$$

where the I denote quantum numbers labelling the finite volume states and N_2 can be found in (4.3.4). Then from (5.2.4)

$$\sqrt{ML}\frac{g}{2} = \frac{N_{NS}}{N_R}\,, \tag{5.2.19}$$

must hold. It is convenient to calculate the logarithm of their ratio:

$$\ln\frac{N_{NS}^2}{N_R^2} = \ln\prod_{n\subset\mathbb{N}^+}\frac{1+\left|K\left(\frac{2\pi}{L}(n-1/2)\right)\right|^2}{1+\left|K\left(\frac{2\pi}{L}(n)\right)\right|^2}\,, \tag{5.2.20}$$

which in Appendix A is shown to be equal to

$$\ln\frac{MM_0L}{(M+M_0)}$$

when $L\to\infty$, so (5.2.19) indeed holds.

5.3 Phase quenches in the sine–Gordon model

Consider the sine–Gordon model defined by the action

$$\mathcal{A} = \int d^2x \left(\frac{1}{2} \partial_\mu \Phi \partial^\mu \Phi + \frac{\mu^2}{\beta^2} \cos \beta \Phi \right) , \tag{5.3.1}$$

in a finite volume L with quasi-periodic boundary conditions

$$\Phi(t, x + L) = \Phi(t, x) + \frac{2\pi}{\beta} n \quad n \in \mathbb{Z} .$$

The quench protocol consists of abruptly shifting the sine–Gordon field $\Phi \to \Phi + \delta/\beta$ at $t = 0$, i.e. changing the phase of the cosine potential and regarding the pre-quench vacuum as initial state for the post-quench evolution. The peculiarity of this protocol is that it is possible to relate the pre- and post-quench ground states by a unitary transformation.

To obtain the relation between the pre-quench and post-quench ground states, consider the definition of the sine–Gordon model as the perturbation of the compactified free massless bosonic conformal field theory (c.f. Section 3.4.2) in finite volume with the Hamiltonian

$$\begin{aligned} H(\Phi) &= \int dx \frac{1}{2} : (\partial_t \Phi)^2 + (\partial_x \Phi)^2 : - \frac{\lambda}{2} \int dx \, (V_1 + V_{-1}) \\ V_a &=: e^{ia\beta\Phi} : , \end{aligned} \tag{5.3.2}$$

where the V_a are the vertex operators (normal ordered exponentials of the boson field). Note that the free bosonic part of (5.3.2) commutes with the zero mode of the conjugate momentum field $\Pi_0 = \partial_t \Phi$, whereas due to the canonical commutation relations

$$[\Phi(x, t), \Pi(y, t)] = i\delta(x - y) ,$$

one finds that the zero-mode

$$\Pi_0 = \int dy \Pi(y, t)$$

of the canonical momentum field satisfies

$$\exp\left(i \frac{\delta}{\beta} \Pi_0 \right) \, : e^{ia\beta\Phi} : = : e^{ia(\beta\Phi + \delta)} : \, \exp\left(i \frac{\delta}{\beta} \Pi_0 \right) . \tag{5.3.3}$$

Hence for the ground state $H(\Phi)|0\rangle_\Phi = E_0 |0\rangle_\Phi$, we have

$$\begin{aligned} \exp\left(i \frac{\delta}{\beta} \Pi_0 \right) H(\Phi) |0\rangle_\Phi &= E_0 \exp\left(i \frac{\delta}{\beta} \Pi_0 \right) |0\rangle_\Phi , \\ H(\Phi + \delta/\beta) \exp\left(i \frac{\delta}{\beta} \pi_0 \right) |0\rangle_\Phi &= E_0 \exp\left(i \frac{\delta}{\beta} \pi_0 \right) |0\rangle_\Phi , \end{aligned} \tag{5.3.4}$$

from which

$$\exp\left(i \frac{\delta}{\beta} \Pi_0 \right) |0\rangle_\Phi = |0\rangle_{\Phi + \frac{\delta}{\beta}} . \tag{5.3.5}$$

Therefore the initial state in the finite volume theory with PBC reads

$$|\Omega\rangle_L = \exp\left(i \frac{\delta}{\beta} \Pi_0 \right) |0\rangle_L , \tag{5.3.6}$$

The overlaps

$$ {}_L\langle\chi|\exp\left(i\frac{\delta}{\beta}\Pi_0\right)|0\rangle_L \tag{5.3.7}$$

can be expanded in terms of finite volume form factors using

$$\Pi_0=\int_0^L\partial_t\Phi(x)dx=i\int_0^L[H,\Phi(x)]dx\ .$$

This allows one to derive a form factor expansion for the overlaps with an arbitrary state $|\chi\rangle$

$$ {}_L\langle\chi|\Omega\rangle_L={}_L\langle\chi|\exp\left(i\frac{\delta}{\beta}\Pi_0\right)|0\rangle_L\,, \tag{5.3.8}$$

by expanding the exponential into power series,

$$\begin{aligned} {}_L\langle\chi|\Omega\rangle_L=\sum_{l=0}^{\infty}\frac{(-1)^l}{l!}\left(\frac{\delta}{\beta}\right)^l\sum_{\alpha_1}\dots\sum_{\alpha_{l-1}}\int\left(\prod_i dx_i\right){}_L\langle\chi|e^{i\hat{P}x_1}\Phi(0)e^{-i\hat{P}x_1}|\alpha_1\rangle_L(E_\chi-E_{\alpha_1})\times\\ {}_L\langle\alpha_1|e^{i\hat{P}x_2}\Phi(0)e^{-i\hat{P}x_2}|\alpha_2\rangle_L(E_{\alpha_1}-E_{\alpha_2})\dots{}_L\langle\alpha_{l-1}|e^{i\hat{P}x_l}\Phi(0)e^{-i\hat{P}x_l}|0\rangle_L(E_{\alpha_{l-1}}-E_0), \end{aligned} \tag{5.3.9}$$

where $\hat{P}$ is the momentum operator and the α_i index $l-1$ complete sets of asymptotic multi-particle eigenstates. As the initial state is the ground state of a translational invariant Hamiltonian, the overlaps are non-zero only for states $|\chi\rangle$ of total spatial momentum zero. Due to the integrals over x_i, this also restricts the intermediate states $|\alpha_i\rangle_L$ to have zero total momentum so we can write

$$ {}_L\langle\chi|\Omega\rangle_L=\sum_{l=0}^{\infty}(-1)^l\left(\frac{\delta}{\beta}\right)^l\frac{L^l}{l!}\tilde{\sum_{\alpha_1}}\dots\tilde{\sum_{\alpha_{l-1}}}{}_L\langle\chi|\Phi(0)|\alpha_1\rangle_L(E_\chi-E_{\alpha_1})\times \tag{5.3.10}$$

$$ {}_L\langle\alpha_1|\Phi(0)|\alpha_2\rangle_L(E_{\alpha_1}-E_{\alpha_2})\dots{}_L\langle\alpha_{l-1}|\Phi(0)|0\rangle_L(E_{\alpha_{l-1}}-E_0)\ , \tag{5.3.11}$$

where the tildes over the sums mean that only zero momentum states are included.

We now compute the overlap with a stationary first breather to first order in δ/β. Matching the finite volume expression of the initial state (5.3.6) with the general case (5.2.18), and using (4.3.4) and the finite volume form factors (3.3.4), we obtain

$$\begin{aligned} \sqrt{m_1L}\,\frac{g}{2}=&{}_L\langle\{0\}|\Omega\rangle_L\\ =&-m_1L\frac{\delta}{\beta}{}_L\langle\{0\}|\Phi(0)|0\rangle_L\\ =&-\left(\frac{\delta}{\beta}\right)m_1L\frac{F^*_{B_1}}{\sqrt{m_1L}}\ , \end{aligned} \tag{5.3.12}$$

from which

$$\frac{g}{2}=-\frac{\delta}{\beta}F^*_{B_1}\ , \tag{5.3.13}$$

where F_{B_1} is the infinite volume one-breather form factor of Φ ((B.0.6)).

Since the form factors of Φ with even number of breathers B_1 vanishes, the lowest non-trivial order for the pair amplitude K is $(\delta/\beta)^2$:

$$\begin{aligned} N_2(\vartheta,L)K(\vartheta)=&{}_L\langle\{I,-I\}|\Omega\rangle_L\\ =&\left(\frac{\delta}{\beta}\right)^2\frac{L^2}{2}\tilde{\sum_{\alpha_1}}{}_L\langle\{I,-I\}|\Phi(0)|\alpha_1\rangle_L(2m_1\cosh\vartheta-E_{\alpha_1}){}_L\langle\alpha_1|\Phi(0)|0\rangle_L E_{\alpha_1}\ , \end{aligned} \tag{5.3.14}$$

where ϑ is related to the quantum number I via the Bethe quantisation condition (4.3.2) $N_2(\vartheta, L)$ is a finite volume normalisation factor (4.3.4) $\delta_{B_1B_1}$ and its derivative $\varphi_{B_1B_1}(\vartheta)$ is defined by $S_{B_1B_1}(\vartheta) = -e^{i\delta_{B_1B_1}(\vartheta)}$, and $\theta_1, ..., \theta_n$ are the particle rapidities in the state $|\alpha_1\rangle_L$ determined by finite volume quantisation relations (3.3.1). Using the expression for finite volume form factors (3.3.4) it can be written as

$$\left(\frac{\delta}{\beta}\right)^2 \frac{L^2}{2} \sum_{n=1}^{\infty} \sum_{\{\beta\}_n} \frac{F_{B_1B_1B_{i_1}...B_{i_n}}(i\pi+\vartheta, i\pi-\vartheta, \theta_1, ...\theta_n)}{\sqrt{(m_1 L\cosh\vartheta)^2 + (m_1 L\cosh\vartheta)\ \varphi_{B_1B_1}(\vartheta)\rho_n(\theta_1, ...\theta_n)}} \times \\ \left(2m_1\cosh\vartheta - \sum_{i=1}^{n} m_i\cosh\theta_i\right) F^*_{B_{i_1}...B_{i_n}}(\theta_1, ...\theta_n) \left(\sum_{i=1}^{n} m_i\cosh\theta_i\right) . \tag{5.3.15}$$

In Appendix B it is shown that in the limits $L \to \infty$ and $\vartheta \to 0$ only the $n = 1$ term survives where the single particle in the intermediate state is also a B_1, from which

$$K(\vartheta) \sim \left(\frac{\delta}{\beta}\right)^2 \frac{F_{B_1B_1B_1}(i\pi+\vartheta, i\pi-\vartheta, 0)(2\cosh\vartheta - 1)F^*_{B_1}}{2\cosh\vartheta} . \tag{5.3.16}$$

Using the form factor kinematical singularity equation (3.2.6) one can extract that for small ϑ

$$F_{B_1B_1B_1}(i\pi+\vartheta, i\pi-\vartheta, 0) \sim -\frac{4i}{\vartheta} F_{B_1} , \tag{5.3.17}$$

so

$$\begin{aligned} K(\vartheta) &\sim -2i\left(\frac{\delta}{\beta}F_{B_1}\right)^2 \frac{1}{\vartheta} + O(\vartheta^0) \\ &= -i\frac{g^2}{2}\frac{1}{\vartheta} + O(\vartheta^0) , \end{aligned} \tag{5.3.18}$$

where we used (5.3.13) which establishes the relation (4.1.12) between the one-particle coupling of the first breather and the singularity of its pair amplitude for this particular quench in the sine–Gordon model.

We remark that it is not known whether this particular quench protocol leads to an integrable initial state of the generalised squeezed form (4.2.7). Note also that the above argument straightforwardly generalises to a much larger class of quench protocols, the "exponential quenches" when the initial state is related to the post-quench ground state via

$$|\Omega\rangle_L = \exp\left(i\lambda \int dx \Psi(x)\right) |0\rangle_L , \tag{5.3.19}$$

where $\Psi(x)$ is a local field which breaks particle number parity.

5.4 Summary

In this chapter we studied (translation invariant) quantum quenches when the expansion of the initial state in the post-quench basis contains a zero momentum one-particle state contribution. Based on an analogy with the case of integrable boundary states, we argued that the zero-momentum particle implies a pole in the pair amplitude. We supported our statement with two concrete examples: a quench in the Ising field theory crossing the phase boundary which is an integrable quench, and a quench in the sine–Gordon model consisting of shifting the phase of the sine-Gordon field, which is not known to be integrable but its treatment yields a perturbative confirmation of our statement. The general argument and also the perturbative proof may seem too heuristic at this level, we return to discussing these singular overlaps in Section 8.2.

Quenches with zero momentum particles are especially interesting as oscillations in expectation values associated with the masses of the particles can be detected in experiments [13], hence suitably small

quenches can be used to determine the mass spectrum of a model in what is known as quench spectroscopy. Another peculiarity of these quenches is that they present serious theoretical challenges in the calculation of expectation values after a quench, which are discussed in Chapter 8.

Chapter 6

Quench overlaps in the sinh-Gordon model

In this chapter we discuss a particular quench protocol for which it is possible to derive integral equations that determine the quench overlaps uniquely. Even though the solution requires the use of numerical methods and some other assumptions, the validity of the assumptions can be easily checked, and based on the integral equations, general features of the overlaps can be studied as well. In particular we show that the quench overlaps decay exponentially with the rapidity variable, which is necessary for a well-defined field theory quench as discussed in Section 2.4.

Whereas the particular example we study is a quench from the ground state of the free massive boson theory with pre-quench mass m_0 to the interacting sinh-Gordon model with post-quench (renormalized) mass m and interaction strength g (see the Lagrangian and the definition of the model in Section 3.4), this method can be extended to the corresponding quench in the sine-Gordon model and affine Toda field theories as well, at least for the $A^{(1)}_{N-1}$ models where the form factors of the exponential fields are known [168]. In this chapter we first discuss this particular quench in the sinh-Gordon model, and find an operator formulation which allows to derive the integral equations involving form factors of the operator for the overlaps. Studying the Dirichlet boundary case the and solution of this system in the free case $(m_0, g = 0) \to (m, g = 0)$ offers arguments for the uniqueness and squeezed-coherent form of the initial state. Finally we discuss the numerical treatment of the problem and show that the numerical solution can be approximated by a simple analytical Ansatz [169] to a good accuracy.

6.1 The infinity hierarchy of integral equations for the initial state

6.1.1 Operator continuity condition

Considering a quench from a free field theory with a mass m_0 to sinh-Gordon theory with (renormalized) mass m and interaction coupling g, the initial state $|\Omega\rangle$ is the ground state of the pre-quench Hamiltonian which is defined through the condition that it is annihilated by the pre-quench free annihilation operators

$$A(p)|\Omega\rangle = 0 \tag{6.1.1}$$

for all momenta p. The annihilation operators $A(p)$ can be easily expressed in terms of the elementary field ϕ and the canonical conjugate field π in the free theory. A key observation for this particular quench is that these fields are continuous through the quench:

$$\phi(x, t \to 0^-) = \phi(x, t \to 0^+) \text{ and } \pi(x, t \to 0^-) = \pi(x, t \to 0^+)\,, \tag{6.1.2}$$

which is easy to see from the Heisenberg picture according to which

$$\frac{d}{dt}\mathcal{O} = i[H, \mathcal{O}]\,.$$

As at $t = 0$ there is a finite jump in the Hamiltonian, in the time derivative of $\mathcal{O}$ there may be utmost a finite jump too, hence the integrated operator with respect to time is continuous. As a consequence the annihilation operators $A(p)$ in the free field theory can be given in terms of the interacting fields ϕ and π by the standard relation

$$A(p) = \frac{1}{\sqrt{2E_0(p)}} \Big(E_0(p)\hat{\phi}(p) + i\hat{\pi}(p) \Big) \ , \tag{6.1.3}$$

where

$$\hat{\phi}(p) = \int dx\, e^{-ipx}\phi(x), \tag{6.1.4}$$

is the Fourier transform of $\phi(x)$ and

$$E_0(p) = \sqrt{p^2 + m_0^2}\,. \tag{6.1.5}$$

Moreover, from the relation $\pi = \partial_t\phi = -i[\phi, H]$ where H is the post-quench Hamiltonian, we obtain the equation

$$\left\{ \hat{\phi}(p) + \frac{1}{E_0(p)} \Big[\hat{\phi}(p), H \Big] \right\} |\Omega\rangle = 0\,, \tag{6.1.6}$$

This equation was first derived in [169] and it has the advantage that all matrix elements of the operator $\hat{\phi}$ are known in the the post-quench field theory, i.e. the Sinh-Gordon model.

Expanding the initial state on a complete set of states gives

$$|\Omega\rangle = \sum_{n=0}^{\infty} \frac{1}{n!} \int \prod_{j=1}^{n} \frac{d\beta_j}{2\pi} K_n(\beta_1, \dots, \beta_n) |\beta_1, \dots, \beta_n\rangle\,, \tag{6.1.7}$$

where $|\beta_1, \dots, \beta_n\rangle$ are the multi-particle eigenstates of the post-quench Hamiltonian. Using the commutation rules of the Zamolodchikov-Faddeev algebra (3.1.7), the functions $K_n(\beta_1, \dots, \beta_n)$ can be assumed to satisfy the symmetry relation

$$K_n(\beta_1, \dots, \beta_i, \beta_{i+1}, \dots, \beta_n) = K_n(\beta_1, \dots, \beta_{i+1}, \beta_i, \dots, \beta_n)\, S(\beta_{i+1} - \beta_i)\,. \tag{6.1.8}$$

Projecting (6.1.6) to all the linearly independent states of the post-quench Hilbert space, we can write an infinite hierarchy of integral equations for the functions K_n

$$\langle \vartheta_1, \dots, \vartheta_N | \left\{ \hat{\phi}(p) + \frac{1}{E_0(p)} \Big[\hat{\phi}(p), H \Big] \right\} |\Omega\rangle = 0\,. \tag{6.1.9}$$

We propose that this set of equations determines all the functions K_n uniquely (up to overall normalization).

Note that due to translational invariance of the global quench, the initial state $|\Omega\rangle$ is in the subspace of zero total momentum, i.e all amplitudes K_n contain a delta function $2\pi\delta\big(\sum_{j=1}^{n} m \sinh\beta_j\big)$. Therefore, nontrivial equations are only obtained for

$$p = -\sum_{j=1}^{N} m \sinh\vartheta_j\ , \tag{6.1.10}$$

i.e. when the momentum p is opposite to the total momentum of the test state. Also note that the number N of particles in the test state must be chosen odd, otherwise the equations are trivially satisfied. This can be seen easily from (6.1.9) since the operator $\hat{\phi}(p) + \big[\hat{\phi}(p), H\big]/E_0(p)$ is odd i.e. antisymmetric under the transformation $\phi \to -\phi$, while the state $|\Omega\rangle$ is even since the pre-quench Hamiltonian is symmetric under the same transformation. This means in particular that it contains only excitations with even number of particles, i.e. all odd amplitudes K_n in (6.1.7) together with the one-particle coupling must vanish.

6.1.2 Integral equations for the initial states

To derive explicit expressions for equations of the hierarchy (6.1.9) we substitute the expansion (3.2.13) for the operator $\hat{\phi}(p) + \big[\hat{\phi}(p), H\big]/E_0(p)$ and the general expansion (6.1.7) of the state $|\Omega\rangle$ into (6.1.9). Then the equation with an N particle test state is the sum of all possible contractions between the N particles of the test state with the operator $\hat{\phi}(p) + \big[\hat{\phi}(p), H\big]/E_0(p)$ and the state $|\Omega\rangle$.

From (6.1.4) and using the translation operator e^{iPx} (where P is the momentum operator) to shift the field $\phi(x)$ to the origin, we can easily find that

$$\begin{aligned}\langle\vartheta_1,\dots,\vartheta_m|\hat{\phi}(p)|\eta_1,\dots,\eta_n\rangle &= \int dx\, e^{-ipx}\langle\vartheta_1,\dots,\vartheta_m|\phi(x)|\eta_1,\dots,\eta_n\rangle \\ &= 2\pi\delta\big(p+\sum_{i=1}^{m} m\sinh\vartheta_i - \sum_{j=1}^{n} m\sinh\eta_j\big)\langle\vartheta_1,\dots,\vartheta_m|\phi(0)|\eta_1,\dots,\eta_n\rangle \end{aligned} \tag{6.1.11}$$

so that the expansion of $\hat{\phi}(p)$ is

$$\begin{aligned}\hat{\phi}(p) = \sum_{m,n=0}^{\infty}\frac{1}{m!n!}\int\prod_{i=1}^{m}\frac{d\vartheta_i}{2\pi}\int\prod_{j=1}^{n}\frac{d\eta_j}{2\pi}\,2\pi\delta\big(p+\sum_{i=1}^{m} m\sinh\vartheta_i - \sum_{j=1}^{n} m\sinh\eta_j\big) \\ \times\, f^{\phi}_{m,n}(\vartheta_1,\dots,\vartheta_m|\eta_1,\dots\eta_n)Z^{\dagger}(\vartheta_1)\dots Z^{\dagger}(\vartheta_m)Z(\eta_1)\dots Z(\eta_n)\,,\end{aligned} \tag{6.1.12}$$

with the expansion coefficients $f^{\phi}_{m,n}(\theta_1,\dots,\theta_m|\eta_1,\dots\eta_n)$ given by the form factors of the elementary Sinh-Gordon field ϕ according to (3.2.14).

Substituting

$$\langle\vartheta_1,\dots,\vartheta_N|H = \langle\vartheta_1,\dots,\vartheta_N|\left(\sum_{s=1}^{N}E(\vartheta_s)\right)\,, \tag{6.1.13}$$

and

$$H|\Omega\rangle = \sum_{n=0}^{\infty}\frac{1}{n!}\int\prod_{j=1}^{n}\frac{d\beta_j}{2\pi}\left(\sum_{k=1}^{n}E(\beta_k)\right)K_n(\beta_1,\dots,\beta_n)|\beta_1,\dots,\beta_n\rangle\,, \tag{6.1.14}$$

into (6.1.9) yields

$$\begin{aligned}\sum_{m,n,\ell=0}^{\infty}\frac{1}{m!n!\ell!}\int\prod_{i=1}^{m}\frac{d\zeta_i}{2\pi}\int\prod_{j=1}^{n}\frac{d\eta_j}{2\pi}\int\prod_{k=1}^{\ell}\frac{d\beta_k}{2\pi}\,2\pi\delta\big(p+\sum_{i=1}^{m} m\sinh\zeta_i - \sum_{j=1}^{n} m\sinh\eta_j\big) \\ \times\, f^{\phi}_{m,n}(\zeta_1,\dots,\zeta_m|\eta_1,\dots\eta_n)\left(E_0(p) - \sum_{s=1}^{N}E(\vartheta_s) + \sum_{k=1}^{\ell}E(\beta_k)\right)K_\ell(\beta_1,\dots,\beta_\ell) \\ \times\,\langle\vartheta_1,\dots,\vartheta_N|Z^{\dagger}(\zeta_1)\dots Z^{\dagger}(\zeta_m)Z(\eta_1)\dots Z(\eta_n)|\beta_1,\dots,\beta_\ell\rangle = 0\,.\end{aligned} \tag{6.1.15}$$

Using the Zamolodchikov-Faddeev algebra (3.1.7) the contractions can be performed and that the matrix element

$$\langle\vartheta_1,\dots,\vartheta_N|Z^{\dagger}(\zeta_1)\dots Z^{\dagger}(\zeta_m)Z(\eta_1)\dots Z(\eta_n)|\beta_1,\dots,\beta_\ell\rangle \tag{6.1.16}$$

is only non-zero when all η_j are contracted with some of the β_k and all ζ_i are contracted with some of the ϑ_s, while the remaining β_k are contracted with the remaining ϑ_s. This means in particular that m and n are constrained to vary between the values $0 \le m \le N$, $0 \le n \le \ell$ and must also satisfy $N-m+n-\ell = 0$. These conditions restrict the sums in the above equation. Moreover, according to earlier comments, $m+n$ must be an odd positive integer, ℓ must be even and N odd. There are $\ell!/(\ell-n)!$ ways to contract η_j and β_k, $N!/(N-m)!$ ways to contract ζ_i and θ_s and $(\ell-n)!$ ways to contract the remaining β_k and ϑ_s, which

are all equivalent up to S-matrix factors due to permutations of the rapidities. Note that S-matrix factors due to permutations of integrated rapidities can always be absorbed by re-ordering the rapidities to some fixed order using (3.2.16) and (6.1.8) and by renaming them since they are dummy integration variables. However there still remain S-matrix factors corresponding to the permutations of the test particle rapidities ϑ_s that are necessary in order to perform the contractions with the ζ_i. There are $\binom{N}{m}$ distinct choices that give terms multiplied by different S-matrix products. Overall the number of combinations of contractions that give identical contributions is

$$\frac{\ell!}{(\ell-n)!}\times\frac{N!}{(N-m)!}\times(\ell-n)!/\binom{N}{m}=m!\ell!\,. \tag{6.1.17}$$

After performing all contractions (6.1.15) becomes

$$\begin{aligned}&\sum_{\ell=0}^{\infty}\sum_{n=0}^{\ell}\frac{1}{n!}\int\prod_{k=1}^{n}\frac{d\beta_k}{2\pi}\,2\pi\delta\big(p+\sum_{s=\ell-n+1}^{N}m\sinh\vartheta_s-\sum_{k=1}^{n}m\sinh\beta_k\big)\\&\quad\times f^{\phi}_{m,n}(\vartheta_N,\dots,\vartheta_{\ell-n+1}|\beta_n,\dots,\beta_1)\left(E_0(p)-\sum_{s=\ell-n+1}^{N}E(\vartheta_s)+\sum_{k=1}^{n}E(\beta_k)\right)\\&\quad\times K_\ell(\beta_1,\dots,\beta_n,\vartheta_{\ell-n},\dots,\vartheta_1)+\text{perms}=0\,,\qquad(m=N+n-\ell)\,,\end{aligned} \tag{6.1.18}$$

where "perms" denotes the other choices of splitting the test particle rapidities ϑ_s into those contracted with ζ_i and those contracted with β_k. As the amplitudes K_ℓ contain a factor $2\pi\delta\big(\sum_{j=1}^{\ell}m\sinh\beta_j\big)$ expressing the translational invariance of $|\Omega\rangle$, the δ-function in the above equation can be replaced by $\delta\big(p+\sum_{s=1}^{N}m\sinh\vartheta_s\big)$ which can be factored out of the integral and sum. This overall factor means that the only nontrivial equations are those for which p is opposite to the total momentum of the test state (6.1.10) as was already noted. Provided that this condition is fulfilled, the final form of the N test particle equation is

$$\begin{aligned}&\sum_{\ell=0}^{\infty}\sum_{n=0}^{\ell}\frac{1}{n!}\int\prod_{k=1}^{n}\frac{d\beta_k}{2\pi}\\&\quad\times f^{\phi}_{m,n}(\vartheta_N,\dots,\vartheta_{\ell-n+1}|\beta_n,\dots,\beta_1)\left(E_0(p)-\sum_{s=\ell-n+1}^{N}E(\vartheta_s)+\sum_{k=1}^{n}E(\beta_k)\right)\\&\quad\times K_\ell(\beta_1,\dots,\beta_n,\vartheta_{\ell-n},\dots,\vartheta_1)+\text{perm.s}=0\,,\qquad(m=N+n-\ell)\,,\end{aligned} \tag{6.1.19}$$

In particular, for a single test particle, there are only two possible values of m are either 0 or 1 and so $n=\ell-1$ or $n=\ell$ respectively. Therefore the $N=1$ equation is

$$\begin{aligned}&f^{\phi}_{1,0}(\theta|)\,(E_0(p(\theta))-E(\vartheta))\\&+\sum_{\substack{\ell=2\\\text{even}}}^{\infty}\frac{1}{(\ell-1)!}\int\prod_{k=1}^{\ell-1}\frac{d\beta_k}{2\pi}\left[f^{\phi}_{0,\ell-1}(|\beta_{\ell-1},\dots,\beta_1)\left(E_0(p(\vartheta))+\sum_{k=1}^{\ell-1}E(\beta_k)\right)K_\ell(\beta_1,\dots,\beta_{\ell-1},\vartheta)\right.\\&\quad\left.+\frac{1}{\ell}\int\frac{d\beta_\ell}{2\pi}\,f^{\phi}_{1,\ell}(\vartheta|\beta_\ell,\dots,\beta_1)\left(E_0(p(\vartheta))-E(\vartheta)+\sum_{k=1}^{\ell}E(\beta_k)\right)K_\ell(\beta_1,\dots,\beta_\ell)\right]=0\,.\end{aligned} \tag{6.1.20}$$

with $p(\vartheta)=m\sinh\vartheta$ and therefore $E_0(p(\vartheta))=\sqrt{m^2\sinh^2\vartheta+m_0^2}$. For $N=1$ and $l=4$, the corresponding equations were derived in [169].

The above equations can be represented diagrammatically as in Figure 6.1.1. The terms

$$G_{m,n}(\vartheta_N,\dots,\vartheta_{\ell-n+1}|\beta_n,\dots,\beta_1) \equiv f^{\phi}_{m,n}(\vartheta_N,\dots,\vartheta_{\ell-n+1}|\beta_n,\dots,\beta_1)\left(E_0(p)-\sum_{s=\ell-n+1}^{N}E(\vartheta_s)+\sum_{k=1}^{n}E(\beta_k)\right) \tag{6.1.21}$$

in the expansion of the operator $\hat{\phi}(p)+\left[\hat{\phi}(p),H\right]/E_0(p)$ are represented as square boxes with m legs on the left and n legs on the right, which should be contracted with the N rapidities of the test state, represented as external legs on the left side of the graph, and with the ℓ rapidities of K_ℓ, represented as legs emerging from the rectangular box on the right, respectively. The remaining rapidities of K_ℓ should be contracted with the remaining rapidities of the test state. The sum is over all possible orders n,ℓ and all possible combinations of contractions. Note that in principle the ordering of rapidities in such graphs matters and that exchange of two consecutive rapidities results in multiplication with the corresponding S-matrix factor.

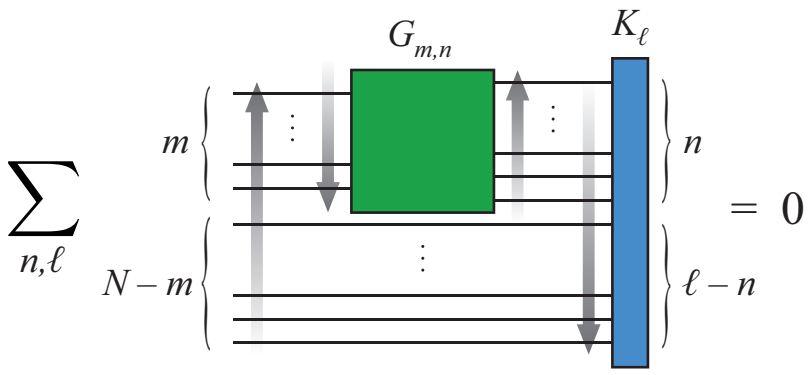

Figure 6.1.1: Diagrammatic representation of the hierarchy of integral equations (6.1.19). The external lines on the left correspond to the N rapidities of the test state $\langle\vartheta_1,\dots,\vartheta_n|$. The green square represents the (m,n)-order term in the expansion of the operator $\hat{\phi}(p)+\left[\hat{\phi}(p),H\right]/E_0(p)$, while the blue rectangle on the right represents the ℓ-order term in the expansion of the initial state $|\Omega\rangle$. The sum is over ℓ and $n\leq\ell$, while m is fixed to $N+n-\ell$. The arrows show the ordering of contracted rapidities in equation (6.1.19).

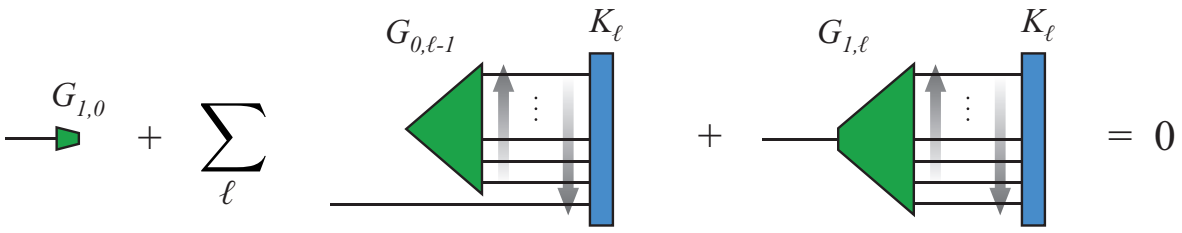

Figure 6.1.2: Diagrammatic representation of one test particle equation (6.1.20).

The above derivation was based directly on the infinite volume formulation of Integrable Field Theories through the use of the Zamolodchikov-Faddeev operators and the related operator and state expansions. In order to verify the validity of the equations from the finite volume formulation of integrable models, we present an alternative derivation of the above equations (up to a certain order) based on the Bethe-Yang equations in Appendix C.

Given the integral equations (6.1.19) and assuming uniqueness of the solution (for which we shortly argue) it is possible to determine all the overlaps in principle. Of course this is still a rather difficult problem. In fact without any further assumptions, all the overlaps K_{2n} in (6.1.7) are independent functions,

therefore finding a solution for all of them generally requires considering (6.1.19) with all possible test states. However, in the limits of $g \to 0$ and of large initial mass $m_0 \to \infty$ the solution of these equations is known. Sending the pre-quench mass to infinity, (6.1.6) transforms into

$$\hat{\phi}(p)|\Omega\rangle = 0\,, \tag{6.1.22}$$

which is identical to the condition that defines the Dirichlet boundary state for the sinh-Gordon model in (4.1.9) for which the K-function K_D (4.1.9) is known, and the squeezed state structure is guaranteed as well. Dropping all the factors in the round brackets in the above equations, the overlaps composed of the products of K_D must solve the equations, which was checked numerically as discussed in Section 6.2. However, as shown in Section 4.1, $K_D(\vartheta)$ does not decay for large momenta and the initial state is not normalizable. This is easily understood: initial state excitations are cut-off at large momenta by the mass scale m_0 which in this case is taken to be infinite. However, for finite m_0 this problem no longer persists as demonstrated in Section 6.2. The other limiting case $g = 0$ corresponding to a mass quench in the free boson theory is discussed below.

6.1.3 Free case

To argue for the statement that the hierarchy uniquely determines the initial state up to normalization, consider first the case when the interaction is zero, corresponding to the free bosonic theory with the Hamiltonian

$$H = \frac{1}{2}\int [\pi^2 + (\nabla\phi)^2 + m\phi^2]\, dx\,, \tag{6.1.23}$$

where the canonical momentum is $\pi = \partial_t\phi$. Defining annihilation operators as follows

$$A(p) = \frac{1}{\sqrt{2E(p)}}\left(E(p)\hat{\phi}(p) + i\hat{\pi}(p)\right)\,, \tag{6.1.24}$$

where $E(p) = \sqrt{m^2 + p^2}$, the canonical commutation relations are

$$[A(p), A^\dagger(p')] = 2\pi\delta(p - p')\,. \tag{6.1.25}$$

For the free case, parametrization of the modes using the momentum instead of the rapidity variable is preferred.

Consider a global quantum quench when at time $t = 0$ the mass parameter is abruptly changed in the theory $m_0 \to m$. Taking the spatial Fourier transform of the fields ϕ and π at time $t = 0$ and defining the creation and annihilation operators, the following equations must hold:

$$\begin{aligned} \frac{1}{\sqrt{2E_0(p)}}\left(A_0(p) + A_0^\dagger(-p)\right) &= \frac{1}{\sqrt{2E(p)}}\left(A(p) + A^\dagger(-p)\right) \\ \frac{-i}{2}\sqrt{2E_0(p)}\left(A_0(p) - A_0^\dagger(-p)\right) &= \frac{-i}{2}\sqrt{2E(p)}\left(A(p) - A^\dagger(-p)\right) \end{aligned}\,, \tag{6.1.26}$$

where $E_0(p) = m_0^2 + p^2$, $E(p) = m^2 + p^2$ and $A_0(p)$ and $A(p)$ are the pre- and post-quench mode operators. This is the Bogoliubov transformation, which allows one to express $|\Omega\rangle$ using $A_0(p)|\Omega\rangle = 0$. We now demonstrate that the usual squeezed expression for the initial state can also be obtained from the integral equation hierarchy.

Using (6.1.24), the operator form of the hierarchy can be written as

$$\left(\frac{1}{\sqrt{2E(p)}}(A(p) + A^\dagger(-p)) + \frac{\sqrt{2E(p)}}{2E_0(p)}(A(p) - A^\dagger(-p))\right)|\Omega\rangle = 0\,. \tag{6.1.27}$$

The fact that $A(p)$ and $A^\dagger(-p)$ occur together means that the equations only link components which differ by pairs of particles of opposite momenta. The lowest component is the post-quench vacuum, so $|\Omega\rangle$ can be expressed in terms of states composed entirely of pairs of particles with opposite momenta

$$|\Omega\rangle = \mathcal{N}\sum_{n=0}^{\infty}\left(-\frac{1}{2}\right)^n \int_{-\infty}^{+\infty}\left(\prod_{i=1}^{n}\frac{dk_i}{2\pi}A^\dagger(k_i)A^\dagger(-k_i)\right)K_{2n}^{free}(k_1\dots k_n)|0\rangle\,. \tag{6.1.28}$$

Due to Bose symmetry, the functions K_{2n}^{free} can be taken to be invariant under permutations of their arguments and under $k_i \to -k_i$.

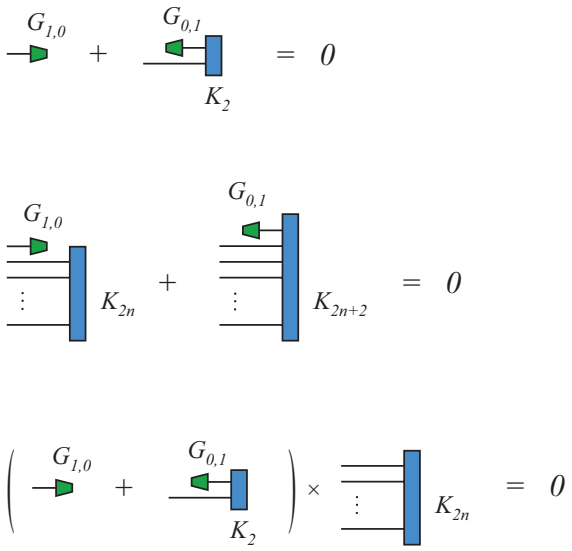

Figure 6.1.3: Diagrammatic expansion of the integral equations for a free theory. The first line represents the one-particle equation, while the second line shows the general multi-particle equation. As can be easily seen in the third line, a factorized solution $K_{2n+2} \sim K_{2n} \times K$ automatically satisfies the multi-particle equation which then reduces to the one-particle equation for the function K. The latter is therefore equal to the pair amplitude $K = K_2$. This explains the exponential form of the solution (6.1.35).

In order to find K_{2n}, Eq. (6.1.27) can be further specified by applying a given test state on the left side of Eq. (6.1.27), which gives the individual equations of the hierarchy. To find K_2, we apply a one-particle test state $\langle p_1| = \langle 0|A(p_1)$ to Eq. (6.1.27) and substitute the expansion of (6.1.28) to obtain

$$\begin{aligned}&\left(\frac{1}{E(p)}-\frac{1}{E_0(p)}\right)\langle 0|A(p_1)A^\dagger(-p)|0\rangle \\ &-\frac{1}{2}\left(\frac{1}{E(p)}+\frac{1}{E_0(p)}\right)\int_{-\infty}^{+\infty}\frac{dk}{2\pi}\langle 0|A(p_1)A(p)A^\dagger(k)A^\dagger(-k)|0\rangle K_2^{free}(k) = 0\,,\end{aligned} \tag{6.1.29}$$

where the matrix elements can be evaluated using the canonical commutation relations (or, equivalently, Wick's theorem) which leads to

$$\left(\frac{1}{E(p)}-\frac{1}{E_0(p)}\right)-\left(\frac{1}{E(p)}+\frac{1}{E_0(p)}\right)K_2^{free}(p) = 0\,, \tag{6.1.30}$$

from which

$$K_2^{free}(p) = \frac{E_0(p)-E(p)}{E_0(p)+E(p)} \tag{6.1.31}$$

follows.

To determine the functional form of $K_{2n}^{free}(k)$ for a general n, test states with higher number of particles are applied on the left side of (6.1.27); only test states with odd numbers of particles give a nonzero result. Let there be $2n-1$ particles in the test state; then only two terms from (6.1.28) give a nonzero contribution leading to

$$\left[nK_{2n}^{free}(k_1,\dots k_{n-1},p)\left(\frac{1}{E(p)}+\frac{1}{E_0(p)}\right)-K_{2(n-1)}^{free}(k_1,\dots k_{n-1})\left(\frac{1}{E(p)}-\frac{1}{E_0(p)}\right)\right]=0\,. \tag{6.1.32}$$

Therefore

$$\frac{K_{2n}^{free}(k_1,\dots k_{n-1},p)}{K_{2(n-1)}^{free}(k_1,\dots k_{n-1})}=\frac{1}{n}\frac{E_0(p)-E(p)}{E_0(p)+E(p)}\,. \tag{6.1.33}$$

Due to the symmetry properties of K_{2n}^{free}, and using (6.1.31)

$$K_{2n}^{free}(k_1,\dots k_n)=\frac{1}{n!}\prod_{i=1}^{n}K_2^{free}(k_i)\,, \tag{6.1.34}$$

that is

$$|\Omega\rangle=\mathcal{N}\exp\left[-\frac{1}{2}\int_{-\infty}^{+\infty}\frac{dk}{2\pi}K^{free}(k)A^\dagger(k)A^\dagger(-k)\right]|0\rangle \tag{6.1.35}$$

where

$$K^{free}(k)=K_2^{free}(k)=\frac{E_0(k)-E(k)}{E_0(k)+E(k)}\,. \tag{6.1.36}$$

This is exactly the squeezed state form that can also be obtained via a direct application of the Bogoliubov transformation (6.1.26) to the condition $A_0(p)|\Omega\rangle=0$.

6.1.4 Uniqueness

As shown above the hierarchy (6.1.9) has a unique solution (up to normalization) for a mass quench in a free field theory, which coincides with the well-known squeezed state resulting from the Bogoliubov transformation. We now argue that for the interacting case (Sinh-Gordon theory) we expect the same uniqueness property.

The interacting systems is much more involved than the free one since each of the equations (6.1.15) involve all of the K_l excitation amplitudes and therefore it does not have the chain-like organization of the equations of the free case, where only two terms were present for each equation, which allowed the calculation of each amplitude of arbitrary order one-by-one from its predecessors. However, since the zero-coupling limit gives back the free equation, and at least for a small enough value of the coupling the dynamics and form factors of Sinh-Gordon theory are known to be well-described by perturbation theory, the introduction of a small coupling does not spoil the uniqueness of the solution. We only expect the solution to be slightly deformed from the free solution, but to preserve most of its properties. Therefore if a given Ansatz can give a solution, or at least a very good approximation of a solution, we can argue it is close to the unique solution of the hierarchy.

We note that a remnant of the chain structure is still present in the interacting case. Denoting the number of particles in the bra state by n_L and in the ket state by n_R, for a free field theory the only nonzero matrix elements are the ones with $n_L-n_R=\pm1$. From perturbation theory, it is clear that these terms dominate for weak coupling. However, in a two-dimensional field theory this argument goes even further: as a simple consideration of available phase space shows, the Feynman graphs corresponding to form factors with larger differences in the number of incoming and outgoing particles are suppressed. The reason for this is that the difference in number of particles can be interpreted as particle creation by the operator inserted; however, in two space time dimensions the available phase space eventually decreases with increasing particle multiplicity [170], therefore processes involving a change in particle number are

suppressed; the larger the change, the stronger the suppression. As a result, we expect that the terms are hierarchically organized by the value of $\Delta n = n_L - n_R$, the ones with $\Delta n = \pm 1$ being the largest, followed by the terms with $\Delta n = \pm 3$ and so on[1]. This fact is important for our ability to treat the infinitely many integral equations, each composed of an infinite number of terms, making up the hierarchy, as it implies that they can be well-approximated by equations that are truncated to a finite number of terms, and more terms can be gradually included to improve the approximation.

6.2 Solution of the hierarchy

In this section we present a solution of the integral equations (6.1.19) for the sinh-Gordon quench problem. The solution of the hierarchy is very involved but using appropriate assumption supported with plausible physical considerations the structure of the equations simplifies and they can be solved numerically by a natural truncation of the hierarchy. The main assumption is that initial state of the quench, i.e. the ground state of the free boson theory can be cast in a squeezed-coherent form (4.2.6) (due to $\mathbb{Z}_2$ symmetry (4.2.7) is excluded) when expanded in terms of the sinh-Gordon creation operators. This means that the only unknown function is the pair overlap $K_2 = K$ and

$$K_{2n}(\vartheta_1, \beta_1, \vartheta_2, \beta_2, ...\vartheta_n, \beta_n) = \prod_{i=1}^{n} 2\pi\delta(\vartheta_i + \beta_i)K(\vartheta_i)\,, \tag{6.2.1}$$

K can be determined from the hierarchy when acting with only one test-state to right of (6.1.6). In particular, for a one-particle test state, (6.1.20) determines K and the numerical solution of the equation can be obtained by iteration. We also provide a simple analytical Ansatz that is an excellent approximation of the numerical solution in the parameter range of the quench studied and show the solution is consistent with the assumption on squeezed-coherent form of the initial state.

6.2.1 Argument for the pair structure of the initial state

As ground states of local Hamiltonians satisfy the cluster decomposition principle, the existence of pair structure together with $\mathbb{Z}_2$ symmetry implies the squeezed-coherent form (4.2.6) (c.f. Section 4.2). Here we present two arguments to support the pair structure or equivalently the integrable squeezed-coherent form of the initial state.

The first argument is based on boundary renormalization group theory. In conformal field theories there exists special boundary conditions compatible with conformal symmetry. Such boundary conditions can be formulated as boundary states, which, similarly to the Dirichlet state, are not normalizable. To regularize such states the authors of [27, 28] used the concept of "extrapolation length" and replaced the original boundary state $|B\rangle_{CFT}$ by $e^{-\tau_0 H_{CFT}}|B\rangle_{CFT}$. The parameter τ_0 expresses the difference of the actual boundary state from the idealized state, which can interpreted using RG concepts. Although massive IQFTs are off-critical theories, for quenches with finite m_0 a similar idea might apply and the initial state can be written as $e^{-\tau_0 H}|D\rangle$. In fact, the generalization $e^{-\sum_s Q_s \tau_s}|D\rangle$ is also sensible and it is eventually justified from the point of view of the previous boundary formulation: RG theory teaches us that, in estimating the difference of the actual boundary state from the idealized Dirichlet state $|D\rangle$, any boundary irrelevant operator could be inserted as a boundary perturbation [171]. In an IQFT such boundary irrelevant operators include (but are not limited to) all conserved charges of the bulk theory. Indeed adding such perturbations does not change the system's behaviour drastically [172]. This means that, in the same way that the extrapolation length τ_0 is introduced essentially as a perturbative parameter associated to the Hamiltonian, one could in principle introduce a different parameter τ_s for each conserved charge $Q_s = \int d\vartheta q_s(\vartheta) Z^\dagger(\vartheta) Z(\vartheta)$, which is equivalent to writing $K_D(\vartheta) \to K_D(\vartheta) e^{-2E(\vartheta)\tau(\vartheta)}$ in the Dirichlet state resulting $|\Omega\rangle$ satisfying (4.2.6).

[1]Note that Δn must always be odd, as even form factors of the elementary field ϕ vanish.

This argument is very heuristic and is therefore not fully satisfactory. There is, however, a stronger argument for the pair structure which can be formulated considering how switching on the integrable interaction dresses the initial state. As a starting point, any quench in the free case $g = 0$ corresponds to an initial state consisting of pairs.

Now a quench to an interacting point $g \neq 0$ can be considered perturbatively and the issue now is how the state is dressed by turning on an integrable interaction. Note that such a dressing must map the non-interacting vacuum state $|0\rangle_{free}$ to the interacting vacuum state $|0\rangle_{shG}$ and the free one-particle states to the asymptotic one-particle states of the interacting theory, which is rather nontrivial. However, there is at least one case in which we know the result of such a dressing: integrable boundary states. Considering only the parity invariant case, let us start from the free field theory with Robin boundary condition

$$\mathcal{L} = \frac{1}{2}(\partial\phi)^2 - \frac{m^2}{2}\phi^2 \qquad \partial_x\phi|_{x=0} = -\lambda\phi|_{x=0} \tag{6.2.2}$$

for which the boundary state has the form

$$|R\rangle = \mathcal{N}\exp\left[\frac{1}{2}\int_{-\infty}^{+\infty}\frac{d\vartheta}{2\pi}K_R(\vartheta)A^\dagger(\vartheta)A^\dagger(-\vartheta)\right]|0\rangle \tag{6.2.3}$$

with

$$K_R(\vartheta) = R_R\left(\frac{i\pi}{2} - \vartheta\right) = \frac{\cosh\vartheta - \lambda/m}{\cosh\vartheta + \lambda/m} \tag{6.2.4}$$

where

$$R_R(\vartheta) = \frac{\sinh\vartheta - i\lambda/m}{\sinh\vartheta + i\lambda/m} \tag{6.2.5}$$

is the Robin reflection factor. When switching to Sinh-Gordon theory (with an integrable boundary condition), this gets dressed up into [173]

$$|S\rangle = \mathcal{N}\exp\left[\frac{1}{2}\int_{-\infty}^{+\infty}\frac{d\vartheta}{2\pi}K_S(\vartheta)A^\dagger(\vartheta)A^\dagger(-\vartheta)\right]|0\rangle_{shG} \tag{6.2.6}$$

with

$$K_S(\vartheta) = -\frac{\cosh\vartheta - \cos\pi E/2}{\cosh\vartheta + \cos\pi E/2}K_D(\vartheta) \tag{6.2.7}$$

where E parametrizes the boundary interaction, and can be considered as a dressed version of λ.

We see that in the above case turning on an integrable interaction dresses the state so that the pair structure is preserved. It is plausible that a perturbative proof can be given, similar in spirit to the mechanism of how particle number changing amplitudes cancel at each order of perturbation theory in the Sinh-Gordon model [174]. We expect the pair structure of the dressed state to be the consequence of the pair structure of the starting state and the integrability of the dressing interaction, and to hold in general. In any case, by analogy we expect the initial state to have this pair structure for any quench from some mass and zero interaction to any other mass and any interaction.

Building upon the idea of integrable dressing, we can even write down an Ansatz for the solution of the sinh-Gordon quench problem considered in this chapter. As a first step, let us consider the initial state on the basis of our heuristic argument for the pair structure. We attributed the preservation of the pair structure to the fact that when switching on the coupling, the state gets dressed by an integrable interaction. In the free case, the state can be expanded as

$$|\Omega\rangle = \mathcal{N}\left\{|0\rangle_{free} - \frac{1}{2}\int_{-\infty}^{+\infty}\frac{dk}{2\pi}K^{free}(k)|k,-k\rangle_0 + \dots\right\}, \tag{6.2.8}$$

where index 0 of the two-particle state refers to $g = 0$. In the interacting case the initial state takes the form

$$|\Omega\rangle = \mathcal{N}\left\{|0\rangle_{shG} + \frac{1}{2}\int_{-\infty}^{+\infty}\frac{d\theta}{2\pi}K(\vartheta)|\vartheta,-\vartheta\rangle + \dots\right\}. \tag{6.2.9}$$

Note that the interaction gives a non-trivial renormalization of the vacuum state and also of the particles.

Motivated by the dressing argument let us look for the pair amplitude K in the form

$$K(\theta) = K^{free}(k)D(k)\,, \tag{6.2.10}$$

where k is expressed as [2] $m\sinh\vartheta$ and the dressing factor $D(k)$ only depends on the parameters of the post-quench Hamiltonian, i.e. it is independent of the pre-quench mass m_0. Now consider the limit for the pre-quench mass $m_0 \to \infty$. In this case the free amplitude tends to 1, while the amplitude K is expected to become identical to (4.1.9) for the integrable Dirichlet boundary state, which means that $D(k) = K_D(\vartheta)$. This leads to the proposal of the following solution

$$K(\vartheta) = K^{free}(k)K_D(\vartheta)\,, \tag{6.2.11}$$

which gives

$$|\Omega\rangle = \mathcal{N}\exp\left[\frac{1}{2}\int_{-\infty}^{+\infty}\frac{d\vartheta}{2\pi}K(\vartheta)Z^\dagger(\vartheta)Z^\dagger(-\vartheta)\right]|0\rangle_{shG} \tag{6.2.12}$$

for the initial state, where

$$\begin{aligned} K(\vartheta) &= \frac{E_0(p)-E(\vartheta)}{E_0(p)+E(\vartheta)}K_D(\vartheta)\,, \\ & p = m\sinh\vartheta \quad , \quad E(\vartheta) = m\cosh\vartheta \quad , \quad E_0(p) = \sqrt{p^2+m_0^2}\,. \end{aligned} \tag{6.2.13}$$

We remark that the relative sign between (6.2.8) and (6.2.9) corresponds to the property that K_D becomes -1 in the free field limit $B \to 0$.

Note that the above Ansatz, which was first proposed first in Ref. [169] on a slightly different basis, has no freely adjustable parameters.

6.2.2 Integral equation with the pair assumption and asymptotics of K

Following the arguments of the previous section we assume that the initial state has the form

$$\begin{aligned} |\Omega\rangle &= \mathcal{N}\exp\left(\frac{1}{2}\int_{-\infty}^{\infty}\frac{d\vartheta}{2\pi}\,K(\vartheta)Z^\dagger(-\vartheta)Z^\dagger(\vartheta)\right)|0\rangle_{shG} \\ &= \mathcal{N}\sum_{n=0}^{\infty}\frac{1}{n!}\prod_{j=1}^{n}\left(\frac{1}{2}\int_{-\infty}^{\infty}\frac{d\vartheta_j}{2\pi}K(\vartheta_j)\right)|-\vartheta_1,\vartheta_1,...,-\vartheta_n,\vartheta_n\rangle\,, \end{aligned} \tag{6.2.14}$$

which results in the integral equation with one text-particle (6.1.20) taking the form

$$f^\phi_{1,0}(\theta|)\left(E_0(p(\theta))-E(\vartheta)\right) \tag{6.2.15}$$

$$\begin{aligned} &+2\sum_{\ell=1}^{\infty}\frac{1}{(\ell-1)!}\int\prod_{k=1}^{\ell-1}\frac{d\beta_k}{2\pi} \\ &\times\left[f^\phi_{0,2\ell-1}(|-\vartheta,\beta_{\ell-1},-\beta_{\ell-1},\ldots,\beta_1,-\beta_1)\left(E_0(p(\vartheta))+E(\vartheta)+2\sum_{k=1}^{\ell-1}E(\beta_k)\right)K(\beta_1)\ldots K(\beta_{\ell-1})K(\vartheta)\right. \\ &\left.+\frac{1}{2\ell}\int\frac{d\beta_\ell}{2\pi}\,f^\phi_{1,2\ell}(\vartheta|\beta_\ell,-\beta_\ell,\ldots,\beta_1,-\beta_1)\left(E_0(p(\vartheta))-E(\vartheta)+2\sum_{k=1}^{\ell}E(\beta_k)\right)K(\beta_1)\ldots K(\beta_\ell)\right]=0\,, \end{aligned} \tag{6.2.16}$$

[2] The transition from integration over k to integration over θ involves a Jacobi determinant factor, but it is eventually included in the way $K_D(\vartheta)$ is given in Eq. (4.1.9).

with expansion coefficients $f^{\phi}_{m,n}(\theta_1,\dots,\theta_m|\eta_1,\dots\eta_n)$ given by the form factors of the elementary Sinh-Gordon field ϕ according to (3.2.14). As we show to obtain a numerical solution for the function K one needs to consider analytic continuation of the equations (6.2.16) to complex rapidities. These can be derived by deforming the integration contours and taking into account the residues of kinematical poles given by (3.2.6) or alternatively by the finite volume formalism briefly reviewed in Appendix C, where we also give the explicit form of the equations used in the numerical computations.

Before presenting the numerical solution of (6.2.16) it is important to mention the leading order behaviour of the solution for large rapidities. Unlike the Dirichlet case, where $\lim_{|\vartheta|\to\infty}|K_D| = 1$, for finite pre-quench mass $m_0 \neq m$, the K-function behaves as $e^{-2|\vartheta|}$, which is easy to see from (6.2.16). From the technical point of view, this fact is the consequence of the squeezed coherent structure of the initial state and the exponential decay of the sinh-Gordon form factors for large rapidities. It is also apparent, however, that the leading asymptotics of the K-function for the interacting quench is dictated by the factor

$$\frac{E_0(p(\vartheta)) - E(\vartheta)}{E_0(p(\vartheta)) + E(\vartheta)}\,, \tag{6.2.17}$$

which is exactly the K-function of in the free massive theory. This is not surprising as for large rapidities, i.e. large energies, the effects of relevant interaction become small: the form factors of the elementary field vanish exponentially, and the scattering of particles becomes energy independent.

Discussing this finding a little further leads to a simple generalization that can be potentially valid to any quench, and we come back to this point in the following chapter at the end of Section 7.2. The decay of the K-function is eventually related to the question if a quantum quench is well-defined in a field theory. As mentioned in Section 2.4, field theories considered as an effective low-energy description of a given physical system possess a high energy cut-off. A quantum quench injects extensive amount of energy and if excitations near or above the cut-off are prominent in the initial state, cut-off effects prevent us to arrive at a universal description. Unlike for Dirichlet-like initial states, where K remains finite at arbitrary large rapidities, the observed $e^{-2|\vartheta|}$ behaviour of the K-function means that the overlaps of pairs with large energy are suppressed and states with all particles having $\mathcal{O}(1)$ rapidity give the dominant contribution to the initial state. One can analyze this further by considering the root density of the representative state that corresponds to the initial state [88]. The asymptotics of the K-function determines the large rapidity behaviour of ρ to be of the form $e^{-3|\vartheta|}$. This means that although infinite energy is injected to the infinite volume system, high energy particles are suppressed as $e^{-3|\vartheta|}$ in the representative state and the effects of the UV cut-off can be safely neglected as long as the quench energy density is not too large.

6.2.3 Numerical solution of the hierarchy: keeping the vacuum and two-particle terms

Keeping the first few terms in the expansion (6.2.14) and applying a one-particle test state $\langle\vartheta|$, the integral equation (C.1.4) can be written for the Dirichlet case $m_0 = \infty$, when the operator equation (6.1.6) simplifies to $\hat{\phi}(p)|D\rangle = 0$ [169]. For the iteration procedure we need to generalize (C.1.4) to complex test rapidities. As long as $\mathrm{Im}\vartheta < \varepsilon$, (C.1.4) turns out to be valid, but for $\mathrm{Im}\vartheta > \varepsilon$, (C.1.5) has to be used. This can be derived from (C.1.4) by analytical continuation using the analytical properties of the form factors. In the case of finite mass quenches (C.1.2) holds for $\mathrm{Im}\vartheta < \varepsilon$ and (C.1.3) for $\mathrm{Im}\vartheta > \varepsilon$ [169]. The structure of the integral equation is shown in Fig 6.2.1.

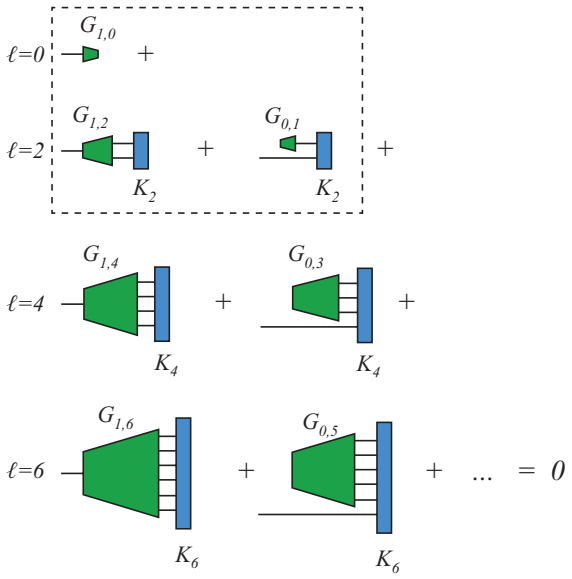

Figure 6.2.1: Diagrammatic expansion of the one test particle equation. The dashed frame encloses those diagrams in which the bra and ket states differ by only one particle. These three terms are the ones kept in the truncated equation of Section 6.2.3.

Numerical calculations immediately show that the vacuum and two-particle terms (those that are zeroth and first order in K) in Eqs. (C.1.2)-(C.1.5) are much larger than the rest, which is expected from the considerations of Subsection 6.1.4 as they correspond to $\Delta n = \pm 1$. As a consequence, it makes sense to construct an iterative method based on the truncated version of (C.1.2)-(C.1.5) that includes only the first three terms, while the rest are omitted:

$$\begin{aligned} 0 \approx & F_1^\phi + \frac{1}{2} F_1^\phi K_D(\vartheta)(1 + S(-2\vartheta)) \\ & + \frac{1}{2} \int_{-\infty+i\varepsilon}^{+\infty+i\varepsilon} \frac{d\vartheta'}{2\pi} F_3^\phi(\vartheta + i\pi, -\vartheta', \vartheta') K_D(\vartheta') \quad (\text{if Im } \vartheta < \varepsilon) \,, \end{aligned} \tag{6.2.18}$$

$$\begin{aligned} 0 \approx & F_1^\phi + F_1^\phi K_D(\vartheta) \\ & + \frac{1}{2} \int_{-\infty+i\varepsilon}^{+\infty+i\varepsilon} \frac{d\vartheta'}{2\pi} F_3^\phi(\vartheta + i\pi, -\vartheta', \vartheta') K_D(\vartheta') \quad (\text{if Im } \vartheta > \varepsilon) \,, \end{aligned} \tag{6.2.19}$$

for the Dirichlet, and

$$\begin{aligned} 0 \approx & F_1^\phi \frac{E_0(p(\vartheta)) - E(\vartheta)}{E_0(p(\vartheta)) + E(\vartheta)} + \frac{1}{2} F_1^\phi K(\vartheta)(1 + S(-2\vartheta)) \\ & + \frac{1}{2} \int_{-\infty+i\varepsilon}^{+\infty+i\varepsilon} \frac{d\vartheta'}{2\pi} \frac{E_0(p(\vartheta)) - E(\vartheta) + 2E(\vartheta')}{E_0(p(\vartheta)) + E(\vartheta)} F_3^\phi(\vartheta + i\pi, -\vartheta', \vartheta') K(\vartheta') \quad (\text{if Im } \vartheta < \varepsilon) \,, \end{aligned} \tag{6.2.20}$$

$$\begin{aligned} 0 \approx & F_1^\phi \frac{E_0(p(\vartheta)) - E(\vartheta)}{E_0(p(\vartheta)) + E(\vartheta)} + F_1^\phi K(\vartheta) \\ & + \frac{1}{2} \int_{-\infty+i\varepsilon}^{+\infty+i\varepsilon} \frac{d\vartheta'}{2\pi} \frac{E_0(p(\vartheta)) - E(\vartheta) + 2E(\vartheta')}{E_0(p(\vartheta)) + E(\vartheta)} F_3^\phi(\vartheta + i\pi, -\vartheta', \vartheta') K(\vartheta') \quad (\text{if Im } \vartheta > \varepsilon) \,, \end{aligned} \tag{6.2.21}$$

for the finite mass quench.

Discussing first the Dirichlet problem, our aim is to numerically calculate the $K_D(\vartheta)$ function for real test rapidities, however, the equations contain this function for complex rapidities $\vartheta' + i\varepsilon$ as well. Consequently, to obtain a closed iterative scheme, we also have to plug in complex test rapidities with imaginary part larger than the shift of the contour to the equations, that is, in each iteration we have to calculate two iterative functions. Instead of calculating the iterative functions at real and shifted rapidities, for practical reasons, both of them are calculated at shifted rapidities $0 < \varepsilon_1 < \varepsilon_2$. At first, $K(\vartheta + i\varepsilon_1)^{(k+1)}$ denoted by $K(\vartheta)_{\varepsilon_1}^{(k+1)}$ is calculated based on (6.2.18) as the integration contour is shifted with ε_2, and then $K(\vartheta)_{\varepsilon_2}^{(k+1)}$ is calculated based on (6.2.19) as the integration contour is now shifted with ε_1. The equations of this iterative scheme derived from (6.2.18) and (6.2.19) read

$$\begin{aligned}
K(\vartheta)_{\varepsilon_1}^{(k+1)} &= \frac{1}{2}\frac{-1}{\gamma_1}\frac{1}{1+S(-2(\vartheta+i\varepsilon_1))}\left(2+(1-\gamma_1)\left(1+S(-2(\vartheta+i\varepsilon_1))\right)K(\vartheta)_{\varepsilon_1}^{(k)}\right. \\
&\left. + \frac{1}{F_1^{\phi}}\int_{-\infty}^{+\infty}\frac{d\vartheta'}{2\pi}F_3^{\phi}(\vartheta+i(\pi+\varepsilon_1),-\vartheta'-i\varepsilon_2,\vartheta'+i\varepsilon_2)K(\vartheta')_{\varepsilon_2}^{(k)}\right)+\frac{1}{2}K(\vartheta)_{\varepsilon_1}^{(k)}\,, \\
K(\vartheta)_{\varepsilon_2}^{(k+1)} &= \frac{1}{2}\frac{-1}{\gamma_2}\left(1+(1-\gamma_2)K(\vartheta)_{\varepsilon_2}^{(k+1)}\right. \\
&\left. + \frac{1}{2F_1^{\phi}}\int_{-\infty}^{+\infty}\frac{d\vartheta'}{2\pi}F_3^{\phi}(\vartheta+i(\pi+\varepsilon_2),-\vartheta'-i\varepsilon_1,\vartheta'+i\varepsilon_1)K(\vartheta')_{\varepsilon_1}^{(k)}\right)+\frac{1}{2}K(\vartheta)_{\varepsilon_2}^{(k)}\,.
\end{aligned} \tag{6.2.22}$$

In the equations above, γ_1 and γ_2 are damping parameters, which were set to one to make the scheme do its best. In addition to this, averaging with the previous iterative function is also performed in the scheme.

Once a satisfactory level of convergence is reached, the solution along the real axis can be obtained by the following equation

$$K(\vartheta) = \frac{-1}{1+S(-2\vartheta)}\left(2+\frac{1}{F_1^{\phi}}\int_{-\infty}^{+\infty}\frac{d\vartheta'}{2\pi}F_3^{\phi}(\vartheta+i\pi,-\vartheta'-i\varepsilon_2,\vartheta'+i\varepsilon_2)K(\vartheta')_{\varepsilon_2}^{(k)}\right)\,. \tag{6.2.23}$$

The above iteration scheme will be denoted by S2D. The iterations under this scheme rapidly converge, as can be seen also in Fig.6.2.2. Besides the convergence of the functions with shifted rapidities in their arguments, the real rapidity solutions obtained with (6.2.23) converge as well. The iterative solution is always very close to the expected exact result (4.1.9) over all the fundamental range $0 \leq B \leq 1$ of the coupling strength. The small deviation between the numerical and the exact solution can be attributed to the truncation of the infinite integral equation to the vacuum and two-particle terms.

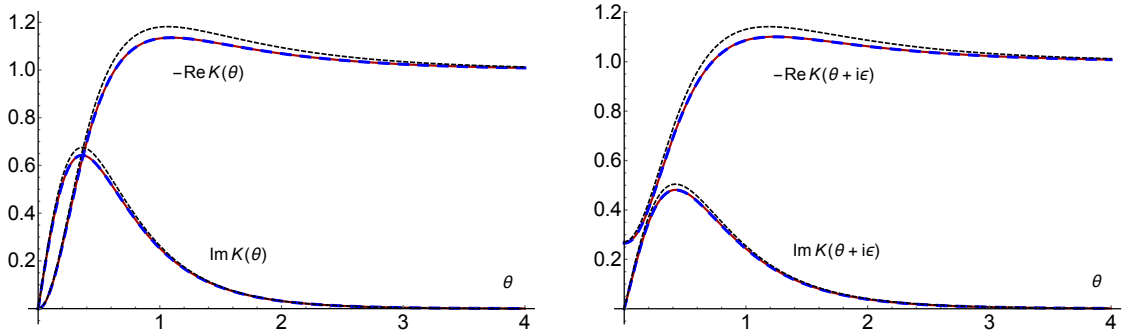

Figure 6.2.2: *6th (continuous red) and 7th (blue dashed) iterative functions for the Dirichlet problem together with the Dirichlet solution $K_D(\vartheta)$ (black dashed line) for real and shifted rapidities. $\varepsilon_1 = 0.05, \varepsilon = \varepsilon_2 = 0.1, B = 0.6$. The input of the first iteration was the Dirichlet solution (4.1.9) itself.*

For the finite mass problem using Eq. (6.2.16) involving the pair assumption as a starting point, (6.2.22) is modified as

$$\begin{aligned} K(\vartheta)_{\varepsilon_1}^{(k+1)} = \frac{1}{2}\frac{-1}{\gamma_1}\frac{1}{1+S(-2(\vartheta+i\varepsilon_1))}\Bigg(2\frac{E_0(p(\vartheta+i\varepsilon_1))-E(\vartheta+i\varepsilon_1)}{E_0(p(\vartheta+i\varepsilon_1))+E(\vartheta+i\varepsilon_1)} \\ + (1-\gamma_1)\left(1+S(-2(\vartheta+i\varepsilon_1))\right)K(\vartheta)_{\varepsilon_1}^{(k)} \\ + \frac{1}{F_1^{\phi}}\int_{-\infty}^{+\infty}\frac{d\vartheta'}{2\pi}\frac{E_0(p(\vartheta+i\varepsilon_1))-E(\vartheta+i\varepsilon_1)+2E(\vartheta'+i\varepsilon_2)}{E_0(p(\vartheta+i\varepsilon_1))+E(\vartheta+i\varepsilon_1)} \\ F_3^{\phi}(\vartheta+i(\pi+\varepsilon_1),-\vartheta'-i\varepsilon_2,\vartheta'+i\varepsilon_2)K(\vartheta')_{\varepsilon_2}^{(k)}\Bigg)+\frac{1}{2}K(\vartheta)_{\varepsilon_1}^{(k)}, \end{aligned} \tag{6.2.24}$$

$$\begin{aligned} K(\vartheta)_{\varepsilon_2}^{(k+1)} = \frac{1}{2}\frac{-1}{\gamma_2}\Bigg(1\frac{E_0(p(\vartheta+i\varepsilon_2))-E(\vartheta+i\varepsilon_2)}{E_0(p(\vartheta+i\varepsilon_2))+E(\vartheta+i\varepsilon_2)}+(1-\gamma_2)K(\vartheta)_{\varepsilon_2}^{(k+1)} \\ + \frac{1}{2F_1^{\phi}}\int_{-\infty}^{+\infty}\frac{d\vartheta'}{2\pi}\frac{E_0(p(\vartheta+i\varepsilon_2))-E(\vartheta+i\varepsilon_2)+2E(\vartheta'+i\varepsilon_1)}{E_0(p(\vartheta+i\varepsilon_2))+E(\vartheta+i\varepsilon_2)} \\ F_3^{\phi}(\vartheta+i(\pi+\varepsilon_2),-\vartheta'-i\varepsilon_1,\vartheta'+i\varepsilon_1)K(\vartheta')_{\varepsilon_1}^{(k)}\Bigg)+\frac{1}{2}K(\vartheta)_{\varepsilon_2}^{(k)}, \end{aligned}$$

yielding scheme S2F. The solution along the real axis is obtained by

$$\begin{aligned} K(\vartheta) = \frac{-1}{1+S(-2\vartheta)}\Bigg(2\frac{E_0(p(\vartheta))-E(\vartheta)}{E_0(p(\vartheta))+E(\vartheta)}+ \\ + \frac{1}{F_1^{\phi}}\int_{-\infty}^{+\infty}\frac{d\vartheta'}{2\pi}\frac{E_0(\vartheta)-E(\vartheta)+2E(\vartheta'+i\varepsilon_2)}{E_0(\vartheta)+E(\vartheta)}F_3^{\phi}(\vartheta+i\pi,-\vartheta'-i\varepsilon_2,\vartheta'+i\varepsilon_2)K(\vartheta')_{\varepsilon_2}^{(k)}\Bigg). \end{aligned} \tag{6.2.25}$$

For the finite mass quench problem fast convergence is witnessed again, furthermore, the iterative solution appears to be close to the proposed Ansatz (6.2.13) (Fig. 6.2.3). Just like in the Dirichlet case, these observations hold for a large regime of the coupling strength B and the quench parameter m_0. Note that the deviation between the iterative solution and the Ansatz (6.2.13) is of the same magnitude as in the Dirichlet case, therefore it can safely be attributed to the truncation of the form factor series, which will be further confirmed after taking into account the four-particle contribution in Subsection 6.2.4.

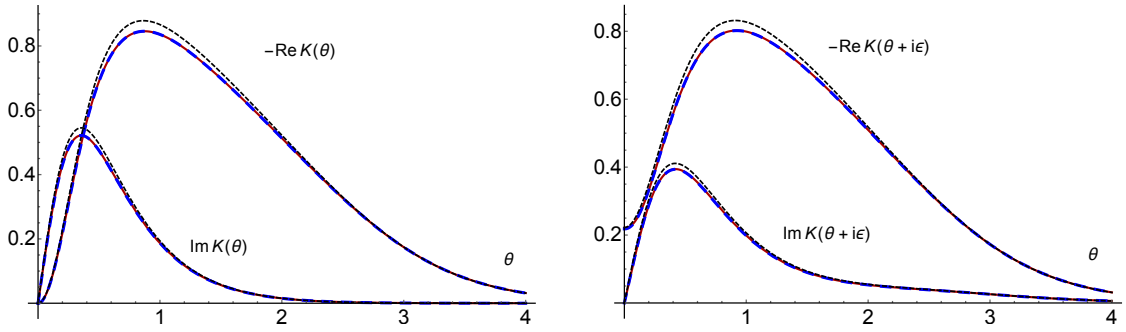

Figure 6.2.3: *6th (continuous red) and 7th (blue dashed) iterations for the finite mass quench problem together with the proposed solution (6.2.13) (black dashed line) for real and shifted rapidities.* $\varepsilon_1 = 0.05, \varepsilon = \varepsilon_2 = 0.1, B = 0.6, m = 1, m_0 = 10$. *The input of the first iteration was (6.2.13) itself.*

6.2.4 Numerical solution of the hierarchy: adding the $O(K^2)$ terms

To construct an iteration scheme including the four-particle contributions of (C.1.2)-(C.1.5), we can simply add them (6.2.18)-(6.2.21). For a closed iteration, however, we now need also an iterative function that is defined for real rapidities. Although it is possible to construct a scheme working with only two iterative functions, the one presented below uses three of them: for $K(\theta)^{(k+1)}$ and $K(\theta)_{\varepsilon_1}^{(k+1)}$ the integration contour is shifted with ε_2, and for $K(\theta)_{\varepsilon_2}^{(k+1)}$ the contour is shifted with ε_1. Unlike in the equation for $K(\theta)_{\varepsilon_1}^{(k+1)}$, where the denominator is $1 + S(-2(\theta + i\varepsilon_1))$, in the equation for $K(\theta)^{(k+1)}$, the denominator is $1 + \frac{1}{2F_1^\phi}\int_{-\infty}^{+\infty}\frac{d\theta'}{2\pi}\left(S(-2\theta) + S(\theta - \theta')S(\theta + \theta')\right)F_3^\phi(-\theta, -\theta', \theta')K(\theta')^{(k)}$ instead. The equations for this scheme S4D read

$$
\begin{aligned}
K(\vartheta) = \frac{1}{2}\frac{-1}{\gamma_1}\frac{1}{1 + S(-2(\vartheta + i\varepsilon_1))}\Bigg(&2 + (1-\gamma_1)\left(1 + S(-2(\vartheta + i\varepsilon_1))\right)K(\vartheta)_{\varepsilon_1}^{(k)} \\
&+ \frac{1}{F_1^\phi}\int_{-\infty}^{+\infty}\frac{d\vartheta'}{2\pi}F_3^\phi(\vartheta + i(\pi + \varepsilon_1), -\vartheta' - i\varepsilon_2, \vartheta' + i\varepsilon_2)K(\vartheta')_{\varepsilon_2}^{(k)} \\
&+ \frac{1}{2F_1^\phi}\int_{-\infty}^{+\infty}\frac{d\vartheta'}{2\pi}\Big(S(-2(\vartheta + i\varepsilon_1))K(\vartheta)_{\varepsilon_1}^{(k)} + S(\vartheta + i\varepsilon_1 - \vartheta')S(\vartheta + i\varepsilon_1 + \vartheta')K(\vartheta)_{\varepsilon_1}^{(k)}\Big) \\
&F_3^\phi(-\vartheta - i\varepsilon_1, -\vartheta', \vartheta')K(\vartheta')^{(k)} \\
&+ \frac{1}{4F_1^\phi}\int_{-\infty}^{+\infty}\frac{d\vartheta_1'}{2\pi}\int_{-\infty}^{+\infty}\frac{d\vartheta_2'}{2\pi}F_5^\phi(\vartheta + i(\pi + \varepsilon_1), -\vartheta_1' - i\varepsilon_2, \vartheta_1' + i\varepsilon_2, -\vartheta_2' - i\varepsilon_2, \vartheta_2' + i\varepsilon_2) \\
&K(\vartheta_1')_{\varepsilon_2}^{(k)}K(\vartheta_2')_{\varepsilon_2}^{(k)}\Bigg) + \frac{1}{2}K(\vartheta)_{\varepsilon_1}^{(k+1)}\,,
\end{aligned}
\tag{6.2.26}
$$

$$
\begin{aligned}
K(\vartheta)^{(k+1)}_{\varepsilon_2} = \frac{1}{2}\frac{-1}{\gamma_2}\Bigg(&1 + (1-\gamma_2)K(\vartheta)^{(k)}_{\varepsilon_2} \\
&+ \frac{1}{2F_1^\phi}\int_{-\infty}^{+\infty}\frac{d\vartheta'}{2\pi}F_3^\phi(\vartheta + i(\pi+\varepsilon_2), -\vartheta' - i\varepsilon_1, \vartheta' + i\varepsilon_1)K(\vartheta')^{(k)}_{\varepsilon_1} \\
&+ \frac{1}{2F_1^\phi}\int_{-\infty}^{+\infty}\frac{d\vartheta'}{2\pi}\Big(S(\vartheta + i\varepsilon_2 - \theta')S(\vartheta + i\varepsilon_2 + \vartheta')K(\vartheta)^{(k)}_{\varepsilon_1}\Big) \\
&F_3^\phi(-\vartheta - i\varepsilon_2, -\vartheta', \vartheta')K(\vartheta')^{(k)} \\
&+ \frac{1}{8F_1^\phi}\int_{-\infty}^{+\infty}\frac{d\vartheta_1'}{2\pi}\int_{-\infty}^{+\infty}\frac{d\vartheta_2'}{2\pi}F_5^\phi(\vartheta + i(\pi+\varepsilon_2), -\vartheta_1' - i\varepsilon_1, \vartheta_1' + i\varepsilon_1, -\vartheta_2' - i\varepsilon_1, \vartheta_2' + i\varepsilon_1) \\
&K(\vartheta_1')^{(k)}_{\varepsilon_1}K(\vartheta_2')^{(k)}_{\varepsilon_1}\Bigg) + \frac{1}{2}K(\vartheta)^{(k+1)}_{\varepsilon_2}\,,
\end{aligned}
\tag{6.2.27}
$$

$$
\begin{aligned}
K(\theta)^{(k+1)} = \frac{-1}{2}\Bigg[&1 + \frac{1}{2F_1^\phi}\int_{-\infty}^{+\infty}\frac{d\vartheta'}{2\pi}\left(S(-2\vartheta) + S(\vartheta - \vartheta')S(\vartheta + \vartheta')\right) \\
&F_3^\phi(-\vartheta, -\vartheta', \vartheta')K(\vartheta')^{(k)}\Bigg]^{-1}\Bigg(2 + S(-2\theta)K(\theta)^{(k)} \\
&+ \frac{1}{F_1^\phi}\int_{-\infty}^{+\infty}\frac{d\vartheta'}{2\pi}F_3^\phi(\vartheta + i\pi, -\vartheta' - i\varepsilon_2, \vartheta' + i\varepsilon_2)K(\vartheta')^{(k)}_{\varepsilon_2} \\
&+ \frac{1}{4F_1^\phi}\int_{-\infty}^{+\infty}\frac{d\vartheta_1'}{2\pi}\int_{-\infty}^{+\infty}\frac{d\vartheta_2'}{2\pi}F_5^\phi(\vartheta + i\pi, -\vartheta_1' - i\varepsilon_2, \vartheta_1' + i\varepsilon_2, -\vartheta_2' - i\varepsilon_2, \vartheta_2' + i\varepsilon_2) \\
&K(\vartheta_1')^{(k)}_{\varepsilon_2}K(\vartheta_2')^{(k)}_{\varepsilon_2}\Bigg) + \frac{1}{2}K(\vartheta)^{(k)}\,.
\end{aligned}
\tag{6.2.28}
$$

We omit the equations of the iteration scheme for the finite mass case, as the corresponding finite mass scheme S4F is easily obtained from S4D by plugging the extra $\frac{E_0-E}{E_0+E}$ type factors. Similarly to schemes S2D and S2F, the parameters γ_1 and γ_2 were set 1, and the averaging with the previous iterative functions is present in each iterative step.

This scheme was chosen from other possibilities by observing that it always performed better than all other schemes we tried. Unlike S2D and S2F and just like other schemes including the four-particle terms, S4D and S4F iterations are unstable. To overcome this issue we stopped the iteration when the difference between two consecutive iterative functions was the smallest. The functional difference was measured by the integral

$$
\int d\theta \left|\mathrm{Re}[K(\vartheta)^{(k+1)} - K(\vartheta)^{(k)}]\right|\,,
$$

as the difference between the imaginary parts tends to be much smaller and slowly varying.

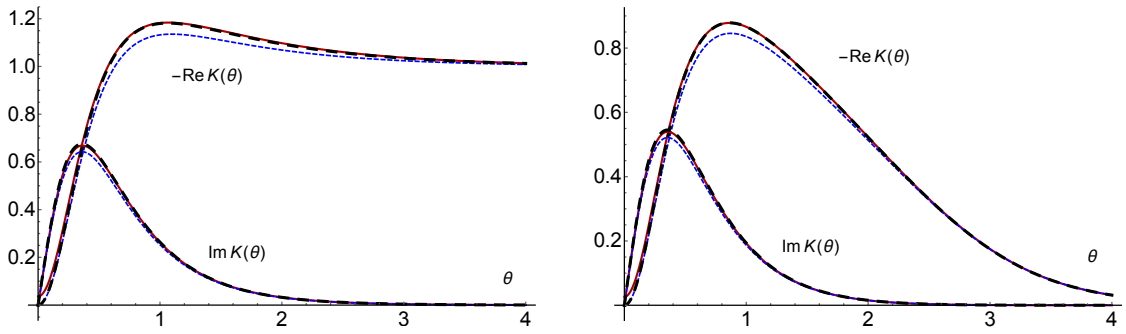

Figure 6.2.4: *Left: 7th (blue dashed) iterative functions obtained by S2D and the optimal iterative function (red continuous) obtained by S4D for the Dirichlet problem together with the Dirichlet solution $K_D(\vartheta)$ (black dashed line) for real rapidities.$\varepsilon_1 = 0.05, \varepsilon = \varepsilon_2 = 0.1, B = 0.6$. The input of the first S2D iteration was the Dirichlet solution itself, whereas the S4D input was the 7th S2D iterative function. Right: 7th (blue dashed) iterative functions obtained by S2F and the optimal iterative function (red continuous) obtained by S4F for the finite mass quench problem together with the proposed solution (6.2.13) (black dashed line) for real rapidities. $\varepsilon_1 = 0.05, \varepsilon = \varepsilon_2 = 0.1, B = 0.6, m = 1, m_0 = 10$. The input of the first S2F iteration was (6.2.13) itself, wheres the S4F input was the 7th S2F iterative function.*

As demonstrated in Fig. 6.2.4 the solutions of S4D and S4F schemes are indeed remarkably close to the exact Dirichlet solution and the Ansatz, respectively. In fact, the solution curves now lie on top of the exact Dirichlet amplitude and the Ansatz, respectively. This pattern again holds for all values of the coupling strength B and a large range of the quench parameter m_0.

6.2.5 Checking the validity of the pair assumption via the three-particle condition

Here we provide a numerical verification of the pair structure and hence exponential form (4.2.6), (6.2.14) of the initial state by considering higher members of the hierarchy. This rapidly becomes impractical due to the computational cost of the integrals involving very high particle form factors. In addition, constructing the form of the equation with the integration contours arranged conveniently for numerical evaluation is also quite tedious.

For this reason, we restrict ourselves here to the case of three-particle test states. The three-particle condition is a sum

$$0 = T_0 + T_2 + T_4 + T_6 + \dots \tag{6.2.29}$$

with T_n denoting the n-particle contribution from initial state(4.2.6), (6.2.14). Since the iterative solution of the one-particle condition is very well described by the Ansatz (6.2.13), the latter can be used to perform the evaluations. We have computed the first three terms explicitly with the result given in (C.1.7). For the contribution T_6, deriving the integral form proved to be so tedious that we decided to estimate its contribution directly evaluating the corresponding term in the finite volume form (C.1.1) for a large value of the volume ($mL = 250$).

To verify that (6.2.29) holds, we computed the sum for several values of the Sinh-Gordon coupling in the fundamental range $0 \leq B \leq 1$, for different values of the test rapidities at each point, and for several different quenches, parametrized by the mass ratio m_0/m.

To make certain that the integral form (C.1.7) of the condition was derived correctly, we supplemented the calculation of T_2 and T_4 by a direct evaluation of the finite volume sum for $mL = 250$. The finite volume form was always found to agree with the integral form within the numerical precision of the former. Note that for practical evaluation the finite volume sum must be truncated to states below some upper energy cutoff. For T_2 and T_4 it was possible to keep this truncation high enough to achieve better than 3 digits accuracy; however, for T_6 this was not always the case, as we discuss below.

A sample of the resulting data is presented in Appendix D. As a benchmark, we always quote the Dirichlet case $m_0/m = \infty$, which can be obtained by omitting the energy factors in square brackets from each term. For the Dirichlet case, the equation must hold exactly when terms T_n are included for all n, since then (4.2.6), (6.2.14) correspond to a boundary state known exactly from reflection factor bootstrap [122, 155]. We can see that the terms T_2 and T_4 (corresponding to $\Delta n = \pm 1$) are always dominant, and typically cancel each other within a few percent. To go further, it is necessary to include T_0 and T_6, corresponding to $\Delta n = \pm 2$. In most cases, this improves the cancellation to better than a percent. There are two exceptions to this, however. First, when the sum $T_0+T_2+T_4$ is relatively small, to verify the improvement T_6 would need to be evaluated to a very high precision which is not possible using the finite volume summation. Second, when some of the test rapidities are relatively large, the cut-off necessary to evaluate the finite volume sum for T_6 prevents the evaluation of all the dominant contributions, as these come from regions which cannot be explored within reasonable computer time. However, in all these cases we also see the same deviations for the $m_0/m = \infty$ case, for which we known the full equation should hold exactly. Taken altogether, these facts show that the deviations can be explained by the approximations made during numerical evaluation. On the other hand, we have data for a much larger number of couplings and rapidities than shown in Appendix D, and all of them fall in the same pattern.

Summing up, the numerical evaluation of the three-particle member of the hierarchy strongly confirms the exponential form of the initial state.

6.3 Summary

Here we briefly summarize the most important points and results presented in this chapter. We studied a particular class of quenches within the Sinh-Gordon model, starting from the ground state of mass m_0 with zero coupling, to a post-quench system with a mass m and a nonzero value of g. For this quench the initial state can be specified via an operator condition allowing the derivation of an infinite hierarchy of integral equations involving form factors of the model and the unknown overlap functions K_{2n}. Each integral equation can be written as a form factor expansion, consisting of an infinite number of terms.

We presented the general derivation of the hierarchy and a number of arguments concerning the nature of its solutions. Some of these arguments are likely valid for more general models (such as sine-Gordon or $A^{(1)}_{N-1}$ affine Toda theories) and initial states, described by similar integral hierarchies. The results we expect to be generally valid are the following:

1. For a free field, the unique solution of the hierarchy is the usual squeezed state obtained from the Bogoliubov transformation, and perturbation theory considerations imply the existence and uniqueness of its solution for the interacting case.

2. The terms in the hierarchy are ordered in magnitude by the difference between the bra and ket state particle numbers Δn; the larger Δn, the smaller is the corresponding term, with the $\Delta n = \pm 1$ terms dominating for odd operators (such as the elementary field ϕ considered in this paper). This means that each equation in the hierarchy can be well approximated by a finite truncation, and that higher equations corresponding to test states with more particles probe overlap amplitudes with states containing more particles.

3. The iterative solution method that was developed on the basis of the aforementioned truncatability property.

We presented a numerical solution for this hierarchy based on the pair assumption for the initial state and argued for its validity based on "integrable dressing" and on analogies with boundary conformal field theories. Due to the heuristic nature of the pairing arguments our considerations were supplemented by numerical checks. We found that the iterative solution of the numerical methods confirms to high precision that the proposed factorized Ansatz (6.2.13) indeed solves the one-particle test state condition, which is

the lowest member of the hierarchy. Second, an independent test of the squeezed state form, which includes the pair structure and the exponentiation, was provided by checking the next member of the hierarchy, i.e. the three-particle condition. Note that since the Ansatz contains no free parameters, there is no way to adjust it: it either fails or passes. In the end, the Ansatz passed all the tests we could pose; while these are limited by computing power, they still impose very stringent constraints. This shows that the Ansatz is at least a very good approximation to the solution of the quench problem, at least in the range of parameters studied in our investigations. Based on the analytical Ansatz, steady state expectation values were obtained in Ref. [88]. Using the pair assumption, we also showed from the integral equations that the K-function behaves asymptotically as $e^{-2|\vartheta|}$ for quenches with a finite difference in the pre- and post-quench masses, and thus demonstrated that the given quantum quench is well-defined in the field theory sense as well.

Chapter 7

Mass quenches in the sine-Gordon model

In the previous chapter it was demonstrated how the overlaps for a specific quench protocol can be calculated. For the computation a crucial ingredient was the operator formulation of the quench problem and the existence of the hierarchy of infinite integral equations as a consequence. For a general quench, however, such integral equations cannot be written down, and the determination of the overlaps remains an unsolved problem. For the numerical determination of the overlaps, truncated spectrum approaches (TSA) offer a notable choice [55, 164, 175]. In addition, TSA methods have a direct access to the time evolution of various quantities including one-point functions [55, 164, 167, 176, 177] and even multi-point correlation functions [176] after quantum quenches. These methods hence offer an insight not only into the quench overlaps but also into the time evolution in relativistic QFTs for short time scales and can be applied in non-integrable models as well.

The central idea of TSA methods is to consider the QFT in a finite volume L resulting in a discrete spectrum and to introduce an energy cut-off, i.e. only finite number of states are kept from the entire Hilbert space. Our main focus in this chapter is on the determination of overlaps for a mass quench in the sine-Gordon model via the truncated conformal space approach (TCSA), and for the particular case of TCSA, the starting point is to regard the QFT as a perturbation of its UV limiting conformal field theory. If the matrix elements of the perturbing operator are known in the conformal basis, the Hamiltonian of the deformed CFT is easily represented as a finite dimensional matrix in the above scheme.

TSA methods are mainly used to study ground state and low energy properties of interacting QFTs and it is not obvious whether they can correctly describe the physics in non-equilibrium situations, when the initial state is a highly excited state in the post-quench basis. This potential problem is of similar nature as the question of the applicability of the quench paradigm in field theories. Whereas in effective theories the UV cut-off is generally large, the available energy cut-offs in TSA methods are usually much more restricted. Indeed, a necessary criterion for the applicability of TSA is that the overlaps decay sufficiently fast with energy, and consequently large energy modes have overlaps negligible with the initial state. The magnitude of the quench for which TSA is expected to describe correctly the out-of-equilibrium physics is the small and moderate size quenches, when the injected energy is well-below the energy cut-off. It is very fortunate that, as demonstrated in the previous chapter and further discussed in Section 7.2, the overlaps after a quench usually decay with the energy, and therefore large energy modes have overlaps often negligible with the initial state. This finding confirms again the applicability of the quantum quench protocol in field theories and enables the use of TSA for suitably small quenches.

In this chapter we first discuss how TCSA is implemented for the sine-Gordon model and then turn to the discussion of the two-particle for the first breather after a mass quench [175]. We show that continuing analytically the Ansatz for the sinh-Gordon problem (6.2.13) as $B = -2\xi$ (cf. (3.4.4) and (3.4.14)) the result agrees with the numerical values of the pair overlaps, although in the quench in the sinh-Gordon model the interaction was changed as well. Furthermore, by calculating the overlaps for 4-breather states, we demonstrate that the integrable squeezed-coherent state assumption is consistent with the TCSA data.

7.1 TCSA in the sine-Gordon model

The truncated conformal space approach (TCSA) is an efficient numerical method to study perturbed conformal field theories. The main idea is to consider the theory of interest in a finite volume L resulting in a discrete spectrum of the unperturbed CFT, which can be truncated to a finite subspace by introducing an upper energy cut-off parameter $e_{\rm cut}$ [18]. For many perturbations of CFTs it is possible to calculate exact matrix elements of the perturbing field and various operators in the truncated Hilbert space. Therefore, computing the spectrum of the perturbed theory and other physical quantities reduces to manipulations with finite dimensional matrices.

For the sine-Gordon TCSA [178] the starting point is the Hamiltonian (3.4.26) of a compactified free massless boson in finite volume L, perturbed by a relevant cosine operator with the Hilbert space in finite volume spanned by the basis (3.4.29). Using the simplest truncation scheme described above, the truncated space is given by

$$\mathcal{H}_{\rm TCSA}(e_{\rm cut}) = \text{span}\left\{ a_{-k_1}...a_{-k_r}\bar{a}_{-p_1}...\bar{a}_{-p_l}|n\rangle : \frac{(n\beta)^2}{4\pi} + \sum_{i=1}^{r} k_i + \sum_{j=1}^{l} p_j - \frac{1}{12} \leq e_{\rm cut} \right\} \tag{7.1.1}$$

which is the scheme commonly employed in the literature.

Matrix elements of the vertex operators V_m can easily be computed in the conformal basis using the mode expansion of the canonical field ϕ on the cylinder:

$$\phi(x,t) = \phi_0 + \frac{4\pi}{L}\pi_0 t + i\sum_{k\neq 0}\frac{1}{k}\left[a_k \exp\left(i\frac{2\pi}{L}k(x-t)\right) + \bar{a}_k \exp\left(-i\frac{2\pi}{L}k(x+t)\right)\right]. \tag{7.1.2}$$

It is straightforward to show that the matrix elements of the vertex operators

$$\langle n'|a_{k'_1}...a_{k'_{r'}}\bar{a}_{p'_1}...\bar{a}_{p'_{l'}}V_m a_{-k_1}...a_{-k_r}\bar{a}_{-p_1}...\bar{a}_{-p_l}|n\rangle \tag{7.1.3}$$

are independent on the Fock module index of the states apart from a selection rule $\delta_{n',n+m}$. Therefore, using the Fock decomposition of the free boson Hilbert space

$$\mathcal{H} = \bigoplus_n \mathcal{F}_n\,,$$

the Hamiltonian of sine-Gordon model has a simple modular structure which can be represented as a tridiagonal block matrix, where the entries correspond to operators acting either within each block (the conformal part H_0) or between neighboring Fock modules (the blocks $\mathcal{V}_{\pm 1}$ from the vertex operators $V_{\pm 1}$):

$$H_{\rm TCSA} = \begin{pmatrix} \ddots & \ddots & \ddots & & & & \\ & \mathcal{V}_1 & H_0^{(n+1)} & \mathcal{V}_{-1} & & & \\ & & \mathcal{V}_1 & H_0^{(n)} & \mathcal{V}_{-1} & & \\ & & & \mathcal{V}_1 & H_0^{(n-1)} & \mathcal{V}_{-1} & \\ & & & & \ddots & \ddots & \ddots \end{pmatrix}. \tag{7.1.4}$$

This matrix is finite dimensional when restricted to the space (7.1.1), and its numerical diagonalization yields an approximation of the energy levels and corresponding eigenstates of the model.

In the particular quench protocol of changing the mass scale in the system, the initial state corresponds to the ground state of the same Hamiltonian (3.4.22) with λ replaced by λ_0 corresponding to M_0. The overlaps are therefore easily calculated by the scalar product of ground state of the pre-quench Hamiltonian with λ_0 and the eigenstates of the post-quench Hamiltonian with coupling λ. When considering the post-quench evolution in dimensionless volume $l = ML$, implementing the quench can also be regarded as using

the ground state computed in the rescaled volume $l_0 = M_0 l/M$ [167]. This fact imposes a restriction on the magnitude of the quench available by TCSA since on the one hand it must be ensured that neither the pre-quench nor the post-quench volumes are too small, in order to avoid large finite size effects (c.f. Section 3.3). On the other hand the volumes cannot be too large, where a very high $e_{\rm cut}$ is required for a given accuracy.

In a suitable volume window and for small and moderate size quenches, where the excitations are dominated by few-particle states, the finite volume corrections become exponentially suppressed. Nevertheless TCSA inevitably involves an energy cut-off $e_{\rm cut}$ to truncate the Hilbert space to a finite dimensional one. Therefore all quantities computed from TCSA show explicit dependence on the cut-off, which can be (at least partially) eliminated using renormalisation group methods [179–181]. RG methods introduce running couplings in the Hamiltonian and additional perturbing operators determined by the operator product expansion of the perturbing field with itself. In particular, in the sine-Gordon model we consider an effective Hamiltonian in the form

$$H_{eff} = \int dx \frac{1}{2} : (\partial_t \Phi)^2 + (\partial_x \Phi)^2 : + \lambda_0 \mathbb{I} + \frac{\lambda_1}{2} \int dx \, (V_1 + V_{-1}) + \frac{\lambda_2}{2} \int dx \, (V_2 + V_{-2})$$

where we included counter terms generated at leading order according to the fusion rules $V_a V_b \sim V_{a+b}$. Introducing the dimensionless couplings

$$\tilde{\lambda}_a = \frac{\lambda_a L^{2-2h_a}}{(2\pi)^{1-2h_a}} \quad h_a = \frac{a^2\beta^2}{8\pi} \tag{7.1.5}$$

the running couplings $\tilde{\lambda}_i$ are determined by the RG equations [182]:

$$\tilde{\lambda}_c(n) - \tilde{\lambda}_c(n-1) = \frac{1}{2n - d_0(l)} \sum_{a,b} \tilde{\lambda}_a(n) \tilde{\lambda}_b(n) C_{ab}^c \frac{n^{2h_{abc}-2}}{\Gamma(h_{abc})^2} \left(1 + O(1/n)\right) \tag{7.1.6}$$

where C_{ab}^c is the operator product coefficient, $h_{abc} = h_a + h_b - h_c$ and $d_0(l)$ is the vacuum scaling function (cf. [182]). The parameter n denotes the highest descendant level retained after truncation. In the free boson CFT the descendant level is given by

$$n = \sum_{i=1}^{r} k_i = \sum_{j=1}^{l} p_j \, , \tag{7.1.7}$$

and the Hilbert space can be restricted to its zero-momentum subspace as a consequence of the homogeneity of the quench.

The couplings must be followed using (7.1.6) down from $n = \infty$ to the appropriate value of n_{cut} corresponding to the given cut-off e_{cut} and at the lowest order it is only necessary to run the couplings λ_0 and λ_2, from their starting values $\lambda_0 = 0$ and $\lambda_2 = 0$ at $n = \infty$. The effective Hamiltonian can now be written as

$$H_{\rm TCSA}^{eff} = \begin{pmatrix} \ddots & \ddots & \ddots & & & & \\ \mathcal{V}_2 & \mathcal{V}_1 & H_0^{(n+1)} & \mathcal{V}_{-1} & \mathcal{V}_{-2} & & \\ & \mathcal{V}_2 & \mathcal{V}_1 & H_0^{(n)} & \mathcal{V}_{-1} & \mathcal{V}_{-2} & \\ & & \mathcal{V}_2 & \mathcal{V}_1 & H_0^{(n-1)} & \mathcal{V}_{-1} & \mathcal{V}_{-2} \\ & & & & \ddots & \ddots & \ddots \end{pmatrix}$$

were we used a modified version of the running coupling prescription in [182] making the eventual value of n_{cut} dependent on the block one considers. Namely, when computing the coefficient of the block V_2 between $\mathcal{F}_a$ and $\mathcal{F}_{a+2}$, the intermediate states in the OPE $V_1 V_1 \sim V_2$ are from $\mathcal{F}_{a+1}$ which determines the

level n_{cut} appropriate for the given block, and similarly for V_{-2} between $\mathcal{F}_a$ and $\mathcal{F}_{a-2}$ n_{cut} is fixed from $\mathcal{F}_{a-1}$. For the identity term between $\mathcal{F}_a$ and $\mathcal{F}_a$ there are two possible intermediate modules $\mathcal{F}_{a\pm1}$, so the identity coupling must be split into two pieces $\lambda_{0\pm}$, each of them running down to the appropriate n_{cut} determined by the highest level in $\mathcal{F}_{a\pm1}$.

The block-dependent running coupling corresponds to including a non-local counter term. The appearance of such counter terms was first observed in [183]; they account for $1/n$ corrections in the running coupling. In the sine-Gordon there is a large $1/n$ effect resulting from the fact that the cut-off level is heavily module dependent, ranging from e_{cut} in Fock module $\mathcal{F}_0$ to 0 for the Fock modules with the largest indices $\mathcal{F}_{\pm a_{max}}$. The consistency of this scheme was verified by numerically checking the cut-off dependence of the 15 lowest-lying levels in the TCSA spectrum, which proved to be negligible with this method.

7.2 Overlaps from TCSA

7.2.1 The $B_1 - B_1$ pair amplitude

For the mass quench considered here the initial state is translation and parity invariant. Under parity all the odd breather transform as $\mathcal{P}|\vartheta\rangle_{B_{2k+1}} = (-1)|-\vartheta\rangle_{B_{2k+1}}$, therefore the lowest excited states including only first breathers with a non-zero overlap consist of two first breathers. Here we present numerical results for the $B_1 - B_1$ pair amplitudes and compare them with the infinite volume prediction offered by the analytic continuation of the sinh-Gordon Ansatz (6.2.13), which can be written as

$$K_{B_1B_1}(\vartheta) = \frac{E_0(\vartheta) - E(\vartheta)}{E_0(\vartheta) + E(\vartheta)} K_D(\vartheta) \tag{7.2.1}$$

$$K_D(\vartheta) = i \tanh\left(\frac{\vartheta}{2}\right) \frac{\cosh\left(\frac{\vartheta}{2} + \frac{i\pi\xi}{4}\right)}{\sinh\left(\frac{\vartheta}{2} - \frac{i\pi\xi}{4}\right)} \frac{\sinh\left(\frac{\vartheta}{2} + \frac{i\pi(1-\xi)}{4}\right)}{\cosh\left(\frac{\vartheta}{2} - \frac{i\pi(1-\xi)}{4}\right)},$$

where ξ is given by (3.4.14).

For the numerical overlaps one first has to identify states corresponding to $B_1 - B_1$ pairs in the numerical spectrum of the post-quench Hamiltonian. Solving the constrained Bethe-Yang system (4.3.2) one obtains the possible rapidities from which the energy levels can be computed. However, apart from the lowest lying levels, the identification is not feasible by merely comparing the TCSA and the Bethe-Yang energies due the density of the TCSA spectrum. This issue can be overcome by supplementing the energy selection procedure with a comparison of the finite volume form factors of the fields V_1 and V_2 obtained using the formalism developed in [144], to the TCSA matrix elements (for an exposition of how this works in sine-Gordon theory cf. [184]). As the form factors depend sensitively on the particle content of the state, the identification can unambiguously be performed.

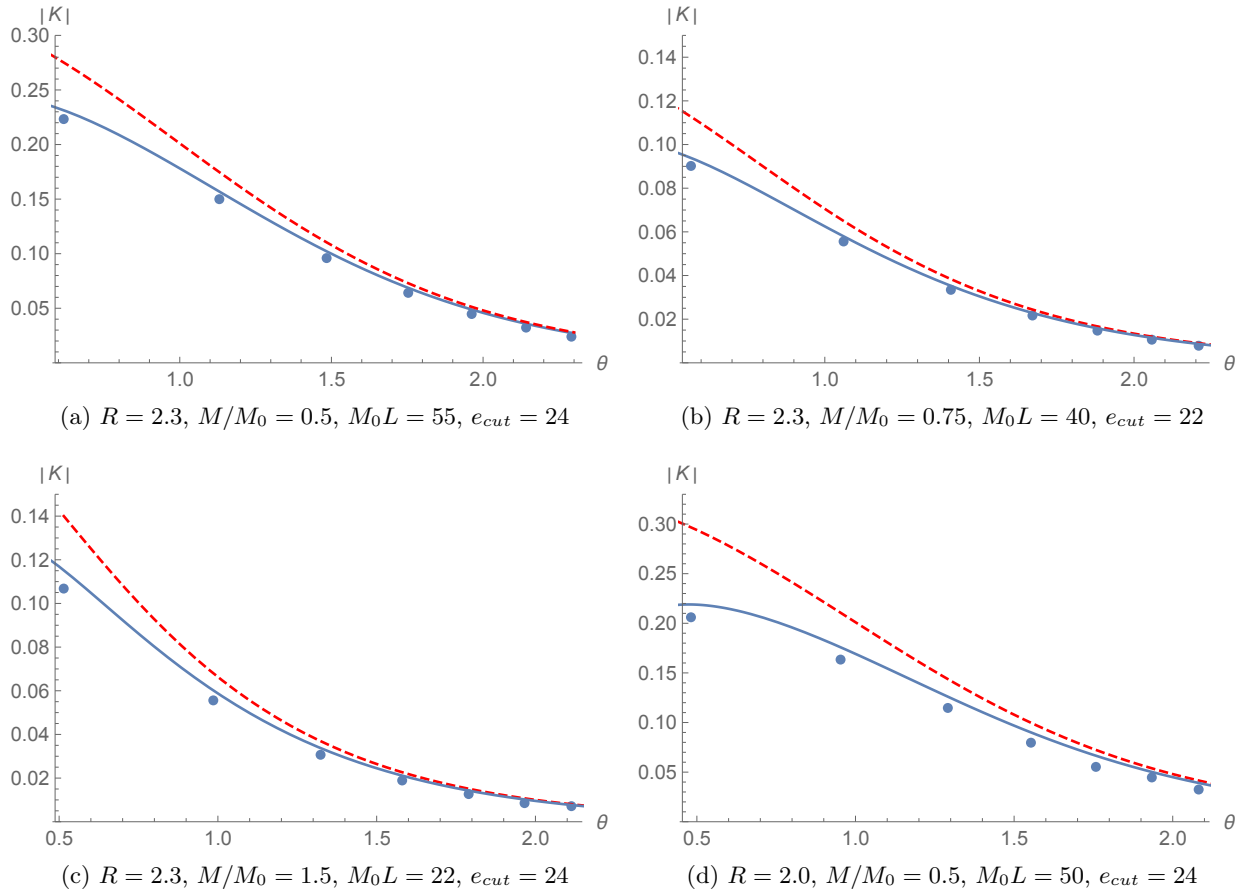

(a) $R = 2.3$, $M/M_0 = 0.5$, $M_0 L = 55$, $e_{cut} = 24$

(b) $R = 2.3$, $M/M_0 = 0.75$, $M_0 L = 40$, $e_{cut} = 22$

(c) $R = 2.3$, $M/M_0 = 1.5$, $M_0 L = 22$, $e_{cut} = 24$

(d) $R = 2.0$, $M/M_0 = 0.5$, $M_0 L = 50$, $e_{cut} = 24$

Figure 7.2.1: The pair amplitude for some mass quenches in sine-Gordon theory. The sine-Gordon coupling β is parametrised as $\beta = \sqrt{4\pi}/R$. The blue (continuous) curves correspond to the sine-Gordon Ansatz (7.2.1), and the red (dashed) ones to the free theory solutions.

Having identified the proper states in the set of numerical eigenstates the numerical overlaps can be obtained from their scalar product with the initial state, divided by the vacuum overlap to eliminate the normalisation factor $\mathcal{N}$ in (4.2.6). As the TCSA matrix elements of the perturbing operator are real numbers, all the numerically computed eigenvectors are also real, corresponding to a specific convention for the phases of the post-quench eigenstates. Therefore the phase of the overlap function $K(\vartheta)$ is absent from the data, so after normalising the TCSA overlap values with the inverse of N_2 (4.3.4)[1] we compare their modulus to the value obtained from (7.2.1). Note that using (4.3.4) for the pair overlap is independent of whether the quench in the first breather sector is integrable or not. This comparison is shown in Fig. 7.2.1 for a few quenches; the data strongly confirm that the prediction (7.2.1) and it is also clear that both the free particle and the Dirichlet parts of the analytic formula (7.2.1) are important.

In some cases, deviations in the low energy range can be seen, which can be attributed to two sources. First, the initial state is different from the free massive vacuum for which (7.2.1) (or more precisely, its sinh-Gordon counterpart (6.2.13)) was obtained. However, the difference is the presence of a relevant perturbation in the pre-quench Hamiltonian, which is a relevant operator and so its effect decreases with energy. Second, when modelling the finite size effects in Section 3.3 we used a formalism that neglects exponential corrections in the volume, which affect the lower lying states more. Unfortunately, it is

[1]Unfortunately a slight mistake was made in the work Ref. [175], on which this Section is based, namely the TCSA overlaps were multiplied incorrectly by N_2 instead of its inverse. This has no essential effect on the quality of the match between the TCSA data and the analytic predictions for the overlaps. However, the plots presented in Fig. 7.2.1 are not identical with that of Ref. [175] and were created using the correct procession of the TCSA data.

Rapidities $\vartheta_1^*, \vartheta_2^*$	BY energy	TCSA energy	Normalized overlap	Factorized prediction
{0.671828, 1.44047}	1.13089	1.13133	0.0255928	0.0244265
{0.651971, 1.72849}	1.34668	1.34742	0.0168602	0.0162507
{1.19428, 1.70726}	1.51794	1.51918	0.0108541	0.0108043
{0.642841, 1.95028}	1.56712	1.56853	0.0117727	0.0113951
{0.637471, 2.1315}	1.73764	1.79245	0.0083998	0.0083603

(a) $R = 2.3$, $M/M_0 = 0.5$, $M_0 L = 55$, $e_{cut} = 24$

Rapidities $\vartheta_1^*, \vartheta_2^*$	BY energy	TCSA energy	Normalized overlap	Factorized prediction
{0.549607, 1.22608}	1.33758	1.33916	0.0296001	0.0278547
{0.524061, 1.51576}	1.56955	1.57217	0.0139780	0.0195048
{1.03577, 1.48932}	1.74274	1.74686	0.0142756	0.0149960
{0.512645, 1.73741}	1.80847	1.81308	0.0137404	0.0141252
{1.00938, 1.72497}	1.98019	1.98813	0.0130837	0.0108970

(b) $R = 2.0$, $M/M_0 = 0.5$, $M_0 L = 50$, $e_{cut} = 24$

Rapidities $\vartheta_1^*, \vartheta_2^*$	BY energy	TCSA energy	Normalized overlap	Factorized prediction
{0.618879, 1.36023}	1.60354	1.60489	0.00454695	0.00344512
{0.599521, 1.64559}	1.89691	1.89943	0.00292898	0.00219769
{1.12225, 1.62472}	2.12314	2.12725	0.00176750	0.00132404
{0.590723, 1.866}	2.19785	2.20287	0.00203194	0.00150384
{1.10091, 1.85633}	2.42300	2.43139	0.00128401	0.00091002

(c) $R = 2.3$, $M/M_0 = 0.75$, $M_0 L = 40$, $e_{cut} = 22$

Table 7.2.1: Overlaps for 4-B_1 paired states $|-\vartheta_1^*, \vartheta_1^*, -\vartheta_2^*, \vartheta_2^*\rangle$. The sine-Gordon coupling β is parametrised as $\beta = \sqrt{4\pi}/R$. To eliminate differences in phase conventions of energy eigenstates the modulus of the overlaps is reported.

not easy to separate these effects, and so we cannot say anything more definite about the low-energy behaviour. However, the analytically continued solution (7.2.1) definitely provides a good description of the amplitudes in the mid-to-high energy range.

7.2.2 Amplitudes for 4 B_1 particles and factorisation

Here we aim to check if the squeezed-coherent form of the initial state (4.2.6) is a valid assumption in the sector of the first breathers. Once the amplitude $K(\vartheta)$ is pinned down, all higher overlaps are determined by the exponential form, which entails the factorisation property claiming that states which do not have an exclusive pair structure in terms of particles have zero overlap, and for paired states the overlap is just equal to the product of individual pair state overlaps.

Another prediction from factorisation is that the overlaps for paired 4-B_1 states is the product of pair overlaps. This is also consistent with the TCSA data as shown in Table 7.2.1. For the quenches in sub-tables (a) and (b), the overlaps are large enough so that one can observe a quantitative agreement between the predictions of (7.2.1) and the TCSA results. For the example in sub-table (c), the overlap is too small to be measured and the agreement is only qualitative.

The question is whether this constitutes a non-trivial test of overlap factorisation. As discussed in Section (4.2), when the quench is small factorisation is expected to be valid to a very good approximation. A small quench means that the average energy density $\mathcal{E}$ after the quench satisfies

$$\mathcal{E} = \frac{1}{L}\left(\langle\Psi(0)|H|\Psi(0)\rangle - \langle 0|H|0\rangle\right) \ll m_1^2$$

where m_1 is the mass of the lightest particle. In such a case the density of even the lightest pairs is so small that the average distance d between pairs is much larger than the correlation length m_1^{-1}. Since the interactions are suppressed by the distance as $e^{-m_1 d}$, the multi-pair amplitudes are expected to factorise irrespective of integrability when the quench is small.

We evaluated $\mathcal{E}$ for all the quenches for which we could produce reliable TCSA data and found that d was at least an order of magnitude larger than m_1^{-1}, therefore all observed deviations from factorisation are expected to be TCSA related (either truncation errors or unmodeled finite size effects). Indeed, when testing the overlaps for non-paired 4-B_1 states, they proved to be an order of magnitude smaller than the overlaps for paired states, and were of the same order as the deviations between the prediction (7.2.1) and the measured two-particle overlap, which is consistent with factorisation.

7.3 Summary

In this chapter we studied mass quenches in the sine-Gordon model by the truncated conformal space approach (TCSA). We extracted the finite volume pair overlaps for the first breathers and calculated the corresponding infinite volume predictions for the pair overlaps. It was demonstrated offered (infinite volume) pair overlaps from TCSA match to a good accuracy with the analytic continuation of the sinh-Gordon pair overlap (6.2.13). Although the two quench protocols slightly differ (in the sine-Gordon model only the mass is changes, whereas in the sinh-Gordon, the coupling constant is also altered), this difference is expected to affect only the low-energy behaviour of the overlaps. The observed match between the numerical and analytical overlaps therefore further supports the validity of the Ansatz for the sinh-Gordon model, since TCSA by construction is devoid of the assumptions made in the previous chapter. We also studied the overlaps for states composed of 4 first breathers, and showed that the TCSA data is consistent with the factorisation of the overlaps, expected to occur for the given quenches within the first breathers.

TCSA also gives access to amplitudes for higher breathers and soliton–anti-soliton pairs. Here and in the work [175] we refrained from reporting the corresponding numerical data, since at present we have no theoretical description for them. Since the appearance of [175], another work was published applying TCSA to extract the overlaps. In Ref. [164] mass quenches in the E_8 longitudinal field Ising field theory were studied, where it was possible to study the large energy asymptotics of the overlaps for the lightest particle and, which found to be $e^{-E(\vartheta)}$ rather than $e^{-2|\vartheta|}$. Together with the results presented here and in the previous chapter, this contributed to better although still partial understanding the asymptotic behaviour, which is worth discussing here and can be summarised as follows [164]. The high-energy behaviour of the overlaps is strongly influenced by the UV conformal field theory or more precisely by presence of interaction between the particles represented in the UV theory of the post-quench model. Concerning the sinh- or sine-Gordon models and E_8 model, the UV limiting theory is a free theory in all these cases, i.e. the free boson and the free fermion CFT. Nevertheless for the E_8 model the basis of particles $A_1, ..., A_8$ is essentially different from the free fermions, and these particles do not become free in the ultraviolet limit, unlike the elementary particle in the sinh-Gordon model and the first breathers in the sine-Gordon theory. This is not a contradiction as there is no unique notion of a particle basis in the limiting conformal field theory, and considering the massless limit from different massive directions produces different results. Therefore the presence of interaction between the particles represented in the UV theory seems to be essential for high energy behaviour of the overlaps.

Finally, it is also important to mention that the asymptotics of the overlaps always decays with energy. This behaviour enables not only the use of TCSA in these particular situations but also guarantees that the quantum quench protocol in field provides cut-off independent physics at least for moderate size quenches.

Chapter 8

Time evolution of one point functions after a quench

The previous chapters were devoted to the overlaps after quantum quenches, and we presented important examples when the overlaps can be computed. Although the overlaps themselves are interesting quantities, as discussed in the introductory chapters, the knowledge of the overlaps is crucial to come up with predictions for the steady-state and also for the quench dynamics at least with the currently available techniques in IQFTs.

Whereas important features of the steady state, such as the emergence of the GGE [6,19], are believed to be understood in integrable systems, and in integrable quenches it is also possible to give a representation of the steady state, the theoretical description of the out-of-equilibrium time evolution is much more difficult and less understood than the characterisation of the steady state. Describing the actual time evolution and possibly identifying universal features of the non-equilibrium dynamics are also of great interest but analytical results have mainly been restricted to systems that can be mapped to free particles [86, 87, 90–102], to conformal field theory [27, 28] and to a few cases in interacting integrable systems [73, 74, 83, 103–106].

Our aim in this chapter is to study the time evolution of one-point functions after homogeneous quenches in massive IQFTs using analytical tools. As discussed in Section 2.3, one advantage of the Quench Action approach is that it describes the late time evolution in a uniform fashion, but the necessary ingredients, i.e. form factors of local operators with respect to the quasi-particle and hole excitations over the steady state are not known. Many of the earlier results and our findings follow therefore the way provided by Eq. (2.1.1). i.e. the decomposition of the initial state with respect to the post-quench eigenstates, which is a very natural approach in IQFTs due to the available exact form factors.

In massive integrable quantum field theories, for suitably small quenches, the semi-classical approach [113, 185–187] and approaches based on form factor expansions [107–109, 111, 112] can lead to analytical predictions for the time evolution of certain observables. The perturbative approach in [111, 112] can be applied to any quench in which the *pre-quench* Hamiltonian is integrable, however, analytical results have only been obtained by perturbation theory up to first order in the quench amplitude, which is often too restrictive [164]. The method developed in [107–109, 113] can be applied whenever the post-quench Hamiltonian is integrable but it requires that the quench is integrable according to the discussion in Section 4 and the post-quench particle density is suitably small.

Particular examples include mass quenches within the paramagnetic phase of the Ising field theory [107], where due to the existence of a Bogoliubov transformation the structure (4.2.6) is guaranteed and the K-function is explicitly known, and the repulsive regime of the sine-Gordon model [108, 113], where (4.2.6) is an assumption, but is known to hold is the small quench limit (c.f. Section 4.2). In Ref. [107] the time evolution of the magnetisation operator in the Ising field theory was shown to decay exponentially in the leading order and in the long time limit with a time constant

$$\tau_{Ising}^{-1} = \frac{2M}{\pi}\int_0^\infty d\vartheta\, |K_{Ising}(\vartheta)|^2 \sinh\vartheta\ . \tag{8.0.1}$$

For the sine-Gordon model, similar results were reported in [108, 113] for vertex operators V_a with half-integer a resulting in a time constant

$$\tau_\alpha^{-1} = \frac{4M_s}{\pi}\sin^2\left(\frac{\pi\alpha}{\beta}\right)\int_0^\infty d\vartheta\, |K_{s\bar{s}}(\vartheta)|^2 \sinh\vartheta\ , \tag{8.0.2}$$

where $\alpha = a\beta$. Interestingly, the "simple" semi-classical treatment [113] gives the same predictions as a linked cluster calculation involving form factor expressions and the resummation of secular terms.i.e. terms that grow polynomially with time and are the consequence of the kinematic pole axiom (3.2.6). This method was first used in [107] and then in [108] for the sine-Gordon model.

Based on (8.0.1) and (8.0.2) one may assume that the one-point functions after a quench exhibit an exponential relaxation, at least for integrable quenches. Unfortunately, both cases discussed seem to be too special, as the magnetisation operator has vanishing expectation value and non-vanishing form factors with odd number of fermions only, and the vertex operators V_a with half-integer a have non-local properties with respect to the solitonic excitations (3.2.5)-(3.2.7), which is extensively used in the computation in [108]. At the moment the relaxation of local operators to their steady state expectation value is not known in general, but in many cases a power-law relaxation is expected instead of an exponential one [87, 108–112], which is consistent with the predictions of the Quench Action approach as well [83].

For an initial state (4.2.7), time evolution of the vertex operator $e^{i\beta\phi/2}$ in the attractive regime of the sine–Gordon model was studied in [109]. In the homogeneous (translationally invariant) quenches considered here, the presence of zero-momentum solitons or anti-solitons is excluded if the initial state is annihilated by the topological charge which is a typical situation including quenches from the ground state of the model with a different coupling. For stationary breathers B_n, however, the one-particle couplings g_{B_n} can appear in (4.2.7). The conclusion of [109] was that besides the relaxation associated with the solitons (8.0.2), one-particle oscillations with a time dependence of the form e^{-imt} are present due to the zero-momentum breathers and m corresponds to the breather mass. These oscillations show an exponential decay with several different relaxation rates. In particular, with only one breather species in the model the contribution of the first breather to the relaxation rate of one-particle oscillations is

$$\tau_{B_1}^{-1} = \frac{m_{B_1}}{\pi}\int_0^\infty d\vartheta\, (1 - S_{B_1B_1}(\vartheta))\, |K_{B_1B_1}(\vartheta)|^2 \sinh\vartheta\ . \tag{8.0.3}$$

As discussed in Section 5, the existence of a one-particle coupling implies a first order pole in the corresponding K function at the origin and as an immediate consequence, the integral in (8.0.3) becomes divergent since $S_{B_1B_1}(0) = -1$. Since this contribution was omitted in [109], the results derived there are eventually incomplete and ill-defined. Even though much of the derivation in [109] remains valid, the singular expressions clearly need to be corrected, which was performed in [110].

In this chapter we implement the same linked-cluster calculation for the one-point functions [107–109], but using finite volume to regularise the singular expression originating from the either the form factors or the K-function. Unfortunately, the proper treatment of the problem. i.e. the calculation of one-point functions after integrable quenches with one-particle coupling (4.2.7) is extremely technical and long, and unlike in [107–109], the calculation of high order terms and hence the resummation of secular contributions has not yet been performed. Focusing primarily on the one-particle oscillations in the expectation value relevant to certain experiments [13] and on the non-oscillatory part of the expectation value related to the diagonal elements in the expectation value, we present results for the time dependence including terms up to five particles. Therefore we concentrate on the case (4.2.7) and hence the presence of zero-momentum terms in the initial state, but the calculation includes the regular case as well, for which it agrees with [107, 108].

The structure of this chapter is the following. In Section 8.1 we perform a linked cluster expansion for the time-dependent one-point function, using a finite volume regularisation which was first introduced in [144]. This allows us to refine the argument of Chapter 5 for the existence of the singularity in Section 8.2, and also the explicit construction of the contributions for $\langle\mathcal{O}(t)\rangle$ up to four particle terms, from which the terms corresponding to one-particle oscillations are extracted. We then consider the five-particle terms, but only present the leading order secular contributions in Section 8.3. Our formulas describing the time evolution are collected and interpreted in Section 8.4, where we address the question of resummation in the linked cluster expansion and attempt to guess its effect on the eventual time evolution. We also generalise our results to cases involving more than one particle species. Finally we discuss a class of secular terms linked to a mechanism analogous to parametric resonance, and summarise our results in Section 8.5. Due to the large amount of tedious calculations involved, most of their details are relegated to appendices. The technical details of the linked cluster expansion and the calculation of the time evolution can be found in Appendices E, F, H, I and J. To confirm the validity of our calculations they were numerically cross-checked at several points; details of these checks are presented in Appendix K. The results presented in this chapter were published in [110].

8.1 Linked cluster calculation in finite volume

To describe the time evolution of expectation values of local operator, we follow the approach developed in [107–109] and apply a linked cluster expansion, combined with the finite volume regularisation scheme used in [165, 188]. The latter is based on the finite volume form factor technique developed in [144]; the ingredients necessary for our calculations are described in Sections 3.3 and 4.3.1.

For a quench starting from an initial state written in terms of post-quench multi-particle states as in (4.2.7), a natural approach to compute the one-point function of a local operator $\mathcal{O}$ is to decompose it into contributions from states with different number of particles, which results in an expansion in terms of form factors of the local operator. However, form factors possess pole singularities due to the presence of disconnected contributions (cf. (3.2.6)), and for quenches with one-particle coupling the K-functions are also singular. As a result, the contributions are ill-defined and need to be regularised, which can be achieved by putting the theory in finite volume, where due to the quantisation of the particle momenta neither the kinematic singularities of the form factors nor the singularities of the pair amplitude contribute directly. The finite volume L can be considered as a physical regulator since for any finite L the theory is sensible and the infinite volume results can be obtained in the limit $L\to\infty$. The expectation value is then written as

$$\begin{aligned}\langle\mathcal{O}(t)\rangle =&\frac{\langle\Omega|\ e^{itH}\mathcal{O}(0)\ e^{-itH}|\Omega\rangle}{\langle\Omega|\Omega\rangle}\\ =&\lim_{L\to\infty}\frac{{}_L\langle\Omega|\ e^{itH}\mathcal{O}(0)\ e^{-itH}|\Omega\rangle_L}{{}_L\langle\Omega|\Omega\rangle_L}\ ,\end{aligned}\tag{8.1.1}$$

which is first evaluated for finite L where one can verify the cancellation of singular terms explicitly and then take the limit $L\to\infty$.

To perform the calculation, one needs an expression for the initial state in finite volume (4.3), which was derived in [165]:

$$\begin{aligned}|\Omega\rangle_L =\mathcal{N}(L)\Big(&|0\rangle_L+\frac{g}{2}\sqrt{mL}|\{0\}\rangle_L+\sum_I K(\vartheta)N_2(\vartheta,L)|\{-I,I\}\rangle_L\\ &+\sum_I\frac{g}{2}K(\vartheta)N_3(\vartheta,L)|\{-I,I,0\}\rangle_L+\frac{1}{2}\sum_{I\neq J}K(\vartheta_1)K(\vartheta_2)N_4(\vartheta_1,\vartheta_2,L)|\{-I,I,-J,J\}\rangle_L\Big)+\dots\ ,\end{aligned}\tag{8.1.2}$$

where I, J are Bethe quantum numbers and we used the notations introduced in Section 4.3. To simplify expressions, we use the following shorthand notation:

$$|\Omega\rangle_L = \mathcal{G}(L) \sum_{n=0}^{\infty} |\Omega\rangle^{(n)} ,$$

where $|\Omega\rangle^{(0)} = |0\rangle_L$, $|\Omega\rangle^{(1)} = \frac{g}{2} N_1(L)|\{0\}\rangle_L$, etc. denote the contributions with a fixed number of particles.

To ensure the convergence of the expansion for high energies one can introduce a further regulator parameter R and consider

$$\langle \mathcal{O}(t,R)\rangle = \frac{\langle\Omega|\ e^{\left(-\frac{R}{2}+it\right)H}\mathcal{O}(0)\ e^{\left(-\frac{R}{2}-it\right)H}|\Omega\rangle}{\langle\Omega|e^{-RH}|\Omega\rangle} , \tag{8.1.3}$$

where $R > 0$. When later the sums on quantum numbers are recast in terms of contour integrals, R ensures that the integrals themselves are convergent and therefore allows appropriate manipulations of the contours. At the end of the calculation the parameter R is sent to zero.

Following the procedure introduced in [189], one can separate contributions indexed by particle number as follows

$$C_{kl} = {}^{(k)}\langle\Omega|e^{\left(-\frac{R}{2}+it\right)H}\mathcal{O}(0)\ e^{\left(-\frac{R}{2}-it\right)H}|\Omega\rangle^{(l)} ,$$

and for a proper normalisation of the state one must also divide by the "partition function"

$$Z = \sum_n Z_n = \sum_n {}^{(n)}_{L}\langle\Omega|e^{-RH}|\Omega\rangle^{(n)}_{L} .$$

In particular for Z, the first few terms are

$$Z_0 = 1 , \qquad Z_1 = \frac{g^2}{4} mLe^{-mR} , \tag{8.1.4}$$

and

$$Z_2 = \sum_I K^*(\vartheta)K(\vartheta)N_2(\vartheta, L)^2 e^{-2mR\cosh\vartheta} . \tag{8.1.5}$$

Let us turn to the issue of the expansion parameter. Whereas in our calculations R is eventually sent to zero at the end, for $\langle\mathcal{O}(t,R)\rangle$ is expected to be well-defined for any finite R. Therefore let us first treat R as a large positive quantity, and introduce the parameters $z = e^{-m(R/2+it)}$ and $\bar{z} = e^{-m(R/2-it)}$. Then the order of C_{kl} is $\bar{z}^k z^l$, and that of Z_n is $(z\bar{z})^n$. The inverse of the partition function, thus can be expanded in powers of $z\bar{z}$ as

$$Z^{-1} = \sum_n \bar{Z}_n ,$$

where the first few terms read

$$\bar{Z}_0 = 1 , \qquad \bar{Z}_1 = -Z_1 , \qquad \bar{Z}_2 = Z_1^2 - Z_2 .$$

Putting these ingredients together, in a finite volume L we obtain

$$\langle\mathcal{O}(t,R)\rangle_L = \frac{1}{Z}\sum C_{kl} = \sum \tilde{D}_{kl} , \tag{8.1.6}$$

where analogously to to [165] and [189], $\tilde{D}_{nm}$ is introduced as

$$\tilde{D}_{kl} = \sum_j C_{k-j,l-j}\bar{Z}_j , \tag{8.1.7}$$

with the first few terms having the form

$$\tilde{D}_{1l} = C_{1l} - Z_1 C_{0,l-1} \ , \qquad l = 1, 2, \dots \ ,$$
$$\tilde{D}_{2l} = C_{2l} - Z_1 C_{1,l-1} + (Z_1^2 - Z_2) C_{0,l-2} \ , \qquad l = 2, 3, \dots \ .$$

Since the $\tilde{D}_{kl}$ are of order $z^k \bar{z}^l$, they must separately be well-defined as $L \to \infty$:

$$D_{kl} = \lim_{L\to\infty} \tilde{D}_{kl} \ , \tag{8.1.8}$$

and so the infinite volume limit can be written as

$$\langle \mathcal{O}(t, R) \rangle = \sum_{k,l} D_{kl} \ .$$

For convenience and later use, we also introduce the quantities

$$\tilde{G}_n = \sum_{l=0}^{n} \tilde{D}_{n-l,l} \ , \tag{8.1.9}$$

whose infinite volume limit is denoted by G_n.

The expressions individual C_{kl} contain finite volume form factors, which in general are given by [144]

$${}_L\langle \{I_1, \dots, I_k | O | \{J_1, \dots, J_l\} \rangle_L = \frac{F^{\mathcal{O}}_{k+l}(\vartheta_1 + i\pi, \dots, \vartheta_k + i\pi, \vartheta'_1, \dots, \vartheta'_l)}{\sqrt{\rho_k(\vartheta_1, \dots, \vartheta_k)\rho_l(\vartheta'_1, \dots, \vartheta'_l)}} + \mathcal{O}(e^{-\mu L}) \ , \tag{8.1.10}$$

where it is understood that the rapidities $\{\vartheta_1, \dots, \vartheta_k\}$ and $\{\vartheta'_1, \dots, \vartheta'_l\}$ are solutions to the corresponding Bethe–Yang equations with quantum numbers $\{I_n\}, \{J_n\}$. Formula (8.1.10) is valid whenever there are no coinciding rapidities; otherwise a more complicated formula taking into account disconnected contributions is necessary. In this paper we are interested in contributions to one-particle oscillations, for which coinciding rapidities cannot occur, and so the numbers of particles in the two multi-particle states differ by an odd number which excludes the two possible cases with disconnected terms (cf. [144]).

Note that the equality (8.1.10) is valid up to a suitably chosen phase factor which can be changed by redefining the phases of the finite volume eigenstates $|\{I_1, \dots, I_n\}\rangle_L$. This includes also the fact that the ordering of the particles is not determined by first principles and any exchange leads to an S-matrix factor according to (3.2.4). It is clear that all such ambiguities cancel in the expectation value (8.1.3); however, for a practical calculation one must fix the phases of the multi-particle contributions to the matrix elements consistently. Here we make use of the consistent prescription introduced in [165]: any time the amplitudes $K(\vartheta_i)$ and $K^*(\vartheta_i)$ appear with some ϑ_i, the explicit order of the rapidities substituted into the relevant form factor is given by $(-\vartheta_i, \vartheta_i)$ and $(\vartheta_i + i\pi, -\vartheta_i + i\pi)$, respectively. Exchanging any two pairs of rapidities does not make any difference, therefore the phase of the form factors is completely fixed by the above rule. Note that the presence of zero-momentum particles does not produce any additional ambiguities.

8.2 Refined argument for the singularity of the pair overlap

Here we revisit the singularity of the two-particle overlap in the presence of a one-particle coupling discussed in Section 5. Our previous argument was based on an analogy with a boundary problem [165] which we can now put on a more firmer footing. Recall that the boundary problem consisted of the calculation of a one-point function within integrable boundary states, where the ordering of the terms was performed according to powers of $e^{-m(\mathcal{R}-x)}$ and e^{-mx}. The resulting expression for $\tilde{D}_{kl}$ is the same as (8.1.7) but with the expansion parameters continued analytically to $z = e^{-m(R/2+it)}$ and $\bar{z} = e^{-m(R/2-it)}$. In the

boundary problem, the existence of the infinite volume limit (8.1.8) and eventually $\langle\mathcal{O}(x)\rangle^B$ requires the presence of the singularity

$$K_B(\vartheta) \sim -\frac{i}{2}\frac{g_B^2}{\vartheta} ,$$

therefore

$$K(\vartheta) \sim -\frac{i}{2}\frac{g^2}{\vartheta}$$

must hold for the quench problem as well. The easiest way to see that is to consider the one-particle contribution $-Z_1$ which behaves as mL. To make $C_{12} - Z_1 C_{01}$ finite in the infinite volume limit, C_{12} must have a similar volume-dependence, which is ensured by the singularity of K involved in C_{12}.

At the end of the calculations the regulator R is sent to zero. The contribution G_n (8.1.9) is of order $|z|^n = (e^{-mR/2})^n$ and (just as in [165]) it turns out that the coefficient of the largest power of the mL term is always of order g^n. Focusing on the behaviour of the singular term, the small parameter of the linked-cluster calculation can be identified with g. As the singularity of the K is of order g^2 one can formally treat K as a term of order g^2. This method of counting the orders results in the same classification of contributions $\tilde{D}_{kl}$ (8.1.9) that is obtained by considering z and $\bar{z}$ as the expansion parameters.

This counting of orders works most obviously in the case of a perturbative quench corresponding to changing the Hamiltonian as

$$\delta H = \lambda \int dx \Psi(x) ,$$

where Ψ is a purely odd operator (i.e. whose form factors with an even number of particles in the pre-quench system is zero). Using perturbation theory to compute the overlaps following [111, 112] the one-particle coupling is of order λ, while the pair amplitude K is of order λ^2.

When the perturbing operator has even matrix elements as well, the pair amplitude can also have a λ order term. Although this term is not singular due to the regular behaviour of $F(i\pi + \vartheta, i\pi - \vartheta)$ at $\vartheta = 0$, at order λ^2 a singular term is present similarly to the one found in Section 5.3 for the phase quenches in the sine-Gordon model. Therefore the zero-rapidity pole singularity of K is generic. It is important that the above arguments do not rely on the integrability of the quench, and only use the translational invariance of the initial state. Hence even in the non-integrable case the presence of the one-particle coupling implies a pole in the pair amplitude with the proper residue.

8.3 Time dependence

The calculation of even the leading order time dependence is extremely technical and long, therefore the detailed computations are relegated to Appendices E-K. Here we merely quote the most important results. We concentrate on the case with a one-particle contribution and therefore a singular K function in the integrable initial state (4.2.7), but the results corresponding to the case of (4.2.6), i.e. the lack of standing particles is easily recovered from the results below.

8.3.1 Contributions up to 4^{th} order: analytic continuation of the boundary result

In this section we construct all the terms up to fourth order using continuing the Euclidean quantities computed in [165]. The contributions D_{kl} for the Euclidean one-point function

$$\langle\mathcal{O}(x)\rangle^B = \frac{\langle B|\ e^{-Hx}\mathcal{O}(0)\ e^{-H(R-x)}\ |B\rangle}{\langle B|e^{-HR}|B\rangle} = \sum_{k,l} D_{kl} \tag{8.3.1}$$

with $k + l \leq 4$ are listed in Appendix F.

For the analytic continuation, we apply the $R \to 0$ and $x \to -it$ substitutions together with $K_B \to K$ and $g_B \to g$ which give

$$\begin{aligned}
G_0: &\quad \langle 0|\mathcal{O}|0\rangle \quad , \\
G_1: &\quad g\,\Re e F_1^{\mathcal{O}} e^{-imt}, \\
G_2: &\quad \frac{g^2}{4}F_2^{\mathcal{O}}(i\pi,0) + \Re e\int_{-\infty}^{\infty}\frac{d\theta}{2\pi}K(\theta)F_2^{\mathcal{O}}(-\vartheta,\vartheta)e^{-imt2\cosh\vartheta}\ , \\
G_3: &\quad \frac{g}{2}\Re e\int_{-\infty}^{\infty}\frac{d\vartheta}{2\pi}K(\vartheta)F_3^{\mathcal{O}}(-\vartheta,\vartheta,0)e^{-imt(2\cosh\vartheta+1)}\ , \\
&\quad + \frac{g}{2}\Re e\int_{-\infty}^{\infty}\frac{d\vartheta}{2\pi}\left\{K(\vartheta)F_3^{\mathcal{O}}(i\pi,-\vartheta,\vartheta)e^{-imt(2\cosh\vartheta-1)} - 2g^2\frac{\cosh\vartheta}{\sinh^2\vartheta}F_1^{\mathcal{O}}e^{-imt}\right\} \\
&\quad + 2g^3\varphi(0)\Re e F_1^{\mathcal{O}}e^{-imt}\ , \\
G_4: &\quad \frac{1}{4}\Re e\int_{-\infty}^{\infty}\frac{d\vartheta_1}{2\pi}\frac{d\vartheta_2}{2\pi}K(\vartheta_1)K(\vartheta_2)F_4^{\mathcal{O}}(-\vartheta_1,\vartheta_1,-\vartheta_2,\vartheta_2)e^{-imt(2\cosh\vartheta_1+2\cosh\vartheta_2)} \\
&\quad + \frac{g^2}{4}\Re e\int_{-\infty}^{\infty}\frac{d\vartheta}{2\pi}K(\vartheta)F_4^{\mathcal{O}}(-\vartheta+i\pi,\vartheta+i\pi,i\pi,0)e^{-imt2\cosh\vartheta} \\
&\quad + \frac{1}{4}\int_{-\infty}^{\infty}\frac{d\vartheta_1}{2\pi}\frac{d\vartheta_2}{2\pi}K(\vartheta_1)K(\vartheta_2)F_4^{\mathcal{O}}(i\pi-\vartheta_1 i\pi+\vartheta_1,-\vartheta_2,\vartheta_2)e^{imt2(\cosh\vartheta_1-\cosh\vartheta_2)} \\
&\quad + F_2^{\mathcal{O}}(i\pi,0)\int_{-\infty}^{\infty}\frac{d\vartheta}{2\pi}\left\{|K(\vartheta)|^2 - \frac{g^4\cosh\vartheta}{4\sinh^2\vartheta}\right\} \\
&\quad + \frac{g^4}{8}F_2^{\mathcal{O}}(i\pi,0)\varphi(0) \quad ,
\end{aligned} \tag{8.3.2a}$$

$$\tag{8.3.2b}$$

where $F_{2,s}^{\mathcal{O}} = F_2^{\mathcal{O}}(i\pi,0)$ and

$$\varphi(\vartheta) = -i\frac{\partial\log S(\vartheta)}{\partial\vartheta}\ . \tag{8.3.2c}$$

Note that these integrals remain well-defined even when there is a pole in the amplitude $K(\vartheta)$ at $\vartheta = 0$ because the form factors possess a zero $\vartheta_i = 0$ as a consequence of the exchange axiom (3.2.4) and the general property $S(0) = -1$. Concerning the large rapidity behaviour, normalizability of the initial state requires that K tends to zero fast enough for large ϑ ensuring the existence of the integrals.

We now turn to analysing the time dependence originating from (8.3.2). Due to the oscillatory integrands it is convenient to apply the stationary phase approximation (SPA) briefly discussed in Appendix E.4. Both SPA and direct analysis leads to the following type of terms expected from (8.3.2):

$$e^{-inmt}t^{\alpha}\ , \tag{8.3.3}$$

where α is either integer or half integer and n is an integer. For terms D_{kl} the lower bound of the oscillation frequency is always $nm = (k-l)m$.

As our main objective is to study the time dependence of one-particle oscillations, we concentrate here on terms with $n = 1$ but we will also briefly comment on the time dependence of the non-oscillatory part of $\langle\mathcal{O}\rangle$. The non-oscillatory parts include the static contributions

$$\begin{aligned}
G_0: &\quad \langle 0|\mathcal{O}|0\rangle\ , \\
G_2: &\quad \frac{g^2}{4}F_2^{\mathcal{O}}(i\pi,0)\ , \\
G_4: &\quad F_2^{\mathcal{O}}(i\pi,0)\int_{-\infty}^{\infty}\frac{d\vartheta}{2\pi}\left\{|K(\vartheta)|^2 - \frac{g^4\cosh\vartheta}{4\sinh^2\vartheta}\right\} \\
&\quad + \frac{g^4}{8}F_2^{\mathcal{O}}(i\pi,0)\varphi(0)\ ,
\end{aligned} \tag{8.3.4}$$

whereas for the only time dependent integral,

$$\frac{1}{4}\int_{-\infty}^{\infty}\frac{d\vartheta_1}{2\pi}\frac{d\vartheta_2}{2\pi}K(\vartheta_1)K(\vartheta_2)F_4^{\mathcal{O}}(i\pi-\vartheta_1 i\pi+\vartheta_1,-\vartheta_2,\vartheta_2)e^{imt2(\cosh\vartheta_1-\cosh\vartheta_2)}\,, \tag{8.3.5}$$

the SPA (E.4.1) can be applied, yielding

$$\frac{\mathcal{C}}{16\pi mt}\,,\qquad 1\ll mt\,, \tag{8.3.6}$$

where

$$\mathcal{C}=\lim_{\vartheta_2\to 0}\lim_{\vartheta_1\to 0}K(\vartheta_1)K(\vartheta_2)F_4^{\mathcal{O}}(i\pi-\vartheta_1 i\pi+\vartheta_1,-\vartheta_2,\vartheta_2) \tag{8.3.7}$$

which is finite. Notice, that if there are no zero-momentum particles in the initial state, i.e. no pole in K, then the $1/t$ is modified to $1/t^3$.

For terms with one-particle oscillation, one finds

$$\begin{aligned}
&G_1: \quad g\Re e\, F_1^{\mathcal{O}}e^{-imt}\,,\\
&G_3: \quad 2g^3\varphi(0)\Re e\, F_1^{\mathcal{O}}e^{-imt}\\
&\qquad +\frac{g}{2}\Re e\int_{-\infty}^{\infty}\frac{d\vartheta}{2\pi}\left\{K(\vartheta)F_3^{\mathcal{O}}(i\pi,-\vartheta,\vartheta)e^{-imt(2\cosh\vartheta-1)}-2g^2\frac{\cosh\vartheta}{\sinh^2\vartheta}F_1^{\mathcal{O}}e^{-imt}\right\}.
\end{aligned} \tag{8.3.8}$$

For the last term, SPA cannot be applied directly, therefore we shift the contour off the real axis where (as shown in [165]) the contribution from the term

$$\frac{\cosh\vartheta}{\sinh^2\vartheta}$$

vanishes and reintroduce the regulator R. We rewrite the resulting expression using (E.3.4) after which the SPA (E.4.1) can be applied, and finally perform the $R\to 0$ limit. The result is

$$\frac{g^3F_1^{\mathcal{O}}\left(\varphi^2(0)-2/3\right)}{2\sqrt{4\pi mt}}\Re e\, e^{-imt}e^{-i\pi/4}+g^3\sqrt{\frac{mt}{\pi}}\Re e\, F_1^{\mathcal{O}}e^{-imt}\frac{-\sqrt{2}-\sqrt{2}i}{2}\,,\qquad mt\gg 1\,. \tag{8.3.9}$$

For a more detailed derivation, the interested reader is referred to in Appendix G. While the first term has the standard $\sim 1/\sqrt{t}$ time dependence, the second one behaves as $\sim\sqrt{t}$ for large time. We return to this peculiar finding in Sec. 8.4.3.

8.3.2 Leading order time dependence from G_5

The contributions involving five particles are D_{05}, D_{14}, D_{23} and their complex conjugates D_{50},D_{41}, D_{32} . Based on (8.1.7), the expressions to evaluate are

$$\begin{aligned}
D_{05}&=\lim_{L\to\infty}C_{05}\\
D_{14}&=\lim_{L\to\infty}C_{14}-Z_1C_{03}\\
D_{23}&=\lim_{L\to\infty}C_{23}-Z_1C_{12}-(Z_2-Z_1^2)C_{01}\,.
\end{aligned} \tag{8.3.10}$$

The calculation of these expressions is very tedious; even in Appendices H, I and J where the details of the calculations are presented, we focused only on leading secular contributions to the one-particle oscillations, i.e. terms of the form $e^{-imt}t^\alpha$ with the highest power α. As one-particle oscillations originate exclusively from D_{kl} with $|k-l|=1$, we can focus on D_{23} and its conjugate D_{32}.

The leading order secular terms originate from two sources: a residue contribution from encircling the poles of the form factors $F_5(i\pi+\vartheta_1, i\pi-\vartheta_1, -\vartheta_2, \vartheta_2, 0)$ when $\vartheta_1 \approx \vartheta_2$ and a contribution from these poles when a contour integral is performed with an integration contour just above the real axis.

Concerning the first term, the explicit expression reads

$$D_{23}^{Res}(t) = \frac{g}{2} F_1^{\mathcal{O}} e^{-imt}\,(imt) \int_{-\infty}^{\infty} \frac{d\vartheta}{2\pi} |K(\vartheta)|^2 \Im\mathrm{m} S(\vartheta) \sinh\vartheta\,, \tag{8.3.11}$$

whose derivation can be found in Appendix H. Unlike time dependent terms discussed so far, deriving (8.3.11) involves no SPA and so it is also valid for small times. Note that the coefficient of the oscillatory factor e^{-imt} is purely imaginary and linear in time.

For the other term denoted by $D_{23}^{CInt}(t)$, the explicit formula reads

$$\begin{aligned} D_{23}^{CInt}(t) =& \frac{g}{2} F_1^{\mathcal{O}} e^{-imt}\,(-imt) \int_{-\infty}^{\infty} \frac{d\vartheta}{2\pi} |K(\vartheta)|^2 \tanh(\vartheta_1)\,(Ker_a(\vartheta,t))' \\ &+ \frac{g}{2} F_1^{\mathcal{O}} e^{-imt}\,(-imt) \int_{-\infty}^{\infty} \frac{d\vartheta}{2\pi} |K(\vartheta)|^2 Ker(\vartheta,t) \\ &+ \frac{g}{2} F_1 e^{-imt} \int_{-\infty}^{\infty} \frac{d\vartheta}{2\pi} \frac{1}{4\sinh\vartheta} \frac{d}{d\vartheta} \Big\{ |K(\vartheta)|^2 \Re e\, Ker(\vartheta,t,0) \times \\ &\qquad \times \Re e \left(\frac{F_5^{\varepsilon}(\vartheta)}{F_1\Omega(\vartheta)} + \frac{K'(\vartheta)}{K(\vartheta)} - \frac{F_5^{\varepsilon}(-\vartheta)}{F_1\Omega(\vartheta)} - \frac{K'(-\vartheta)}{K(-\vartheta)} \right) \tanh\vartheta \Big\} \\ &+ \mathcal{O}(\sqrt{t}) \quad , \end{aligned} \tag{8.3.12}$$

where

$$Ker^a(\vartheta_1,t) = \lim_{R\to 0} e^{imt}\Omega(\vartheta_1) \int_{-\infty}^{\infty} \frac{d\vartheta_2}{2\pi} \frac{\left[h(\vartheta_1|\vartheta_2,\{0\})_R \left(\sinh\vartheta_2 - \frac{\sinh\vartheta_1}{\cosh\vartheta_2 - \vartheta_1} \right) \right]}{\sinh\vartheta_2 - \vartheta_1}\,, \tag{8.3.13}$$

and

$$Ker(\vartheta_1,t) = e^{imt}\Omega(\vartheta_1) \int_{-\infty}^{\infty} \frac{d\vartheta_2}{2\pi} \frac{[h(\vartheta_1|\vartheta_2,\{0\}) - h(\vartheta_1|\vartheta_1,\{0\})] \sinh\vartheta_1}{\sinh(\vartheta_2-\vartheta_1)\cosh(\vartheta_2-\vartheta_1)} \tag{8.3.14}$$

with

$$\Omega(\vartheta) = (1 - S(-\vartheta))\,(1 - S(\vartheta))\,, \tag{8.3.15}$$

$$h(\vartheta_1|\vartheta_2,\{0\})_R = e^{imt(2\cosh\vartheta_1 - 2\cosh\vartheta_2 - 1)} e^{-mR/2(2\cosh\vartheta_1 + 2\cosh\vartheta_2 + 1)}\,, \tag{8.3.16}$$

$$h(\vartheta_1|\vartheta_2,\{0\}) = h(\vartheta_1|\vartheta_2,\{0\})_{R=0}\,. \tag{8.3.17}$$

Their derivation can be found in Appendices I and J. It is shown in Appendix J that in the large time limit $mt \gg 1$ the integral kernels behave as

$$Ker^a_{stac}(\vartheta,t) = e^{imt}\Omega(\vartheta) \frac{1}{\sqrt{4\pi mt}} \frac{e^{2imt(\cosh\vartheta - 1)} e^{-i\pi/4}}{\cosh\vartheta}, \quad 1 \ll mt\,, \tag{8.3.18}$$

and

$$
\begin{aligned}
Ker_{stac}(\vartheta,t) =& \frac{\sqrt{2(\cosh\vartheta-1)}}{\cosh\vartheta}\Omega(\vartheta) \\
&\times\left\{\frac{1}{2}\left(F_S\left(\sqrt{\frac{4mt(\cosh(\vartheta)-1)}{\pi}}\right)-F_C\left(\sqrt{\frac{4mt(\cosh(\vartheta)-1)}{\pi}}\right)\right)\right. \\
&-\frac{1}{2}i\left(F_C\left(\sqrt{\frac{4mt(\cosh(\vartheta)-1)}{\pi}}\right)+F_S\left(\sqrt{\frac{4mt(\cosh(\vartheta)-1)}{\pi}}\right)\right) \\
&\left.+i\left(\frac{1}{2}-\frac{\cosh\vartheta\sqrt{\sinh^2\vartheta}}{2\sqrt{2(\cosh(\vartheta)-1)}}\right)\right\}, \quad 1\ll mt\,,
\end{aligned}
\tag{8.3.19}
$$

where F_S and F_C are the Fresnel sine and cosine functions, respectively. This leads to the final result

$$
D_{23}(t)=\frac{g}{2}F_1^{\mathcal{O}}e^{-imt}mt\left(\frac{g^4}{4}\left(-\frac{\log(mt)}{\pi}\right)+\gamma_1+i\gamma_2\right)+\mathcal{O}(e^{-imt}\sqrt{t}) \tag{8.3.20}
$$

with

$$
\begin{aligned}
\gamma_1 =& \mathcal{K}+\frac{g^4}{4}\frac{3}{\pi}\,, \\
\gamma_2 =& \frac{g^4}{8}+\int_{-\infty}^{\infty}\frac{d\vartheta}{2\pi}|K(\vartheta)|^2\Im m\, S(\vartheta)\sinh\vartheta\,,
\end{aligned}
\tag{8.3.21}
$$

where

$$
\begin{aligned}
\mathcal{K}=\lim_{t\to\infty}\left\{-\frac{1}{2}\int_{-\infty}^{\infty}\frac{d\vartheta}{2\pi}\Omega(\vartheta)|K(\vartheta)|^2\left[\frac{\sqrt{2(\cosh\vartheta-1)}}{\cosh\vartheta}\times\right.\right. \\
\left.\left(F_C\left(\sqrt{\frac{4mt(\cosh(\vartheta)-1)}{\pi}}\right)+F_S\left(\sqrt{\frac{4mt(\cosh(\vartheta)-1)}{\pi}}\right)-1\right)+\sqrt{\sinh^2\vartheta}\right] \\
\left.+\frac{g^4}{4}\left(\frac{\log(mt)}{\pi}\right)\right\}\,.
\end{aligned}
\tag{8.3.22}
$$

8.4 Discussion of the results

Before discussing the time evolution of the one-point function, we collect the leading order time-dependent contributions for the non-oscillatory and one-particle-oscillatory part of $\langle\mathcal{O}\rangle$ from each term D_{kl} we considered in the previous section. In the long-time limit $1\ll mt$, these are

$$
\begin{aligned}
G_0:&\quad \langle 0|\mathcal{O}|0\rangle\,, \\
G_2:&\quad \frac{g^2}{4}F_2^{\mathcal{O}}(i\pi,0)\,, \\
G_4:&\quad F_2^{\mathcal{O}}(i\pi,0)\int_{-\infty}^{\infty}\frac{d\vartheta}{2\pi}\left\{|K(\vartheta)|^2-\frac{g^4\cosh\vartheta}{4\sinh^2\vartheta}\right\}+\frac{g^4}{8}F_2^{\mathcal{O}}(i\pi,0)\varphi(0) \\
&+\frac{\mathcal{C}}{16\pi mt}\,,
\end{aligned}
\tag{8.4.1}
$$

and

$$\begin{aligned} G_1: &\quad g\Re e\, F_1^{\mathcal{O}} e^{-imt}\,, \\ G_3: &\quad 2g^3\varphi(0)\Re e\, F_1^{\mathcal{O}} e^{-imt} \\ &\quad +g^3\sqrt{\frac{mt}{\pi}}\Re e\, F_1^{\mathcal{O}} e^{-imt}\frac{-\sqrt{2}-\sqrt{2}i}{2} \\ &\quad +\mathcal{O}(1/\sqrt{t})\,, \\ G_5: &\quad g\Re e\, F_1^{\mathcal{O}} e^{-imt} mt\left(\frac{g^4}{4}\left(-\frac{\log(mt)}{\pi}\right)+\gamma_1+i\gamma_2\right) \\ &\quad +\mathcal{O}(\sqrt{t})\,, \end{aligned} \tag{8.4.2}$$

where $\mathcal{C}$ is given in (8.3.7) and $\gamma_{1,2}$ in (8.3.21).

In the non-oscillatory terms given by G_0, G_2 and G_4 up to the four-particle contribution there is no secular term which grows with t. The only explicitly time dependent term behaves as $1/t$ or $1/t^3$ depending on if the squeezed-coherent initial state contains one-particle states or not. Without the knowledge of the terms G_6 and G_8, it is difficult to reach a final conclusion about the time evolution, but the result is consistent with a power-law relaxation. Even if the finite volume regularised linked cluster calculation only yields an asymptotic series of the eventual time evolution, our results predict a $1/t$ behaviour in the time window $1 \ll mt \ll g^{-4}$, or a $1/t^3$ time dependence if $1 \ll mt \ll K^{-2}$, K denoting the typical magnitude of the K-function.

In the preceding subsections we studied terms with one-particle oscillations and found that the long time asymptotics of the leading order contributions to oscillations contain, besides the original oscillation e^{-imt} from G_1, two new types of terms: one with time dependence $\sqrt{t}e^{-imt}$ from G_3 and terms of time dependence te^{-imt} and $t\ln te^{-imt}$ from G_5.

Since these are secular terms growing for large t, it is necessary to sum up higher order contributions coming from G_{2n+1}. Computing terms G_7 and higher is extremely tedious and has not yet been performed, therefore we can only present a limited discussion of their resummation based on insights gained from earlier works [107–109].

One could also try to get some hints by analysing the $FM \to PM$ quench in the Ising model considered in Subsection 5.2; however, we show that this is unfortunately not possible. In Section 5.2 it was shown that in the continuum limit the time evolution of the magnetisation is

$$\langle\sigma^x(x,t)\rangle = \bar{\sigma}\left(\frac{1}{2}\right)^{\frac{1}{4}}\left(\frac{M_0}{M}\right)^{\frac{1}{8}}\left[\cos\left(\sqrt{M^2+MM_0}t+\alpha'\right)+...\right]e^{-t/\tau}\,, \tag{8.4.3}$$

where the relaxation time is given by

$$\tau^{-1} = \frac{1}{\pi}\left\{\sqrt{M^2+M\,M_0}\ln\left(\frac{\sqrt{M^2+M\,M_0}+M}{\sqrt{M^2+M\,M_0}-M}\right)-\frac{1}{2}\sqrt{M^2-M_0^2}\ln\left(\frac{M+\sqrt{M^2-M_0^2}}{M-\sqrt{M^2-M_0^2}}\right)\right\} \tag{8.4.4}$$

for $M > M_0$ and

$$\tau^{-1} = \frac{1}{\pi}\left\{\sqrt{M^2+M\,M_0}\ln\left(\frac{\sqrt{M^2+M\,M_0}+M}{\sqrt{M^2+M\,M_0}-M}\right)-\sqrt{M_0^2-M^2}\left[\tan^{-1}\left(\frac{M}{\sqrt{M_0^2-M^2}}\right)-\frac{\pi}{2}\right]\right\} \tag{8.4.5}$$

for $M < M_0$. At first sight, since the K function is known for this particular quench, the expansion of (8.4.3) can be matched with the form factor expansion evaluated in our work. However, note that (8.4.3)

and (8.4.4) are non-analytic functions of the pre-quench mass M_0 around the origin, and therefore are also non-analytic in g around $g = 0$ due to the relation (5.2.17). This is not surprising since a quench across a quantum critical point is expected to be a large quench with potentially non-analytic behaviour, and therefore the form factor expansion is not expected to be valid at all. This situation is in marked contrast with the phase quenches in the sine–Gordon model considered in Subsection 5.3 where the shift δ/β can play the role of a small parameter.

8.4.1 Connection with previous results and discussion of possible resummation of G_{4n+1}

Considering first the contributions G_{4n+1} one-particle oscillations originate from the terms $D_{2n,2n+1}$. In [109] these terms served as the sole source of secular terms which were shown to sum up to an exponential function to order t^2, i.e. the result including the two leading order corrections had the form

$$\Re e\, \frac{g}{2} F_1^{\mathcal{O}} e^{-imt} \left(1 - \frac{t}{\tau} + \frac{1}{2}\frac{t^2}{\tau^2} + \dots\right)$$

which is the expansion of

$$\Re e\, \frac{g}{2} F_1^{\mathcal{O}} e^{-imt} e^{-t/\tau} \ ,$$

where

$$\tau^{-1} = \frac{m}{\pi} \int_0^\infty d\vartheta \, (1 - S(\vartheta)) \, |K(\vartheta)|^2 \sinh\vartheta \ . \tag{8.4.6}$$

The real part of the above integral is the relaxation time, while the imaginary part is a frequency shift. It is easy to see that sending $g \to 0$ in our expressions (8.3.20), which is equivalent to removing the singularity of K, reproduces the result for τ above as the integrand is non-singular and

$$\lim_{x\to\infty} F_C(x) = \lim_{x\to\infty} F_S = \frac{1}{2} \ . \tag{8.4.7}$$

The relaxation time (8.4.6) originates from the kinematic singularities (i.e. disconnected pieces) of the form factors. In our calculation we have a singularity from K which results in some new contributions according to (8.3.20). Assuming an exponentiation similar to that observed in [107–109], the leading order time dependence from G_{4n+1} is

$$D_{2n,2n+1}(t) = \frac{g}{2} F_1^{\mathcal{O}} e^{-imt} \frac{(mt)^n}{n!} \left(-\frac{g^4}{4}\frac{\log(mt)}{\pi} + \gamma_1 + i\gamma_2\right)^n + \dots \ , \tag{8.4.8}$$

which can be resummed into

$$\frac{g}{2} F_1^{\mathcal{O}} e^{-imt} \exp\left[mt\left(-\frac{g^4}{4}\frac{\log(mt)}{\pi} + \gamma_1 + i\gamma_2\right)\right] \ . \tag{8.4.9}$$

Therefore, besides the frequency shift, the relaxation for late time is naively expected to be super-exponential with a dependence of the form $e^{-t\ln t}$. This means that τ^{-1} in (8.4.6) is to be replaced with $m\left(\frac{g^4}{4}\frac{\log(mt)}{\pi} - \gamma_1 - i\gamma_2\right)$ in the exponential function. However, this cannot be concluded safely without computing at least $D_{45}(t)$ and checking whether one obtains the correct combinatorial coefficients for the terms involving higher powers of $-\frac{g^4}{4}\frac{\log(mt)}{\pi}mt$, which is the condition for exponentialisation. Based on analogy with [109], one can argue that terms containing $\gamma_{1,2}$ exponentialise and their resummation leads to a relaxation rate and a frequency shift; however, the fate of the logarithmic term cannot be decided without examining higher order contributions, whose straightforward evaluation is extremely complicated. Assuming that the relaxation is of the usual exponentially decaying form (i.e. the logarithmic part does not exponentialise) also means that it is not clear at the moment what part of the real terms (involving γ_1) exponentialises and determines the relaxation rate.

8.4.2 Multiple species

It is easy to generalise our results to the case of multiple species following the reasoning in [109] which studied relaxation in the attractive regime of the sine–Gordon model for operators semi-local to soliton excitations (and consequently local with respect to the soliton–anti-soliton bound states, i.e. the breathers B_n). In the following we write down the result for semi-local operators

$$\begin{aligned}\langle\mathcal{O}(t)\rangle =&\left(\langle 0|\mathcal{O}|0\rangle+\sum_j \frac{g_j^2}{4}F_{jj}^{\mathcal{O}}(i\pi,0)\right)\left[1-\frac{t}{\tau_s}+...\right]\\ &+\sum_j g_j\Re e\left\{F_j^{\mathcal{O}}e^{-im_jt}\left[1-\frac{t}{\tau_{sj}}-\sum_k\frac{t}{\tau_{jk}}+...\right]\right\}\\ &+\sum_{j\neq k}\frac{g_jg_k}{2}\Re e\left\{F_{jk}^{\mathcal{O}}(i\pi,0)e^{i(m_j-m_k)t}\left[1-\frac{t}{\tau_{jks}}-\sum_l\frac{t}{\tau_{jkl}}+...\right]\right\}\ ,\end{aligned} \tag{8.4.10}$$

where

$$\begin{aligned}\tau_s^{-1}=&\frac{2m_s}{\pi}\int_0^\infty d\vartheta|K_{s\bar{s}}(\vartheta)|^2\sinh\vartheta\ ,\\ \tau_{sj}^{-1}=&\frac{m_s}{\pi}\int_0^\infty d\vartheta\left(1+S_{sj}(\vartheta)\right)|K_{s\bar{s}}(\vartheta)|^2\sinh\vartheta\ ,\\ \tau_{jk}^{-1}=&\frac{m_j}{\pi}\int_0^\infty d\vartheta\left(1-S_{jk}(\vartheta)\right)|K_j(\vartheta)|^2\sinh\vartheta\ ,\qquad j\neq k\ ,\\ \tau_{jks}^{-1}=&\frac{m_s}{\pi}\int_0^\infty d\vartheta\left(1+S_{sj}(\vartheta)S_{sk}(-\vartheta)\right)|K_{s\bar{s}}(\vartheta)|^2\sinh\vartheta\ ,\\ \tau_{jkl}^{-1}=&\frac{m_l}{\pi}\int_0^\infty d\vartheta\left(1-S_{kl}(\vartheta)S_{jl}(-\vartheta)\right)|K_l(\vartheta)|^2\sinh\vartheta\ ,\qquad j\neq l,k\neq l\ ,\end{aligned} \tag{8.4.11}$$

and

$$\begin{aligned}\tau_{jj}^{-1}(t)=&-m_j\left(-\frac{g_j^4}{4}\frac{\log(m_jt)}{\pi}+\gamma_1^{(j)}+i\gamma_2^{(j)}\right)\ ,\\ \tau_{lkl}^{-1}(t)=\tau_{kll}^{-1}(t)=&-m_l\left(-\frac{g_l^4}{4}\frac{\log(m_lt)}{\pi}+\gamma_1^{(llk)}+i\gamma_2^{(llk)}\right)\ ,\end{aligned} \tag{8.4.12}$$

where j,k,l,o index breather excitations, and $\gamma_{1,2}^{(n)}$ are obtained by substituting S in (8.3.21) with the B_n-B_n scattering amplitude S_{nn} and g with the B_n one-particle coupling g_n. The expressions for $\gamma_1^{(llk)}$ and $\gamma_2^{(llk)}$ are obtained from (8.3.21), by replacing g with g_j and also

$$\Omega(\vartheta)=\left(1-S(\vartheta)\right)\left(1-S(-\vartheta)\right)\to\left(1-S_{lk}(\vartheta)S_{ll}(-\vartheta)\right)\left(1-S_{ll}(\vartheta)S_{lk}(-\vartheta)\right) \tag{8.4.13}$$

in (8.3.13) and (8.3.14); in addition, in the residue term D_{23}^{Res} (8.3.11) it is necessary to replace

$$\Im m\,S(\vartheta)\to\frac{1}{2i}\left(S_{ll}(\vartheta)S_{lk}(-\vartheta)-S_{ll}(-\vartheta)S_{lk}(\vartheta)\right)\ . \tag{8.4.14}$$

Since solitons can have no one-particle coupling in the quench due to topological charge conservation, the amplitude $K_{s\bar{s}}$ is regular at the origin.

Note that the (8.4.11) are identical to the results in [109]. It is easy to understand this from the fact the expressions given in [109] for τ_{jk}^{-1} with $j \neq k$ and for τ_{jkl}^{-1} with $j \neq l, k \neq l$, are regular even if the K_j are singular. The only terms to be revised are τ_{jj}^{-1} and τ_{lkl}^{-1} where the naive application of (8.4.11) results in divergent contributions and must be modified using our calculations performed above.

Results for theories with multiple species with fully diagonal scattering can be obtained by omitting the solitonic contributions from the above results and replacing the breathers with the actual particle spectrum.

8.4.3 Parametric resonance

Finally, we turn to contribution (8.3.9) from G_3

$$g^3\sqrt{\frac{mt}{\pi}}\Re e\, F_1^{\mathcal{O}} e^{-imt}\frac{-\sqrt{2}-\sqrt{2}i}{2} \qquad mt \gg 1\,. \tag{8.4.15}$$

The origin of this term is the integral

$$\frac{g}{2}\Re e\int_{-\infty}^{\infty}\frac{d\vartheta}{2\pi}\left\{K(\vartheta)F_3^{\mathcal{O}}(i\pi,-\vartheta,\vartheta)e^{-imt(2\cosh\vartheta-1)} - 2g^2\frac{\cosh\vartheta}{\sinh^2\vartheta}F_1^{\mathcal{O}}e^{-imt}\right\}\,, \tag{8.4.16}$$

which is derived from a finite volume contribution of the form

$$\sum_{I>0}\langle\{0\}|\mathcal{O}|\{-I,I\}\rangle_L N_2(\vartheta,L)K(\vartheta)e^{-imt(2\cosh\vartheta-1)}\,, \tag{8.4.17}$$

where ϑ is determined by the quantisation rule

$$mL\sinh\vartheta + \delta(2\vartheta) = 2\pi I\,.$$

Let us recall the phenomenon of parametric resonance, for which the simplest example is the Mathieu equation describing a system with only one degree of freedom,

$$\frac{d^2x}{dt^2} + \left[\omega_0^2 - 2q\cos\omega_p t\right]x = 0\,. \tag{8.4.18}$$

This equation has a region of instability in which the solution of the equation oscillates with an exponentially growing amplitude. This region is when the ratio ω_p/ω_0 is sufficiently close to 2, where the width of the region of proportional to q.

It is clear that the term (8.4.17) couples the one-particle mode with the two-particle modes and satisfies the condition for resonance on the threshold; however, the interplay between the integration over rapidity and the singularity of the form factor $F_3^{\mathcal{O}}(i\pi,-\vartheta,\vartheta)$ results in a growth of $\sqrt{t}$ instead of being exponential. This cannot be the final story: since a quench pumps a finite energy density in the system, the oscillations cannot grow without bound and therefore higher terms G_{4n+1} must modify this behaviour to keep the amplitude bounded. Since at present we do not have control over these higher order terms, we cannot predict the eventual fate of this class of contributions.

A heuristic analogy can be drawn by noting that in the Mathieu equation the driving oscillator is external, while in the quench the two-particle modes are also dynamical and the total energy stored in the system is conserved. A closer analogy for this dynamics is provided by the following system of differential equations describing two non-linearly coupled modes

$$\frac{d^2x}{dt^2} + \left[\omega_1^2 + qy\right]x = 0 \qquad \frac{d^2y}{dt^2} + \omega_2^2 y + \frac{q}{2}x^2 = 0\,.$$

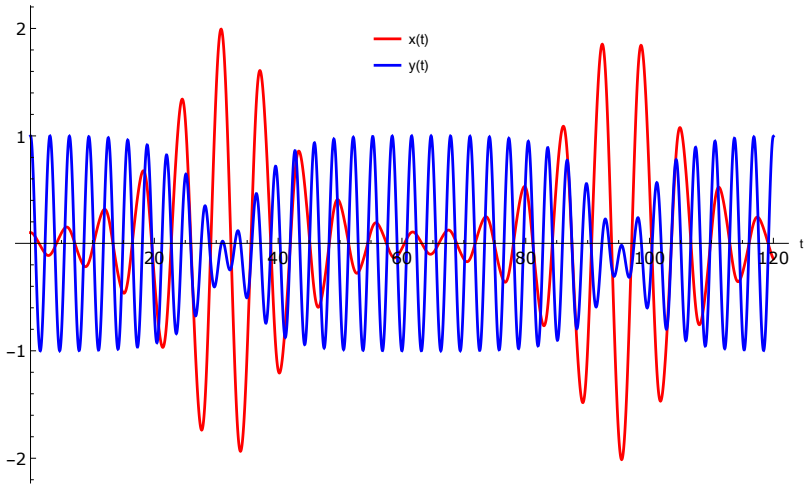

Figure 8.4.1: An example of a parametric resonance in a closed system with two modes. The frequencies are chosen $\omega_1 = 1$ and $\omega_2 = 2$, corresponding to parametric resonance, while the mode coupling is $q = 0.5$. Initial conditions for the particular motion shown are $x(0) = 0.1$, $y(0) = 1$ and $\dot{x}(0) = \dot{y}(0) = 0$.

The mode x is parity odd and is the analogue of the one-particle mode, while the mode y is parity even and is the analogue of the two-particle mode. Depending on the choice of the parameters, this system has solutions in which the energy stored in the modes shows an oscillatory behaviour in time. With the choice $\omega_2 = 2\omega_1$ the condition of parametric resonance is satisfied, but in contrast to the Mathieu equation, the system has a total energy

$$H = \frac{1}{2}\left(\dot{x}^2 + \omega_1^2 x^2\right) + \frac{1}{2}\left(\dot{y}^2 + \omega_2^2 y^2\right) + \frac{q}{2} y x^2$$

which is conserved since the driving and driven modes now form a closed system. An example of a resonance solution is shown in Fig. 8.4.1; notice the long plateau in the amplitude of the driving mode y showing the non-linearity of this system. This is in contrast to linearly coupled oscillators where the energy transfer would itself have a harmonic dependence on time.

It is an interesting question whether in the full quench situation such a non-trivial behaviour can be observed in the time evolution for some choice of the parameters. Since the $\sqrt{t}$ term is of order g^2 and the next secular contribution is of order g^4, it is quite possible that for small enough quenches there is some intermediate time window in which the parametric resonance dominates. To study this requires the detailed analysis and resummation of higher order terms which is left for further investigation.

8.5 Summary

In this chapter we studied the time evolution of one-point functions of local operators in massive IQFTs after integrable quenches. We first reviewed the already existing results and then moved onto the explicit computation of the time evolution of one-point functions focusing on mainly the one-particle oscillations with time dependence e^{-imt} in integrable initial states with one-particle coupling. Part of our motivation was to correct previous results which ignored the singularity in the K-function and hence gave divergent expressions for various quantities. We used a modification of the linked cluster expansion introduced in [107–109], where instead of rapidity space point splitting, we applied a finite volume regulator first proposed in [144]. The advantage of this regulator is that it uses a physical parameter, i.e. the system size L, and since the thermodynamic limit must be well-defined, the computed one-point function must have a finite limit as $L \to \infty$. The cancellation of terms containing positive powers of the volume (resulting from kinematical singularities) provides an important consistency check for the computation.

We found a $1/t$ type time dependence for the non-oscillatory part which modifies to $1/t^3$ in the absence

of the one particle coupling. The $1/t^3$ contribution was found also in Ref. [83], but it varies depending on the properties of form factors between highly excited states, which is quite non-trivial. When the one-particle coupling is non-zero in the initial state, oscillatory terms with the angular frequency related to the particle mass are also present and two important secular contributions were found to the one-particle oscillations. The first one takes the following form at leading order

$$\Re e\, g F_1^{\mathcal{O}} e^{-imt} mt \left(-\frac{g^4}{4} \frac{\log(mt)}{\pi} + \gamma_1 + i\gamma_2 \right) . \tag{8.5.1}$$

The terms γ_1 and γ_2 are directly analogous to the contributions found in [109], with two essential differences. First, the integrals expressing the coefficients $\gamma_{1,2}$ are now entirely well-defined. If there was no pole in $K(\vartheta)$ (which we argued to be impossible for $g \neq 0$), these terms would reduce to the expressions given in [109]. The second difference is the presence of the logarithmic time-dependence for $g \neq 0$. In analogy to [109] it is expected that either higher order terms G_{4n+1} get resummed to an exponential function $e^{-t/\tau}$ with $\tau^{-1} \to m \left(\frac{g^4}{4} \frac{\log(mt)}{\pi} - \gamma_1 - i\gamma_2 \right)$, or alternatively, only terms containing $\gamma_{1,2}$ are resummed into a relaxation rate and a frequency shift of the one-particle oscillations. We stress that the fate of the logarithmic term is unclear at present, which also implies that the part of γ_1 entering the resummation is not defined until this issue is dealt with, which requires further investigation.

Our results can be easily extended to local operators in theories with more than one species with diagonal scattering, and also to operators semi-local with respect to solitons in the sine–Gordon model.

The other class of secular contributions to one-particle oscillations is a novel one having the form

$$\Re e\, g F_1^{\mathcal{O}} e^{-imt} g^2 \sqrt{\frac{mt}{\pi}} \frac{-\sqrt{2} - \sqrt{2}i}{2} , \tag{8.5.2}$$

and its leading order is g^3. The origin of this secular term is a physical effect analogous to parametric resonance, and is caused by the effective coupling between one- and two-particle modes. This coupling is established by the corresponding form factor of the operator and the K function resulting in a singularity at the threshold of the two-particle continuum. At this point the ratio between the frequencies is exactly two satisfying the condition of parametric resonance. Note that the singularity of the K function is an essential ingredient as it is the origin of enhancement in the effective coupling between the modes.

Unfortunately, it is rather difficult to calculate the next secular contribution from G_7 and even having an expression for the next term, it is not guaranteed that they can be resummed in an effective manner to extract the long time behaviour. Therefore it is presently unclear how this phenomenon influences the fate of the one-particle oscillations. However, it is clear that despite the initial growth indicated by the presence of $\sqrt{t}$, the amplitude must eventually saturate as only finite energy density is injected in the system during the quench.

As seen from this chapter, the analytical description of time evolution followed by a quench is a very challenging problem, with lots of open questions remaining. Even if our analysis and partial understanding is valid only for integrable squeezed-coherent states, it is worth mentioning that for quenches that are not exactly integrable, the deviations from the integrable structure, say for the case of the four-particle overlap

$$\delta(\vartheta_1 - \vartheta_3)\delta(\vartheta_2 - \vartheta_4)K(\vartheta_1)K(\vartheta_2)|-\vartheta_1, \vartheta_1, -\vartheta_2, \vartheta_2\rangle - \delta(\sum p(\vartheta_i))K(\vartheta_1, \vartheta_2, \vartheta_3, \vartheta_4)|\vartheta_1, \vartheta_2, \vartheta_3, \vartheta_4\rangle \tag{8.5.3}$$

is expected to only result in perturbative corrections to the integrable case in various physical quantities. To develop a formalism implementing this idea, after understanding the time evolution in pure integrable quenches of course, is an interesting open direction for future works.

It must be emphasised again, that TSA methods [167] and in particular TCSA [55, 164, 177] are able able to follow the time evolution of various quantities (one-point functions, Loschmidt echo) and even correlation functions [176], and therefore these methods play an important role in the study and understanding of time evolution.

Finally, we wish to comment on the relevance of the phase quenches in the sine–Gordon model introduced in Subsection 5.3. Being both experimentally realisable and analytically tractable, the sine–Gordon theory has attracted a lot of attention. The sine–Gordon model emerges as an effective description in cold atom experiments involving tunnel coupled quasi-one-dimensional condensates, where the sine–Gordon field corresponds to the relative phase of the condensate [12, 13]. Therefore, phase quenches can be an ideal protocol to compare experimental and theoretical results. This is especially true for moderate sized quenches, where the small post-quench density of excitations makes the form factor series valid and it is possible to extract analytic results about the time evolution.

Chapter 9

Conclusions

In recent decades the spectacular advances in cold atom experiments and the studies of the non-equilibrium properties of isolated quantum many-body systems have stimulated considerable activity in the understanding of quantum statistical mechanics. For its rigorous foundation particularly important questions arise in the context of quantum integrable models. Via studying quantum quenches in integrable quantum field theories (IQFTs), this thesis focused on the relaxation towards the equilibrium i.e. the time evolution of local observables after a quench, general properties and the determination of the quench overlaps and eventually the applicability of the quench paradigm in field theories.

In Chapter 4 integrable quenches in massive IQFTs were investigated, which are defined by the condition, that the initial state $|\Omega\rangle$ is annihilated by all the odd conserved charges. i.e. $Q_s^o|\Omega\rangle = 0$. It was shown that if the initial state satisfies the cluster decomposition principle then integrable initial state in a generic massive integrable model can be written in a squeezed-coherent form (4.2.6), (4.2.7) resembling integrable boundary states in the context of boundary field theory.

Integrable quenches are important since they include all cases in which it was possible to find exact analytic results for the steady state expectation values and/or the time evolution of observables. Although a given quench protocol is not guaranteed to yield an integrable initial state, we showed that in massive IQFTs with one particle species and for quenches with sufficiently low energy density, the integrable structure of the quench holds to a good accuracy and thus the integrable quench assumption can apply in various situations. In the small quench limit the integrable structure of the initial state is ensured also in the repulsive regime of the sine-Gordon model, whose spectrum consists of solitons and anti-solitons and somewhat surprisingly also in any massive but non-integrable QFTs with one particle species. The connection between small integrable quenches and the consequences of the extensivity of local charges on the initial state were established in Ref. [159].

In Chapter 5 we studied translationally invariant quenches for which the expansion of the initial state in the post-quench basis contains a zero momentum one-particle state contribution. Based on an analogy with the case of integrable boundary states, it was argued that the zero-momentum particle implies a pole in the pair amplitude. Our statement was supported with two concrete examples: a quench in the Ising field theory crossing the phase boundary, i.e. a quench from the ferromagnetic to the paramagnetic phase, which in an integrable quench, and the interesting quench in the sine–Gordon model consisting of shifting the phase of the sine-Gordon field. The latter quench is not known to be integrable but a perturbative treatment yields a confirmation of our statement not relying on the integrability of the quench. The general and the perturbative argument for the pole in the pair amplitude was further supported by considering a linked-cluster expansion of time-dependent one-point functions after a quench in Section 8.2. This chapter relies on the publication Ref. [110].

Chapter 6 was devoted to the determination of overlaps and the study of a particular class of quenches within the Sinh-Gordon model, starting from the ground state of mass m_0 with zero coupling, to a post-quench system with a mass m and a nonzero value of g. For this quench the initial state can be specified via an operator condition allowing the derivation of an infinite hierarchy of integral equations involving

form factors of the model and the unknown overlap functions. Each integral equation can be written as a form factor expansion, consisting of an infinite number of terms. Besides the general derivation of the hierarchy and a number of arguments concerning the nature of its solutions were presented. Some of these findings are likely to be valid for more general models (such as sine-Gordon or $A^{(1)}_{N-1}$ affine Toda theories) and initial states, described by similar integral hierarchies. These are the existence and uniqueness of its solution for the interacting cases, the truncatability of the hierarchy and the applicability of an iterative solution method exploiting the truncation.

We also presented the numerical solution of the hierarchy, which is based on the pair assumption for the initial state. The validity of this assumption was supported by an argument based on 'integrable dressing', on analogies with boundary conformal field theories and due to the heuristic nature of these arguments our considerations were supplemented by numerical checks. We found that the iterative solution of the numerical methods confirms to high precision that a proposed factorized Ansatz (6.2.13) indeed solves the one-particle test state condition, which is the lowest member of the hierarchy. Second, an independent test of the squeezed state form, which includes the pair structure and the exponentiation, was provided by checking the next member of the hierarchy, i.e. the three-particle condition. The derivation the three-particle equation was carried out in two different ways: using the expansion of operators in terms of the Zamolodchikov-Faddeev creation and annihilation operators [137] and the finite volume regularization method too to check the validity of the former approach. Using the pair assumption for the overlaps, it was also shown by means of the integral equations that the asymptotics of the K-function behaves as $e^{-2|\vartheta|}$ for quenches with a finite difference in the pre- and post-quench masses, and thus provided an example in an interacting theory, where it can be demonstrated that the given quantum quench is well-defined in the field theory sense as well. The results presented in this chapter were published in Ref. [159].

In Chapter 7 mass quenches in the sine-Gordon model were studied by the truncated conformal space approach (TCSA). With TCSA the pair overlaps for the first breather were extracted and it was demonstrated that the infinite volume predictions for the pair overlaps extracted from the finite volume ones obtained by TCSA match to a accurate with the analytic continuation of the sinh-Gordon pair overlap (6.2.13). The $e^{-2|\vartheta|}$ asymptotics of the pair overlaps enables the usage of TCSA and the good accuracy match of the pair overlaps supports the validity of the factorised Ansatz in the sinh-Gordon quench. We also showed that the TCSA data are consistent with the factorisation of the four-particle overlaps. These results were published in Ref. [175].

In Chapter 8 the time evolution of one-point functions of local operators was investigated in massive IQFTs after integrable quenches. An explicit computation of the time evolution of one-point functions was presented based on Eq. (2.1.1) focusing on mainly the one-particle oscillations with time dependence e^{-imt} in integrable initial states with one-particle coupling. Part of our motivation was to correct previous results which ignored the singularity in the pair amplitude and hence give divergent expressions for various quantities. For the calculation a linked cluster expansion was applied using finite volume as a regulator and the expansion was terminated after terms containing five particles.

For the non-oscillatory part of the one-point function a $1/t$ type time dependence was found which modifies to $1/t^3$ in the absence of the one-particle coupling. When the one-particle coupling is non-zero in the initial state, oscillatory terms with the angular frequency related to the particle mass are also present and two important secular contributions were found. For the first one, the one-particle oscillation $gF_1^{\mathcal{O}}e^{-imt}$ (g being the one-particle coupling in the initial state) is multiplied a term linear in time $(\gamma_1 + i\gamma_2)\,mt$ where γ_1, γ_2 are of $\mathcal{O}\left(g^4\right)$ and by $-g^4\frac{\log(mt)}{4\pi}mt$ at leading order in time. The calculation of higher order and hence the resummation of secular contributions has not been achieved, but it is expected that either higher order terms G_{4n+1} get resummed to an exponential function $e^{-t/\tau}$ with $\tau^{-1} \to m\left(\frac{g^4}{4}\frac{\log(mt)}{\pi} - \gamma_1 - i\gamma_2\right)$, or alternatively, only terms containing $\gamma_{1,2}$ are resummed into a relaxation rate and a frequency shift of the one-particle oscillations. These results are easy to extend to local operators in theories with more than one species with diagonal scattering, and also to operators semi-local with respect to solitons in the sine–Gordon model.

The other class of secular contributions to one-particle oscillations is a novel one, where $gF_1^{\mathcal{O}}e^{-imt}$ is multiplied by $-g^2\sqrt{\frac{mt}{2\pi}}\,(1+i)$, and hence its leading order is g^3. The origin of this secular term is a physical effect analogous to parametric resonance, and is caused by the effective coupling between one- and two-particle modes. At the threshold of the two-particle continuum, the ratio between the frequencies is exactly two satisfying the condition of parametric resonance and singularity of the K function at the origin of enhances the effective coupling between the modes. The calculation of the next secular contribution from G_7 has not been performed and, therefore, it is presently unclear how this phenomenon influences the fate of the one-particle oscillations.

Although expressions for higher order terms are important and their calculation together with the question of resummation are relegated to future works, it is worth noting that these results describe the leading order time dependence in the time window $1 \ll mt \ll g^{-4}$, or $1 \ll mt \ll K^{-2}$, K denoting the typical magnitude of the K-function with the absence of one-particle terms in the integrable initial state. These results were published in Ref. [110].

Now we turn to the significance of the results summarized above, and also give an outlook. Considering first quenches with zero momentum particles it is worth mentioning that these quenches are especially interesting as oscillations in expectation values associated with the masses of the particles can be detected in experiments [13]. Suitably small quenches can, therefore, be used to determine the mass spectrum of a model, which is the idea of quench spectroscopy. As seen in this thesis, time evolution after such quenches present serious theoretical challenges and the calculation of higher order contribution for the time evolution or the resummation of secular terms are difficult problems which remain for further studies. As discussed in Chapter 2, the question of time evolution can be addressed in the Quench Action approach and the missing pieces of information are the form factors of operators between highly excited states and the set of quasi-particles above the representative state. Whereas these issues present a serious obstacle at the moment, our results for the time evolution provide an important benchmark for future advances.

The relevance of the phase quenches in the sine–Gordon model introduced in Subsection 5.3. The sine–Gordon model emerges as an effective description in cold atom experiments involving tunnel coupled quasi-one-dimensional condensates, where the sine–Gordon field corresponds to the relative phase of the condensate [12, 13]. Therefore phase quenches including zero-momentum particles in the initial state can be an ideal protocol to compare experimental and theoretical results. This is especially true for moderate sized quenches, where the small post-quench density of excitations makes the form factor series valid and the analytic results about the post-quench time evolution presented in Chapter 8 are expected to give sufficiently accurate results. Note that in the sine-Gordon phase quenches the overlaps can be determined by a perturbative form factor series as well as TCSA, which makes them more amenable to a theoretical treatment compared to other quench protocols.

The determination of overlaps was accomplished in Chapters 6 and 7 for particular cases, and these results have already been used to compute steady state expectation values in the sinh-Gordon model in Ref. [88]. Although overlaps are very important quantities, their general calculation remains a difficult problem. Nevertheless our results of Chapters 6 and 7 and studies in free theories and in the E_8 model [164] offered an increasing body of evidence that confirm that the overlaps generally decay at high energies, and in particular the role of the UV limiting CFT in the asymptotic behaviour was pointed out in Ref. [175]. The high-energy suppression of the overlaps implies that the quantum quench paradigm is well-defined in QFTs for moderate-size quenches, which means that the QFT framework can offer a cut-off independent, universal description of the quench and can eventually be applied in describing universal features of out-of-equilibrium physics in quantum systems near quantum critical points.

This conclusion has another noteworthy implication, namely the applicability of TCSA for small quenches in QFTs. Whereas the analytical calculation of the overlaps is an extremely complicated task, with TCSA it is relatively easy to extract the overlaps numerically. In fact, although the numerical results were not reported due to the lack of theoretical description, it is also possible to extract amplitudes for higher breathers and soliton–anti-soliton pairs in the sine-Gordon model. TCSA was successfully applied

to determine overlaps in the E_8 model as well [164]. However, the usefulness of TCSA is not restricted to the overlaps and it was demonstrated that TCSA [55,164,177] and other truncated spectrum methods [167] can follow the time evolution of various quantities (one-point functions, Loschmidt echo) and even correlation functions [176]. TCSA can be applied to study integrability breaking situations as well [55]. The very effective and non-perturbative truncated spectrum methods in out-of-equilibrium situation in QFTs initiated in [167, 175] already have a diverse range of applications and these methods are expected to have a further important role in the study and understanding the out-of-equilibrium physics in quantum systems.

Acknowledgments I would like to thank my supervisor, Gábor Takács for his guidance and coordination during my PhD studies, for the innumerable interesting discussions that gave me an insight not only into the most exciting fields of modern physics but broadened my overall horizons too and for his inspiring and encouraging enthusiasm and optimism. I am grateful to him for the knowledge I acquired in these years, for his continuous support and for the numerous opportunities I could seize thanks to him. I am also indebted to him for carefully reading and commenting on my thesis.

I am grateful to Márton Kormos and Spyros Sotiriadis for their contribution to my research and for many important and helpful discussions. I would like to thank Balázs Pozsgay for reading my thesis and Gergely Zaránd, György Fehér, Izabella Lovas, Kristóf Hódsági and Miklós Werner for the numerous interesting and illuminating discussions.

Finally, I would like to express my gratitude to my parents, to Mária Szikszay and Mariann Gyenis for their personal support.

Bibliography

[1] J. M. Deutsch, *Phys. Rev.* **A 43** (1991) 2046–2049.

[2] M. Srednicki, *Phys. Rev.* **E 50** (1994) 888–901, arXiv:cond-mat/9403051.

[3] T. Kinoshita, T. Wenger, and D. S. Weiss, *Nature* **440** (2006) 900–903.

[4] S. Trotzky, Y.-A. Chen, A. Flesch, I. P. McCulloch, U. Schollwöck, J. Eisert and I. Bloch, *Nature Phys.* **8** (2012) 325-330, arXiv:1101.2659 [cond-mat.quant-gas].

[5] M. Gring, M. Kuhnert, T. Langen, T. Kitagawa, B. Rauer, M. Schreitl, I. Mazets, D. A. Smith, E. Demler and J. Schmiedmayer, *Science* **337** (2012) 1318-1322, arXiv:1112.0013.

[6] T. Langen, S. Erne, R. Geiger, B. Rauer, T. Schweigler, M. Kuhnert, W. Rohringer, I. E. Mazets, T. Gasenzer and J. Schmiedmayer, *Science* **348** (2015) 207–211, arXiv:1411.7185 [cond-mat.quant-gas].

[7] S. Hofferberth, I. Lesanovsky, B. Fischer, T. Schumm and J. Schmiedmayer, *Nature* **449**, 324 (2007), arXiv:0706.2259 [cond-mat.other].

[8] T. Langen, R. Geiger, M. Kuhnert, B. Rauer and J. Schmiedmayer, *Nature Physics* **9**, 640 (2013), arXiv:1305.3708 [cond-mat.quant-gas].

[9] F. Meinert, M. J. Mark, E. Kirilov, K. Lauber, P. Weinmann, A. J. Daley and H.-C. Nägerl, *Phys. Rev. Lett.* **111** (2013) 053003, arXiv:1304.2628 [cond-mat.quant-gas].

[10] T. Fukuhara, P. Schauss, M. Endres, S. Hild, M. Cheneau, I. Bloch and C. Gross, *Nature* **502** (2013) 76, arXiv:1305.6598 [cond-mat.quant-gas].

[11] A. M. Kaufman, M. E. Tai, A. Lukin, M. Rispoli, R. Schittko, P. M. Preiss and M. Greiner, `Quantum thermalization through entanglement in an isolated many-body system`, ArXiv e-prints (2016), 1603.04409.

[12] T. Schweigler, V. Kasper, S. Erne, B. Rauer, T. Langen, T. Gasenzer, J. Berges and J. Schmiedmayer, *Nature* **545**, 323 (2017), arXiv:1505.03126 [cond-mat.quant-gas].

[13] M. Pigneur, T. Berrada, M. Bonneau, T. Schumm, E. Demler and J. Schmiedmayer, *Phys. Rev. Lett.* **120** (2018) 173601, arXiv:1711.06635 [quant-ph].

[14] J.-S. Caux and J. Mossel, *J. Stat. Mech.* **2011** (2011) 02023, arXiv:1012.3587 [cond-mat.str-el].

[15] M. Cheneau, P. Barmettler, D. Poletti, M. Endres, P. Schauss, T. Fukuhara, C. Gross, I. Bloch, C. Kollath and S. Kuhr, *Nature* **481** (2012) 484-487, arXiv:1111.0776 [cond-mat.quant-gas].

[16] M. Kormos, M. Collura, G. Takács and P. Calabrese, *Nature Physics* **13** (2017) 246-249, arXiv:1604.03571 [cond-mat.stat-mech].

[17] G. Vidal, *Phys. Rev. Lett.* **91** (2003) 147902, arXiv:quant-ph/0301063, M. Zwolak and G. Vidal, *Phys. Rev. Lett.* **93** (2004) 207205, arXiv:cond-mat/0406440.

[18] V.P. Yurov and A.B. Zamolodchikov, *Int. J. Mod. Phys.* **A5** (1990) 3221-3246.

[19] M. Rigol, V. Dunjko, V. Yurovsky and M. Olshanii, *Phys. Rev. Lett.* **98** (2007) 050405, arXiv:cond-mat/0604476 [cond-mat.other].

[20] J. M. P. Carmelo and T. Prosen, *Nucl. Phys.* **B 914** (2017) 62-98, arXiv:1611.08582 [cond-mat.str-el], M. Ljubotina, M. Znidaric and T. Prosen, *Nature Commun.* **8** (2017) 16117, arXiv:1702.04210 [cond-mat.stat-mech].

[21] L. Piroli, J. De Nardis, M. Collura, B. Bertini and M. Fagotti, *Phys. Rev.* **B 96** (2017)115124, arXiv:1706.00413 [cond-mat.stat-mech].

[22] O. A. Castro-Alvaredo, B. Doyon and T. Yoshimura, *Phys. Rev.* **X 6** (2016) 041065, arXiv:1605.07331 [cond-mat.stat-mech].

[23] B. Bertini, M. Collura, J. De Nardis and M. Fagotti, *Phys. Rev. Lett.* **117** (2016) 207201, arXiv:1605.09790 [cond-mat.stat-mech].

[24] J. De Nardis, D. Bernard and B. Doyon, *Phys. Rev. Lett.* **121** (2018)160603, arXiv:1807.02414 [cond-mat.stat-mech].

[25] P. Calabrese and J. Cardy, *J. Stat. Mech.* **0504** (2005) 04010, arXiv:cond-mat/0503393 [cond-mat.stat-mech].

[26] V. Alba and P. Calabrese, S*ciPost Phys.* **4** (2018) 017, arXiv:1712.07529 [cond-mat.stat-mech].

[27] P. Calabrese and J. Cardy, *Phys. Rev. Lett.* **96** (2006) 136801.

[28] P. Calabrese and J. Cardy, *J. Stat. Mech.* **0706** (2007) P06008.

[29] F. J. Dyson, *J. Math. Phys.* **3** (1962) 140.

[30] M. Rigol, V. Dunjko and M. Olshanii, *Nature* **452** (2008) 854-858, arXiv:0708.1324 [cond-mat.stat-mech].

[31] S. Sotiriadis and P. Calabrese, *J. Stat. Mech.* (2014) 07024, arXiv:1403.7431 [cond-mat.stat-mech].

[32] M. Rigol, *Phys. Rev. Lett.* **103** (2009) 100403.

[33] M. Rigol, *Phys. Rev.* **A 80** (2009) 053607.

[34] R. Steinigeweg, J. Herbrych and P. Prelovsek, *Phys. Rev.* **E 87** (2013) 012118.

[35] W. Beugeling, R. Moessner and M. Haque, *Phys. Rev.* **E 89** (2014) 042112.

[36] H. Kim, T.N. Ikeda and D.A. Huse, *Phys. Rev.* **E 90** (2014) 052105.

[37] R. Steinigeweg, A. Khodja, H. Niemeyer, C. Gogolin and J. Gemmer, *Phys. Rev. Lett.* **112** (2014)130403.

[38] A. Khodja, R. Steinigeweg and J. Gemmer, *Phys. Rev.* **E 91** (2015) 012120.

[39] W. Beugeling, R. Moessner and M. Haque, *Phys. Rev.* **E 91** (2015) 012144.

[40] E. Khatami, M. Rigol, A. Relano and A.M. Garcia-Garcia, *Phys. Rev.* **E 85** (2012) 050102(R).

[41] S. Genway, A.F. Ho, and D.K.K. Lee, *Phys. Rev.* **A 86** (2012) 023609.

[42] G. Biroli, C. Kollath and A.M. Läuchli, *Phys. Rev. Lett.* **105** (2010) 250401, arXiv:0907.3731 [cond-mat.quant-gas].

[43] G. Roux, *Phys. Rev.* **A 81** (2010) 053604.

[44] S. Sorg, L. Vidmar, L. Pollet and F. Heidrich-Meisner, *Phys. Rev.* **A 90** (2014) 033606.

[45] R. Mondaini, K.R. Fratus, M. Srednicki and M. Rigol, *Phys. Rev.* **E 93** (2016) 032104.

[46] L. F. Santos and M. Rigol, *Phys. Rev.* **E 82** (2010) 031130, arXiv:1006.0729 [cond-mat.stat-mech].

[47] L. F. Santos and M. Rigol, *Phys. Rev.* **E 81** (2010) 036206, arXiv:0910.2985 [cond-mat.stat-mech].

[48] T. N. Ikeda, Y. Watanabe and M. Ueda, *Phys. Rev.* **E 87** (2013) 012125, arXiv:1202.1965 [cond-mat.stat-mech].

[49] W. Beugeling, R. Moessner and Masudul Haque, *Phys. Rev.* **E 89** (2014) 042112, arXiv:1308.2862 [cond-mat.stat-mech].

[50] F. H. L. Essler and R. M. Konik, *'Applications of Massive Integrable Quantum Field Theories to Problems in Condensed Matter Physics'* in From Fields to Strings: Circumnavigating Theoretical Physics, edited by M. Shifman, A. Vainshtein, and J. Wheater (World Scientific, Singapore, 2005) arXiv:0412421 (2004).

[51] T. Langen, T. Gasenzer and J. Schmiedmayer, J. Stat. Mech. **1606** (2016) 064009, arXiv:1603.09385 [cond-mat.quant-gas].

[52] B. Bertini, F. H. L. Essler, S. Groha and N. J. Robinson, Phys. Rev. **B 94** (2016) 245117, arXiv:1608.01664 [cond-mat.stat-mech].

[53] T. Mori, T. N. Ikeda, E. Kaminishi and M. Ueda, *J. Phys.* **B 51** (2018)112001, arXiv:1712.08790 [cond-mat.stat-mech].

[54] V. Alba and M. Fagotti, Phys. Rev. Lett. **119**, 010601 (2017), arXiv:1701.05552 [cond-mat.stat-mech].

[55] A. J. A. James, R. M. Konik and N. J. Robinson: `Nonthermal states arising from confinement in one and two dimensions`, ArXiv Preprint, arXiv:1804.09990 [cond-mat.stat-mech]; N. J. Robinson, A. J. A. James, R. M. Konik: `Signatures of rare states and thermalization in a theory with confinement`, ArXiv Preprint, arXiv:1808.10782 [cond-mat.str-el].

[56] E. Fermi, J. Pasta, S. Ulam, Studies of nonlinear problems. *I. Los Alamos Scientific Laboratory Report* **LA-1940** (1955) 977-988.

[57] R. Nandkishore and D. A. Huse, *Ann. Rev. of Cond. Matt. Phys.* **6** (2015) 15-38, arXiv:1404.0686 [cond-mat.stat-mech].

[58] E. T. Jaynes, *Phys. Rev.* **106** (1957) 620–630.

[59] B. Wouters, J. De Nardis, M. Brockmann, D. Fioretto, M. Rigol and J.-S. Caux, *Phys. Rev. Lett.* **113** (2014) 117202, arXiv:1405.0172, arXiv:1405.0172 [cond-mat.str-el].

[60] B. Pozsgay, M. Mestyán, M. A. Werner, M. Kormos, G. Zaránd and G. Takács, *Phys. Rev. Lett.* **113** (2014) 117203, arXiv:1405.2843 [cond-mat.stat-mech].

[61] M. Mestyan, B. Pozsgay, G. Takacs and M. A. Werner, *J. Stat. Mech.* **1504** (2015) 04001 arXiv:1412.4787 [cond-mat.stat-mech].

[62] B. Pozsgay, *J. Stat. Mech.* **9** (2014) 09026, arXiv:1406.4613 [cond-mat.stat-mech].

[63] G. Goldstein and N. Andrei, *Phys. Rev.* ***A*** **90** (2014) 043625, arXiv:1405.4224 [cond-mat.quant-gas].

[64] F. H. L. Essler, G. Mussardo and M. Panfil, *Phys. Rev.* ***A*** **91** (2015) 051602, arXiv:1411.5352 [cond-mat.quant-gas].

[65] E. Ilievski, J. De Nardis, B. Wouters, J.-S. Caux, F. H. L. Essler and T. Prosen, *Phys. Rev. Lett.* **115** (2015) 157201, arXiv:1507.02993 [quant-ph].

[66] E. Ilievski, M. Medenjak, T. Prosen and L. Zadnik, *J. Stat. Mech.* **1606** (2016) 064008, arXiv:1603.00440 [cond-mat.stat-mech].

[67] B. Pozsgay, E. Vernier and M. A. Werner, *J. Stat. Mech.* **2017** (2017) 093103, arXiv:1703.09516 [cond-mat.stat-mech].

[68] E. Ilievski, E. Quinn and J.-S. Caux, *Phys. Rev.* **B 95** (2017) 115128, arXiv:1610.06911 [cond-mat.stat-mech].

[69] A. C. Cassidy, C. W. Clark and M. Rigol, *Phys. Rev. Lett.* **106** (2011) 140405, arXiv:1008.4794 [cond-mat.stat-mech].

[70] B. Pozsgay, *J. Stat. Mech.* **1101** (2011) P01011, arXiv:1009.4662 [hep-th].

[71] E. Ilievski, E. Quinn, J. De Nardis and M. Brockmann, *J. Stat. Mech.* **1606** (2016) 063101, arXiv:1512.04454 [cond-mat.stat-mech].

[72] A. Klümper, *Ann. Phys.* **504** (1992) 540; A. Klümper, *Z. Phys.* **B 91** (1993) 507.

[73] L. Piroli, B. Pozsgay and E. Vernier, *J. Stat. Mech.* (2017) 023106, arXiv:1611.06126 [cond-mat.stat-mech].

[74] L. Piroli, B. Pozsgay and E. Vernier: `Non-analytic behavior of the Loschmidt echo in XXZ spin chains: exact results`, arXiv:1803.04380 [cond-mat.stat-mech].

[75] L. Piroli, B. Pozsgay and E. Vernier, *Nucl. Phys.* **B 925**(2017) 362, arXiv:1709.04796[cond-mat.stat-mech].

[76] L. Piroli, E. Vernier, P. Calabrese and B. Pozsgay: `Integrable quenches in nested spin chains I-II` (Preprints), arXiv:1811.00432 [cond-mat.stat-mech], arXiv:1812.05330 [cond-mat.stat-mech].

[77] F.H.L. Essler, G. Mussardo and M. Panfil, *Phys. Rev.* **A 91** (2015) 051602, arXiv:1411.5352 [cond-mat.quant-gas].

[78] E. Vernier and A. C. Cubero, *J. Stat. Mech.* **1702** (2017) 023101, arXiv:1609.03220 [cond-mat.stat-mech].

[79] B. Pozsgay, *J. Stat. Mech.* **1406** (2014) P06011, arXiv:1309.4593 [cond-mat.stat-mech].

[80] M. Brockmann, *J. Stat. Mech.* **1405** (2014) P05006, arXiv:1402.1471 [cond-mat.stat-mech].

[81] M. Brockmann, J. De Nardis, B. Wouters and J.-S. Caux, *J. Phys.* **A47** (2014) 345003, arXiv:1403.7469 [cond-mat.stat-mech].

[82] L. Piroli and P. Calabrese, *J. Phys.* **A 47** (2014) 385003, arXiv:1407.2242 [cond-mat.stat-mech].

[83] J. De Nardis, L. Piroli and J.-S. Caux, *J.Phys. A: Math. Theor.* **48**, (2015) 43FT01, arXiv:1505.03080 [cond-mat.quant-gas].

[84] B. Bertini, E. Tartaglia and P. Calabrese, *J. Stat. Mech.* **1710** (2017) 103107, arXiv:1707.01073 [cond-mat.stat-mech].

[85] J. D. Nardis, B. Wouters, M. Brockmann and J.-S. Caux, *Phys. Rev.* **A 89** (2014) 033601, arXiv:1308.4310 [cond-mat.stat-mech].

[86] L. Bucciantini, M. Kormos and P. Calabrese, *J. Phys. A: Math. Theor.* **47** (2014)175002, arXiv:1401.7250 [cond-mat.stat-mech].

[87] D. Fioretto and G. Mussardo, *New J. Phys.* **12** (2010) 055015, arXiv:0911.3345 [cond-mat.stat-mech].

[88] B. Bertini, L. Piroli and P. Calabrese, *J. Stat. Mech.* **1606** (2016) 063102, arXiv:1602.08269 [cond-mat.stat-mech].

[89] A. Bastianello, L. Piroli, P. Calabrese, *Phys. Rev. Lett.* **120** (2018) 190601, arXiv:1802.02115 [cond-mat.quant-gas].

[90] M. A. Cazalilla, *Phys. Rev. Lett.* **97**(15), (2006)156403, arXiv:cond-mat/0606236v2 [cond-mat.stat-mech].

[91] A. Silva, *Phys. Rev. Lett.* **101** (2008) 120603, arXiv:0806.4301 [cond-mat.stat-mech].

[92] S. Sotiriadis, P. Calabrese and J. Cardy, *EPL (Europhysics Letters)* **87** (2009) 20002, arXiv:0903.0895 [cond-mat.stat-mech].

[93] B. Dóra, M. Haque and G. Zaránd, *Phys. Rev. Lett.* **106**(15) (2011) 156406, arXiv:1011.6655 [cond-mat.str-el].

[94] P. Calabrese, F. H. L. Essler and M. Fagotti, *Phys. Rev. Lett.* **106** (2011) 227203, arXiv:1104.0154 [cond-mat.str-el].

[95] P. Calabrese, F. H. L. Essler and M. Fagotti, *J. Stat. Mech.* **7** (2012) 07016, arXiv:1204. 3911 [cond-mat.quant-gas].

[96] P. Calabrese, F. H. L. Essler and M. Fagotti, *J. Stat. Mech.* **7** (2012) 07022, arXiv:1205.2211 [cond-mat.stat-mech].

[97] M. Heyl, A. Polkovnikov and S. Kehrein, *Phys. Rev. Lett.* **110** (2013)135704, arXiv:1206.2505 [cond-mat.stat-mech].

[98] F. H. L. Essler, S. Evangelisti and M. Fagotti, *Phys. Rev. Lett.* **109**(24) (2012) 247206, arXiv:1208.1961 [cond-mat.stat-mech].

[99] M. Collura, S. Sotiriadis and P. Calabrese, *Phys. Rev. Lett.* **110**(24) (2013) 245301, arXiv:1303.3795 [cond-mat.quant-gas].

[100] M. Kormos, M. Collura and P. Calabrese, *Phys. Rev.* ***A*** **89**(1) (2014) 013609, arXiv:1307.2142 [cond-mat.quant-gas].

[101] S. Sotiriadis and P. Calabrese, *J. Stat. Mech.* **7** (2014) 07024, arXiv:1403.7431 [cond-mat.stat-mech].

[102] S. Sotiriadis, *Phys. Rev.* **A 94**(3) (2016) 031605, arXiv:1507.07915 [cond-mat.stat-mech].

[103] D. Iyer and N. Andrei, *Phys. Rev. Lett.* **109**, (2012) 115304, arXiv:1206.2410 [cond-mat.quant-gas].

[104] D. Iyer, H. Guan and N. Andrei, *Phys. Rev.* **A 87**, (2013) 053628, arXiv:1304.0506 [cond-mat.quant-gas].

[105] W. Liu and N. Andrei, *Phys. Rev. Lett.* **112**, (2014) 257204, arXiv:1311.1118 [cond-mat.quant-gas].

[106] H. Guan and N. Andrei: `Quench Dynamics of the Gaudin-Yang Model,` arXiv:1803.04846 [cond-mat.quant-gas].

[107] D. Schuricht and F.H.L. Essler, *J. Stat. Mech.* **1204** (2012) P04017, arXiv:1203.5080 [cond-mat.str-el].

[108] B. Bertini, D. Schuricht and F.H.L. Essler, *J. Stat. Mech.* **1410** (2014) P10035, arXiv:1405.4813 [cond-mat.stat-mech].

[109] A. C. Cubero, and D. Schuricht, *J. Stat. Mech.* **1710** (2017) 103106, arXiv:1707.09218v2 [cond-mat.stat-mech].

[110] D.X. Horváth, M. Kormos and G. Takács, *JHEP* **08** (2018) 170, arXiv:1805.08132 [cond-mat.stat-mech].

[111] G. Delfino, *J. Phys. A: Math. Theor.* **47** (2014) 402001, arXiv:1405.6553 [cond-mat.stat-mech].

[112] G. Delfino, J. Viti, *J. Phys. A: Math. Theor.* **50** (2017) 084004, arXiv:1608.07612 [cond-mat.stat-mech].

[113] M. Kormos and G. Zaránd, *Phys. Rev.* **E93** (2016) 062101, arXiv:1507.02708 [cond-mat.stat-mech]; C. P. Moca, M. Kormos and G. Zaránd, *Phys. Rev. Lett.* **119** (2016) 100603, arXiv:1609.00974 [cond-mat.stat-mech].

[114] J-S. Caux and F. H. L. Essler, *Phys. Rev. Lett.* **110**, 257203 (2013), arXiv:1301.3806 [cond-mat.stat-mech].

[115] J-S. Caux, *J. Stat. Mech.* **1606** (2016) 064006, arXiv:1603.04689 [cond-mat.str-el].

[116] A. LeClair and G. Mussardo, *Nucl. Phys.* **B 552** (1999) 624–642, arXiv:hep-th/9902075.

[117] B. Doyon, *J.Stat.Mech.* **0511** (2005) 11006, arXiv:hep-th/0506105.

[118] B. Doyon: *'Finite-Temperature Form Factors: a Review'*, Proc. of the O'Raifeartaigh Symposium on Non-Perturbative and Symmetry Methods in Field Theory (June 2006, Budapest, Hungary), published in SIGMA (Symmetry, Integrability and Geometry: Methods and Applications), arXiv:hep-th/0611066.

[119] M. Mestyán and B. Pozsgay, *J. Stat. Mech.* **1409** (2014) 09020, arXiv:1405.0232 [cond-mat.stat-mech].

[120] B. Pozsgay and I. M. Szécsényi, *JHEP* **05** (2018) 170, arXiv:1802.05890 [hep-th]

[121] A. C. Cubero and M. Panfil, `Thermodynamic bootstrap program for integrable QFT's: Form factors and correlation functions at finite energy density` (Preprint), arXiv:1809.02044 [hep-th].

[122] S. Ghoshal and A. B. Zamolodchikov, *Int. J. Mod. Phys.* **A9** (1994) 3841–3886, arXiv:hep-th/9306002.

[123] R. J. Eden, P. V. Landshoff, D. I. Olive and J. C. Polkinghorne, *'The Analytic S-Matrix'* Cambridge University Press (1966)

[124] C.-N. Yang, *Phy. Rev. Lett.* **19** (1967) 1312-1314.

[125] R. J. Baxter, *Annals Phys.* **70** (1972) 193-228.

[126] A. B. Zamolodchikov and Al. B. Zamolodchikov, *Annals Phys.* **120** (1979) 253-291.

[127] J. L. Miramontes, *Phys. Lett.* **B455** (1999) 231-238, arXiv:hep-th/9901145.

[128] G. Lechner, *Comm. Math. Phys.* **277** (2008) 821–860, math-ph/0601022.

[129] G. Lechner, `Algebraic constructive quantum field theory: Integrable models and deformation techniques`, arXiv e-prints (2015), arXiv:1503.03822 [math-ph].

[130] E. Gutkin, *Physics Reports* **167** (1988) 1 – 131.

[131] F. A. Smirnov: Form Factors in Completely Integrable Models of Quantum Field Theory. World Scientific, 1992, 10.1142/1115.

[132] G. Delfino, P. Simonetti and J. L. Cardy, *Phys.Lett.* **B 387** (1996) 327-333, arXiv:hep-th/9607046.

[133] M. Karowski and P. Weisz, *Nucl. Phys.* **B 139** (1978) 455 – 476.

[134] A. B. Zamolodchikov, *Nucl. Phys.* **B 348** (1991) 619-641.

[135] B. Berg, M. Karowski and P. Weisz, *Phys. Rev.* **D 19** (1979) 2477.

[136] G. Delfino and G. Mussardo, *Nucl. Phys.* **B 455** (1995) 724-758.

[137] H. Bostelmann and D. Cadamuro, *Comm. Math. Phys.* **337** (2015) 1199-1240.

[138] M. Lüscher, *Commun. Math. Phys.* **104** (1986) 177-206.

[139] M. Lüscher, *Commun. Math. Phys.* **105** (1986) 153-188.

[140] H. Bethe, *Zeitschrift für Physik* **A 71** (1931) 205-226.

[141] T. R. Klassen and E. Melzer, *Nucl. Phys.* **B 362** (1991) 329–388.

[142] Z. Bajnok and R. A. Janik, *Nucl. Phys.* **B 807** (2009) 625–650, arXiv: 0807.0399 [hep-th].

[143] Y. Hatsuda and R. Suzuki, *JHEP* **0809** (2008) 025, arXiv: 0807.0643 [hep-th].

[144] B. Pozsgay and G. Takács, *Nucl. Phys.* **B 788** (2008) 167-208, arXiv: 0706.1445 [hep-th].
B. Pozsgay and G. Takács, *Nucl. Phys.* **B 788** (2008) 209-251, arXiv: 0706.3605 [hep-th].

[145] A. E. Arinshtein, V. A. Fateev and A. B. Zamolodchikov, *Phys. Lett.* **B 87** (1979) 389.

[146] A. Fring, G. Mussardo and P. Simonetti, *Nucl. Phys.* **B 393** (1993) 413-441, [arXiv:hep-th/9211053].

[147] A. Koubek and G. Mussardo, [arXiv:hep-th/9306044].

[148] S. L. Lukyanov and A.B. Zamolodchikov, *Nucl. Phys.* **B 493** (1997) 571-587, [arXiv:hep-th/9611238].

[149] S. L. Lukyanov, *Mod. Phys. Lett.* **A 12** (1997) 2543–2550, arXiv: hep-th/9703190.

[150] A. A. Belavin, A. M. Polyakov and A. B. Zamolodchikov, *Nucl. Phys.* **B 241** (1984) 333-380.

[151] Al. B. Zamolodhikov, *Int. J. Mod. Phys.* **A 10** (1995) 1125-1150.

[152] E. Lieb, T. Schultz, and D. Mattis, *Annals of Physics* **16** (1961) 407–466.

[153] P. Pfeuty, *Annals of Physics* **57** (1970) 79–90.

[154] I. Cherednik. *Theor. Math.Phys.* **61**:1 (1984) 977.

[155] S. Ghoshal, *Int. J. Mod. Phys.* **A 9** (1994) 4801.

[156] P. Dorey, M. Pillin, R. Tateo, and G. M. T. Watts, *Nucl. Phys.* **B 594** (2001) 625–659, arXiv:hep-th/0007077.

[157] Z. Bajnok, L. Palla, and G. Takács, *Nucl. Phys.* **B 716** (2005) 519–542, arXiv:hep-th/0412192.

[158] Z. Bajnok, L. Palla, and G. Takács, *Nucl. Phys.* **B 772** (2007) 290–322, arXiv:hep-th/0611176.

[159] D. X. Horvath, S. Sotiriadis, and G. Takács, *Nucl. Phys.* **B 902** (2016) 508, arXiv:1510.01735 [cond-mat.stat-mech].

[160] P. P. Mazza, J.-M. Stephan, E. Canovi, V. Alba, M. Brockmann, and M. Haque, *J. Stat. Mech.* (2016) 013104, arXiv:1509.04666 [cond-mat.str-el],

[161] K. K. Kozlowski and B. Pozsgay, *J. Stat. Mech.* **1205** (2012) P05021, arXiv:1201.5884 [nlin.SI].

[162] M. Brockmann, J. De Nardis, B. Wouters and J.-S. Caux, *J. Phys.* **A 47** (2014) 145003, arXiv:1401.2877 [cond-mat.stat-mech].

[163] B. Pozsgay, *J. Stat. Mech.* **1805** (2018) 053103, arXiv:1801.03838 [cond-mat.stat-mech].

[164] K. Hódsági, M. Kormos, and G. Takács, *SciPost Phys.* **5** (2018) 027, arXiv:1803.01158 [cond-mat.stat-mech].

[165] M. Kormos and B. Pozsgay, *JHEP* **1004** (2010) 112, arXiv:1002.2783 [hep-th].

[166] Z. Bajnok, L. Palla, and G. Takács, *Nucl. Phys.* **B 750** (2006) 179-212, arXiv:hep-th/0603171.

[167] T. Rakovszky, M. Mestyán, M. Collura, M. Kormos and G. Takács, *Nucl. Phys.* **B 911** (2016) 805-845, arXiv:1607.01068v2 [cond-mat.stat-mech].

[168] S. Lukyanov, *Phys.Lett.* **B 408** (1997) 192-200.

[169] S. Sotiriadis, G. Takács and G. Mussardo, *Phys. Lett.* **B 734** (2014) 52.

[170] Cf. Section 17C of the monograph G. Mussardo: Statistical Field Theory: An Introduction to Exactly Solved Models in Statistical Physics (Oxford University Press, Oxford, 2010).

[171] J. Cardy: `Quantum Quenches to a Critical Point in One Dimension: some further results`, arXiv:1507.07266 [cond-mat.stat-mech].

[172] R. Egger, A. Komnik and H. Saleur, *Phys. Rev.* **B 60** (1999) R5113(R).

[173] E. Corrigan and A. Taormina, *J. Phys.* **A33** (2000) 8739-8754; E. Corrigan: `Boundary bound states in integrable quantum field theories`, hep-th/0010094.

[174] P. Dorey, *'Exact S matrices'*, hep-th/9810026. In: Z. Horváth and L. Palla: Proceedings of Eotvos Summer School in Physics: Conformal Field Theories and Integrable Models, 13-18 Aug 1996. Budapest, Hungary. Published as Lecture Notes in Physics vol. 498 (Springer, Berlin, 1997).

[175] D.X. Horváth and G. Takács, *Phys. Lett.* **B 771** (2017) 539–545, arXiv:1704.00594 [cond-mat.stat-mech].

[176] I. Kukuljan, S. Sotiriadis and G. Takacs, *Phys. Rev. Lett.* **121** (2018) 110402

[177] D. X. Horvath, I. Lovas, M. Kormos, G. Takacs, G. Zarand: `Non-equilibrium time evolution and rephasing in the quantum sine-Gordon model`, ArXiv Preprint, arXiv:1809.06789 [cond-mat.quant-gas].

[178] G. Feverati, F. Ravanini and G. Takács, *Phys. Lett.* **B 430**, 264-273 (1998)**,** arXiv:hep-th/9803104.

[179] G. Feverati, K. Graham, P. A. Pearce, G. Z. Tóth, and G. Watts: `A renormalization group for TCSA`, arXiv: hep-th/0612203.

[180] R. M. Konik and Y. Adamov, *Phys. Rev. Lett.* **98** (2007) 147205, arXiv:cond-mat/0701605 [cond-mat.str-el].

[181] P. Giokas and G. Watts:`The renormalization group for the truncated conformal space approach on the cylinder`, arXiv:1106.2448 [hep-th].

[182] M. Lencsés and G. Takács, *JHEP* **1509** (2015) 146, arXiv:1506.06477 [hep-th].

[183] M. Hogervorst, S. Rychkov and B. C. van Rees, *Phys. Rev.* **D 91** (2015) 025005, arXiv:1409.1581 [hep-th].

[184] G. Fehér and G. Takács, *Nucl. Phys.* **B 852** (2011) 441-467, arXiv:1106.1901 [hep-th].

[185] H. Rieger and F. Iglói, *Phys. Rev.* **B 84**(16) (2011) 165117, arXiv:1106.5248 [cond-mat.stat-mech].

[186] B. Blass, H. Rieger and F. Iglói, *EPL (Europhysics Letters)* **99** (2012) 30004, arXiv:1205.3303 [cond-mat.stat-mech].

[187] S. Evangelisti, *J. Stat. Mech.* **4** (2013) 04003, arXiv:1210.4028 [cond-mat.stat-mech].

[188] B. Pozsgay and G. Takács, *J. Stat. Mech.* **1011** (2010) 11012, arXiv: 1008.3810 [hep-th].
I.M. Szécsényi and G. Takács, *J. Stat. Mech.* **1212** (2012) P12002, arXiv: 1210.0331 [hep-th].

[189] F.H.L. Essler and R.M. Konik, *J. Stat. Mech.* **0909** (2009) P09018, arXiv: 0907.0779 [cond-mat.str-el].

Appendix A

The singularity of the Ising K function

To complete the proof for the pole strength of the K-function for the $FM \to PM$ quench in the Ising model (c.f. Section 5.2), our aim is to show that $\frac{N_{NS}}{N_R} = \sqrt{ML}\sqrt{\frac{M_0}{M_0+M}}$ holds where M and M_0 are the post- and pre-quench masses and N_R and N_{NS} are the normalisation constants of the Ramond and Neveu-Schwartz components of the initial state.

It is convenient to calculate the logarithm of the ratio, which we write as

$$\begin{aligned}
\ln \frac{N_{NS}^2}{N_R^2} =& \ln \prod_{n\subset\mathbb{N}^+} \frac{1+\left|K\left(\frac{2\pi}{L}(n-1/2)\right)\right|^2}{1+\left|K\left(\frac{2\pi}{L}(n)\right)\right|^2} \\
=& A + B \,, \\
A =& \ln \prod_{n\subset\mathbb{N}^+} \frac{1+\frac{x}{(n-\frac{1}{2})^2}}{1+\frac{x}{i^2}} \,, \\
B =& \ln \prod_{n\subset\mathbb{N}^+} \frac{1+\frac{x}{n^2}}{1+|K\left(\frac{2\pi}{L}n\right)|^2} \\
& - \ln \prod_{n\subset\mathbb{N}^+} \frac{1+\frac{x}{(n-\frac{1}{2})^2}}{1+|K\left(\frac{2\pi}{L}(n-\frac{1}{2})\right)|^2} \,,
\end{aligned} \tag{A.0.1}$$

and x is introduced as

$$x = \frac{4M^2M_0^2L^2}{(M+M_0)^2(2\pi)^2} \,.$$

When $ML \to 0$, the expression denoted by B in (A.0.1) is zero, which can be easily seen by considering the Euler-Maclaurin formula: for the two terms in B the difference between the lower endpoints for the integration and for the boundary terms consisting of the functions and their derivatives goes as $1/L$ and the expressions in the logarithms are smooth, well-behaved functions. The term A in (A.0.1) can explicitly be computed, therefore when $L \to \infty$,

$$\begin{aligned}\ln\frac{N_{NS}^2}{N_R^2} &= \ln\prod_{i\subset\mathbb{N}^+}\frac{1+\frac{x}{(i-\frac{1}{2})^2}}{1+\frac{x}{i^2}} \\ &= -\frac{1}{2}\left[-2\ln\Gamma\left(1-\sqrt{-x}\right)+2\ln\Gamma\left(\frac{1}{2}-\sqrt{-x}\right)\right. \\ &\quad \left.-2\ln\Gamma\left(\sqrt{-x}+1\right)+2\ln\Gamma\left(\sqrt{-x}+\frac{1}{2}\right)\right] \\ &\quad +\ln\pi\,,\end{aligned} \tag{A.0.2}$$

and consequently, leading order behaviour of $\ln\frac{N_{NS}^2}{N_R^2}-\ln L$ from (A.0.2) is $\ln(\pi\sqrt{x})$. Then, one finds that

$$\frac{N_{NS}}{N_R} = \sqrt{ML}\sqrt{\frac{M_0}{M_0+M}}\,, \tag{A.0.3}$$

from which $g = 2\sqrt{\frac{M_0}{M_0+M}}$ follows (c.f. Section 5.2).

Appendix B

Phase quenches in the sine–Gordon model and exponential quenches

In this appendix we discuss some details conserning the phase quench in the sine-Gordon model that were not dealt with in the main part of the thesis. We recall that the phase quenches in the sine–Gordon model consist of abruptly shifting the sine–Gordon field $\phi \to \phi + \delta/\beta$, i.e. changing the phase in the model and regarding the pre-quench vacuum as the initial state for the post-quench evolution and it is possible to relate the pre- and post-quench vacua by a similarity transformation

$$|\Omega\rangle_L = \exp\left(i\frac{\delta}{\beta}\Pi_0\right)|0\rangle_L\,, \tag{B.0.1}$$

where L indicates that the theory is considered in finite volume and PBC are assumed. It is possible to write down a form factor expansion for the overlaps in finite volume,

$${}_L\langle\chi|\exp\left(i\frac{\delta}{\beta}\Pi_0\right)|0\rangle_L\,, \tag{B.0.2}$$

yielding

$$\begin{aligned}\frac{(-1)^l L^l}{l!}\left(\frac{\delta}{\beta}\right)^l \tilde{\sum_{\alpha_1}}\cdots\tilde{\sum_{\alpha_{l-1}}} {}_L\langle\chi|\Phi(0)|\alpha_1\rangle_L(E_\chi - E_{\alpha_1})\times \\ {}_L\langle\alpha_1|\Phi(0)|\alpha_2\rangle_L(E_{\alpha_1}-E_{\alpha_2})\ldots{}_L\langle\alpha_{l-1}|\Phi(0)|0\rangle_L(E_{\alpha_{l-1}}-E_0)\,,\end{aligned} \tag{B.0.3}$$

where the tildes over the sums signal that only zero momentum states are included due to translation invariance and accordingly, overlaps with zero momentum states are non-vanishing only.

As was shown for a state containing only zero-momentum first breather and to first order in δ in the main part (see Section 5.3), the correspondoing overlap in finite volume is

$$\begin{aligned}\sqrt{m_1 L}\frac{g}{2} =& {}_L\langle\{0\}|\Omega\rangle_L \\ =&(-1)L\left(\tfrac{\delta}{\beta}\right){}_L\langle\{0\}|\Phi(0)|0\rangle_L m_1\,,\end{aligned} \tag{B.0.4}$$

with

$${}_L\langle\{0\}|\Phi(0)|0\rangle_L = \frac{F^*_{B_1}}{\sqrt{m_1 L}}\,,$$

which gives

$$\frac{g}{2} = -\frac{\delta}{\beta} F^*_{B_1} \,, \tag{B.0.5}$$

where F denotes the form factor of the field Φ in the sine–Gordon theory which has only has non-vanishing matrix elements with states composed first breathers when their total number is odd. In particular [149],

$$F_{B_1} = F^*_{B_1} = \frac{\bar{\lambda}(\xi)\pi\xi}{\beta \sin \pi\xi} \,, \tag{B.0.6}$$

with

$$\begin{aligned} \xi =& \frac{\beta^2}{\beta^2 - 8\pi} \,, \\ \bar{\lambda}(\xi) =& 2\cos\frac{\pi\xi}{2}\sqrt{2\sin\frac{\pi\xi}{2}}\exp\left(-\int_0^{\pi\xi}\frac{dt}{2\pi}\frac{t}{\sin t}\right) \,, \end{aligned} \tag{B.0.7}$$

and we remark that the form factors of the sine–Gordon field ϕ can be obtained from that of the vertex operators $:e^{i\alpha\phi}:$ by differentiating with respect to α. For the pair overlap the lowest non-trivial order is δ^2 and one obtains

$$\begin{aligned} N_2(\vartheta, L)K(\vartheta) =& {}_L\langle I, -I|\Omega\rangle_L \\ =& \left(\frac{\delta}{\beta}\right)^2 \frac{L^2}{2} \tilde{\sum_{\alpha_1}} {}_L\langle I, -I|\Phi(0)|\alpha_1\rangle_L (2m_1\cosh\vartheta - E_{\alpha_1})_L\langle\alpha_1|\Phi(0)|0\rangle_L E_{\alpha_1} \\ =& \left(\frac{\delta}{\beta}\right)^2 \frac{L^2}{2} \sum_{n=1}^{\infty}\sum_{\{\theta_k\}} \frac{F_{B_1,B_1,A_1\dots A_n}(i\pi+\vartheta, i\pi-\vartheta, \theta_1, \dots\theta_n)}{\sqrt{(m_1 L\cosh\vartheta)^2 + (m_1 L\cosh\vartheta)\ \varphi_{B_1B_1}(\vartheta)}\rho_n(\theta_1,\dots\theta_n)} \times \\ & \left(2m_1\cosh\vartheta - \sum_{i=1}^n m_i\cosh\theta_i\right) F^*_{A_1\dots A_n}(\theta_1,\dots\theta_n)\left(\sum_{i=1}^n m_i\cosh\theta_i\right) \,, \end{aligned} \tag{B.0.8}$$

where the particles A_k are either breathers or solitons and their is an implicit summation over all possible choice of their species.

Now we are interested in the singular behaviour of K which can only originate from those of the form factors. The infinite volume limit itself is finite, since the numerator contains an explicit L^2, and in the n-particle term the denomination contributes $1/L$ and also $1/L^n$ from the density factor, while rewriting the discrete summation in terms of integrals results in a state density factor of behaviour L^{n-1}, so the leading term is independent of L.

First let us focus on terms where all particles $A_1 \dots A_n$ are first breathers. We now proceed to analyse the singularity of these terms by setting ϑ to a value ϵ and to consider the limit of small ϵ. The form factor has a kinematical singularity when some subset of m particles among the $A_1 \dots A_n$ has similarly small rapidities, which we take to be a multiple of ϵ. The dependence of the most singular term can be obtained from the kinematical residue equation (3.2.6) but also taking into account that the form factor having a first order zero when two rapidities coincide due to (3.2.4) and $S(0) = -1$. There are three cases:

- $m < n-1$: The behaviour of $F(i\pi+\vartheta, i\pi-\vartheta, \theta_1, \dots\theta_n)$ is $\epsilon^{1+(m-1)m/2-2m}$, where the 1 comes from the coincidence of $i\pi-\vartheta$ and $i\pi+\vartheta$, the $m(m-1)/2$ comes from the coincidence of the m rapidities in the set $\theta_1, \dots\theta_n$, and the $-2m$ are from the kinematical singularities "activated" in the limit. For $F^*(\theta_1, \dots\theta_n)$ one obtains a factor $\epsilon^{(m-1)m/2}$, therefore the overall behaviour is $\epsilon^{1+(m-1)m-2m}$ which is only singular for $m = 1$ or 2.

- $m = n - 1$: one must be aware that the condition of zero total momentum, that sending $m = n - 1$ rapidities to zero results in all the n of them going to zero, leading to the behaviour $\epsilon^{1+(n-1)n-2n}$ which is singular for $n = 2$.

- $m = n$: same behaviour $\epsilon^{1+(n-1)n-2n}$ as for the case $m = n - 1$, resulting in $n = 1$ or $n = 2$.

Note that whenever there is a singularity it is always of order one. For the case when all the $A_1 \dots A_n$ are first breathers, n must also be odd for the form factor not to vanish due to parity invariance. The $n = 1$ contribution is

$$\left(\frac{\delta}{\beta}\right)^2 \frac{L^2}{2} \frac{F_{B_1B_1B_1}(i\pi + \vartheta, i\pi - \vartheta, 0)(2m_1 \cosh\vartheta - m_1)F_1^* m_1}{\sqrt{(m_1 L \cosh\vartheta)^2 + (m_1 L \cosh\vartheta)\ \varphi_{B_1B_1}(\vartheta)} m_1 L} \ . \tag{B.0.9}$$

Using the form factor equations

$$F_{B_1B_1B_1}(i\pi + \vartheta, i\pi - \vartheta, 0) \approx -\frac{4i}{\vartheta} F_{B_1} \ , \tag{B.0.10}$$

this contribution alone gives the expected pole contribution

$$\begin{aligned} K(\vartheta) &= -\left(\frac{\delta}{\beta}\right)^2 \frac{2i\,|F_{B_1}|^2}{2} \frac{1}{\vartheta} + \mathcal{O}(\vartheta^0) \\ &= -i\frac{g^2}{2}\frac{1}{\vartheta} \ . \end{aligned} \tag{B.0.11}$$

Now we demonstrate that contributions with $n \geq 3$ are regular at the origin $\vartheta = 0$. Observe that in finite volume the rapidity ϑ in finite volume is eventually quantised according to

$$mL \sinh\vartheta + \delta(2\vartheta) = 2\pi I$$

with some half-integer quantum number I, so it is always displaced by an amount of order $1/L$ from the origin. Fixing I results in the parameter ϵ being essentially $1/L$, therefore the singularity $1/\epsilon$ manifests itself as a divergence of (B.0.8) proportional to L when L goes to infinity with I fixed. A simple power counting then gives that the contribution is

$$\frac{L^2}{L^{n+1}} \times L \times L^r = L^{r+2-n} \ ,$$

where L^r is the state density factor resulting for the r particle rapidities among the $\theta_1, ...\theta_n$ whose summation is left free once fixing the positions of those needed for the singularity and also taking into account the zero-momentum constraint. Clearly one obtains $r \leq n-2$ resulting in a cancellation of any divergence for $L \to \infty$.

To finish this discussion, let us consider the case when the set of particles $A_1 \dots A_n$ contains other species (higher breathers or solitons) as well. Let us suppose that the total number of first breathers among $A_1 \dots A_n$ is k with $k < n$. The counting of the degree of singularity only involves first breathers, so we obtain that the only possible cases are again $k = 1$ or 2. However, in the denominator of (B.0.8) now one has a density ρ_n with a behaviour L^n with $n > k$, which leads to a regular limit for $L \to \infty$.

Appendix C

Finite volume derivation of the integral equations

Here we briefly summarize the finite volume regularization for the hierarchy and show that after an appropriate redefinition of integration contours the resulting equations are equivalent to those obtained from the form factor representation (3.2.13) of the field.

C.1 One- and three-particle test states

In Section 3.3, we discussed how to construct scattering states in finite volume based on the Bethe-Yang equations (3.3.1) and how form factors between these finite volume states can be computed (3.3.4) and in Section 4.3, the finite volume regularized version of the squeezed-coherent initial state 4.3.1 was presented. With these ingredients, the finite volume counterpart of the integral equation hierarchy can be straightforwardly written as

$$\sum_{k=0}^{\infty}\frac{1}{k!}\sum_{I_1'}\cdots\sum_{I_k'}N_{2k}(\vartheta_1',\dots,\vartheta_k')_L K(\vartheta_1')\dots K(\vartheta_k')\langle\vartheta_1,\dots,\vartheta_n|\mathcal{O}(p)|-\vartheta_1',\vartheta_1',\dots,-\vartheta_k',\vartheta_k'\rangle_L=0\,, \quad \text{(C.1.1)}$$

for an n-particle test state, where $\vartheta_1,\dots,\vartheta_n$ must also be a state satisfying the quantization relations with some arbitrarily chosen quantum numbers.

In the Supplementary Material of the work [169] it was shown an explicit example of this sort of calculation for the one-particle test state; therefore here we refrain from going into more details and refer to instead the original paper.

For one-particle test states, the resulting equation up to (and including) four-particle terms from the

initial state can be written as

$$\begin{aligned}0 =&[E_0(p) - E(\vartheta)]F_1^\phi + \frac{1}{2}[E_0(p) + E(\vartheta)]F_1^\phi K(\vartheta)(1 + S(-2\vartheta))\\ &+ \frac{1}{2}\int_{-\infty+i\varepsilon}^{+\infty+i\varepsilon}\frac{d\vartheta'}{2\pi}[E_0(p) - E(\vartheta) + 2E(\vartheta')]F_3^\phi(\vartheta + i\pi, -\vartheta', \theta')K(\vartheta')\\ &+ \frac{1}{4}\int_{-\infty}^{+\infty}\frac{d\vartheta'}{2\pi}[E_0(p) + E(\vartheta) + 2E(\vartheta')](S(-2\vartheta)K(\vartheta) + S(\vartheta - \vartheta')S(\vartheta + \vartheta')K(\vartheta))\\ &\qquad\times F_3^\phi(-\vartheta, -\vartheta', \vartheta')K(\vartheta')\\ &+ \frac{1}{8}\int_{-\infty+i\varepsilon}^{+\infty+i\varepsilon}\frac{d\theta\vartheta_1'}{2\pi}\int_{-\infty+i\varepsilon}^{+\infty+i\varepsilon}\frac{d\vartheta_2'}{2\pi}[E_0(p) - E(\vartheta) + 2E(\vartheta_1') + 2E(\vartheta_2')]\\ &\qquad\times F_5^\phi(\vartheta + i\pi, -\vartheta_1', \vartheta_1', -\vartheta_2', \vartheta_2')K(\theta_1')K(\theta_2')\\ &+ \dots,\end{aligned} \tag{C.1.2}$$

valid as long as Im $\vartheta < \varepsilon$, where $p = m\sinh\vartheta$, $E_0(p) = \sqrt{m_0^2 + p^2}$, and $E(\vartheta) = m\cosh\vartheta$.

For Im $\vartheta > \varepsilon$, the equation is changed by kinematic poles of the form factors F_3^ϕ and F_5^ϕ crossing the contours of integrations; the appropriate analytic continuation of the equation reads

$$\begin{aligned}0 =&[E_0(p) - E(\vartheta)]F_1^\phi + [E_0(p) + E(\vartheta)]F_1^\phi K(\vartheta)\\ &+ \frac{1}{2}\int_{-\infty+i\varepsilon}^{+\infty+i\varepsilon}\frac{d\vartheta'}{2\pi}[E_0(p) - E(\vartheta) + 2E(\vartheta')]F_3^\phi(\vartheta + i\pi, -\vartheta', \vartheta')K(\vartheta')\\ &+ \frac{1}{2}\int_{-\infty}^{+\infty}\frac{d\vartheta'}{2\pi}[E_0(p) + E(\vartheta) + 2E(\vartheta')]S(\vartheta - \vartheta')S(\vartheta + \vartheta')K(\vartheta)F_3^\phi(-\vartheta, -\vartheta', \vartheta')K(\vartheta')\\ &+ \frac{1}{8}\int_{-\infty+i\varepsilon}^{+\infty+i\varepsilon}\frac{d\vartheta_1'}{2\pi}\int_{-\infty+i\varepsilon}^{+\infty+i\varepsilon}\frac{d\vartheta_2'}{2\pi}[E_0(p) - E(\vartheta) + 2E(\vartheta_1') + 2E(\theta\vartheta_2')]\\ &\qquad\times F_5^\phi(\vartheta + i\pi, -\vartheta_1', \vartheta_1', -\vartheta_2', \vartheta_2')K(\vartheta_1')K(\vartheta_2') + \dots.\end{aligned} \tag{C.1.3}$$

In the limit $m_0 \to \infty$, the energy terms $E(\vartheta)$ can be dropped and the equation divided through by $E_0(p)$, leading to the simplified form

$$\begin{aligned}0 =&F_1^\phi + \frac{1}{2}F_1^\phi K_D(\vartheta)(1 + S(-2\vartheta))\\ &+ \frac{1}{2}\int_{-\infty+i\varepsilon}^{+\infty+i\varepsilon}\frac{d\vartheta'}{2\pi}F_3^\phi(\vartheta + i\pi, -\vartheta', \vartheta')K_D(\vartheta')\\ &+ \frac{1}{4}\int_{-\infty}^{+\infty}\frac{d\vartheta'}{2\pi}(S(-2\vartheta)K_D(\vartheta) + S(\vartheta - \vartheta')S(\vartheta + \vartheta')K_D(\vartheta))F_3^\phi(-\vartheta, -\vartheta', \vartheta')K_D(\vartheta')\\ &+ \frac{1}{8}\int_{-\infty+i\varepsilon}^{+\infty+i\varepsilon}\frac{d\vartheta_1'}{2\pi}\int_{-\infty+i\varepsilon}^{+\infty+i\varepsilon}\frac{d\vartheta_2'}{2\pi}F_5^\phi(\vartheta + i\pi, -\vartheta_1', \vartheta_1', -\vartheta_2', \vartheta_2')K_D(\theta\vartheta_1')K_D(\vartheta_2') + \dots\end{aligned} \tag{C.1.4}$$

for Im $\vartheta < \varepsilon$, and

$$\begin{aligned}0 =&F_1^\phi + F_1^\phi K_D(\vartheta)\\ &+ \frac{1}{2}\int_{-\infty+i\varepsilon}^{+\infty+i\varepsilon}\frac{d\vartheta'}{2\pi}F_3^\phi(\vartheta + i\pi, -\vartheta', \vartheta')K_D(\vartheta')\\ &+ \frac{1}{2}\int_{-\infty}^{+\infty}\frac{d\vartheta'}{2\pi}S(\vartheta - \vartheta')S(\vartheta + \vartheta')K_D(\vartheta)F_3^\phi(-\vartheta, -\vartheta', \vartheta')K_D(\vartheta')\\ &+ \frac{1}{8}\int_{-\infty+i\varepsilon}^{+\infty+i\varepsilon}\frac{d\vartheta_1'}{2\pi}\int_{-\infty+i\varepsilon}^{+\infty+i\varepsilon}\frac{d\vartheta_2'}{2\pi}F_5^\phi(\vartheta + i\pi, -\vartheta_1', \vartheta_1', -\vartheta_2', \vartheta_2')K_D(\vartheta_1')K_D(\vartheta_2') + \dots\end{aligned} \tag{C.1.5}$$

for Im $\vartheta > \varepsilon$. These express the condition

$$\phi(x)|D\rangle = 0 \tag{C.1.6}$$

satisfied by the Dirichlet state.

For three-particle test states, the result was calculated in [159] and reads

$$0 = T_0 + T_2 + T_4 + \dots \tag{C.1.7}$$

with T_n denoting the n-particle contribution from the state $|\Omega\rangle$:

$$T_0 = [E_0(p) - E(\vartheta_1) - E(\vartheta_2) - E(\vartheta_3)]\, F(\vartheta_3 + i\pi, \vartheta_2 + i\pi, \vartheta_1 + i\pi) \quad , \tag{C.1.8}$$

$$\begin{aligned}
T_2 =& \frac{1}{2}\int_{-\infty}^{+\infty} \frac{\mathrm{d}\vartheta'}{2\pi}\Big[[E_0(p) - E(\vartheta_1) - E(\vartheta_2) - E(\vartheta_3) + 2E(\vartheta' + i\varepsilon)] \\
&\times F(\vartheta_3 + i\pi, \vartheta_2 + i\pi, \vartheta_1 + i\pi, -\vartheta' - i\varepsilon, \vartheta' + i\varepsilon)K(\vartheta' + i\varepsilon)\Big] \\
&+ \frac{1}{2}[E_0(p) + E(\vartheta_1) - E(\vartheta_2) - E(\vartheta_3)][S(\vartheta_2 - \vartheta_1)S(\vartheta_3 - \vartheta_1) + S(-2\vartheta_1)]F(\vartheta_3 + i\pi, \vartheta_2 + i\pi, -\vartheta_1)K(\vartheta_1) \\
&+ \frac{1}{2}[E_0(p) - E(\vartheta_1) + E(\vartheta_2) - E(\vartheta_3)][S(\vartheta_3 - \vartheta_2) + S(\vartheta_2 - \vartheta_1)S(-2\vartheta_2)]F(\vartheta_3 + i\pi, \vartheta_1 + i\pi, -\vartheta_2)K(\vartheta_2) \\
&+ \frac{1}{2}[E_0(p) - E(\vartheta_1) - E(\vartheta_2) + E(\vartheta_3)][1 + S(\vartheta_3 - \vartheta_2)S(\vartheta_3 - \vartheta_1)S(-2\vartheta_3)]F(\vartheta_2 + i\pi, \vartheta_1 + i\pi, -\vartheta_3)K(\vartheta_3)\,,
\end{aligned} \tag{C.1.9}$$

$$\begin{aligned}
T_4 =& \frac{1}{8}\int_{-\infty}^{+\infty} \frac{\mathrm{d}\vartheta_1'}{2\pi}\int_{-\infty}^{+\infty} \frac{\mathrm{d}\vartheta_2'}{2\pi}\Big[[E_0(p) - E(\vartheta_1) - E(\vartheta_2) - E(\vartheta_3) + 2E(\vartheta_1' + i\varepsilon) + 2E(\vartheta_2' + i\varepsilon)] \\
&\times F(\vartheta_3 + i\pi, \vartheta_2 + i\pi, \vartheta_1 + i\pi, -\vartheta_1' - i\varepsilon, \vartheta_1' + i\varepsilon, -\vartheta_2' - i\varepsilon, \vartheta_2' + i\varepsilon)K(\vartheta_1' + i\varepsilon)K(\vartheta_2' + i\varepsilon)\Big] \\
&+ \frac{1}{4}\int_{-\infty}^{+\infty} \frac{\mathrm{d}\vartheta'}{2\pi}[E_0(p) + E(\vartheta_1) - E(\vartheta_2) - E(\vartheta_3) + 2E(\vartheta' + i\varepsilon)]F(\vartheta_3 + i\pi, \vartheta_2 + i\pi, -\vartheta_1, -\vartheta' - i\varepsilon, \vartheta' + i\varepsilon) \\
&\times [S(\vartheta_3 - \vartheta_1)S(\vartheta_2 - \vartheta_1)S(\vartheta_1 - \vartheta' - i\varepsilon)S(\vartheta_1 + \vartheta' + i\varepsilon) + S(-2\vartheta_1)]K(\vartheta' + i\varepsilon)K(\vartheta_1) \\
&+ \frac{1}{4}\int_{-\infty}^{+\infty} \frac{\mathrm{d}\vartheta'}{2\pi}[E_0(p) - E(\vartheta_1) + E(\vartheta_2) - E(\vartheta_3) + 2E(\vartheta' + i\varepsilon)]F(\vartheta_3 + i\pi, \vartheta_1 + i\pi, -\vartheta_2, -\vartheta' - i\varepsilon, \vartheta' + i\varepsilon) \\
&\times [S(\vartheta_3 - \vartheta_2)S(\vartheta_2 - \vartheta' - i\varepsilon)S(\vartheta_2 + \vartheta' + i\varepsilon) + S(\vartheta_2 - \vartheta_1)S(-2\vartheta_2)]K(\vartheta' + i\varepsilon)K(\vartheta_2) \\
&+ \frac{1}{4}\int_{-\infty}^{+\infty} \frac{\mathrm{d}\vartheta'}{2\pi}[E_0(p) - E(\vartheta_1) - E(\vartheta_2) + E(\vartheta_3) + 2E(\vartheta' + i\varepsilon)]F(\vartheta_2 + i\pi, \vartheta_1 + i\pi, -\vartheta_3, -\vartheta' - i\varepsilon, \vartheta' + i\varepsilon) \\
&\times [S(\vartheta_3 - \vartheta' - i\varepsilon)S(\vartheta_3 + \vartheta' + i\varepsilon) + S(\vartheta_3 - \vartheta_1)S(\vartheta_3 - \vartheta_2)S(-2\vartheta_3)]K(\vartheta' + i\varepsilon)K(\vartheta_3) \\
&+ \frac{1}{4}[E_0(p) + E(\vartheta_1) + E(\vartheta_2) - E(\vartheta_3)]F(\vartheta_3 + i\pi, -\vartheta_1, -\vartheta_2)[S(\vartheta_3 - \vartheta_1)S(\vartheta_2 + \vartheta_1)S(\vartheta_3 - \vartheta_2)K(\vartheta_1)K(\vartheta_2) \\
&+ S(\vartheta_3 - \vartheta_1)K(\vartheta_1)K(-\vartheta_2) + S(\vartheta_3 - \vartheta_2)K(-\vartheta_1)K(\vartheta_2) + S(-\vartheta_2 - \vartheta_1)K(-\vartheta_1)K(-\vartheta_2)] \\
&+ \frac{1}{4}[E_0(p) + E(\vartheta_1) - E(\vartheta_2) + E(\vartheta_3)]F(\vartheta_2 + i\pi, -\vartheta_1, -\vartheta_3)[S(\vartheta_2 - \vartheta_1)S(\vartheta_3 + \vartheta_1)K(\vartheta_1)K(\vartheta_3) \\
&+ S(\vartheta_2 - \vartheta_1)S(\vartheta_3 - \vartheta_2)K(\vartheta_1)K(-\vartheta_3) + K(-\vartheta_1)K(\vartheta_3) + S(\vartheta_3 - \vartheta_2)S(-\vartheta_3 - \vartheta_1)K(-\vartheta_1)K(-\vartheta_3)] \\
&+ \frac{1}{4}[E_0(p) - E(\vartheta_1) + E(\vartheta_2) + E(\vartheta_3)]F(\vartheta_1 + i\pi, -\vartheta_2, -\vartheta_3)[S(\vartheta_2 + \vartheta_3)K(\vartheta_2)K(\vartheta_3) \\
&+ S(\vartheta_3 - \vartheta_1)K(\vartheta_2)K(-\vartheta_3) + S(\vartheta_2 - \vartheta_1)K(-\vartheta_2)K(\vartheta_3) \\
&+ S(-\vartheta_3 - \vartheta_2)S(\vartheta_3 - \vartheta_1)S(\vartheta_2 - \vartheta_1)K(-\vartheta_1)K(-\vartheta_3)]\,,
\end{aligned} \tag{C.1.10}$$

and $p = m\sinh\vartheta_1 + m\sinh\vartheta_2 + m\sinh\vartheta_3$, valid as long as Im $\vartheta_i < \varepsilon$. For other complex values of the test rapidities it can be continued analytically similarly to the one-particle equation; the condition satisfied by

the Dirichlet function K_D can be obtained by dropping the terms containing combinations of E_0 and E in the square brackets.

C.2 Comparing to the infinite volume formalism

The equation hierarchy can be obtained directly from substituting the infinite volume matrix element (3.2.14) into (6.1.15). Considering the case of a one-particle test state, from (6.2.16) one obtains

$$\begin{aligned}
0 =&[E_0(p)-E(\vartheta)]F_1^\phi+[E_0(p)+E(\vartheta)]F_1^\phi K(\vartheta)\\
&+\frac{1}{2}\int_{-\infty}^{+\infty}\frac{d\vartheta'}{2\pi}[E_0(p)-E(\vartheta)+2E(\vartheta')]F_3^\phi(\vartheta+i\pi+i0,-\vartheta'-i0,\vartheta'-i0)K(\vartheta')\\
&+\frac{1}{2}\int_{-\infty}^{+\infty}\frac{d\vartheta'}{2\pi}[E_0(p)+E(\vartheta)+2E(\vartheta')]F_3^\phi(-\vartheta'-i0,\vartheta'-i0,-\vartheta-i0)K(\vartheta')K(\vartheta)\\
&+\frac{1}{8}\int_{-\infty}^{+\infty}\frac{d\vartheta_1'}{2\pi}\int_{-\infty}^{+\infty}\frac{d\vartheta_2'}{2\pi}[E_0(p)-E(\vartheta)+2E(\vartheta_1')+2E(\vartheta_2')]\\
&\qquad\times F_5^\phi(\vartheta+i\pi+i0,-\vartheta_1'-i0,\vartheta_1'-i0,-\vartheta_2'-i0,\vartheta_2'-i0)K(\vartheta_1')K(\vartheta_2')+\dots\,.
\end{aligned}\tag{C.2.1}$$

In the finite volume formula it is necessary to take the form (C.1.3) valid for $\mathrm{Im}\theta>\varepsilon$ to have the same ordering of the imaginary parts between the unprimed and primed rapidity variables as in (C.2.1) above. Shifting back the contours to the real axis, and absorbing S-matrix factors by reordering the rapidity variables in the corresponding form factor gives

$$\begin{aligned}
0 =&[E_0(p)-E(\vartheta)]F_1^\phi+[E_0(p)+E(\vartheta)]F_1^\phi K(\vartheta)\\
&+\frac{1}{2}\int_{-\infty}^{+\infty}\frac{d\vartheta'}{2\pi}[E_0(p)-E(\vartheta)+2E(\vartheta')]F_3^\phi(\vartheta+i\pi+i\varepsilon,-\vartheta',\vartheta')K(\vartheta')\\
&+\frac{1}{2}\int_{-\infty}^{+\infty}\frac{d\vartheta'}{2\pi}[E_0(p)+E(\vartheta)+2E(\vartheta')]K(\vartheta)F_3^\phi(-\vartheta',\vartheta',-\vartheta)K(\vartheta')\\
&+\frac{1}{8}\int_{-\infty}^{+\infty}\frac{d\vartheta_1'}{2\pi}\int_{-\infty}^{+\infty}\frac{d\vartheta_2'}{2\pi}[E_0(p)-E(\vartheta)+2E(\vartheta_1')+2E(\vartheta_2')]\\
&\qquad\times F_5^\phi(\theta+i\pi+i\varepsilon,-\vartheta_1',\vartheta_1',-\vartheta_2',\vartheta_2')K(\vartheta_1')K(\vartheta_2')+\dots\,.
\end{aligned}$$

Due to the $+i0$ shifts in the unprimed rapidities, the $-i0$ shifts in (C.2.1) can be eliminated, making the two equations identical.

Similar identity can be demonstrated for the three-test particle condition; as it contains no essential novelty compared to the one-particle case, for the sake of brevity we omit the details here.

Appendix D

Tables for the three particle test states

The tables in this Section contain a sample of numerical data obtained from numerical evaluation of the three-particle condition (C.1.7). The first three terms T_0, T_2 and T_4 were evaluated using the integral formulae. The first line labeled "sum" gives the sum of these three terms, and verifies how precisely the condition is satisfied in this truncation. For the evaluation of T_6 it proved practical to use the finite volume sum form (3.3.4). The second line labeled "sum" gives the value of the three-particle condition once the computed result for T_6 is included as well.

D.1 B=0.1

$\{\theta_1,\theta_2,\theta_3\}=\{0.0607,0.1277,0.2606\}$				$\{\theta_1,\theta_2,\theta_3\}=\{-0.0866,0.0495,0.1621\}$		
m_0	∞	10	2	∞	10	2
T_0	-0.0138-0.0067 i	-0.0963-0.0464 i	0.0137 +0.0066 i	-0.0175-0.0175 i	-0.1222-0.1222 i	0.0178 +0.0178 i
T_2	-1.8826-0.908 i	-13.8152-6.6628 i	-0.6397-0.3085 i	26.5853 +26.5881 i	195.393 +195.413 i	8.7483 +8.7492 i
T_4	1.9096 +0.9209 i	13.9958 +6.7499 i	0.6241 +0.301 i	-26.9231-26.9261 i	-197.666-197.688 i	-8.7886-8.7895 i
sum	0.0131 +0.0063 i	0.0843 +0.0406 i	-0.0019-0.0009 i	-0.3553-0.3556 i	-2.3951-2.3972 i	-0.0225-0.0226 i
T_6	-0.0122-0.0059 i	-0.0826-0.0398 i	-0.0015-0.0007 i	0.3523 +0.3524 i	2.4211 +2.4213 i	0.0492 +0.0492 i
sum	0.0009 +0.0004 i	0.0017 +0.0008 i	-0.0034-0.0016 i	-0.0029-0.0032 i	0.026 +0.0241 i	0.0267 +0.0266 i

$\{\theta_1,\theta_2,\theta_3\}=\{-0.078,0.4879,0.2606\}$				$\{\theta_1,\theta_2,\theta_3\}=\{0.7633,0.8322,0.9462\}$		
m_0	∞	10	2	∞	10	2
T_0	0.0415 -0.0275 i	0.2859 -0.1889 i	-0.0446+0.0295 i	-0.013-0.0046 i	-0.0813-0.0289 i	0.0086 +0.0031 i
T_2	-21.9148+14.4858 i	-159.244+105.261 i	-6.7734+4.4773 i	-0.0402-0.0143 i	-0.2756-0.0978 i	-0.0201-0.0071 i
T_4	22.1749 -14.6577 i	160.966 -106.399 i	6.7582 -4.4672 i	0.0424 +0.0151 i	0.2876 +0.1021 i	0.0109 +0.0039 i
sum	0.3016 -0.1994 i	2.0086 -1.3278 i	-0.0598+0.0395 i	-0.0108-0.0038 i	-0.0692-0.0246 i	-0.0006-0.0002 i
T_6	-0.3085+0.2039 i	-2.0947+1.3846 i	-0.0402+0.0265 i	0.0112 +0.004 i	0.0695 +0.0247 i	0.0009 +0.0003 i
sum	-0.0068+0.0045 i	-0.0861+0.0568 i	-0.1+0.0661 i	0.0003 +0.0001 i	0.0003 +0.0001 i	0.0003 +0.0001 i

$\{\theta_1,\theta_2,\theta_3\}=\{-0.9706,1.5852,-2.13\}$				$\{\theta_1,\theta_2,\theta_3\}=\{0.5267,1.5444,2.1303\}$		
m_0	∞	10	2	∞	10	2
T_0	0.0095 +0.0009 i	0.0199 +0.0018 i	-0.0451-0.0041 i	0.0411 -0.0194 i	0.177 -0.0838 i	-0.0263+0.0124 i
T_2	-0.6149-0.0565 i	-2.6313-0.2417 i	0.0003	0.0509 -0.0241 i	0.2783 -0.1317 i	0.0221 -0.0104 i
T_4	0.6181 +0.0568 i	2.687 +0.2469 i	0.0311 +0.0029 i	-0.0542+0.0257 i	-0.2771+0.1311 i	-0.0052+0.0024 i
sum	0.0127 +0.0012 i	0.0757 +0.007 i	-0.0137-0.0013 i	0.0377 -0.0179 i	0.1783 -0.0844 i	-0.0094+0.0044 i
T_6	0.0044 +0.0004 i	0.0191 +0.0018 i	0.0001	0.0016 -0.0007 i	0.008 -0.0038 i	0.0001
sum	0.0171 +0.0016 i	0.0948 +0.0087 i	-0.0136-0.0012 i	0.0393 -0.0186 i	0.1862 -0.0881 i	-0.0093+0.0044 i

D.2 B=0.5

$\{\theta_1,\theta_2,\theta_3\}=\{0.0534,0.1261,0.2692\}$				$\{\theta_1,\theta_2,\theta_3\}=\{-0.0958,0.05,0.1708\}$		
m_0	∞	10	2	∞	10	2
T_0	-0.005+0.0072 i	-0.0346+0.0504 i	0.0049 -0.0072 i	-0.012+0.0132 i	-0.0836+0.0919 i	0.0122 -0.0134 i
T_2	-0.5063+0.7382 i	-3.7154+5.4174 i	-0.1732+0.2526 i	10.3305 -11.353 i	75.9036 -83.4169 i	3.3881 -3.7235 i
T_4	0.5317 -0.7753 i	3.8838 -5.6629 i	0.1681 -0.2452 i	-10.7851+11.8527 i	-78.8828+86.6909 i	-3.4052+3.7423 i
sum	0.0205 -0.0299 i	0.1338 -0.1951 i	-0.0001+0.0002 i	-0.4666+0.5128 i	-3.0628+3.366 i	-0.005+0.0055 i
T_6	-0.0201+0.0293 i	-0.134+0.1954 i	-0.0023+0.0033 i	0.4811 -0.5287 i	3.2224 -3.5414 i	0.0552 -0.0606 i
sum	0.0004 -0.0006 i	-0.0002+0.0003 i	-0.0024+0.0035 i	0.0145 -0.0159 i	0.1596 -0.1754 i	0.0502 -0.0552 i

$\{\theta_1,\theta_2,\theta_3\}=\{-0.0775,-0.4968,0.1173\}$				$\{\theta_1,\theta_2,\theta_3\}=\{0.7577,0.8313,0.9519\}$		
m_0	∞	10	2	∞	10	2
T_0	0.0579 -0.1144 i	0.398 -0.7868 i	-0.0625+0.1236 i	-0.0035+0.0059 i	-0.0221+0.0366 i	0.0023 -0.0039 i
T_2	-16.5658+32.7473 i	-120.284+237.778 i	-5.0646+10.0117 i	-0.0086+0.0143 i	-0.0597+0.0991 i	-0.0047+0.0078 i
T_4	17.2361 -34.0724 i	124.58 -246.27 i	5.1212 -10.1237 i	0.0104 -0.0173 i	0.0712 -0.118 i	0.0026 -0.0043 i
sum	0.7282 -1.4395 i	4.6937 -9.2786 i	-0.0059+0.0116 i	-0.0017+0.0028 i	-0.0106+0.0176 i	0.0002 -0.0003 i
T_6	-0.7247+1.4325 i	-4.7758+9.4408 i	-0.0747+0.1476 i	0.0017 -0.0028 i	0.01 -0.0166 i	0.0001 -0.0002 i
sum	0.0035 -0.007 i	-0.0821+0.1622 i	-0.0806+0.1593 i	-0.0001+0.0001 i	-0.0006+0.001 i	0.0003 -0.0005 i

$\{\theta_1,\theta_2,\theta_3\}=\{-0.9692,1.5855,-2.1307\}$				$\{\theta_1,\theta_2,\theta_3\}=\{0.5223,1.5347,2.1319\}$		
m_0	∞	10	2	∞	10	2
T_0	0.1249 +0.0499 i	0.2626 +0.105 i	-0.5949-0.238 i	-0.0439-0.4658 i	-0.1891-2.0068 i	0.0282 +0.2994 i
T_2	-6.3313-2.5327 i	-26.9395-10.7763 i	0.0664 +0.0266 i	-0.0486-0.5161 i	-0.2742-2.9104 i	-0.0215-0.2286 i
T_4	6.4396 +2.576 i	27.724 +11.0901 i	0.3068 +0.1227 i	0.0606 +0.6434 i	0.3182 +3.3773 i	0.0054 +0.057 i
sum	0.2331 +0.0932 i	1.0471 +0.4189 i	-0.2216-0.0887 i	-0.0319-0.3384 i	-0.1451-1.54 i	0.012 +0.1278 i
T_6	0.0389 +0.0156 i	0.1561 +0.0624 i	0.0004 +0.0002 i	0.0003 +0.0029 i	0.0019 +0.0203 i	0.0001 +0.0005 i
sum	0.272 +0.1088 i	1.2032 +0.4813 i	-0.2212-0.0885 i	-0.0316-0.3355 i	-0.1432-1.5197 i	0.0121 +0.1283 i

D.3 B=0.9

$\{\theta_1,\theta_2,\theta_3\}=\{0.0526,0.1259,0.2702\}$				$\{\theta_1,\theta_2,\theta_3\}=\{-0.097,0.05,0.1719\}$		
m_0	∞	10	2	∞	10	2
T_0	-0.0039+0.0084 i	-0.0275+0.0586 i	0.0039 -0.0084 i	-0.0098+0.0164 i	-0.0686+0.1144 i	0.01 -0.0167 i
T_2	-0.3545+0.7563 i	-2.6022+5.5512 i	-0.1218+0.2598 i	7.2362 -12.0605 i	53.1652 -88.6102 i	2.3711 -3.9519 i
T_4	0.3772 -0.8046 i	2.7507 -5.868 i	0.1176 -0.2509 i	-7.6368+12.7282 i	-55.7598+92.9346 i	-2.3777+3.963 i
sum	0.0187 -0.0399 i	0.121 -0.2582 i	-0.0002+0.0005 i	-0.4105+0.6841 i	-2.6632+4.4387 i	0.0034 -0.0057 i
T_6	-0.0179+0.0381 i	-0.1182+0.2523 i	-0.0019+0.0041 i	0.4182 -0.697 i	2.7766 -4.6278 i	0.045 -0.0751 i
sum	0.0009 -0.0018 i	0.0028 -0.006 i	-0.0021+0.0046 i	0.0077 -0.0128 i	0.1134 -0.189 i	0.0484 -0.0807 i

$\{\theta_1,\theta_2,\theta_3\}=\{-0.0771,-0.4988,0.1191\}$				$\{\theta_1,\theta_2,\theta_3\}=\{0.7571,0.8312,0.9526\}$		
m_0	∞	10	2	∞	10	2
T_0	0.0582 -0.1498 i	0.4 -1.0295 i	-0.0629+0.1619 i	-0.0027+0.0066 i	-0.0171+0.0412 i	0.0018 -0.0044 i
T_2	-13.8111+35.5416 i	-100.262+258.014 i	-4.2068+10.8259 i	-0.006+0.0145 i	-0.042+0.1009 i	-0.0034+0.0083 i
T_4	14.5091 -37.3378 i	104.671 -269.361 i	4.2464 -10.9278 i	0.0077 -0.0186 i	0.0527 -0.1268 i	0.0019 -0.0045 i
sum	0.7562 -1.9459 i	4.8094 -12.3765 i	-0.0233+0.06 i	-0.001+0.0025 i	-0.0064+0.0153 i	0.0003 -0.0006 i
T_6	-0.7363+1.8948 i	-4.804+12.3627 i	-0.0705+0.1815 i	0.0008 -0.0019 i	0.0048 -0.0116 i	0.0001 -0.0001 i
sum	0.0198 -0.0511 i	0.0054 -0.0138 i	-0.0938+0.2414 i	-0.0002+0.0006 i	-0.0015+0.0037 i	0.0003 -0.0007 i

$\{\theta_1, \theta_2, \theta_3\} = \{-0.9687, 1.5857, -2.131\}$				$\{\theta_1, \theta_2, \theta_3\} = \{0.5205, 1.5437, 2.1324\}$		
m_0	∞	10	2	∞	10	2
T_0	0.2713 +0.1465 i	0.5702 +0.3079 i	-1.2928-0.6982 i	-0.4238-0.7565 i	-1.8254-3.2585 i	0.2728 +0.487 i
T_2	-12.4191-6.7073 i	-52.7054-28.465 i	0.1829 +0.0988 i	-0.4415-0.7882 i	-2.5287-4.5139 i	-0.1971-0.3518 i
T_4	12.6765 +6.8463 i	54.3523 +29.3545 i	0.5922 +0.3198 i	0.5858 +1.0456 i	3.0962 +5.5269 i	0.0496 +0.0885 i
sum	0.5287 +0.2855 i	2.2171 +1.1974 i	-0.5177-0.2796 i	-0.2796-0.4991 i	-1.2579-2.2455 i	0.1253 +0.2237 i
T_6	-0.013-0.007 i	-0.0768-0.0415 i	-0.0012-0.0007 i	0.0174 +0.0311 i	0.0901 +0.1609 i	0.0009 +0.0015 i
sum	0.5157 +0.2785 i	2.1403 +1.1559 i	-0.5189-0.2802 i	-0.2621-0.4679 i	-1.1678-2.0846 i	0.1262 +0.2252 i

Appendix E

Some useful relations

Here we collect some useful formulae regarding the K function and form factors, identities from the theory of distributions and relations for the stationary phase approximation (SPA) that are useful in the text.

E.1 The K function

The K function possesses a singularity at the origin, if the one particle coupling to the boundary denoted by g is non-zero. In this case, the singular term in K is

$$K(\vartheta) \propto -i\frac{g^2}{2}\frac{1}{\vartheta}\,. \tag{E.1.1}$$

Due to the relation $K(-\vartheta) = S(-2\vartheta)K(\vartheta)$ the constant term in the expansion of K is also expressible with g. Writing K as

$$K(\vartheta) = -i\frac{g^2}{2}\frac{1}{\vartheta} + K_0 + K_1\vartheta + \dots\,, \tag{E.1.2}$$

and expanding

$$S(\vartheta) = -1 - i\varphi(0)\vartheta + \frac{1}{2}\varphi^2(0)\vartheta^2 + \dots\,, \tag{E.1.3}$$

one obtains

$$K_0 = \frac{\varphi(0)g^2}{2}\,, \tag{E.1.4}$$

hence

$$K(\vartheta) = -i\frac{g^2}{2}\frac{1}{\vartheta} + \frac{\varphi(0)g^2}{2} + K_1\vartheta + \dots\,. \tag{E.1.5}$$

Also note that due to real analyticity $K(-\vartheta) = K^*(\vartheta)$, all even/odd coefficients in the expansion of K around $\vartheta = 0$ are purely real/imaginary, respectively.

E.2 Form factor singularities and expansions

Consider form factors for a single species, such as the the multi-B_1 form factors of the sine–Gordon model. Using the form factor equations (3.2.4) and (3.2.6) one can derive the universal expression

$$F_3(i\pi, -\varepsilon, \varepsilon) = \frac{4i}{\varepsilon}F_1 - 4iF_1\frac{f''_{min}(0)}{f'_{min}(0)} + \mathcal{O}(\varepsilon)\,, \tag{E.2.1}$$

where

$$\frac{f''_{min}(0)}{f'_{min}(0)} = i\varphi(0) \,, \tag{E.2.2}$$

i.e. the first derivative of the S-matrix at the origin. Another form factor we need is $F_5(i\pi, -\varepsilon, \varepsilon, -\vartheta, \vartheta)$, where ϑ is non-zero. Using (3.2.10), one can explicitly compute

$$F_5(i\pi, -\varepsilon, \varepsilon, -\vartheta, \vartheta) = \frac{4i}{\varepsilon} F_3(-\vartheta, \vartheta, 0) + 4F_3(-\vartheta, \vartheta, 0)\varphi(0) + \mathcal{O}(\varepsilon) \tag{E.2.3}$$

which is universal as well.

For $F_5(i\pi + \vartheta + \varepsilon, i\pi - \vartheta - \varepsilon, -\vartheta, \vartheta, 0)$ the most singular term is $O(\epsilon^{-2})$, however, we also need the ε^{-1} terms. Denoting the coefficient of the sub-leading singularity by $F_5^{\varepsilon}(\vartheta)$, it can be shown based on (3.2.10) that

$$\begin{aligned} F_5(i\pi + \vartheta, i\pi - \vartheta, -\vartheta - \varepsilon, \vartheta + \varepsilon, 0) =& \frac{1}{\varepsilon^2} \left(1 - S(\vartheta)\right) \left(1 - S(-\vartheta)\right) F_1 \\ &+ \frac{1}{\varepsilon} F_5^{\varepsilon}(\vartheta) + \text{regular} \,, \\ F_5(i\pi + \vartheta, i\pi - \vartheta, \vartheta - \varepsilon, -\vartheta + \varepsilon, 0) =& \frac{1}{\varepsilon^2} S(2\vartheta) \left(1 - S(\vartheta)\right) \left(1 - S(-\vartheta)\right) F_1 \\ &+ \frac{1}{\varepsilon} S(2\vartheta) F_5^{\varepsilon}(-\vartheta) + \text{regular} \,, \end{aligned} \tag{E.2.4}$$

where

$$F_5^{\varepsilon}(\vartheta) \approx \frac{8F_1}{\vartheta} \,, \qquad \vartheta \to 0 \,. \tag{E.2.5}$$

E.3 Some distribution identities

Suppose that $f(x)$ is a well behaved function with vanishing at infinity. Then it is well-known that

$$\int_{-\infty}^{\infty} dx \frac{f(x)}{x - x_0 + i\epsilon} = P \int_{-\infty}^{\infty} dx \frac{f(x)}{x - x_0} - i\pi f(x_0) \,, \tag{E.3.1}$$

where $P\int$ denotes the principal value. This identity has the following counterpart for second order singularity

$$\int_{-\infty}^{\infty} dx \frac{f(x)}{(x - x_0 + i\epsilon)^2} = P \int_{-\infty}^{\infty} dx \frac{f'(x)}{x - x_0} - i\pi f'(x_0) \,. \tag{E.3.2}$$

One can also write

$$\int_{-\infty}^{\infty} dx \frac{f(x)}{\sinh\left(x - x_0 + i\epsilon\right)} = P \int_{-\infty}^{\infty} dx \frac{f(x)}{\sinh\left(x - x_0\right)} - i\pi f(x_0) \,, \tag{E.3.3}$$

and

$$\int_{-\infty}^{\infty} dx f(x) \frac{\cosh\left(x - x_0 + i\epsilon\right)}{\sinh^2\left(x - x_0 + i\epsilon\right)} = P \int_{-\infty}^{\infty} dx \frac{f'(x)}{\sinh\left(x - x_0\right)} - i\pi f'(x_0) \,. \tag{E.3.4}$$

hold as well. A useful way of evaluating the principal value integral is

$$P \int_{-\infty}^{\infty} dx \frac{f(x)}{x - x_0} = \int_{-\infty}^{\infty} dx \frac{f(x) - f(x_0)/g(x - x_0)}{x - x_0} \,, \tag{E.3.5}$$

where $g(x)$ is an appropriate mask function that is even, grows at the infinity and satisfies $g(0) = 1$, a convenient choice being $g(x) = \cosh x$.

E.4 Stationary phase approximation

Consider the following integral with oscillatory argument:

$$\frac{1}{2\pi}\int dx f(x) e^{itg(x)} ,$$

in which $g(x)$ has one global extremum at x_0, and $f(x)$ is regular and decays fast enough for large $|x|$. The asymptotic behaviour of this integral for large t can then be evaluated as

$$\frac{1}{2\pi}\int_{-\infty}^{\infty} dx f(x) e^{itg(x)} = \frac{f(x_0) e^{itg(x_0)} e^{i\pi/4 \mathrm{sign}(g"(x_0))}}{\sqrt{2\pi t |g"(x_0)|}} + \mathcal{O}(t^{-3/2}) . \tag{E.4.1}$$

Appendix F

The finite volume 1-point function in the presence of boundaries

The expectation value of a local operator in a finite volume with boundaries

$$\langle \mathcal{O}(x)\rangle^B = \frac{\langle B|\ e^{-Hx}\mathcal{O}(0)\ e^{-H(\mathcal{R}-x)}\ |B\rangle}{\langle B|e^{-H\mathcal{R}}|B\rangle} = \sum_{k,l} D_{kl} \tag{F.0.1}$$

was calculated in [165] up to contributions D_{kl} with $k+l \leq 4$. We quote here the result:

$$\begin{aligned}
D_{10} &= \frac{g_B}{2} F_1^{\mathcal{O}} e^{-mx}\ , \\
D_{20} &= \frac{1}{2}\int \frac{d\vartheta}{2\pi} K_B(\vartheta) F_2^{\mathcal{O}}(-\vartheta,\vartheta) e^{-2m\cosh\vartheta\ x}\ , \\
D_{30} &= \frac{1}{2}\int \frac{d\vartheta}{2\pi} K_B(\vartheta) \frac{g_B}{2} F_3^{\mathcal{O}}(-\vartheta,\vartheta,0) e^{-m(2\cosh\vartheta+1)\ x}\ , \\
D_{40} &= \frac{1}{8}\int \frac{d\vartheta_1}{2\pi}\frac{d\vartheta_2}{2\pi} K_B(\vartheta_1) K_B(\vartheta_2) F_4^{\mathcal{O}}(-\vartheta_1,\vartheta_1,-\vartheta_2,\vartheta_2) e^{-2m(\cosh\vartheta_1+\cosh\vartheta_2)\ x}\ , \\
D_{01} &= \frac{g_B}{2} F_1^{\mathcal{O}} e^{-m(\mathcal{R}-x)}\ , \\
D_{02} &= \frac{1}{2}\int \frac{d\vartheta}{2\pi} K_B(\vartheta) F_2^{\mathcal{O}}(-\vartheta,\vartheta) e^{-2m\cosh\vartheta\ (\mathcal{R}-x)}\ , \\
D_{03} &= \frac{1}{2}\int \frac{d\vartheta}{2\pi} K_B(\vartheta) \frac{g_B}{2} F_3^{\mathcal{O}}(-\vartheta,\vartheta,0) e^{-m(2\cosh\vartheta+1)\ (\mathcal{R}-x)}\ , \\
D_{04} &= \frac{1}{8}\int \frac{d\vartheta_1}{2\pi}\frac{d\vartheta_2}{2\pi} K_B(\vartheta_1) K_B(\vartheta_2) F_4^{\mathcal{O}}(-\vartheta_1,\vartheta_1,-\vartheta_2,\vartheta_2) e^{-2m(\cosh\vartheta_1+\cosh\vartheta_2)\ (\mathcal{R}-x)}\ ,
\end{aligned} \tag{F.0.2}$$

and

$$
\begin{aligned}
D_{11} &= \frac{g_B^2}{4} F_{2,s}^{\mathcal{O}} e^{-m\mathcal{R}} \ , \\
D_{21} &= \frac{g_B}{4} \int \frac{d\vartheta}{2\pi} \left(F_3^{\mathcal{O}}(-\vartheta + i\pi, \vartheta + i\pi, 0) K_B(\vartheta) e^{-2m\cosh\vartheta x - m(\mathcal{R}-x)} - \frac{2g_B^2 F_1^{\mathcal{O}} \cosh\vartheta}{\sinh^2\vartheta} e^{-m(\mathcal{R}+x)} \right) \\
&\quad + e^{-m(x+\mathcal{R})} g_B^3 F_1^{\mathcal{O}} \frac{\varphi(0)}{4} \ , \\
D_{12} &= \frac{g_B}{4} \int \frac{d\vartheta}{2\pi} \left(F_3^{\mathcal{O}}(i\pi, -\vartheta, \vartheta) K_B(\vartheta) e^{-2m\cosh\vartheta(\mathcal{R}-x) - mx} - \frac{2g_B^2 F_1^{\mathcal{O}} \cosh\vartheta}{\sinh^2\vartheta} e^{-m(2\mathcal{R}-x)} \right) \\
&\quad + e^{-m(2\mathcal{R}-x)} g_B^3 F_1^{\mathcal{O}} \frac{\varphi(0)}{4} \ , \\
D_{31} &= \frac{g_B^2}{8} e^{-m\mathcal{R}} \int \frac{d\vartheta}{2\pi} K_B(\vartheta) F_4^{\mathcal{O}}(-\vartheta + i\pi, \vartheta + i\pi, i\pi, 0) e^{-2m\cosh\vartheta \ x} \ , \\
D_{13} &= \frac{g_B^2}{8} e^{-m\mathcal{R}} \int \frac{d\theta}{2\pi} K_B(\vartheta) F_4^{\mathcal{O}}(-\vartheta + i\pi, \vartheta + i\pi, i\pi, 0) e^{-2m\cosh\vartheta \ (\mathcal{R}-x)} \ , \\
D_{22} &= \frac{1}{4} \int \frac{d\vartheta_1}{2\pi} \frac{d\vartheta_2}{2\pi} K_B(\vartheta_1) K_B(\vartheta_2) F_4^{\mathcal{O}}(-\vartheta_1 + i\pi, \vartheta_1 + i\pi, -\vartheta_2, \vartheta_2) e^{-2m\cosh\vartheta_1 x - 2m\cosh\vartheta_2(\mathcal{R}-x)} \\
&\quad + F_{2,s}^{\mathcal{O}} \int \frac{d\vartheta}{2\pi} \Big(K_B(-\vartheta) K_B(\vartheta) e^{-2m\cosh\vartheta\mathcal{R}} - \frac{g_B^4 \cosh\vartheta}{4\sinh^2\vartheta} e^{-2m\mathcal{R}} \Big) + F_{2,s}^{\mathcal{O}} \frac{g_B^4}{8} e^{-2m\mathcal{R}} \varphi(0) \ ,
\end{aligned}
\tag{F.0.3}
$$

where $F_{2,s}^{\mathcal{O}} = F_2^{\mathcal{O}}(i\pi, 0)$ and

$$
\varphi(\vartheta) = -i \frac{\partial \log S(\vartheta)}{\partial \vartheta} \ .
$$

Appendix G

Evaluating D_{12}

In order to analyse the time dependence of the term

$$\frac{g}{2}\Re e\int_{-\infty}^{\infty}\frac{d\vartheta}{2\pi}\left\{K(\vartheta)F_3^{\mathcal{O}}(i\pi,-\vartheta,\vartheta)e^{-imt(2\cosh\vartheta-1)}-2g^2\frac{\cosh\vartheta}{\sinh^2\vartheta}F_1^{\mathcal{O}}e^{-imt}\right\}, \tag{G.0.1}$$

we reintroduce the regulator R enabling us to shift the contour off the real axis where (as shown in [165]), the contribution from the term

$$\frac{\cosh\vartheta}{\sinh^2\vartheta}$$

vanishes, i.e., we end up with

$$\frac{g}{2}\Re e\int_{-\infty+i\varepsilon}^{\infty+i\varepsilon}\frac{d\vartheta}{2\pi}\left\{K(\vartheta)F_3^{\mathcal{O}}(i\pi,-\vartheta,\vartheta)e^{-imt(2\cosh\vartheta-1)}e^{-mR/2(2\cosh\vartheta+1)}\right\}. \tag{G.0.2}$$

Using now (E.3.4), we find

$$\begin{aligned}
D_{12}(R)=&\frac{g}{2}\Re e\int_{-\infty+i\varepsilon}^{\infty+i\varepsilon}\frac{d\vartheta}{2\pi}\frac{\left(\sinh^2\vartheta K(\vartheta)F_3^{\mathcal{O}}(i\pi,-\vartheta,\vartheta)e^{-imt(2\cosh\vartheta-1)}e^{-mR/2(2\cosh\vartheta+1)}/\cosh\vartheta\right)'}{\sinh\vartheta}\\
D_{12}=&\frac{g}{2}\Re e\int_{-\infty}^{\infty}\frac{d\vartheta}{2\pi}\frac{\left(\sinh^2\vartheta K(\vartheta)F_3^{\mathcal{O}}(i\pi,-\vartheta,\vartheta)/\cosh\vartheta\right)e^{-imt(2\cosh\vartheta-1)}\left(-2imt\sinh\vartheta\right)}{\sinh\vartheta}\\
&+\frac{g}{2}\Re e\int_{-\infty}^{\infty}\frac{d\vartheta}{2\pi}\frac{\left(\sinh^2\vartheta K(\vartheta)F_3^{\mathcal{O}}(i\pi,-\vartheta,\vartheta)e^{-imt(2\cosh\vartheta-1)}/\cosh\vartheta\right)'e^{-imt(2\cosh\vartheta-1)}}{\sinh\vartheta},
\end{aligned} \tag{G.0.3}$$

where we placed the integration contour back to the real axis as the integrands are now free of poles for real rapidities and also got rid off the regulator by setting its value to zero. Performing the SPA (E.4.1) results in

$$\frac{g^3F_1^{\mathcal{O}}\left(\varphi^2(0)-2/3\right)}{2\sqrt{4\pi mt}}\Re e\,e^{-imt}e^{-i\pi/4}+g^3\sqrt{\frac{mt}{\pi}}\Re e\,F_1^{\mathcal{O}}e^{-imt}\frac{-\sqrt{2}-\sqrt{2}i}{2},\qquad mt\gg1. \tag{G.0.4}$$

While the first term has the standard $\sim 1/\sqrt{t}$ time dependence, the second one behaves as $\sim\sqrt{t}$ for large time. This peculiar finding is discussed in Section 8.4.3.

Appendix H

Evaluating G_5, part I. Notations, D_{05}, D_{14} and residue terms from D_{23}

In this and the following appendix we describe how to compute the five-particle contribution G_5. According to the discussion in Section 8.3 it can be obtained as (the real part of) the infinite volume limit of

$$\begin{aligned}&\tilde{D}_{05}+\tilde{D}_{14}+\tilde{D}_{23}\ ,\\ &\tilde{D}_{05}=C_{05}\ ,\\ &\tilde{D}_{14}=C_{14}-Z_1C_{03}\ ,\\ &\tilde{D}_{23}=C_{23}-Z_1C_{12}-(Z_2-Z_1^2)C_{01}\ .\end{aligned} \tag{H.0.1}$$

The calculation of $\tilde{D}_{05}$ and $\tilde{D}_{14}$ is easy; we show explicitly the cancellation of terms with positive powers of mL and extract the time dependence based on stationary phase approximation (SPA). It turns out that this time-dependence is only of sub-leading order.

The calculation of $\tilde{D}_{23}$ is, however, so long and tedious that we only extract terms accounting for the leading time-dependence and then carefully argue why other terms produce only sub-leading effects. In particular, in this Appendix we only focus on residue terms and leave contributions resulting from a contour integration for Appendix I. Finally, we provide numerical evidence for the existence of the infinite volume limit demonstrating the cancellation of terms behaving as mL and $(mL)^2$ in Appendix K.

We use the following notation to abbreviate formulas involving form form factors: whenever a vertical line is seen in the argument of the form factors, rapidities in the argument refer to rapidity pairs, and a single rapidity is indicated by putting it into brackets $\{\}$. Rapidities to the right of the line are understood to be shifted by $i\pi$. For example,

$$F_5(\vartheta_1|\vartheta_2,\{0\})=F_5(i\pi+\vartheta_1,i\pi-\vartheta_1,-\vartheta_2,\vartheta_2,0)\ ,$$

and

$$F_5(|\vartheta_1,\vartheta_2,\{0\})=F_5(-\vartheta_1,\vartheta_1,-\vartheta_2,\vartheta_2,0)\ .$$

In a similar spirit, we introduce

$$h(\vartheta_1|\vartheta_2,\{0\})_R=e^{imt(2\cosh\vartheta_1-2\cosh\vartheta_2-1)}e^{-mR/2(2\cosh\vartheta_1+2\cosh\vartheta_2+1)}\ ,$$

and

$$h(\vartheta_1,\vartheta_2,\{0\}|)_R=e^{imt(2\cosh\vartheta_1+2\cosh\vartheta_2+1)}e^{-mR/2(2\cosh\vartheta_1+2\cosh\vartheta_2+1)}\ , \tag{H.0.2}$$

and

$$h(\vartheta_1|\vartheta_2,\{0\}) = h(\vartheta_1|\vartheta_2,\{0\})_{R=0}\ . \tag{H.0.3}$$

H.1 Evaluation of $\tilde{D}_{05} = C_{05}$ and $\tilde{D}_{14} = C_{14} - Z_1 C_{03}$

Let us start with

$$\begin{aligned}\tilde{D}_{05} =& \frac{1}{2}\sum_{I\neq J}\frac{g}{2}K(\vartheta_1)K(\vartheta_2)N_5(\vartheta_1,\vartheta_2,L)_L\langle 0|\mathcal{O}(0)|\{I,-I,J,-J,0\}\rangle_L\times \\ & e^{-imt(2\cosh\vartheta_1+2\cosh\vartheta_2+1)}e^{-Rm/2(2\cosh\vartheta_1+2\cosh\vartheta_2+1)}\end{aligned} \tag{H.1.1}$$

which is free of divergences, therefore its infinite volume and $R\to 0$ limit is simply

$$D_{05} = \frac{g}{8}\int_{-\infty}^{\infty}\frac{d\vartheta_1}{2\pi}\int_{-\infty}^{\infty}\frac{d\vartheta_2}{2\pi}K(\vartheta_1)K(\vartheta_2)F_5(0,-\vartheta_1,\vartheta_1,-\vartheta_2,\vartheta_2)e^{-imt(2\cosh\vartheta_1+2\cosh\vartheta_2+1)}\ . \tag{H.1.2}$$

Concerning the long time asymptotics of this term, the stationary points are $\vartheta_1=\vartheta_2=0$ where the product of the form factor and the K factors can be expanded in non-negative powers $\vartheta_1^n\vartheta_2^m$. Applying a Gaussian approximation $\int\frac{d\vartheta_1}{2\pi}\int\frac{d\vartheta_2}{2\pi}\vartheta_1^n\vartheta_2^m e^{-itm\left(1+2\vartheta_1^2+2\vartheta_2^2\right)}$ yields time dependence of the form t^{-1-m-n} which we neglect.

Turning now to

$$\begin{aligned}C_{14} =& \frac{1}{2}\sum_{I\neq J}\frac{g}{2}K(\vartheta_1)K(\vartheta_2)N_1N_4(\vartheta_1,\vartheta_2,L)_L\langle\{0\}|O(0)|\{-I,I,J,-J\}\rangle_L\times \\ & e^{-imt(2\cosh\vartheta_1+2\cosh\vartheta_2-1)}e^{-Rm/2(2\cosh\vartheta_1+2\cosh\vartheta_2+1)}\ ,\end{aligned} \tag{H.1.3}$$

the corresponding form factor $F_5(i\pi,-\vartheta_1,\vartheta_1,-\vartheta_2,\vartheta_2)$ has a ϑ^2 behaviour around the origin when $\vartheta_1=\vartheta_2=\vartheta$, therefore it remains regular even when multiplied with the two K functions. However when only one of the rapidities is close to zero then it has a first order pole $F_5\propto\frac{1}{\vartheta}$, hence taking into account the singularity of the appropriate K function leads to a second order pole. Following the formalism introduced in [188], one can write the sum using contour integrals

$$\begin{aligned}C_{14} =& \frac{g}{4}\left(-\frac{1}{2}\right)\sum_{I\neq 0}\oint_{C_I}\frac{d\vartheta_1}{2\pi}\left(-\frac{1}{2}\right)\sum_{J\neq 0}\oint_{C_J}\frac{d\vartheta_2}{2\pi}K(\vartheta_1)K(\vartheta_2)\frac{F_5(i\pi,-\vartheta_1,\vartheta_1,-\vartheta_2,\vartheta_2)}{\left(e^{i\bar{Q}_{4,1}}+1\right)\left(e^{i\bar{Q}_{4,2}}+1\right)}\times \\ & e^{-imt(2\cosh\vartheta_1+2\cosh\vartheta_2-1)}e^{-Rm/2(2\cosh\vartheta_1+2\cosh\vartheta_2+1)}\ ,\end{aligned} \tag{H.1.4}$$

where the two-dimensional product contour $C_I\times C_J$ encircles the solution of the Bethe-Yang equation determining ϑ_1 and ϑ_2 with quantum numbers I and J . To open the contours it is necessary to subtract the residue terms when $\vartheta_1=0$ or $\vartheta_2=0$. Hence

$$\begin{aligned}C_{14} =& \frac{g}{16}\int_{-\infty+i\varepsilon}^{\infty+i\varepsilon}\frac{d\vartheta_1}{2\pi}\int_{-\infty+i\varepsilon}^{\infty+i\varepsilon}\frac{d\vartheta_2}{2\pi}K(\vartheta_1)K(\vartheta_2)\frac{F_5(\{0\}|\vartheta_1,\vartheta_2)}{\left(e^{i\bar{Q}_{4,1}}+1\right)\left(e^{i\bar{Q}_{4,2}}+1\right)}h(\{0\}|\vartheta_1,\vartheta_2)_R \\ & +\frac{g}{4}\left(-\frac{1}{2}\right)\sum_{I\neq 0}\oint_{C_I}\frac{d\vartheta_1}{2\pi}\left(\frac{1}{2}\right)\oint_{C_0}\frac{d\vartheta_2}{2\pi}K(\vartheta_1)K(\vartheta_2)\frac{F_5(\{0\}|\vartheta_1,\vartheta_2)}{\left(e^{i\bar{Q}_{4,1}}+1\right)\left(e^{i\bar{Q}_{4,2}}+1\right)}h(\{0\}|\vartheta_1,\vartheta_2)_R \\ & +\frac{g}{4}\left(-\frac{1}{2}\right)\sum_{J\neq 0}\oint_{C_J}\frac{d\vartheta_2}{2\pi}\left(\frac{1}{2}\right)\oint_{C_0}\frac{d\vartheta_1}{2\pi}K(\vartheta_1)K(\vartheta_2)\frac{F_5(\{0\}|\vartheta_1,\vartheta_2)}{\left(e^{i\bar{Q}_{4,1}}+1\right)\left(e^{i\bar{Q}_{4,2}}+1\right)}h(\{0\}|\vartheta_1,\vartheta_2)_R\ ,\end{aligned} \tag{H.1.5}$$

where we used that on the contours with imaginary parts $-i\varepsilon$ $e^{i\bar{Q}_{4,k}} \to \infty$ in the infinite volume limit. Now we split C_{14} according to the lines in (H.1.5) as $C_{14} = C_{14}^{int} + C_{14}^{res1} + C_{14}^{res2}$. Clearly, $C_{14}^{res1} = C_{14}^{res2} =: C_{14}^{res}$ and the infinite volume limit of C_{14}^{int} is regular:

$$\lim_{L\to\infty} C_{14}^{int} = \frac{g}{16}\int_{-\infty+i\varepsilon}^{\infty+i\varepsilon}\frac{d\vartheta_1}{2\pi}\int_{-\infty+i\varepsilon}^{\infty+i\varepsilon}\frac{d\vartheta_2}{2\pi}K(\vartheta_1)K(\vartheta_2)F_5(\{0\}|\vartheta_1,\vartheta_2)h(\{0\}|\vartheta_1,\vartheta_2)_R\,,$$

since $e^{i\bar{Q}_{4,k}} \to 0$ in the infinite volume limit on the contours with imaginary parts $+i\varepsilon$. The residue contribution is

$$2C_{14}^{res} = \frac{ig}{4}\left(-\frac{1}{2}\right)\sum_{I\neq 0}\oint_{C_I}\frac{d\vartheta_1}{2\pi}\oint_{C_0}\frac{d\vartheta_2}{2\pi i}K(\vartheta_1)K(\vartheta_2)\frac{F_5(\{0\}|\vartheta_1,\vartheta_2)}{\left(e^{i\bar{Q}_{4,1}}+1\right)\left(e^{i\bar{Q}_{4,2}}+1\right)}h(\{0\}|\vartheta_1,\vartheta_2)_R\,. \tag{H.1.6}$$

For $\vartheta_2 \approx 0$ based on (E.2.3)

$$\begin{aligned} F_5(\{0\}|\vartheta_1,\vartheta_2)K(\vartheta_2) &= 4iF_3(-\vartheta_1,\vartheta,0)\left(\frac{1}{\vartheta_2}-i\varphi(0)\right)\left(\frac{-ig^2}{2\vartheta_2}+\frac{g^2}{2}\varphi(0)\right)+\text{regular}\\ &= F_3(-\vartheta_1,\vartheta,0)\left(\frac{2g^2}{\vartheta_2^2}\right)+\text{regular}\,, \end{aligned} \tag{H.1.7}$$

in the contour integral around the $\vartheta_2 = 0$ point the $1/\vartheta_2^2$ term acts as a differentiation on the other regular ϑ_2 dependent factor, leading to

$$C_{14}^{res} = \frac{g^3}{16}\int_{-\infty}^{\infty}\frac{d\vartheta}{2\pi}F_3(|\{0\},\vartheta_1)K(\vartheta_1)h(\{0\}|\vartheta_1,0)_R\left(mL+2\varphi(0)+2\varphi(\vartheta_1)\right)+O\left(L^{-1}\right)\,. \tag{H.1.8}$$

Turning to $-Z_1C_{03}$ we have

$$Z_1 = \frac{g^2}{4}mLe^{-mR}$$

and

$$C_{03} = \frac{1}{2}\frac{g}{2}\int\frac{d\vartheta}{2\pi}F_3(0,-\vartheta_1,\vartheta_1)K(\vartheta_1)h(\{0\}|\vartheta_1,0)_R\,.$$

Therefore the $O(L)$ term in (H.1.8) is cancelled, resulting in

$$\begin{aligned} D_{14} &= \lim_{L\to\infty} C_{14} - Z_1C_{03}\\ &= \frac{g}{16}\int_{-\infty+i\varepsilon}^{\infty+i\varepsilon}\frac{d\vartheta_1}{2\pi}\int_{-\infty+i\varepsilon}^{\infty+i\varepsilon}\frac{d\vartheta_2}{2\pi}K(\vartheta_1)K(\vartheta_2)F_5(\{0\}|\vartheta_1,\vartheta_2)h(\{0\}|\vartheta_1,\vartheta_2)_R\\ &+\frac{g^3}{16}\int_{-\infty}^{\infty}\frac{d\vartheta}{2\pi}F_3(|\{0\},\vartheta_1)K(\vartheta_1)h(\{0\}|\vartheta_1,0)_R\left(2\varphi(0)+2\varphi(\vartheta_1)\right)\,. \end{aligned} \tag{H.1.9}$$

Pulling the contours back to the real axis by sending ε to zero, one can then send R to zero as well with the final result

$$\begin{aligned} D_{14} = \frac{g}{16}\int_{-\infty}^{\infty}\frac{d\vartheta_1}{2\pi}\int_{-\infty}^{\infty}\frac{d\vartheta_2}{2\pi}\Big\{&K(\vartheta_1)K(\vartheta_2)F_5(i\pi,-\vartheta_1,\vartheta_1,-\vartheta_2,\vartheta_2)e^{-itm(2\cosh\vartheta_1+2\cosh\vartheta_2-1)}\\ &-2g^2F_3(0,-\vartheta_2,\vartheta_2)\frac{\cosh\vartheta_1}{\sinh^2\vartheta_1}K(\vartheta_2)e^{-itm(2\cosh\vartheta_2+1)}\\ &-2g^2F_3(0,-\vartheta_1,\vartheta_1)\frac{\cosh\vartheta_2}{\sinh^2\vartheta_2}K(\vartheta_1)e^{-itm(2\cosh\vartheta_1+1)}\Big\}\\ &+\frac{g^3}{16}\int_{-\infty}^{\infty}\frac{d\vartheta}{2\pi}F_3(0,-\vartheta_1,\vartheta_1)K(\vartheta_1)e^{-itm(2\cosh\vartheta_1+1)}\left(2\varphi(0)+2\varphi(\vartheta_1)\right)\,. \end{aligned} \tag{H.1.10}$$

Addressing the time dependence of this term, note that the structure of D_{14} is reminiscent of D_{12} discussed in Section 8.4.3 resulting in a $\sqrt{t}$ type behaviour again due to a mechanism analogous to parametric resonance. The difference from the case of D_{12} is that the oscillations are of the form $\cos 3mt$ instead of $\cos mt$. Since our primary focus is on one-particle oscillations, we do not discuss this term further here.

H.2 Evaluation of $D_{23} = C_{23} - Z_1 C_{12} - (Z_2 - Z_1^2) C_{01}$

Consider

$$\begin{aligned} C_{23} &= \frac{g}{2} \sum_{I\geq 0} \sum_{J\geq 0} N_2 N_3 K(-\vartheta_1) K(\vartheta_2)_L \langle \{I,-I\}|\mathcal{O}(0)|\{J,-J,0\}\rangle_L \times \\ &\quad e^{imt(2\cosh\vartheta_1 - 2\cosh\vartheta_2 - 1)} e^{-Rm/2(2\cosh\vartheta_1 + 2\cosh\vartheta_2 + 1)} \\ &= \frac{g}{2} \sum_{I\geq 0} \sum_{J\geq 0} K(-\vartheta_1) K(\vartheta_2) \frac{F_5(i\pi+\vartheta_1, i\pi-\vartheta_1, -\vartheta_2, \vartheta_2, 0)}{\bar\rho_2(\vartheta_1)\bar\rho_3(\vartheta_2)} \times \\ &\quad e^{imt(2\cosh\vartheta_1 - 2\cosh\vartheta_2 - 1)} e^{-Rm/2(2\cosh\vartheta_1 + 2\cosh\vartheta_2 + 1)} + \mathcal{O}(e^{-\mu L}) \,, \end{aligned} \tag{H.2.1}$$

where I and J are the quantum numbers specifying ϑ_1 and ϑ_2, i.e.

$$\bar Q_2(\vartheta_1) = 2\pi I \,, \qquad \bar Q_3(\vartheta_2) = 2\pi J \,,$$

where $\bar Q_2$ and $\bar Q_3$ are defined in (4.3.2) and (4.3.3), respectively. The density factors are given by

$$\bar\rho_2(\vartheta_1) = \frac{\partial \bar Q_2(\vartheta_1)}{\partial \vartheta_1} \,, \qquad \bar\rho_3(\vartheta_1) = \frac{\partial \bar Q_3(\vartheta_2)}{\partial \vartheta_2} \,.$$

Note that I takes half-integer, while J takes integer values, according to the discussion in Appendix 4.3.1. The expression

$$F_5(i\pi+\vartheta_1, i\pi-\vartheta_1, -\vartheta_2, \vartheta_2, 0) K^*(\vartheta_1) K(\vartheta_2)$$

is singular when $\vartheta_1 = \vartheta_2$ or when $\vartheta_1 = 0$ and ϑ_2 is finite, and these singularities are of second order. One can first write the sum over J as a contour integral:

$$C_{23} = \frac{g}{2}\left(\frac{1}{2}\right)^2 \sum_{J\neq 0} \sum_{I\neq 0} \oint_{C_J} \frac{d\vartheta_2}{2\pi} h(\vartheta_1|\vartheta_2,\{0\})_R \, K^*(\vartheta_1) K(\vartheta_2) \frac{F_5(\vartheta_1|\vartheta_2,\{0\})}{\bar\rho_2(\vartheta_1)\left(e^{i\bar Q_3(\vartheta_2)} - 1\right)} \,, \tag{H.2.2}$$

where C_J surrounds the positions ϑ_2 corresponding to J. Opening the contour leads to

$$\begin{aligned} C_{23} &= \frac{g}{2}\left(\frac{1}{2}\right)^2 \sum_{I\neq 0} \int_{-\infty+i\varepsilon}^{\infty+i\varepsilon} \frac{d\vartheta_2}{2\pi} h(\vartheta_1|\vartheta_2,\{0\})_R \, K(-\vartheta_1) K(\vartheta_2) \frac{F_5(\vartheta_1|\vartheta_2,\{0\})}{\bar\rho_2(\vartheta_1)\left(e^{i\bar Q_3(\vartheta_2)} - 1\right)} \\ &\quad + \frac{g}{2}\left(\frac{1}{2}\right)^2 \sum_{I\neq 0} \int_{-\infty-i\varepsilon}^{\infty-i\varepsilon} \frac{d\vartheta_2}{2\pi} h(\vartheta_1|\vartheta_2,\{0\})_R \, K(-\vartheta_1) K(\vartheta_2) \frac{F_5(\vartheta_1|\vartheta_2,\{0\})}{\bar\rho_2(\vartheta_1)\left(e^{i\bar Q_3(\vartheta_2)} - 1\right)} \\ &\quad - i\frac{g}{2}\left(\frac{1}{2}\right)^2 \sum_{I\neq 0} \oint_{C_{\vartheta_1}} \frac{d\vartheta_2}{2\pi i} h(\vartheta_1|\vartheta_2,\{0\})_R \, K(-\vartheta_1) K(\vartheta_2) \frac{F_5(\vartheta_1|\vartheta_2,\{0\})}{\bar\rho_2(\vartheta_1)\left(e^{i\bar Q_3(\vartheta_2)} - 1\right)} \\ &\quad - i\frac{g}{2}\left(\frac{1}{2}\right)^2 \sum_{I\neq 0} \oint_{C_{-\vartheta_1}} \frac{d\vartheta_2}{2\pi i} h(\vartheta_1|\vartheta_2,\{0\})_R \, K(-\vartheta_1) K(\vartheta_2) \frac{F_5(\vartheta_1|\vartheta_2,\{0\})}{\bar\rho_2(\vartheta_1)\left(e^{i\bar Q_3(\vartheta_2)} - 1\right)} \,, \end{aligned} \tag{H.2.3}$$

where in the first two terms we perform the $mL \to \infty$ only for the rapidities ϑ_2, from which only the integration along the contour above the real axis survives. We thus have

$$\begin{aligned} C_{23} = & \frac{g}{2}\left(\frac{1}{2}\right)^2 \sum_{I\neq 0} \int_{-\infty+i\varepsilon}^{\infty+i\varepsilon} \frac{d\vartheta_2}{2\pi} h(\vartheta_1|\vartheta_2,\{0\})_R\, K(-\vartheta_1)K(\vartheta_2) \frac{F_5(\vartheta_1|\vartheta_2,\{0\})}{\bar\rho_2(\vartheta_1)} \\ & - i\frac{g}{2}\left(\frac{1}{2}\right)^2 \sum_{I\neq 0} \oint_{C_{\vartheta_1}} \frac{d\vartheta_2}{2\pi i} h(\vartheta_1|\vartheta_2,\{0\})_R\, K(-\vartheta_1)K(\vartheta_2) \frac{F_5(\vartheta_1|\vartheta_2,\{0\})}{\bar\rho_2(\vartheta_1)\left(e^{i\bar Q_3(\vartheta_2)}-1\right)} \\ & - i\frac{g}{2}\left(\frac{1}{2}\right)^2 \sum_{I\neq 0} \oint_{C_{-\vartheta_1}} \frac{d\vartheta_2}{2\pi i} h(\vartheta_1|\vartheta_2,\{0\})_R\, K(-\vartheta_1)K(\vartheta_2) \frac{F_5(\vartheta_1|\vartheta_2,\{0\})}{\bar\rho_2(\vartheta_1)\left(e^{i\bar Q_3(\vartheta_2)}-1\right)} \,. \end{aligned} \tag{H.2.4}$$

This contour manipulation was checked numerically using known form factor solutions and comparing (H.2.2) and (H.2.4) for finite R. The terms in the three lines in eqn. (H.2.4) are written in short as

$$C_{23} = C_{23}^{int} + C_{23}^{res1A} + C_{23}^{res1B} \,.$$

H.2.1 Time dependence from residue term C_{23}^{res1A} and C_{23}^{res1B}

Consider the residue terms

$$\begin{aligned} C_{23}^{res1A} = & -i\frac{g}{2}\left(\frac{1}{2}\right)^2 \sum_{I\neq 0} \oint_{C_{\vartheta_1}} \frac{d\vartheta_2}{2\pi i} h(\vartheta_1|\vartheta_2,\{0\})_R\, K(-\vartheta_1)K(\vartheta_2) \frac{F_5(\vartheta_1|\vartheta_2,\{0\})}{\bar\rho_2(\vartheta_1)\left(e^{i\bar Q_3(\vartheta_2)}-1\right)} \\ = & -i\frac{g}{2}\left(\frac{1}{2}\right)^2 F_1 \sum_{I\neq 0} \frac{K(-\vartheta_1)\left(1-S(\vartheta_1)\right)\left(1-S(-\vartheta_1)\right) h(\vartheta_1|\vartheta_1,\{0\})_R}{\bar\rho_2(\vartheta_1)} \times \\ & \left\{ K(\vartheta_1)\frac{(-2imt-Rm)\sinh\vartheta_1}{(S(\vartheta_1)-1)} + \frac{K'(\vartheta_1)}{(S(\vartheta_1)-1)} \right. \\ & \left. - \frac{K(\vartheta_1)S(\vartheta_1) i\left(mL\cosh\vartheta_1 + 2\varphi(2\vartheta_1)+\varphi(\vartheta_1)\right)}{(S(\vartheta_1)-1)^2} \right\} \\ & -i\frac{g}{2}\left(\frac{1}{2}\right)^2 F_1 \sum_{I\neq 0} \frac{K(-\vartheta_1)K(\vartheta_1)F_5^{\varepsilon}(\vartheta_1) h(\vartheta_1|\vartheta_1,\{0\})_R}{(S(\vartheta_1)-1)\,\bar\rho_2(\vartheta_1)} \,, \end{aligned} \tag{H.2.5}$$

and

$$\begin{aligned} C_{23}^{res1B} = & -i\frac{g}{2}\left(\frac{1}{2}\right)^2 \sum_{I\neq 0} \oint_{C_{-\vartheta_1}} \frac{d\vartheta_2}{2\pi i} h(\vartheta_1|\vartheta_2,\{0\})_R\, K(-\vartheta_1)K(\vartheta_2) \frac{F_5(\vartheta_1|\vartheta_2,\{0\})}{\bar\rho_2(\vartheta_1)\left(e^{i\bar Q_3(\vartheta_2)}-1\right)} \\ = & -i\frac{g}{2}\left(\frac{1}{2}\right)^2 F_1 \sum_{I\neq 0} \frac{K(-\vartheta_1)S(2\vartheta_1)\left(1-S(\vartheta_1)\right)\left(1-S(-\vartheta_1)\right) h(\vartheta_1|\vartheta_1,\{0\})_R}{\bar\rho_2(\vartheta_1)} \times \\ & \left\{ K(-\vartheta_1)\frac{(-1)\,(-2imt-Rm)\sinh\vartheta_1}{(S(-\vartheta_1)-1)} + \frac{K'(-\vartheta_1)}{(S(-\vartheta_1)-1)} \right. \\ & \left. - \frac{K(-\vartheta_1)S(-\vartheta_1) i\left(mL\cosh\vartheta_1 + 2\varphi(2\vartheta_1)+\varphi(\vartheta_1)\right)}{(S(-\vartheta_1)-1)^2} \right\} \\ & -i\frac{g}{2}\left(\frac{1}{2}\right)^2 F_1 \sum_{I\neq 0} \frac{K(-\vartheta_1)K(-\vartheta_1)F_5^{\varepsilon}(-\vartheta_1)S(2\vartheta_1) h(\vartheta_1|\vartheta_1,\{0\})_R}{(S(-\vartheta_1)-1)\,\bar\rho_2(\vartheta_1)} \,, \end{aligned} \tag{H.2.6}$$

where (E.2.4) was made use of. Note, that both the second and first order singularities are to be taken into account. Adding C_{23}^{res1A} and C_{23}^{res1B}, one has

$$\begin{aligned}
C_{23}^{res1} =& -i\frac{g}{2}\left(\frac{1}{2}\right)^2 F_1 \sum_{I\neq 0} |K(\vartheta_1)|^2 \frac{(-2i\Im m\, S(\vartheta_1))\,(-2imt - Rm)\sinh\vartheta_1}{\bar\rho_2(\vartheta_1)} h(\vartheta_1|\vartheta_1,\{0\})_R \\
& -i\frac{g}{2}\left(\frac{1}{2}\right)^2 F_1 \sum_{I\neq 0} 2\frac{|K(\vartheta_1)|^2 i\,(mL\cosh\vartheta_1 + 2\varphi(2\vartheta_1) + \varphi(\vartheta_1))\,h(\vartheta_1|\vartheta_1,\{0\})_R}{\bar\rho_2(\vartheta_1)} \\
& +i\frac{g}{2}\left(\frac{1}{2}\right)^2 F_1 \sum_{I\neq 0} \frac{K(\vartheta_1)K'(-\vartheta_1)\,(1-S(\vartheta_1)) + K(-\vartheta_1)K'(\vartheta_1)\,(1-S(-\vartheta_1))}{\bar\rho_2(\vartheta_1)} h(\vartheta_1|\vartheta_1,\{0\})_R \\
& -i\frac{g}{2}\left(\frac{1}{2}\right)^2 \sum_{I\neq 0} \frac{|K(\vartheta_1)|^2 h(\vartheta_1|\vartheta_1,\{0\})_R}{\bar\rho_2(\vartheta_1)} \left(\frac{F_5^\varepsilon(\vartheta_1)}{(S(\vartheta_1)-1)} + \frac{F_5^\varepsilon(-\vartheta_1)}{(S(-\vartheta_1)-1)}\right) ,
\end{aligned} \tag{H.2.7}$$

or after some manipulations

$$\begin{aligned}
C_{23}^{res1} =& -\frac{g}{2}\left(\frac{1}{2}\right)^2 F_1 \sum_{I\neq 0} |K(\vartheta_1)|^2 \frac{(2\Im m\, S(\vartheta_1))\,(-2imt - Rm)\sinh\vartheta_1}{\bar\rho_2(\vartheta_1)} h(\vartheta_1|\vartheta_1,\{0\})_R \\
& +\frac{g}{2}\left(\frac{1}{2}\right)^2 F_1 \sum_{I\neq 0} 2\frac{|K(\vartheta_1)|^2\,(mL\cosh\vartheta_1 + 2\varphi(2\vartheta_1) + \varphi(\vartheta_1))\,h(\vartheta_1|\vartheta_1,\{0\})_R}{\bar\rho_2(\vartheta_1)} \\
& -\frac{g}{2}\left(\frac{1}{2}\right)^2 F_1 \sum_{I\neq 0} \frac{\Im m\, S(\vartheta_1)\left(|K(\vartheta_1)|^2\right)' + 2\varphi(2\vartheta_1)|K(\vartheta_1)|^2 \mathrm{Re}\,(1-S(\vartheta_1))}{\bar\rho_2(\vartheta_1)} h(\vartheta_1|\vartheta_1,\{0\})_R \\
& -i\frac{g}{2}\left(\frac{1}{2}\right)^2 \sum_{I\neq 0} \frac{|K(\vartheta_1)|^2 h(\vartheta_1|\vartheta_1,\{0\})_R}{\bar\rho_2(\vartheta_1)} \left(\frac{F_5^\varepsilon(\vartheta_1)}{(S(\vartheta_1)-1)} + \frac{F_5^\varepsilon(-\vartheta_1)}{(S(-\vartheta_1)-1)}\right) ,
\end{aligned} \tag{H.2.8}$$

The four terms of C_{23}^{res1} have singularities at $\vartheta_1 = 0$. However, these singularities can only produce terms with positive powers in mL but no non-trivial time dependence since $h(\vartheta_1|\vartheta_1,\{0\})_R$ contains no ϑ_1 dependent function multiplied by t. We therefore have a single secular term, namely

$$\begin{aligned}
C_{23}^{res/sec} =& \frac{g}{2} F_1 e^{-imt}\,(imt) \int_{-\infty}^{\infty} \frac{d\vartheta}{2\pi} |K(\vartheta)|^2 \Im m\, S(\vartheta) \sinh\vartheta e^{-Rm/2(4\cosh\vartheta+1)} \\
& + \frac{g}{2} F_1 e^{-imt}\,(Rm/2) \int_{-\infty}^{\infty} \frac{d\vartheta}{2\pi} |K(\vartheta)|^2 \Im m\, S(\vartheta) \sinh\vartheta e^{-Rm/2(4\cosh\vartheta+1)} ,
\end{aligned} \tag{H.2.9}$$

and taking the limit $R \to 0$ results in

$$C_{23}^{res/sec} = \frac{g}{2} F_1 e^{-imt}\,(imt) \int_{-\infty}^{\infty} \frac{d\vartheta}{2\pi} |K(\vartheta)|^2 \Im m\, S(\vartheta) \sinh\vartheta . \tag{H.2.10}$$

Appendix I

Evaluating G_5, part II. Contour integral terms from D_{23}

In this appendix we evaluate the contour integral from (H.2.3) which reads

$$C_{23}^{int} = \frac{g}{2}\left(\frac{1}{2}\right)^2 \sum_{I\neq 0} \int_{-\infty+i\varepsilon}^{\infty+i\varepsilon} \frac{d\vartheta_2}{2\pi} h(\vartheta_1|\vartheta_2,\{0\})_R\, K(-\vartheta_1)K(\vartheta_2) \frac{F_5(\vartheta_1|\vartheta_2,\{0\})}{\bar{\rho}_2(\vartheta_1)}\,. \tag{I.0.1}$$

Let us start with a summary of our method first. Manipulating (I.0.1) leads to various terms of which only (I.1.7) and (I.5.4) give rise to interesting time dependence. The origin of these terms was made clear at the beginning of this Appendix, but their actual evaluation needs further non trivial integral manipulations discussed in Appendix J. The largest part of this Appendix is dedicated to showing that apart from (I.1.7) and (I.5.4) no other term yields any interesting time dependence.

Starting from (I.0.1) we can subtract and add back the singularities of the five particle form factors. Using (E.2.4), this leads to

$$\begin{aligned}
C_{23}^{int} =& \frac{g}{2}\left(\frac{1}{2}\right)^2 \sum_{I\neq 0} \int_{-\infty+i\varepsilon}^{\infty+i\varepsilon} \frac{d\vartheta_2}{2\pi} \left\{ \frac{h(\vartheta_1|\vartheta_2,\{0\})_R\, K(-\vartheta_1)K(\vartheta_2)}{\bar{\rho}_2(\vartheta_1)} \left[F_5(\vartheta_1|\vartheta_2,\{0\}) \right.\right. \\
& \left.\left. -\Omega(\vartheta_1) F_1\left(\frac{\cosh(\vartheta_2-\vartheta_1)}{\sinh^2(\vartheta_2-\vartheta_1)} + \frac{S(2\vartheta_1)\cosh(\vartheta_2+\vartheta_1)}{\sinh^2(\vartheta_2+\vartheta_1)}\right) - \frac{F_5^{\varepsilon}(\vartheta_1)}{\sinh(\vartheta_2-\vartheta_1)} - \frac{S(2\vartheta_1)F_5^{\varepsilon}(-\vartheta_1)}{\sinh(\vartheta_2+\vartheta_1)} \right] \right\} \\
& + \frac{g}{2}\left(\frac{1}{2}\right)^2 \sum_{I\neq 0} \int_{-\infty+i\varepsilon}^{\infty+i\varepsilon} \frac{d\vartheta_2}{2\pi} \left\{ \frac{h(\vartheta_1|\vartheta_2,\{0\})_R K(-\vartheta_1)K(\vartheta_2)}{\bar{\rho}_2(\vartheta_1)} \times \right. \\
& \left. \Omega(\vartheta_1) F_1\left(\frac{\cosh(\vartheta_2-\vartheta_1)}{\sinh^2(\vartheta_2-\vartheta_1)} + \frac{S(2\vartheta_1)\cosh(\vartheta_2+\vartheta_1)}{\sinh^2(\vartheta_2+\vartheta_1)}\right) \right\} \\
& + \frac{g}{2}\left(\frac{1}{2}\right)^2 \sum_{I\neq 0} \int_{-\infty+i\varepsilon}^{\infty+i\varepsilon} \frac{d\vartheta_2}{2\pi} \left\{ \frac{h(\vartheta_1|\vartheta_2,\{0\})_R\, K(-\vartheta_1)K(\vartheta_2)}{\bar{\rho}_2(\vartheta_1)} \left(\frac{F_5^{\varepsilon}(\vartheta_1)}{\sinh(\vartheta_2-\vartheta_1)} + \frac{S(2\vartheta_1)F_5^{\varepsilon}(-\vartheta_1)}{\sinh(\vartheta_2+\vartheta_1)} \right) \right\} \\
=& C_{23}^{intA} + C_{23}^{intBI} + C_{23}^{intBII}\,,
\end{aligned} \tag{I.0.2}$$

where $\Omega(\vartheta) = (1-S(\vartheta))\,(1-S(-\vartheta))$.

To make the rather technical evaluation more transparent, we introduce an additional simplification which does not affect the end result. Apart from (I.1.7) and (I.5.4), many other terms also possess singularities that in principle could lead to non-trivial time-dependence, but cancel each other in the end. These singularities emerge from the region where ϑ_1 is around zero. But at zero rapidity $S(0) = -1$, and all other quantities behave similar to the Ising model which has a constant $S = -1$ everywhere, resulting

in $K(\vartheta)$ being an odd function of ϑ. A good example is the sub-leading singularity of the form factor $F_5^{\varepsilon}(\vartheta_1)$ defined in (E.2.4), which for small ϑ_1 behaves as

$$\frac{8F_1}{\vartheta_1}\,,$$

whereas its Ising counterpart is exactly

$$F_5^{\varepsilon}(\vartheta_1) = \frac{8F_1}{\sinh\vartheta_1}\,. \tag{I.0.3}$$

Therefore to keep the reasoning as simple as possible, from now on we perform our calculations for the Ising scattering matrix $S=-1$ and show the cancellation of certain singularities. It turns out that in the only nontrivial time dependent terms (I.5.1) and (I.5.4) the original S matrix can be easily restored.

I.1 Term C_{23}^{intBI} and its descendants

C_{23}^{intBI} reads

$$\begin{aligned} C_{23}^{intBI} =& \frac{g}{2}\left(\frac{1}{2}\right)^2 \sum_{I\neq 0}\int_{-\infty+i\varepsilon}^{\infty+i\varepsilon}\frac{d\vartheta_2}{2\pi}\Bigg\{ h(\vartheta_1|\vartheta_2,\{0\})_R\, K(-\vartheta_1)K(\vartheta_2)\times \\ & \frac{4F_1\left(\frac{\cosh(\vartheta_2-\vartheta_1)}{\sinh^2(\vartheta_2-\vartheta_1)}-\frac{\cosh(\vartheta_2+\vartheta_1)}{\sinh^2(\vartheta_2+\vartheta_1)}\right)}{\bar\rho_2(\vartheta_1)}\Bigg\}\,. \end{aligned} \tag{I.1.1}$$

To proceed we focus on the integral with respect to ϑ_2 and separate the singularities in

$$K(\vartheta_2)\frac{\cosh(\vartheta_2-\vartheta_1)}{\sinh^2(\vartheta_2-\vartheta_1)}$$

to prepare for application of the identities of distribution theory. Using the shorthand $s(\vartheta_2)=K(\vartheta_2)$ and

$$c(\vartheta_2) = \frac{\cosh(\vartheta_2-\vartheta_1)}{\sinh^2(\vartheta_2-\vartheta_1)}\,,$$

where $s(\vartheta_2)$ is singular in 0 and $c(\vartheta_2)$ at $\vartheta_2=\vartheta_1$ one can write the singular terms as

$$\begin{aligned} s(\vartheta_2)c(\vartheta_2) =& \left((s(\vartheta_2)-s(\vartheta_1))+s(\vartheta_1)\right)\left((c(\vartheta_2)-c(0))+c(0)\right) \\ & (s(\vartheta_2)-s(\vartheta_1))\,(c(\vartheta_2)-c(0)) + s(\vartheta_1)c(\vartheta_2) + c(0)s(\vartheta_2) - c(0)s(\vartheta_1)\,, \end{aligned} \tag{I.1.2}$$

from which for fixed, non zero ϑ_1, the first term $(s(\vartheta_2)-s(\vartheta_1))\,(c(\vartheta_2)-c(0))$ is singular only in $\vartheta_2=\vartheta_1$ and this singularity is milder than $1/x^2$, the second term $s(\vartheta_1)c(\vartheta_2)$ is singular only in $\vartheta_2=\vartheta_1$ which is of type $1/x^2$, whereas the third term $c(0)s(\vartheta_2)$ is singular at the origin with $1/x$ behaviour and the last term $c(0)s(\vartheta_1)$ is regular. The terms corresponding to this separation are denoted by $C_{23}^{intBI1}, C_{23}^{intBI2}, C_{23}^{intBI3}$ and C_{23}^{intBI4}.

Considering the first term and using (E.3.3), we have

$$
\begin{aligned}
C_{23}^{intBI1} =& \frac{g}{2}\left(\frac{1}{2}\right)^2 \sum_{I\neq 0}\int_{-\infty+i\varepsilon}^{\infty+i\varepsilon}\frac{d\vartheta_2}{2\pi}\left\{\frac{h(\vartheta_1|\vartheta_2,\{0\})_R\,K(-\vartheta_1)\,(K(\vartheta_2)-K(\vartheta_1))}{\bar\rho_2(\vartheta_1)}4F_1\times\right.\\
&\left.\times\left(\frac{\cosh(\vartheta_2-\vartheta_1)}{\sinh^2(\vartheta_2-\vartheta_1)}-\frac{\cosh\vartheta_1}{\sinh^2\vartheta_1}\right)\right\}\\
&-\frac{g}{2}\left(\frac{1}{2}\right)^2 \sum_{I\neq 0}\int_{-\infty+i\varepsilon}^{\infty+i\varepsilon}\frac{d\vartheta_2}{2\pi}\left\{\frac{h(\vartheta_1|\vartheta_2,\{0\})_R\,K(-\vartheta_1)\,(K(\vartheta_2)-K(-\vartheta_1))}{\bar\rho_2(\vartheta_1)}4F_1\times\right.\\
&\left.\times\left(\frac{\cosh(\vartheta_2+\vartheta_1)}{\sinh^2(\vartheta_2+\vartheta_1)}-\frac{\cosh\vartheta_1}{\sinh^2\vartheta_1}\right)\right\}\\
=&-i\frac{\pi}{2\pi}\frac{g}{2}\left(\frac{1}{2}\right)^2\sum_{I\neq 0}h(\vartheta_1|\vartheta_1,\{0\})_R\,K(-\vartheta_1)K'|_{\vartheta_1}\frac{4F_1}{\bar\rho_2(\vartheta_1)}\\
&+\frac{g}{2}\left(\frac{1}{2}\right)^2\sum_{I\neq 0}\int_{-\infty}^{\infty}\frac{d\vartheta_2}{2\pi}\frac{4F_1}{\bar\rho_2}\frac{K(-\vartheta_1)}{\sinh(\vartheta_2-\vartheta_1)}\left\{h(\vartheta_1|\vartheta_2,\{0\})_R\,(K(\vartheta_2)-K(\vartheta_1))\times\right.\\
&\left.\times\left(\frac{\cosh(\vartheta_2-\vartheta_1)}{\sinh^2(\vartheta_2-\vartheta_1)}-\frac{\cosh\vartheta_1}{\sinh^2\vartheta_1}\right)\sinh(\vartheta_2-\vartheta_1)-\frac{h(\vartheta_1|\vartheta_1,\{0\})_R\,K'|_{\vartheta_1}}{\cosh(\vartheta_2-\vartheta_1)}\right\}\\
&+\vartheta_1\longleftrightarrow-\vartheta_1\ ,
\end{aligned}
\tag{I.1.3}
$$

which equals

$$
\begin{aligned}
&\frac{g}{2}\left(\frac{1}{2}\right)^2\sum_{I\neq 0}\int_{-\infty}^{\infty}\frac{d\vartheta_2}{2\pi}\frac{4F_1}{\bar\rho_2(\vartheta_1)}\frac{K(-\vartheta_1)}{\sinh\vartheta_2-\vartheta_1}\left\{h(\vartheta_1|\vartheta_2,\{0\})_R\,(K(\vartheta_2)-K(\vartheta_1))\times\right.\\
&\left.\times\left(\frac{\cosh(\vartheta_2-\vartheta_1)}{\sinh^2(\vartheta_2-\vartheta_1)}-\frac{\cosh\vartheta_1}{\sinh^2\vartheta_1}\right)\sinh(\vartheta_2-\vartheta_1)-\frac{h(\vartheta_1|\vartheta_1,\{0\})_R\,K'|_{\vartheta_1}}{\cosh(\vartheta_2-\vartheta_1)}\right\}\ ,\\
&+\vartheta_1\longleftrightarrow-\vartheta_1\ .
\end{aligned}
\tag{I.1.4}
$$

One can split it further as

$$
\begin{aligned}
C_{23}^{intBI1} =& C_{23}^{intBI1a}+C_{23}^{intBI1b}\\
C_{23}^{intBI1a} =& \frac{g}{2}\left(\frac{1}{2}\right)^2\sum_{I\neq 0}\int_{-\infty}^{\infty}\frac{d\vartheta_2}{2\pi}4F_1\frac{K(-\vartheta_1)}{\bar\rho_2(\vartheta_1)}\frac{h(\vartheta_1|\vartheta_2,\{0\})_R}{\sinh\vartheta_2-\vartheta_1}\times\\
&\times\left[(K(\vartheta_2)-K(\vartheta_1))\left(\frac{\cosh(\vartheta_2-\vartheta_1)}{\sinh^2(\vartheta_2-\vartheta_1)}-\frac{\cosh\vartheta_1}{\sinh^2\vartheta_1}\right)\sinh(\vartheta_2-\vartheta_1)-\frac{K'(\vartheta_1)}{\cosh(\vartheta_2-\vartheta_1)}\right]\\
&+\frac{g}{2}\left(\frac{1}{2}\right)^2\sum_{I\neq 0}\int_{-\infty}^{\infty}\frac{d\vartheta_2}{2\pi}4F_1\frac{K(\vartheta_1)}{\bar\rho_2(\vartheta_1)}\frac{h(\vartheta_1|\vartheta_2,\{0\})_R}{\sinh\vartheta_2+\vartheta_1}\times\\
&\times\left[(K(\vartheta_2)-K(-\vartheta_1))\left(\frac{\cosh(\vartheta_2+\vartheta_1)}{\sinh^2(\vartheta_2+\vartheta_1)}-\frac{\cosh\vartheta_1}{\sinh^2\vartheta_1}\right)\sinh(\vartheta_2-\vartheta_1)-\frac{K'(-\vartheta_1)}{\cosh(\vartheta_2+\vartheta_1)}\right]\\
C_{23}^{intBI1b} =& \frac{g}{2}\left(\frac{1}{2}\right)^2\sum_{I\neq 0}\int_{-\infty}^{\infty}\frac{d\vartheta_2}{2\pi}4F_1\frac{K(-\vartheta_1)}{\bar\rho_2(\vartheta_1)}\frac{[h(\vartheta_1|\vartheta_2,\{0\})_R-h(\vartheta_1|\vartheta_1,\{0\})_R]\,K'(\vartheta_1)}{\cosh(\vartheta_2-\vartheta_1)\sinh(\vartheta_2-\vartheta_1)}\\
&+\frac{g}{2}\left(\frac{1}{2}\right)^2\sum_{I\neq 0}\int_{-\infty}^{\infty}\frac{d\vartheta_2}{2\pi}4F_1\frac{K(\vartheta_1)}{\bar\rho_2(\vartheta_1)}\frac{[h(\vartheta_1|\vartheta_2,\{0\})_R-h(\vartheta_1|\vartheta_1,\{0\})_R]\,K'(-\vartheta_1)}{\cosh(\vartheta_2+\vartheta_1)\sinh(\vartheta_2+\vartheta_1)}\ .
\end{aligned}
\tag{I.1.5}
$$

The second term C_{23}^{intBI2} reads as follows:

$$\begin{aligned}
C_{23}^{intBI2} =& \frac{g}{2}\left(\frac{1}{2}\right)^2 \sum_{I\neq 0}\int_{-\infty+i\varepsilon}^{\infty+i\varepsilon}\frac{d\vartheta_2}{2\pi}h(\vartheta_1|\vartheta_2,\{0\})_R\frac{|K(\vartheta_1)|^2}{\bar\rho_2(\vartheta_1)}4F_1\left(\frac{\cosh(\vartheta_2-\vartheta_1)}{\sinh^2(\vartheta_2-\vartheta_1)}\right)\\
&+\frac{g}{2}\left(\frac{1}{2}\right)^2 \sum_{I\neq 0}\int_{-\infty+i\varepsilon}^{\infty+i\varepsilon}\frac{d\vartheta_2}{2\pi}h(\vartheta_1|\vartheta_2,\{0\})_R\frac{|K(\vartheta_1)|^2}{\bar\rho_2(\vartheta_1)}4F_1\left(\frac{\cosh(\vartheta_2+\vartheta_1)}{\sinh^2(\vartheta_2+\vartheta_1)}\right)\\
=&\frac{g}{2}\left(\frac{1}{2}\right)^2 \sum_{I\neq 0}\int_{-\infty+i\varepsilon}^{\infty+i\varepsilon}\frac{d\vartheta_2}{2\pi}h(\vartheta_1|\vartheta_2,\{0\})_R\frac{|K(\vartheta_1)|^2}{\bar\rho_2(\vartheta_1)}4F_1\left(\frac{\cosh(\vartheta_2-\vartheta_1)}{\sinh^2(\vartheta_2-\vartheta_1)}+\frac{\cosh(\vartheta_2+\vartheta_1)}{\sinh^2(\vartheta_2+\vartheta_1)}\right)\\
=&-i\frac{\pi}{2\pi}\frac{g}{2}\left(\frac{1}{2}\right)^2 \sum_{I\neq 0}h(\vartheta_1|\vartheta_1,\{0\})_R\frac{|K(\vartheta_1)|^2}{\bar\rho_2(\vartheta_1)}4F_1\left(-2imt-Rm\right)\left(\sinh\vartheta_1+\sinh(-\vartheta_1)\right)\\
&+\left(-2imt-Rm\right)\frac{g}{2}\left(\frac{1}{2}\right)^2 \sum_{I\neq 0}\int_{-\infty}^{\infty}\frac{d\vartheta_2}{2\pi}\frac{|K(\vartheta_1)|^2}{\bar\rho_2(\vartheta_1)}\frac{4F_1}{\sinh(\vartheta_2-\vartheta_1)}\times\\
&\qquad\times\left[h(\vartheta_1|\vartheta_2,\{0\})_R\sinh\vartheta_2-\frac{h(\vartheta_1|\vartheta_1,\{0\})_R\sinh\vartheta_1}{\cosh(\vartheta_2-\vartheta_1)}\right]\\
&+\left(-2imt-Rm\right)\frac{g}{2}\left(\frac{1}{2}\right)^2 \sum_{I\neq 0}\int_{-\infty}^{\infty}\frac{d\vartheta_2}{2\pi}\frac{|K(\vartheta_1)|^2}{\bar\rho_2(\vartheta_1)}\frac{4F_1}{\sinh(\vartheta_2+\vartheta_1)}\times\\
&\qquad\times\left[h(\vartheta_1|\vartheta_2,\{0\})_R\sinh\vartheta_2-\frac{h(\vartheta_1|\vartheta_1,\{0\})_R\sinh(-\vartheta_1)}{\cosh(\vartheta_2+\vartheta_1)}\right],
\end{aligned}\tag{I.1.6}$$

where (E.3.4) was used. Thus,

$$\begin{aligned}
C_{23}^{intBI2} =& \left(-2imt-Rm\right)\frac{g}{2}\left(\frac{1}{2}\right)^2 \sum_{I\neq 0}\int_{-\infty}^{\infty}\frac{d\vartheta_2}{2\pi}\frac{|K(\vartheta_1)|^2}{\bar\rho_2(\vartheta_1)}\frac{4F_1}{\sinh(\vartheta_2-\vartheta_1)}\times\\
&\qquad\times\left[h(\vartheta_1|\vartheta_2,\{0\})_R\sinh\vartheta_2-\frac{h(\vartheta_1|\vartheta_1,\{0\})_R\sinh\vartheta_1}{\cosh(\vartheta_2-\vartheta_1)}\right]\\
&+\left(-2imt-Rm\right)\frac{g}{2}\left(\frac{1}{2}\right)^2 \sum_{I\neq 0}\int_{-\infty}^{\infty}\frac{d\vartheta_2}{2\pi}\frac{|K(\vartheta_1)|^2}{\bar\rho_2(\vartheta_1)}\frac{4F_1}{\sinh(\vartheta_2+\vartheta_1)}\times\\
&\qquad\times\left[h(\vartheta_1|\vartheta_2,\{0\})_R\sinh\vartheta_2-\frac{h(\vartheta_1|\vartheta_1,\{0\})_R\sinh(-\vartheta_1)}{\cosh(\vartheta_2+\vartheta_1)}\right].
\end{aligned}\tag{I.1.7}$$

Turning to the third contribution and using (E.3.4), we have

$$\begin{aligned}
C_{23}^{intBI3} =& \frac{g}{2}\left(\frac{1}{2}\right)^2 \sum_{I\neq 0}\int_{-\infty+i\varepsilon}^{\infty+i\varepsilon}\frac{d\vartheta_2}{2\pi}h(\vartheta_1|\vartheta_2,\{0\})_R\,K(-\vartheta_1)K(\vartheta_2)\frac{4F_1\frac{\cosh\vartheta_1}{\sinh^2\vartheta_1}}{\bar\rho_2(\vartheta_1)}\\
&-\frac{g}{2}\left(\frac{1}{2}\right)^2 \sum_{I\neq 0}\int_{-\infty+i\varepsilon}^{\infty+i\varepsilon}\frac{d\vartheta_2}{2\pi}h(\vartheta_1|\vartheta_2,\{0\})_R\,K(-\vartheta_1)K(\vartheta_2)\frac{4F_1\frac{\cosh\vartheta_1}{\sinh^2\vartheta_1}}{\bar\rho_2(\vartheta_1)}\\
=&0\,.
\end{aligned}\tag{I.1.8}$$

The 4th term reads

$$C_{23}^{intBI4} = -2\frac{g}{2}\left(\frac{1}{2}\right)^2 \sum_{I\neq 0}\int_{-\infty}^{\infty}\frac{d\vartheta_2}{2\pi}\frac{h(\vartheta_1|\vartheta_2,\{0\})_R\,|K(\vartheta_1)|^2}{\bar\rho_2(\vartheta_1)}4F_1\frac{\cosh\vartheta_1}{\sinh^2\vartheta_1}\,.\tag{I.1.9}$$

I.2 Term C_{23}^{intBII} and its descendants

Consider now

$$C_{23}^{intBII} = \frac{g}{2}\left(\frac{1}{2}\right)^2 \sum_{I\neq 0}\int_{-\infty+i\varepsilon}^{\infty+i\varepsilon}\frac{d\vartheta_2}{2\pi}\left\{h(\vartheta_1|\vartheta_2,\{0\})_R K(-\vartheta_1)K(\vartheta_2)\frac{\left[\frac{F_5^\varepsilon(\vartheta_1)}{\sinh(\vartheta_2-\vartheta_1)}-\frac{F_5^\varepsilon(-\vartheta_1)}{\sinh(\vartheta_2+\vartheta_1)}\right]}{\bar\rho_2(\vartheta_1)}\right\}. \quad \text{(I.2.1)}$$

Similarly to C_{23}^{intBI} , we first separate the singularities using the shorthand $s(\vartheta_2) = K(\vartheta_2)$ and

$$c(\vartheta_2) = \frac{1}{\sinh(\vartheta_2-\vartheta_1)}\,,$$

where $s(\vartheta_2)$ is singular at $\vartheta_2 = 0$ and $c(\vartheta_2)$ at $\vartheta_2 = \vartheta_1$, to write

$$\begin{aligned} s(\vartheta_2)c(\vartheta_2) =& \left((s(\vartheta_2)-s(\vartheta_1))+s(\vartheta_1)\right)\left((c(\vartheta_2)-c(0))+c(0)\right)\\ & (s(\vartheta_2)-s(\vartheta_1))\,(c(\vartheta_2)-c(0)) + s(\vartheta_1)c(\vartheta_2) + c(0)s(\vartheta_2) - c(0)s(\vartheta_1)\,, \end{aligned} \quad \text{(I.2.2)}$$

from which for fixed, non zero ϑ_1, the first term $(s(\vartheta_2)-s(\vartheta_1))\,(c(\vartheta_2)-c(0))$ is regular in ϑ_2, the second term $s(\vartheta_1)c(\vartheta_2)$ is singular only in $\vartheta_2 = \vartheta_1$ which is of type $1/x$, whereas the third term $c(0)s(\vartheta_2)$ is singular at the origin with $1/x$ behaviour and the last term $c(0)s(\vartheta_1)$ is regular. The terms corresponding to this separation are denoted by $C_{23}^{intBII1}, C_{23}^{intBII2}, C_{23}^{intBII3}$ and $C_{23}^{intBII4}$ from which we have the first term

$$\begin{aligned} C_{23}^{intBII1} =& \frac{g}{2}\left(\frac{1}{2}\right)^2 \sum_{I\neq 0}\int_{-\infty}^{\infty}\frac{d\vartheta_2}{2\pi}\frac{h(\vartheta_1|\vartheta_2,\{0\})_R\,K(-\vartheta_1)\,(K(\vartheta_2)-K(\vartheta_1))}{\bar\rho_2(\vartheta_1)}\times\\ & \left(\frac{1}{\sinh\vartheta_2-\vartheta_1}+\frac{1}{\sinh\vartheta_1}\right)F_5^\varepsilon(\vartheta_1)\\ & -\frac{g}{2}\left(\frac{1}{2}\right)^2 \sum_{I\neq 0}\int_{-\infty}^{\infty}\frac{d\vartheta_2}{2\pi}\frac{h(\vartheta_1|\vartheta_2,\{0\})_R\,K(-\vartheta_1)\,(K(\vartheta_2)-K(-\vartheta_1))}{\bar\rho_2(\vartheta_1)}\times\\ & \left(\frac{1}{\sinh\vartheta_2+\vartheta_1}-\frac{1}{\sinh\vartheta_1}\right)F_5^\varepsilon(-\vartheta_1) \end{aligned} \quad \text{(I.2.3)}$$

which is regular, and the second term

$$
\begin{aligned}
C_{23}^{intBII2} =& \frac{g}{2}\left(\frac{1}{2}\right)^2 \sum_{I\neq 0}\int_{-\infty+i\varepsilon}^{\infty+i\varepsilon}\frac{d\vartheta_2}{2\pi}\frac{h(\vartheta_1|\vartheta_2,\{0\})_R\,K(-\vartheta_1)K(\vartheta_1)}{\bar\rho_2(\vartheta_1)}\frac{F_5^\varepsilon(\vartheta_1)}{\sinh(\vartheta_2-\vartheta_1)}\\
&-\frac{g}{2}\left(\frac{1}{2}\right)^2 \sum_{I\neq 0}\int_{-\infty+i\varepsilon}^{\infty+i\varepsilon}\frac{d\vartheta_2}{2\pi}\frac{h(\vartheta_1|\vartheta_2,\{0\})_R\,K(-\vartheta_1)K(-\vartheta_1)}{\bar\rho_2(\vartheta_1)}\frac{F_5^\varepsilon(-\vartheta_1)}{\sinh(\vartheta_2+\vartheta_1)}\\
=&-i\frac{\pi}{2\pi}\frac{g}{2}\left(\frac{1}{2}\right)^2\sum_{I\neq 0}\frac{h(\vartheta_1|\vartheta_1,\{0\})_R\,|K(\vartheta_1)|^2}{\bar\rho_2(\vartheta_1)}\left(8/\sinh\vartheta_1+8/\sinh(-\vartheta_1)\right)F_1\\
&+\frac{g}{2}\left(\frac{1}{2}\right)^2\sum_{I\neq 0}\frac{|K(\vartheta_1)|^2}{\bar\rho_2(\vartheta_1)}\frac{8F_1}{\sinh\vartheta_1}\times\\
&\quad\times\int_{-\infty}^{\infty}\frac{d\vartheta_2}{2\pi}\left(\frac{h(\vartheta_1|\vartheta_2,\{0\})_R-h(\vartheta_1|\vartheta_1,\{0\})_R/\cosh(\vartheta_2-\vartheta_1)}{\sinh(\vartheta_2-\vartheta_1)}\right)\\
&+\frac{g}{2}\left(\frac{1}{2}\right)^2\sum_{I\neq 0}\frac{|K(\vartheta_1)|^2}{\bar\rho_2(\vartheta_1)}\frac{8F_1}{\sinh(-\vartheta_1)}\times\\
&\quad\times\int_{-\infty}^{\infty}\frac{d\vartheta_2}{2\pi}\left(\frac{h(\vartheta_1|\vartheta_2,\{0\})_R-h(\vartheta_1|\vartheta_1,\{0\})_R/\cosh(\vartheta_2+\vartheta_1)}{\sinh(\vartheta_2+\vartheta_1)}\right)\,,
\end{aligned}
\tag{I.2.4}
$$

where we used (I.0.3) and (E.3.3). This can be further simplified to

$$
\begin{aligned}
C_{23}^{intBII2} =& C_{23}^{intBII2a}+C_{23}^{intBII2b}\,,\\
C_{23}^{intBII2a} =& \frac{g}{2}\left(\frac{1}{2}\right)^2\sum_{I\neq 0}\int_{-\infty}^{\infty}\frac{d\vartheta_2}{2\pi}\frac{|K(\vartheta_1)|^2}{\bar\rho_2(\vartheta_1)}\left(\frac{h(\vartheta_1|\vartheta_2,\{0\})_R\,(1-1/\cosh(\vartheta_2-\vartheta_1))}{\sinh(\vartheta_2-\vartheta_1)}\right)8F_1/\sinh\vartheta_1\\
&+\frac{g}{2}\left(\frac{1}{2}\right)^2\sum_{I\neq 0}\int_{-\infty}^{\infty}\frac{d\vartheta_2}{2\pi}\frac{|K(\vartheta_1)|^2}{\bar\rho_2(\vartheta_1)}\left(\frac{h(\vartheta_1|\vartheta_2,\{0\})_R\,(1-1/\cosh(\vartheta_2+\vartheta_1))}{\sinh(\vartheta_2+\vartheta_1)}\right)8F_1/\sinh(-\vartheta_1)\,,
\end{aligned}
$$

$$
\begin{aligned}
C_{23}^{intBII2b} =& \frac{g}{2}\left(\frac{1}{2}\right)^2\sum_{I\neq 0}\int_{-\infty}^{\infty}\frac{d\vartheta_2}{2\pi}\frac{|K(\vartheta_1)|^2}{\bar\rho_2(\vartheta_1)}\left(\frac{h(\vartheta_1|\vartheta_2,\{0\})_R-h(\vartheta_1|\vartheta_1,\{0\})_R}{\sinh(\vartheta_2-\vartheta_1)\cosh\vartheta_2-\vartheta_1}\right)8F_1/\sinh\vartheta_1\\
&+\frac{g}{2}\left(\frac{1}{2}\right)^2\sum_{I\neq 0}\int_{-\infty}^{\infty}\frac{d\vartheta_2}{2\pi}\frac{|K(\vartheta_1)|^2}{\bar\rho_2(\vartheta_1)}\left(\frac{h(\vartheta_1|\vartheta_2,\{0\})_R-h(\vartheta_1|\vartheta_1,\{0\})_R}{\sinh(\vartheta_2+\vartheta_1)\cosh(\vartheta_2+\vartheta_1)}\right)8F_1/\sinh(-\vartheta_1)\,.
\end{aligned}
\tag{I.2.5}
$$

Now consider

$$
\begin{aligned}
C_{23}^{intBII3} =& \frac{g}{2}\left(\frac{1}{2}\right)^2\sum_{I\neq 0}\int_{-\infty+i\varepsilon}^{\infty+i\varepsilon}\frac{d\vartheta_2}{2\pi}\frac{h(\vartheta_1|\vartheta_2,\{0\})_R\,K(-\vartheta_1)K(\vartheta_2)}{\bar\rho_2(\vartheta_1)}\frac{F_5^\varepsilon(\vartheta_1)}{\sinh(-\vartheta_1)}\\
&-\frac{g}{2}\left(\frac{1}{2}\right)^2\sum_{I\neq 0}\int_{-\infty+i\varepsilon}^{\infty+i\varepsilon}\frac{d\vartheta_2}{2\pi}\frac{h(\vartheta_1|\vartheta_2,\{0\})_R\,K(-\vartheta_1)K(\vartheta_2)}{\bar\rho_2(\vartheta_1)}\frac{F_5^\varepsilon(-\vartheta_1)}{\sinh\vartheta_1}\\
=&0\,.
\end{aligned}
\tag{I.2.6}
$$

Finally,

$$
\begin{aligned}
C_{23}^{intBII4} =& -\frac{g}{2}\left(\frac{1}{2}\right)^2 \sum_{I\neq 0}\int_{-\infty}^{\infty}\frac{d\vartheta_2}{2\pi}\frac{h(\vartheta_1|\vartheta_2,\{0\})_R\,|K(\vartheta_1)|^2}{\bar\rho_2(\vartheta_1)}\frac{F_5^\varepsilon(\vartheta_1)}{\sinh(-\vartheta_1)} \\
&-\frac{g}{2}\left(\frac{1}{2}\right)^2 \sum_{I\neq 0}\int_{-\infty}^{\infty}\frac{d\vartheta_2}{2\pi}\frac{h(\vartheta_1|\vartheta_2,\{0\})_R\,|K(\vartheta_1)|^2}{\bar\rho_2(\vartheta_1)}\frac{F_5^\varepsilon(-\vartheta_1)}{\sinh\vartheta_1} \\
=&\frac{g}{2}\left(\frac{1}{2}\right)^2 \sum_{I\neq 0}\int_{-\infty}^{\infty}\frac{d\vartheta_2}{2\pi}\frac{h(\vartheta_1|\vartheta_2,\{0\})_R\,|K(\vartheta_1)|^2}{\bar\rho_2(\vartheta_1)}\frac{16F_1}{\sinh^2\vartheta_1} \quad .
\end{aligned}
\tag{I.2.7}
$$

I.3 The term C^{intA}

As a function of ϑ_2 this term has no singularity at the origin so we can pull the contour back to the real axis at once:

$$
\begin{aligned}
C_{23}^{intA} =&\frac{g}{2}\left(\frac{1}{2}\right)^2 \sum_{I\neq 0}\int_{-\infty+i\varepsilon}^{\infty+i\varepsilon}\frac{d\vartheta_2}{2\pi}\left\{\frac{h(\vartheta_1|\vartheta_2,\{0\})_R\,K(-\vartheta_1)K(\vartheta_2)}{\bar\rho_2(\vartheta_1)}\left[F_5(\vartheta_1|\vartheta_2,\{0\})\right.\right. \\
&\left.\left.-4F_1\left(\frac{\cosh(\vartheta_2-\vartheta_1)}{\sinh^2(\vartheta_2-\vartheta_1)}-\frac{\cosh(\vartheta_2+\vartheta_1)}{\sinh^2(\vartheta_2+\vartheta_1)}\right)-\frac{F_5^\varepsilon(\vartheta_1)}{\sinh(\vartheta_2-\vartheta_1)}+\frac{F_5^\varepsilon(-\vartheta_1)}{\sinh(\vartheta_2+\vartheta_1)}\right]\right\} \\
=&\frac{g}{2}\left(\frac{1}{2}\right)^2 \sum_{I\neq 0}\int_{-\infty}^{\infty}\frac{d\vartheta_2}{2\pi}\left\{\frac{h(\vartheta_1|\vartheta_2,\{0\})_R\,K(-\vartheta_1)K(\vartheta_2)}{\bar\rho_2(\vartheta_1)}\left[F_5(\vartheta_1|\vartheta_2,\{0\})\right.\right. \\
&\left.\left.-4F_1\left(\frac{\cosh(\vartheta_2-\vartheta_1)}{\sinh^2(\vartheta_2-\vartheta_1)}-\frac{\cosh(\vartheta_2+\vartheta_1)}{\sinh^2(\vartheta_2+\vartheta_1)}\right)-\frac{F_5^\varepsilon(\vartheta_1)}{\sinh(\vartheta_2-\vartheta_1)}+\frac{F_5^\varepsilon(-\vartheta_1)}{\sinh(\vartheta_2+\vartheta_1)}\right]\right\} ,
\end{aligned}
\tag{I.3.1}
$$

thus a stationary phase evaluation using (E.4.1) yields a $1/\sqrt{t}$ behaviour multiplied by the function value in $\vartheta_2 = 0$. This expression as a function of ϑ_1 has singularities of 4th and 2nd order, but the 4th order ones just cancel due to

$$
\begin{aligned}
&\lim_{\vartheta_1\to 0}K(-\vartheta_1)4\lim_{\vartheta_2\to 0}\frac{F_1K(\vartheta_2)\sinh\vartheta_2}{\sinh\vartheta_2}\left(\frac{\cosh(\vartheta_2-\vartheta_1)}{\sinh^2(\vartheta_2-\vartheta_1)}-\frac{\cosh(\vartheta_2+\vartheta_1)}{\sinh^2(\vartheta_2+\vartheta_1)}\right)=\lim_{\vartheta_1\to 0}g^4 2\frac{\cosh^2\vartheta_1+1}{\sinh^4\vartheta_1}F_1 , \\
&\lim_{\vartheta_1\to 0}K(-\vartheta_1)\lim_{\vartheta_2\to 0}\frac{K(\vartheta_2)\sinh\vartheta_2}{\sinh\vartheta_2}\left(-\frac{F_5^\varepsilon(\vartheta_1)}{\sinh(\vartheta_2-\vartheta_1)}+\frac{F_5^\varepsilon(\vartheta_1)}{\sinh(\vartheta_2+\vartheta_1)}\right)=\lim_{\vartheta_1\to 0}-2g^4 2\frac{\cosh\vartheta_1}{\sinh^4\vartheta_1}F_1
\end{aligned}
$$

as $F_5^\varepsilon(\vartheta_1)\propto\frac{8F_1}{\vartheta_1}$ around the origin. Hence in ϑ_1 no 4th order singularity is present and when the sum over I is converted to an integral the remaining 2nd order singularity can only produce terms of the type mL but no higher power of L. These are expected to be cancelled by terms from Z_1D_{12}.

I.4 Singularities and their cancellation from C_{23}^{intBI} and C_{23}^{intBII}

There are some terms that have an integral regular at $\vartheta_2 = 0$ hence the SPA (E.4.1) can be directly applied yielding a $1/\sqrt{t}$ factor. But the resulting ϑ_1 dependent prefactor has a dangerous $1/\vartheta_1^4$ singularity which must cancel for the volume dependence to be regular when combined with Z_1D_{12}.

I.4.1 4th order singularities from $C_{23}^{intBII1}$, $C_{23}^{intBII4}$ and their cancellation

Now we turn to $C_{23}^{intBII1}$ and $C_{23}^{intBII4}$

$$\begin{aligned}
C_{23}^{intBII1} =& \frac{g}{2}\left(\frac{1}{2}\right)^2 \sum_{I\neq 0}\int_{-\infty}^{\infty}\frac{d\vartheta_2}{2\pi}\frac{h(\vartheta_1|\vartheta_2,\{0\})_R\,K(-\vartheta_1)\,(K(\vartheta_2)-K(\vartheta_1))\,F_5^{\varepsilon}(\vartheta_1)}{\bar{\rho}_2(\vartheta_1)}\times \\
&\times\left(\frac{1}{\sinh(\vartheta_2-\vartheta_1)}+\frac{1}{\sinh\vartheta_1}\right) \\
&-\frac{g}{2}\left(\frac{1}{2}\right)^2 \sum_{I\neq 0}\int_{-\infty}^{\infty}\frac{d\vartheta_2}{2\pi}\frac{h(\vartheta_1|\vartheta_2,\{0\})_R\,K(-\vartheta_1)\,(K(\vartheta_2)-K(-\vartheta_1))\,F_5^{\varepsilon}(-\vartheta_1)}{\bar{\rho}_2(\vartheta_1)}\times \\
&\times\left(\frac{1}{\sinh(\vartheta_2+\vartheta_1)}-\frac{1}{\sinh\vartheta_1}\right)\,, \\
C_{23}^{intBII4} =& \frac{g}{2}\left(\frac{1}{2}\right)^2 \sum_{I\neq 0}\int_{-\infty}^{\infty}\frac{d\vartheta_2}{2\pi}\frac{h(\vartheta_1|\vartheta_2,\{0\})_R\,|K(\vartheta_1)|^2}{\bar{\rho}_2(\vartheta_1)}\frac{F_5^{\varepsilon}(\vartheta_1)-F_5^{\varepsilon}(-\vartheta_1)}{\sinh\vartheta_1}\,,
\end{aligned} \tag{I.4.1}$$

from which we have after the ϑ_2 integration applying the SPA, (E.4.1)

$$\begin{aligned}
C_{23}^{intBII1} &\approx \frac{g}{8}\sum_{I\neq 0} h(\vartheta_1|0,\{0\})_R\left(\frac{ig^2/2}{\sinh^2\vartheta_1}\cosh\vartheta_1\right)8F_1\frac{K(-\vartheta_1)-K(\vartheta_1)}{\bar{\rho}_2\sinh\vartheta_1}/\sqrt{4\pi mt} \\
&\approx -\frac{g}{8}\vartheta_1^{-4}h(\vartheta_1|0,\{0\})_R\,(g^4/4)16F_1/\sqrt{4\pi mt}\,, \\
C_{23}^{intBII4} &\approx \frac{g}{8}\sum_{I\neq 0} h(\vartheta_1|0,\{0\})_R\,K(-\vartheta_1)K(\vartheta_1)\frac{1}{\bar{\rho}_2}\frac{F_5^{\varepsilon}(\vartheta_1)-F_5^{\varepsilon}(-\vartheta_1)}{\sinh\vartheta_1}/\sqrt{4\pi mt} \\
&\approx \frac{g}{8}\vartheta_1^{-4}(g^4/4)16F_1h(\vartheta_1|0,\{0\})_R\,/\sqrt{4\pi mt}\,,
\end{aligned} \tag{I.4.2}$$

hence the 4th order singularity vanishes.

I.4.2 4th order singularities from C_{23}^{intBI4}, $C_{23}^{intBI1a}$ and their cancellation

We begin by C_{23}^{intBI4} and its integration with respect to ϑ_2 using the SPA, (E.4.1):

$$C_{23}^{intBI4} = -2\frac{g}{2}\left(\frac{1}{2}\right)^2\sum_{I\neq 0}\int_{-\infty}^{\infty}\frac{d\vartheta_2}{2\pi}\frac{h(\vartheta_1|\vartheta_2,\{0\})_R\,|K(\vartheta_1)|^2}{\bar{\rho}_2(\vartheta_1)}4F_1\frac{\cosh\vartheta_1}{\sinh^2\vartheta_1}\,, \tag{I.4.3}$$

from which, neglecting the sum, the following behaviour is obtained for $\vartheta_1\approx 0$

$$C_{23}^{intBI4} \approx -2\frac{g}{8}\vartheta_1^{-4}h(\vartheta_1|0,\{0\})_R\,g^4\frac{F_1}{\bar{\rho}_2(\vartheta_1)}/\sqrt{4\pi mt}\,, \tag{I.4.4}$$

whereas for $C_{23}^{intBI1a}$, which reads

$$
\begin{aligned}
C_{23}^{intBI1a} =& \frac{g}{2}\left(\frac{1}{2}\right)^2 \sum_{I\neq 0}\int_{-\infty}^{\infty}\frac{d\vartheta_2}{2\pi} 4F_1 \frac{K(-\vartheta_1)}{\bar{\rho}_2(\vartheta_1)}\frac{h(\vartheta_1|\vartheta_2,\{0\})_R}{\sinh\vartheta_2-\vartheta_1}\times \\
&\times\left[(K(\vartheta_2)-K(\vartheta_1))\left(\frac{\cosh(\vartheta_2-\vartheta_1)}{\sinh^2(\vartheta_2-\vartheta_1)}-\frac{\cosh\vartheta_1}{\sinh^2\vartheta_1}\right)\sinh(\vartheta_2-\vartheta_1)-\frac{K'(\vartheta_1)}{\cosh(\vartheta_2-\vartheta_1)}\right] \\
&+\frac{g}{2}\left(\frac{1}{2}\right)^2 \sum_{I\neq 0}\int_{-\infty}^{\infty}\frac{d\vartheta_2}{2\pi} 4F_1 \frac{K(\vartheta_1)}{\bar{\rho}_2(\vartheta_1)}\frac{h(\vartheta_1|\vartheta_2,\{0\})_R}{\sinh\vartheta_2+\vartheta_1}\times \\
&\times\left[(K(\vartheta_2)-K(-\vartheta_1))\left(\frac{\cosh(\vartheta_2+\vartheta_1)}{\sinh^2(\vartheta_2+\vartheta_1)}-\frac{\cosh\vartheta_1}{\sinh^2\vartheta_1}\right)\sinh(\vartheta_2+\vartheta_1)-\frac{K'(-\vartheta_1)}{\cosh(\vartheta_2+\vartheta_1)}\right],
\end{aligned}
\tag{I.4.5}
$$

we have after integration on ϑ_2 applying the SPA, (E.4.1)

$$
\begin{aligned}
C_{23}^{intBI1a} \approx& \frac{g}{8}\left\{4F_1\frac{K(-\vartheta_1)}{\bar{\rho}_2(\vartheta_1)}h(\vartheta_1|0,\{0\})_R\left(\left(-ig^2/2\right)(-1)\frac{\cosh^2\vartheta_1+1}{\sinh^3(-\vartheta_1)}+\frac{K'(\vartheta_1)}{\sinh\vartheta_1\cosh\vartheta_1}\right)+\right. \\
&\left.+4F_1\frac{K(\vartheta_1)}{\bar{\rho}_2(\vartheta_1)}h(\vartheta_1|0,\{0\})_R\left(\left(-ig^2/2\right)(-1)\frac{\cosh^2\vartheta_1+1}{\sinh^3\vartheta_1}-\frac{K'(-\vartheta_1)}{\sinh\vartheta_1\cosh\vartheta_1}\right)\right\}/\sqrt{4\pi mt} \\
=& \frac{g}{8}\left\{4F_1\frac{K(-\vartheta_1)}{\bar{\rho}_2(\vartheta_1)}h(\vartheta_1|0,\{0\})_R\left(-ig^2/2\right)\left(\frac{\cosh^2\vartheta_1+1}{\sinh^3\vartheta_1}+\frac{-1}{\sinh^3\vartheta_1\cosh\vartheta_1}\right)+\right. \\
&\left.+4F_1\frac{K(\vartheta_1)}{\bar{\rho}_2(\vartheta_1)}h(\vartheta_1|0,\{0\})_R\left(-ig^2/2\right)\left(-\frac{\cosh^2\vartheta_1+1}{\sinh^3\vartheta_1}+\frac{1}{\sinh^3\vartheta_1\cosh\vartheta_1}\right)\right\}/\sqrt{4\pi mt} \\
\approx& 2\frac{g}{8}\vartheta_1^{-4}F_1\frac{1}{\bar{\rho}_2(\vartheta_1)}h(\vartheta_1|0,\{0\})_R\, g^4/\sqrt{4\pi mt}
\end{aligned}
\tag{I.4.6}
$$

that cancels the 4th order singularity from C_{23}^{intBI4}.

I.4.3 Singularities from $C_{23}^{intBII2a}$

We start with $C_{23}^{intBII2a}$ and show that after the ϑ_2 integration with SPA (E.4.1), no 4th order singularity remains. $C_{23}^{intBII2a}$ reads

$$
\begin{aligned}
C_{23}^{intBII2a} =& +\frac{g}{2}\left(\frac{1}{2}\right)^2\sum_{I\neq 0}\int_{-\infty}^{\infty}\frac{d\vartheta_2}{2\pi}\frac{|K(\vartheta_1)|^2}{\bar{\rho}_2(\vartheta_1)}\left(\frac{h(\vartheta_1|\vartheta_2,\{0\})_R\,(1-1/\cosh(\vartheta_2-\vartheta_1))}{\sinh(\vartheta_2-\vartheta_1)}\right)8F_1/\sinh\vartheta_1 \\
&+\frac{g}{2}\left(\frac{1}{2}\right)^2\sum_{I\neq 0}\int_{-\infty}^{\infty}\frac{d\vartheta_2}{2\pi}\frac{|K(\vartheta_1)|^2}{\bar{\rho}_2(\vartheta_1)}\left(\frac{h(\vartheta_1|\vartheta_2,\{0\})_R\,(1-1/\cosh(\vartheta_2+\vartheta_1))}{\sinh(\vartheta_2+\vartheta_1)}\right)8F_1/\sinh(-\vartheta_1)
\end{aligned}
\tag{I.4.7}
$$

and is regular in $\vartheta_2=0$. Hence performing the SPA (E.4.1) for $C_{23}^{intBII2a}$, it is seen that the ϑ_1 dependence is $1/\vartheta_1^2$.

I.5 Terms with non trivial time dependence

As seen in (I.4), a large number of terms originating from (I.0.1) involving integration with respect to ϑ_2 can be evaluated directly using the SPA (E.4.1). Once the SPA is performed, these terms have singularities in ϑ_1, which are of either 4th or second order, and those of 4th order behaviour cancel each other, whereas the second order singularities cannot produce time dependence stronger than $O(t^0)$.

For some terms, however, the ϑ_2 integration cannot be easily performed. The first example is provided by (I.1.7) which we write again as

$$\begin{aligned}
C_{23}^{intBI2} =& (-2imt - Rm)\,\frac{g}{2}\left(\frac{1}{2}\right)^2 \sum_{I\neq 0}\int_{-\infty}^{\infty}\frac{d\vartheta_2}{2\pi}\frac{|K(\vartheta_1)|^2}{\bar\rho_2(\vartheta_1)}\frac{4F_1}{\sinh(\vartheta_2-\vartheta_1)}\times \\
&\times\left[h(\vartheta_1|\vartheta_2,\{0\})_R\sinh\vartheta_2 - \frac{h(\vartheta_1|\vartheta_1,\{0\})_R\sinh\vartheta_1}{\cosh(\vartheta_2-\vartheta_1)}\right] \\
&+(-2imt - Rm)\,\frac{g}{2}\left(\frac{1}{2}\right)^2 \sum_{I\neq 0}\int_{-\infty}^{\infty}\frac{d\vartheta_2}{2\pi}\frac{|K(\vartheta_1)|^2}{\bar\rho_2(\vartheta_1)}\frac{4F_1}{\sinh(\vartheta_2+\vartheta_1)}\times \\
&\times\left[h(\vartheta_1|\vartheta_2,\{0\})_R\sinh\vartheta_2 - \frac{h(\vartheta_1|\vartheta_1,\{0\})_R\sinh(-\vartheta_1)}{\cosh(\vartheta_2+\vartheta_1)}\right]\,,
\end{aligned} \tag{I.5.1}$$

and split into $C_{23}^{intBI2a} + C_{23}^{intBI2b}$ as

$$\begin{aligned}
C_{23}^{intBI2a} =& (-2imt - Rm)\,\frac{g}{2}\left(\frac{1}{2}\right)^2 \sum_{I\neq 0}\int_{-\infty}^{\infty}\frac{d\vartheta_2}{2\pi}\frac{|K(\vartheta_1)|^2}{\bar\rho_2(\vartheta_1)}\frac{4F_1 h(\vartheta_1|\vartheta_2,\{0\})_R\left(\sinh\vartheta_2 - \frac{\sinh\vartheta_1}{\cosh(\vartheta_2-\vartheta_1)}\right)}{\sinh(\vartheta_2-\vartheta_1)} \\
&+(-2imt - Rm)\,\frac{g}{2}\left(\frac{1}{2}\right)^2 \sum_{I\neq 0}\int_{-\infty}^{\infty}\frac{d\vartheta_2}{2\pi}\frac{|K(\vartheta_1)|^2}{\bar\rho_2(\vartheta_1)}\frac{4F_1 h(\vartheta_1|\vartheta_2,\{0\})_R\left(\sinh\vartheta_2 - \frac{\sinh-\vartheta_1}{\cosh(\vartheta_2+\vartheta_1)}\right)}{\sinh(\vartheta_2+\vartheta_1)}\,, \\
C_{23}^{intBI2b} =& (-2imt - Rm)\,\frac{g}{2}\left(\frac{1}{2}\right)^2 \sum_{I\neq 0}\int_{-\infty}^{\infty}\frac{d\vartheta_2}{2\pi}\frac{|K(\vartheta_1)|^2}{\bar\rho_2(\vartheta_1)}\frac{4F_1\sinh\vartheta_1}{\sinh(\vartheta_2-\vartheta_1)\cosh(\vartheta_2-\vartheta_1)}\times \\
&\times\left[h(\vartheta_1|\vartheta_2,\{0\})_R - h(\vartheta_1|\vartheta_1,\{0\})_R\right] \\
&+(-2imt - Rm)\,\frac{g}{2}\left(\frac{1}{2}\right)^2 \sum_{I\neq 0}\int_{-\infty}^{\infty}\frac{d\vartheta_2}{2\pi}\frac{|K(\vartheta_1)|^2}{\bar\rho_2(\vartheta_1)}\frac{4F_1\sinh(-\vartheta_1)}{\sinh(\vartheta_2+\vartheta_1)\cosh(\vartheta_2+\vartheta_1)}\times \\
&\times\left[h(\vartheta_1|\vartheta_2,\{0\})_R - h(\vartheta_1|\vartheta_1,\{0\})_R\right] \quad .
\end{aligned} \tag{I.5.2}$$

$C_{23}^{intBI1b}$ and $C_{23}^{intBII2b}$ provide the second example, which is written again for better transparency as

$$
\begin{aligned}
C_{23}^{intBI1b} =& \frac{g}{2}\left(\frac{1}{2}\right)^2 \sum_{I\neq 0}\int_{-\infty}^{\infty}\frac{d\vartheta_2}{2\pi}4F_1\frac{K(-\vartheta_1)}{\bar\rho_2(\vartheta_1)}\frac{[h(\vartheta_1|\vartheta_2,\{0\})_R - h(\vartheta_1|\vartheta_1,\{0\})_R]\,K'(\vartheta_1)}{\cosh(\vartheta_2-\vartheta_1)\sinh(\vartheta_2-\vartheta_1)} \\
&+\frac{g}{2}\left(\frac{1}{2}\right)^2 \sum_{I\neq 0}\int_{-\infty}^{\infty}\frac{d\vartheta_2}{2\pi}4F_1\frac{K(\vartheta_1)}{\bar\rho_2(\vartheta_1)}\frac{[h(\vartheta_1|\vartheta_2,\{0\})_R - h(\vartheta_1|\vartheta_1,\{0\})_R]\,K'(-\vartheta_1)}{\cosh(\vartheta_2+\vartheta_1)\sinh(\vartheta_2+\vartheta_1)}\,, \\
C_{23}^{intBII2b} =& \frac{g}{2}\left(\frac{1}{2}\right)^2 \sum_{I\neq 0}\int_{-\infty}^{\infty}\frac{d\vartheta_2}{2\pi}\frac{|K(\vartheta_1)|^2}{\bar\rho_2(\vartheta_1)}\left(\frac{h(\vartheta_1|\vartheta_2,\{0\})_R - h(\vartheta_1|\vartheta_1,\{0\})_R}{\sinh(\vartheta_2-\vartheta_1)\cosh(\vartheta_2-\vartheta_1)}\right)8F_1/\sinh\vartheta_1 \\
&+\frac{g}{2}\left(\frac{1}{2}\right)^2 \sum_{I\neq 0}\int_{-\infty}^{\infty}\frac{d\vartheta_2}{2\pi}\frac{|K(\vartheta_1)|^2}{\bar\rho_2(\vartheta_1)}\left(\frac{h(\vartheta_1|\vartheta_2,\{0\})_R - h(\vartheta_1|\vartheta_1,\{0\})_R}{\sinh(\vartheta_2+\vartheta_1)\cosh(\vartheta_2+\vartheta_1)}\right)8F_1/\sinh(-\vartheta_1)\,,
\end{aligned}
\tag{I.5.3}
$$

which we add and denote by $C_{23}^{intBI-II}$. Therefore,

$$
\begin{aligned}
C_{23}^{intBI-II} =& C_{23}^{intBI1b} + C_{23}^{intBII2b} \\
=& \frac{g}{2}\left(\frac{1}{2}\right)^2 \sum_{I\neq 0}\int_{-\infty}^{\infty}\frac{d\vartheta_2}{2\pi}4F_1\frac{K(-\vartheta_1)}{\bar\rho_2(\vartheta_1)}\frac{[h(\vartheta_1|\vartheta_2,\{0\})_R - h(\vartheta_1|\vartheta_1,\{0\})_R]\left(\frac{2K(\vartheta_1)}{\sinh\vartheta_1}+K'(\vartheta_1)\right)}{\cosh(\vartheta_2-\vartheta_1)\sinh(\vartheta_2-\vartheta_1)} \\
&+\frac{g}{2}\left(\frac{1}{2}\right)^2 \sum_{I\neq 0}\int_{-\infty}^{\infty}\frac{d\vartheta_2}{2\pi}4F_1\frac{K(\vartheta_1)}{\bar\rho_2(\vartheta_1)}\frac{[h(\vartheta_1|\vartheta_2,\{0\})_R - h(\vartheta_1|\vartheta_1,\{0\})_R]\left(\frac{2K(-\vartheta_1)}{\sinh(-\vartheta_1)}+K'(-\vartheta_1)\right)}{\cosh(\vartheta_2+\vartheta_1)\sinh(\vartheta_2+\vartheta_1)}\,.
\end{aligned}
\tag{I.5.4}
$$

Both $C_{23}^{intBI2b}$ and $C_{23}^{intBI-II}$ defined in (I.5.4) involve the same integral kernel

$$
\int_{-\infty}^{\infty}\frac{d\vartheta_2}{2\pi}\frac{h(\vartheta_1|\vartheta_2,\{0\})_R - h(\vartheta_1|\vartheta_1,\{0\})_R}{\cosh(\vartheta_2-\vartheta_1)\sinh(\vartheta_2-\vartheta_1)} \tag{I.5.5}
$$

which is a function of t,ϑ_1 and is evaluated in the next Appendix.

I.6 Summary

We have shown that from C_{23}^{int}, i.e. the contour integral, apart from C_{23}^{intBI2} defined in (I.1.7), (I.5.1) and $C_{23}^{intBI-II}$ defined in (I.5.4), only terms with dependence mL contribute to one-particle oscillations. The $\sqrt{tmL}$ term resulting from (I.1.7) (cf. eqn. (J.1.3)) is expected to be cancelled by the denominator of (8.1.1) through Z_1D_{12}, and the only surviving time dependence comes from C_{23}^{intBI2} and $C_{23}^{intBI-II}$ which are analysed in the next section.

Appendix J

Evaluation of the integral kernel and time dependence

In this section we evaluate

$$
\begin{aligned}
C_{23}^{intBI2a} =& (-2imt - Rm)\,\frac{g}{2}\left(\frac{1}{2}\right)^2 \sum_{I\neq 0}\int_{-\infty}^{\infty}\frac{d\vartheta_2}{2\pi}\frac{|K(\vartheta_1)|^2}{\bar{\rho}_2(\vartheta_1)}\frac{\Omega(\vartheta_1)F_1 h(\vartheta_1|\vartheta_2,\{0\})_R}{\sinh(\vartheta_2-\vartheta_1)}\times \\
&\times\left(\sinh\vartheta_2 - \frac{\sinh\vartheta_1}{\cosh(\vartheta_2-\vartheta_1)}\right) \\
&+(-2imt - Rm)\,\frac{g}{2}\left(\frac{1}{2}\right)^2 \sum_{I\neq 0}\int_{-\infty}^{\infty}\frac{d\vartheta_2}{2\pi}\frac{|K(\vartheta_1)|^2}{\bar{\rho}_2(\vartheta_1)}\frac{\Omega(\vartheta_1)F_1 h(\vartheta_1|\vartheta_2,\{0\})_R}{\sinh(\vartheta_2+\vartheta_1)} \\
&\times\left(\sinh\vartheta_2 - \frac{\sinh -\vartheta_1}{\cosh(\vartheta_2+\vartheta_1)}\right)\,, \qquad \text{(J.0.1)}\\
C_{23}^{intBI2b} =& (-2imt - Rm)\,\frac{g}{2}\left(\frac{1}{2}\right)^2 \sum_{I\neq 0}\int_{-\infty}^{\infty}\frac{d\vartheta_2}{2\pi}\frac{|K(\vartheta_1)|^2}{\bar{\rho}_2(\vartheta_1)}\frac{\Omega(\vartheta_1)F_1\sinh\vartheta_1}{\sinh(\vartheta_2-\vartheta_1)\cosh(\vartheta_2-\vartheta_1)}\times \\
&\times\left[h(\vartheta_1|\vartheta_2,\{0\})_R - h(\vartheta_1|\vartheta_1,\{0\})_R\right] \\
&+(-2imt - Rm)\,\frac{g}{2}\left(\frac{1}{2}\right)^2 \sum_{I\neq 0}\int_{-\infty}^{\infty}\frac{d\vartheta_2}{2\pi}\frac{|K(\vartheta_1)|^2}{\bar{\rho}_2(\vartheta_1)}\frac{\Omega(\vartheta_1)F_1\sinh(-\vartheta_1)}{\sinh(\vartheta_2+\vartheta_1)\cosh(\vartheta_2+\vartheta_1)}\times \\
&\times\left[h(\vartheta_1|\vartheta_2,\{0\})_R - h(\vartheta_1|\vartheta_1,\{0\})_R\right]\,,
\end{aligned}
$$

and

$$
\begin{aligned}
C_{23}^{intBI-II} =& \frac{g}{2}\left(\frac{1}{2}\right)^2 \sum_{I\neq 0}\int_{-\infty}^{\infty}\frac{d\vartheta_2}{2\pi}\frac{K(-\vartheta_1)}{\bar{\rho}_2(\vartheta_1)}\frac{(K(\vartheta_1)F_5^{\varepsilon}(\vartheta_1)+\Omega(\vartheta_1)F_1K'(\vartheta_1))}{\cosh(\vartheta_2-\vartheta_1)\sinh(\vartheta_2-\vartheta_1)}\times \\
&\times\left[h(\vartheta_1|\vartheta_2,\{0\})_R - h(\vartheta_1|\vartheta_1,\{0\})_R\right] \\
&+\frac{g}{2}\left(\frac{1}{2}\right)^2 \sum_{I\neq 0}\int_{-\infty}^{\infty}\frac{d\vartheta_2}{2\pi}\frac{K(\vartheta_1)}{\bar{\rho}_2(\vartheta_1)}\frac{(K(-\vartheta_1)F_5^{\varepsilon}(-\vartheta_1)+\Omega(\vartheta_1)F_1K'(-\vartheta_1))}{\cosh(\vartheta_2+\vartheta_1)\sinh(\vartheta_2+\vartheta_1)}\times \\
&\times\left[h(\vartheta_1|\vartheta_2,\{0\})_R - h(\vartheta_1|\vartheta_1,\{0\})_R\right]\,.
\end{aligned}
\qquad \text{(J.0.2)}
$$

Here we restored the S matrix dependence and $\Omega(\vartheta_1) = (1 - S(\vartheta_1))\,(1 - S(-\vartheta_1))$ compared to (I.1.7). For the integration over ϑ_2 the SPA (E.4.1) cannot be directly applied to the second term in (J.0.1) and to (J.0.2).

$C_{23}^{intBI2a}$, $C_{23}^{intBI2b}$ and $C_{23}^{intBI-II}$ are even functions of ϑ_2, therefore we can define the following integral kernels

$$Ker^a(\vartheta_1,t,R) = e^{imt}\Omega(\vartheta_1)\int_{-\infty}^{\infty}\frac{d\vartheta_2}{2\pi}\frac{\left[h(\vartheta_1|\vartheta_2,\{0\})_R\left(\sinh\vartheta_2-\frac{\sinh\vartheta_1}{\cosh(\vartheta_2-\vartheta_1)}\right)\right]}{\sinh(\vartheta_2-\vartheta_1)} \tag{J.0.3}$$

and

$$Ker(\vartheta_1,t,R) = e^{imt}\Omega(\vartheta_1)\int_{-\infty}^{\infty}\frac{d\vartheta_2}{2\pi}\frac{[h(\vartheta_1|\vartheta_2,\{0\})_R - h(\vartheta_1|\vartheta_1,\{0\})_R]\sinh\vartheta_1}{\sinh(\vartheta_2-\vartheta_1)\cosh(\vartheta_2-\vartheta_1)}\,, \tag{J.0.4}$$

which are even functions of ϑ_1. Then Ker_a appears in $C_{23}^{intBI2a}$ in (J.0.1), while Ker in $C_{23}^{intBI2b}$ in (J.0.1) and in $C_{23}^{intBI-II}$, (J.0.2). For Ker_a, the long time limit can be calculated by applying the SPA (E.4.1) resulting in

$$\begin{aligned} Ker^a_{stac}(\vartheta_1,t,R) =& e^{imt}\Omega(\vartheta_1)\frac{1}{\sqrt{2\pi 2mt}}\frac{h(\vartheta_1,0,\{0\})_R\,e^{-i\pi/4}}{\cosh\vartheta_1} \\ =& \frac{\Omega(\vartheta_1)}{\sqrt{\pi mt}}\frac{e^{2imt(\cosh\vartheta_1-1)}e^{-i\pi/4}}{2\cosh\vartheta_1}e^{-mR(\cosh\vartheta_1+3/2)}\,. \end{aligned} \tag{J.0.5}$$

As for Ker the SPA, (E.4.1) cannot be directly applied, we proceed as follows: we first differentiate the integrand with respect to t and apply the SPA which becomes now possible:

$$\begin{aligned} &\Omega(\vartheta_1)\frac{d}{dt}\int_{-\infty}^{\infty}\frac{d\vartheta_2}{2\pi}\frac{e^{imt}\left[h(\vartheta_1|\vartheta_2,\{0\})_R - h(\vartheta_1|\vartheta_1,\{0\})_R\right]\sinh\vartheta_1}{\sinh(\vartheta_2-\vartheta_1)\cosh(\vartheta_2-\vartheta_1)} \\ =&\Omega(\vartheta_1)\int_{-\infty}^{\infty}\frac{d\vartheta_2}{2\pi}\frac{e^{imt}h(\vartheta_1,\vartheta_2,\{0\})_R\,2im\left(\cosh\vartheta_2-\cosh\vartheta_1\right)\sinh\vartheta_1}{\sinh(\vartheta_2-\vartheta_1)\cosh(\vartheta_2-\vartheta_1)} \\ =&\Omega(\vartheta_1)\frac{e^{2imt(\cosh\vartheta_1-1)}e^{-i\pi/4}}{\sqrt{\pi mt}\cosh\vartheta_1}2im\left(\cosh\vartheta_1-1\right)e^{-mR(\cosh\vartheta_1+3/2)}\,. \end{aligned} \tag{J.0.6}$$

Now integrating with respected to t one ends up with the Fresnel sine and cosine functions, denoted here by F_S and F_C respectively:

$$\begin{aligned} Ker_{stac}(\vartheta_1,t,R) =&\Omega(\vartheta_1)\frac{\sqrt{\cosh\vartheta_1-1)}}{\cosh\vartheta_1}e^{-mR(\cosh\vartheta_1+3/2)} \\ &\times\left\{\frac{\sqrt{2}}{2}\left(F_S\left(\sqrt{\frac{4mt(\cosh(\vartheta_1)-1)}{\pi}}\right)-F_C\left(\sqrt{\frac{4mt(\cosh(\vartheta_1)-1)}{\pi}}\right)\right)\right. \\ &-\frac{\sqrt{2}}{2}i\left(F_C\left(\sqrt{\frac{4mt(\cosh(\vartheta_1)-1)}{\pi}}\right)+F_S\left(\sqrt{\frac{4mt(\cosh(\vartheta_1)-1)}{\pi}}\right)\right) \\ &\left.+if(\vartheta_1,R)\right\}\,, \end{aligned} \tag{J.0.7}$$

where f is an integration constant that is independent of time, but is a function of ϑ_1 and R. We do not determine the precise form of $f(\vartheta_1,R)$, only quote its $R=0$ limit:

$$2\frac{\sqrt{(\cosh\vartheta_1-1)}}{\cosh\vartheta_1}f(\vartheta_1,0)=\left(\frac{\sqrt{2(\cosh\vartheta_1-1)}}{\cosh\vartheta_1}-\sqrt{\sinh^2\vartheta_1}\right) \tag{J.0.8}$$

which is determined by noticing that the $t\to\infty$ limit for $Ker(\vartheta_1,t,R)$ is proportional to $|\sinh\vartheta_1|$. Note that $\frac{\sqrt{\cosh\vartheta_1-1)}}{\cosh\vartheta_1}f(\vartheta_1,R)\approx\vartheta_1^2$ around the origin, i.e. its second derivative is continuous at the origin. Hence integrating it with $|K|^2$ gives a finite and well-defined result. In (J.0.2), however, $Ker(\vartheta_1,t,R)$ is integrated with a $1/\sinh^4(\vartheta_1)$ type of function due to $K(\vartheta_1)F_5^{\varepsilon}(\vartheta_1)+F_1\Omega(\vartheta_1)K'(\vartheta_1)$, where the non-analytic behaviour of $f(\vartheta_1)$ must be carefully handled. The origin of the non-analytic term can be summarised as follows: using the SPA, (E.4.1), a term proportional to $1/\sqrt{t}$ is obtained, but in the asymptotic expansion of the oscillatory integral, terms proportional to $t^{-1/2+n}$ are also present. For any finite t, these lead to analytic behaviour as expected from (J.0.4), but in the $t\to\infty$ limit keeping only the leading terms, non-analyticity can emerge.

J.1 Time dependence from Ker_a and $C_{23}^{intBI2a}$.

Substituting Ker^a_{stac} into (J.0.1), the discrete sum to evaluate reads

$$\frac{g}{2}F_1e^{-imt}(-imt-Rm/2)\sum_{I\neq0}\frac{|K(\vartheta_1)|^2Ker^a_{stac}(\vartheta_1,t,R)}{\bar\rho_2(\vartheta_1)} \tag{J.1.1}$$

that has a $1/\vartheta_1^2$ singularity at the origin which we treat with a contour integral representation:

$$\begin{aligned}
&\frac{g}{2}F_1e^{-imt}(-imt-Rm/2)\sum_{I\neq0}\frac{|K(\vartheta_1)|^2Ker^a_{stac}(\vartheta_1,t,R)}{\bar\rho_2(\vartheta_1)}\\
=&-\frac{g}{2}F_1e^{-imt}(-imt-Rm/2)\sum_{I\neq0}\oint_{C_I}\frac{d\vartheta_1}{2\pi}\frac{|K(\vartheta_1)|^2Ker^a_{stac}(\vartheta_1,t,R)}{e^{i\bar Q_2(\vartheta_1)}+1}\\
=&\frac{g}{2}F_1e^{-imt}(-imt-Rm/2)\int_{-\infty+i\varepsilon}^{\infty+i\varepsilon}\frac{d\vartheta_1}{2\pi}|K(\vartheta_1)|^2Ker^a_{stac}(\vartheta_1,t,R)\\
&+i\frac{g}{2}F_1e^{-imt}(-imt-Rm/2)\oint_0\frac{d\vartheta_1}{2\pi i}\frac{|K(\vartheta_1)|^2Ker^a_{stac}(\vartheta_1,t,R)}{e^{i\bar Q_2(\vartheta_1)}+1}\ .
\end{aligned} \tag{J.1.2}$$

As $Ker^a(\vartheta_1,t,R)$ is even in ϑ_1, its derivative vanishes at the origin, and so only the derivative of $e^{i\bar Q_2(\vartheta_1)}+1$ gives a pole contribution resulting in

$$\begin{aligned}
&i\frac{g}{2}F_1e^{-imt}(-imt-Rm/2)\oint_0\frac{d\vartheta_1}{2\pi i}\frac{|K(\vartheta_1)|^2Ker^a_{stac}(\vartheta_1,t,R)}{e^{i\bar Q_2}+1}\\
=&\frac{g}{2}F_1e^{-imt}(-imt-Rm/2)\frac{g^4Ker^a_{stac}(0,t,0)}{16}mL\\
\propto&\sqrt{t}mL\ ,
\end{aligned} \tag{J.1.3}$$

and hence expected to be cancelled by the appropriate counter-term from Z_1D_{12}. The contour integral in the $L\to\infty$ limit reduces to the upper contour and can be rewritten using (E.3.4) as

$$
\begin{aligned}
&\frac{g}{2}F_1 e^{-imt}(-imt - Rm/2)\int_{-\infty+i\varepsilon}^{\infty+i\varepsilon}\frac{d\vartheta_1}{2\pi}|K(\vartheta_1)|^2 Ker^a_{stac}(\vartheta_1,t,R)\\
=&\frac{g}{2}F_1 e^{-imt}(-imt - Rm/2)\int_{-\infty+i\varepsilon}^{\infty+i\varepsilon}\frac{d\vartheta_1}{2\pi}\left(|K(\vartheta_1)|^2\frac{sinh^2\vartheta_1}{\cosh\vartheta_1}Ker^a_{stac}(\vartheta_1,t,R)\right)\frac{\cosh\vartheta_1}{\sinh^2\vartheta_1}\\
=&\frac{g}{2}F_1 e^{-imt}(-imt - Rm/2)\int_{-\infty}^{\infty}\frac{d\vartheta_1}{2\pi}\left(|K(\vartheta_1)|^2\frac{sinh^2\vartheta_1}{\cosh\vartheta_1}Ker^a_{stac}(\vartheta_1,t,R)\right)'\frac{1}{\sinh\vartheta_1}\ ,
\end{aligned}
\tag{J.1.4}
$$

which is integrable since $Ker^a_{stac}(\vartheta_1,t,R)$ is an even and regular function with respect to ϑ_1 . Then the derivative of $|K(\vartheta_1)|^2\frac{sinh^2\vartheta_1}{\cosh\vartheta_1}$ gives a $\sqrt{t}$ contribution which we are not interested in at the moment. The contribution linear in t comes from

$$
\begin{aligned}
&\frac{g}{2}F_1 e^{-imt}(-imt)\int_{-\infty}^{\infty}\frac{d\vartheta_1}{2\pi}|K(\vartheta_1)|^2\tanh(\vartheta_1)\left(Ker^a_{stac}(\vartheta_1,t,0)\right)'\\
=&\frac{g}{2}F_1 e^{-imt}\int_{-\infty}^{\infty}\frac{d\vartheta_1}{2\pi}|K(\vartheta_1)|^2\tanh^2(\vartheta_1)\frac{\Omega(\vartheta_1)\,(-imt)\,e^{-i\pi/4}e^{2imt(\cosh(\vartheta_1)-1)}\,(2imt-\mathrm{sech}(\vartheta_1))}{2\sqrt{\pi mt}}\\
+&\frac{g}{2}F_1 e^{-imt}\int_{-\infty}^{\infty}\frac{d\vartheta_1}{2\pi}|K(\vartheta_1)|^2\tanh(\vartheta_1)\frac{(-imt)}{\sqrt{\pi mt}}\frac{e^{2imt(\cosh\vartheta_1-1)}e^{-i\pi/4}}{\cosh\vartheta_1}\Omega'(\vartheta_1)\\
=&\frac{g}{2}F_1 e^{-imt}\frac{g^4}{4}\frac{(-2imt)}{\sqrt{\pi mt 4mt\pi}}\left(2imt-1+\varphi^2(0)\right)\\
=&\frac{g}{2}F_1 e^{-imt}\frac{g^4}{4}\frac{\left(2mt+i(1-\varphi^2(0))\right)}{\pi}\ .
\end{aligned}
\tag{J.1.5}
$$

J.2 Time dependence from $C_{23}^{intBI2b}$ via Ker: imaginary part

As $Ker\approx\vartheta_1^2$ around the origin, one can naively try to evaluate the integral

$$
\frac{g}{2}F_1 e^{-imt}\int_{-\infty}^{\infty}\frac{d\vartheta_1}{2\pi}|K(\vartheta_1)|^2\Im m\left(-imt-Rm/2\right)Ker_{stac}(\vartheta_1,t,R)\ ,
\tag{J.2.1}
$$

However, as time t grows, due to the asymptotics of the Fresnel function ($F_S\to\frac{1}{2}$ and $F_C\to\frac{1}{2}$), the interval in which $Ker_b\approx\vartheta_1^2$ holds shrinks as $[-\frac{1}{\sqrt{t}},\frac{1}{\sqrt{t}}]$, outside of which $Ker_b\approx 0$ since $\Im m\,Ker_b$ includes the difference of F_C and F_S. On the other hand, at the endpoints of the intervals the integrand behaves as $t/\vartheta_1\to t\sqrt{t}$, so one expects that the integral is linear in t and its coefficient is determined by the small ϑ behaviour of the K function. One can check this assumption numerically and conclude that in the long time limit

$$
\begin{aligned}
&\frac{g}{2}F_1 e^{-imt}i\int_{-\infty}^{\infty}\frac{d\vartheta_1}{2\pi}|K(\vartheta_1)|^2\Im m\left(-imt-Rm/2\right)Ker_{stac}(\vartheta_1,t,R)\\
=&\frac{g}{2}F_1 e^{-imt}\frac{g^4}{4}\frac{1}{2}imt\ ,
\end{aligned}
\tag{J.2.2}
$$

J.3 Time dependence from $C_{23}^{intBI2b}$ via Ker: real part and logarithmic anomaly

Similarly to the imaginary part, $\Re e\,Ker\approx\vartheta_1^2$ around the origin, hence one can once again try to evaluate the integral directly

$$\frac{g}{2}F_1 e^{-imt}\int_{-\infty}^{\infty}\frac{d\vartheta_1}{2\pi}|K(\vartheta_1)|^2\Re e\,(-imt-Rm/2)Ker_{stac}(\vartheta_1,t,R)\;, \tag{J.3.1}$$

Again, as the time t grows, $Ker\approx\vartheta_1^2$ holds in the interval $[-\frac{1}{\sqrt{t}},\frac{1}{\sqrt{t}}]$, while at the endpoints of the intervals the integrand behaves as $t/\vartheta_1\to t\sqrt{t}$, so one expects a term linearly dependent on t whose coefficient is given by the small ϑ behaviour of the K function. However, outside this interval the overall behaviour of the integrand is now of the type $1/\vartheta_1$ accounting for a logarithmic dependence and a $t\ln t$ type behaviour with a coefficient related to the the small ϑ behaviour of the K again. Differentiating Ker_{stac} with respect to t and neglecting $(-imt-Rm/2)$ in (J.3.1), the SPA (E.4.1) can be directly applied resulting in a $1/t$ term whose coefficient can be identified with that of the logarithmic term. Explicit calculation shows that

$$\frac{g}{2}F_1 e^{-imt}mt\left(\frac{g^4}{4}\left(-\frac{\log(mt)}{\pi}\right)+\mathcal{K}\right)\;, \tag{J.3.2}$$

where

$$\begin{aligned}\mathcal{K}=\lim_{t\to\infty}\Bigg\{&-\frac{1}{2}\int_{-\infty}^{\infty}\frac{d\vartheta}{2\pi}\Omega(\vartheta)|K(\vartheta)|^2\Bigg[\frac{\sqrt{2(\cosh\vartheta-1)}}{\cosh\vartheta}\times\\&\left(F_C\left(\sqrt{\frac{4mt(\cosh(\vartheta)-1)}{\pi}}\right)+F_S\left(\sqrt{\frac{4mt(\cosh(\vartheta)-1)}{\pi}}\right)-1\right)+\sqrt{\sinh^2\vartheta}\Bigg]\\&+\frac{g^4}{4}\left(\frac{\log(mt)}{\pi}\right)\Bigg\}\;.\end{aligned} \tag{J.3.3}$$

J.4 Time dependence from $C_{23}^{intBI-II}$

To calculate the time-dependence from $C_{23}^{intBI-II}$ we cannot use Ker_{stac} directly, i.e. the long-time approximation (J.0.7) of (J.0.4) in the sum

$$\frac{g}{2}F_1 e^{-imt}\sum_{I\neq 0}\frac{|K(\vartheta_1)|^2Ker(\vartheta_1,t,R)}{\bar\rho_2(\vartheta_1)}\frac{\frac{F_5^\varepsilon(\vartheta_1)}{F_1\Omega(\vartheta)}+\frac{K'(\vartheta_1)}{K(\vartheta_1)}-\frac{F_5^\varepsilon(-\vartheta_1)}{F_1\Omega(\vartheta)}-\frac{K'(-\vartheta_1)}{K(-\vartheta_1)}}{4\sinh\vartheta_1}\;. \tag{J.4.1}$$

The reason is that the singularity of $|K(\vartheta_1)|^2\frac{\frac{F_5^\varepsilon(\vartheta_1)}{\Omega(\vartheta)}+F_1\frac{K'(\vartheta_1)}{K(\vartheta_1)}-\frac{F_5^\varepsilon(-\vartheta_1)}{\Omega(\vartheta)}-F_1\frac{K'(-\vartheta_1)}{K(-\vartheta_1)}}{4\sinh\vartheta_1}$ is of order four, whereas for any finite t, Ker_{stac} (and also Ker) behave as ϑ_1^2 around the origin and the resulting 2nd order singularity is sensitive to the non-analyticity of f in the long-time approximation of $Ker_{stac}(\vartheta_1,t,R)$ in (J.0.7).

With $Ker(\vartheta_1,t,R)$, which is an analytic function for any finite t without such a singular behaviour, one can formally express the time dependence using the contour manipulations and eventually (E.3.4), yielding

$$\begin{aligned}&\frac{g}{2}F_1 e^{-imt}\int_{-\infty}^{\infty}\frac{d\vartheta}{2\pi}\frac{\left(|K(\vartheta)|^2Ker(\vartheta,t,0)\left(\frac{F_5^\varepsilon(\vartheta)}{F_1\Omega(\vartheta)}+\frac{K'(\vartheta)}{K(\vartheta_1)}-\frac{F_5^\varepsilon(-\vartheta)}{F_1\Omega(\vartheta)}-\frac{K'(-\vartheta)}{K(-\vartheta)}\right)\tanh\vartheta\right)'}{4\sinh\vartheta}\\&+\frac{g}{2}F_1 e^{-imt}\frac{g^4}{4}\frac{mLKer(\vartheta,t,0)''}{8}+....\;,\end{aligned} \tag{J.4.2}$$

where $Ker(\vartheta,t,0)''$ is the second derivative with respect to ϑ_1 and ... refers $(mL)^0$ terms with no time dependence. $Ker(\vartheta,t,0)''$ can be approximated using the SPA, (E.4.1) giving $\frac{\pi}{2}(-1-i)\sqrt{mt}$, hence the

pole term yields an allowed $mL\sqrt{mt}$ factor. The way to actually evaluate $C_{23}^{intBI-II}$ is done by performing numerically the integration in (J.0.4) and its derivative needed for (J.4.2) or to calculate only (J.0.4) and perform the sum in (J.4.1).

After performing the numerical integral, we evaluated the sum for the Ising case and came to the conclusion that the leading order time dependence has the form

$$\frac{g}{2}F_1 e^{-imt}\left(\Upsilon_1 mt + i\Upsilon_2 \log mt\right) , \tag{J.4.3}$$

for large mt. It turns out, however, that for the linear term one can even keep the real part from Ker_{stac} in (J.0.7) which has a milder behaviour than f in (J.0.8) and the contour integral manipulations can formally be performed. The end of the analysis by generalising the Ising result is

$$\Upsilon_1 mt = \int_{-\infty}^{\infty}\frac{d\vartheta}{2\pi}\frac{\left(|K(\vartheta)|^2 \Re e\, Ker_{stac}(\vartheta,t,R)\,\Re e\,\left(\frac{F_5^{\varepsilon}(\vartheta)}{F_1\Omega(\vartheta)}+\frac{K'(\vartheta)}{K(\vartheta_1)}-\frac{F_5^{\varepsilon}(-\vartheta)}{F_1\Omega(\vartheta)}-\frac{K'(-\vartheta)}{K(-\vartheta)}\right)\tanh\vartheta\right)'}{4\sinh\vartheta} . \tag{J.4.4}$$

Note, that for the Ising model $\frac{F_5^{\varepsilon}(\vartheta)}{\Omega(\vartheta)}+F_1\frac{K'(\vartheta)}{K(\vartheta_1)}-\frac{F_5^{\varepsilon}(-\vartheta)}{\Omega(\vartheta)}-F_1\frac{K'(-\vartheta)}{K(-\vartheta)}$ is a real function, whereas for an arbitrary interacting IQFT it has an imaginary part as well.

As argued at the beginning of Appendix (I), the singular structure at the origin of $\frac{F_5^{\varepsilon}(\vartheta)}{\Omega(\vartheta)}+F_1\frac{K'(\vartheta)}{K(\vartheta_1)}-\frac{F_5^{\varepsilon}(-\vartheta)}{\Omega(\vartheta)}-F_1\frac{K'(-\vartheta)}{K(-\vartheta)}$ is the same for the Ising an for any interacting theory, and since the source of time dependence is attributed to the singularity, we can keep the real, i.e. singular part in (J.4.4). As a consequence, it is possible to extract the linear time dependence from (J.4.4), and one is allowed to use again the Ising model, where

$$\frac{F_5^{\varepsilon}(\vartheta)}{\Omega(\vartheta)}+F_1\frac{K'(\vartheta)}{K(\vartheta_1)}-\frac{F_5^{\varepsilon}(-\vartheta)}{\Omega(\vartheta)}-F_1\frac{K'(-\vartheta)}{K(-\vartheta)}=\frac{4F_1}{\sinh\vartheta_1}-2F_1\frac{\cosh\vartheta_1}{\sinh\vartheta_1} . \tag{J.4.5}$$

For Υ_1 it is useful to differentiate (J.4.4) with respect to t because for the resulting function the SPA (E.4.1) can be applied yielding a constant and a $1/t$ type term. Elementary calculation shows that the former term is

$$\Upsilon_1 = \frac{g^4}{4}\frac{1}{\pi} . \tag{J.4.6}$$

The details of the numerical study can be found in the next Appendix.

Appendix K

Numerical checks for the calculations

Our quite lengthy and tedious analytic calculations were extensively cross-checked using numerics out of which we discuss and present here three important parts: the cancellation of mL terms in $\tilde{D}_{23}$, the time dependence from the term $C^{intBI-II}$ (I.5.4), and match between the time dependence of D_{23} and our analytic predictions (8.3.20). Beyond these, we also numerically verified other parts of the calculations, such as: numerically monitoring the validity of our manipulations performed in Appendix H (using sine–Gordon first breather form factors) and in Appendix J. From Appendix I, the calculations in (I.2) and (I.3) were also cross-checked, whereas the validity of the rest of the Appendix (i.e. cancellation of the 4th order singularities) is verified by the match between the predicted time evolution of D_{23} and our analytical considerations, discussed below.

K.1 Cancellation of mL terms in $\tilde{D}_{23}$

During the evaluation of $\tilde{D}_{23}$ in Appendix H and I we ignored discussing and showing the cancellation of $\mathcal{O}(mL)$ type terms. Here we verify their cancellation by considering the numerical values for $\tilde{D}_{23}$ for various time instants and mL system sizes. For simplicity, we use the Ising case $S = -1$ for our checks with analytic expression for the form factors from [**?**] and with a singular K function

$$K_{Ising}(\vartheta) = \frac{-ig^2}{\sinh 2\vartheta} \,. \tag{K.1.1}$$

Note that the only way to obtain a quench with a zero momentum particle in the Ising model is when quenching from the ferromagnetic to the paramagnetic phase [94–96]. For such a quench calculations based on a form factor expansion presupposing a small post-quench density are not expected to give accurate results. Nevertheless, the cancellation of volume dependent terms is related to the order-by-order structure of the expansion independent of the eventual behaviour of the expansion itself. We evaluated

$$\tilde{D}_{23} = C_{23} - Z_1 C_{12} - (Z_2 - Z_1^2) C_{01} \tag{K.1.2}$$

numerically for time instants $mt = 0, 2.5, 5, 10, 20$ and volume sizes $mL = 30, 40, 50, 60$ performing discrete summation on the quantised rapidities. To make the summation finite we introduced a rapidity cut-off $\vartheta_c = 4.834$ for the particles involved. In Fig. (K.1.1) we show the numerical values for $e^{imt\frac{\tilde{D}_{23}}{g/2}}$ with $g = 1$.

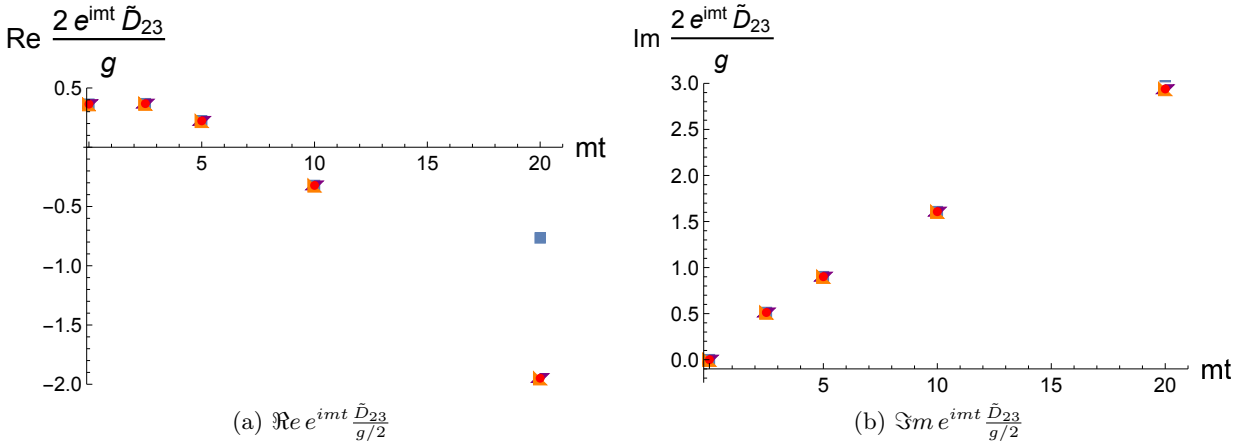

(a) $\Re e\, e^{imt\frac{\tilde{D}_{23}}{g/2}}$ (b) $\Im m\, e^{imt\frac{\tilde{D}_{23}}{g/2}}$

Figure K.1.1: Real and imaginary parts of $e^{imt\frac{\tilde{D}_{23}}{g/2}}$ for time instants $mt = 0, 2.5, 5, 10$ and 20 for a quench in the Ising model. Results for system sizes $mL = 30, 40, 50$ and 60 are shown with blue, purple, orange and red symbols, but with a single exception these cannot really be distinguished due to their almost perfect overlap.

The source of the only observable deviation (for the case $mL = 30$ and $mt = 20$) is numerical inaccuracy resulting from the oscillatory nature of the terms of the sum. In Fig. (K.1.2) we plot the difference between the numerical values obtained for various system sizes at fixed times.

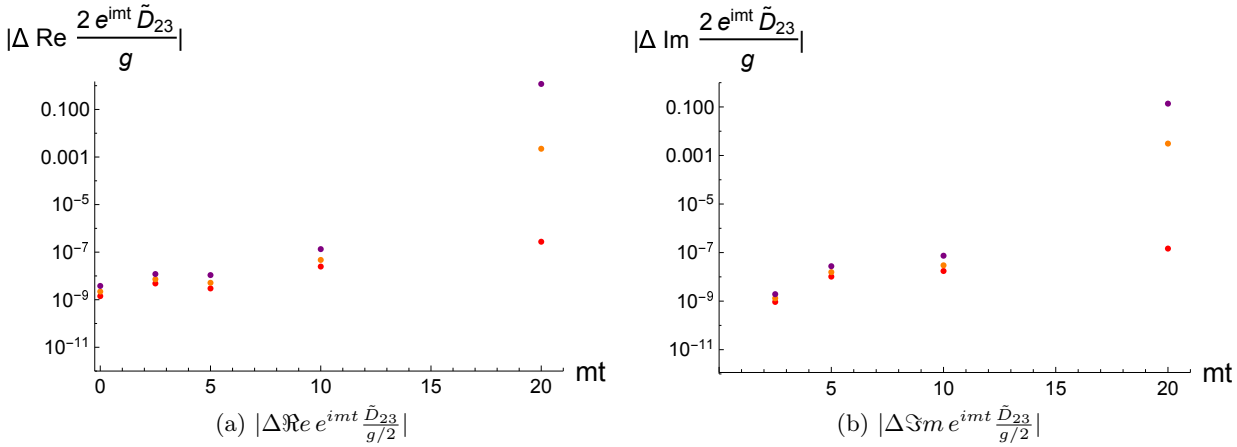

(a) $|\Delta\Re e\, e^{imt\frac{\tilde{D}_{23}}{g/2}}|$ (b) $|\Delta\Im m\, e^{imt\frac{\tilde{D}_{23}}{g/2}}|$

Figure K.1.2: Modulus of differences between real and imaginary parts of $e^{imt\frac{\tilde{D}_{23}}{g/2}}$ for different system sizes at time instants $mt = 0, 2.5, 5, 10$ and 20 for a quench in the Ising model. The purple, orange, and red dots correspond to the difference of the value obtained for $30-40$, $40-50$ and $50-60$ in units of mL.

These results demonstrate that terms growing with mL indeed cancel.

K.2 Time dependence from $C^{intBI-II}$

In this subsection we present numerical results to confirm that the time dependence of

$$\frac{g}{2}F_1 e^{-imt}\sum_{I\neq 0}\frac{|K(\vartheta_1)|^2 Ker(\vartheta_1,t,R)}{\bar{\rho}_2(\vartheta_1)}\frac{\frac{F_5^{\varepsilon}(\vartheta_1)}{F_1\Omega(\vartheta)}+\frac{K'(\vartheta_1)}{K(\vartheta_1)}-\frac{F_5^{\varepsilon}(-\vartheta_1)}{F_1\Omega(\vartheta)}-\frac{K'(-\vartheta_1)}{K(-\vartheta_1)}}{4\sinh\vartheta_1} \tag{K.2.1}$$

in the term $C^{intBI-II}$ defined in (I.5.4), (J.0.2) is of the form

$$\frac{g}{2}F_1 e^{-imt}\left(\Upsilon_1 mt + i\Upsilon_2 \log mt\right) , \tag{K.2.2}$$

and that

$$\Upsilon_1 mt = \int_{-\infty}^{\infty}\frac{d\vartheta}{2\pi}\frac{\left(|K(\vartheta)|^2 \Re e\, Ker_{stac}(\vartheta,t,R)\,\Re e\,\left(\frac{F_5^{\varepsilon}(\vartheta)}{F_1\Omega(\vartheta)}+\frac{K'(\vartheta)}{K(\vartheta_1)}-\frac{F_5^{\varepsilon}(-\vartheta)}{F_1\Omega(\vartheta)}-\frac{K'(-\vartheta)}{K(-\vartheta)}\right)\tanh\vartheta\right)'}{4\sinh\vartheta} . \tag{K.2.3}$$

For the numerical analysis we used the Ising model to demonstrate these statements with

$$K(\vartheta) = -i\frac{g^2}{2\sinh\vartheta} , \tag{K.2.4}$$

where $F_5^{\varepsilon}(\vartheta) = \frac{8F_1}{\sinh\vartheta}$, yielding

$$\frac{g}{2}F_1 e^{-imt}\sum_{I\neq 0}\frac{|K(\vartheta_1)|^2\,(2-\cosh\vartheta_1)\,Ker(\vartheta_1,t,R)}{\bar{\rho}_2(\vartheta_1)2\sinh^2\vartheta_1} \tag{K.2.5}$$

and

$$\Upsilon_1 mt = \int_{-\infty}^{\infty}\frac{d\vartheta}{2\pi}\frac{\left(|K(\vartheta)|^2\,(2-\cosh\vartheta_1)\,/\cosh\vartheta\,\Re e\, Ker_{stac}(\vartheta,t,R)\right)'}{2\sinh\vartheta} . \tag{K.2.6}$$

Figure K.2.1 shows the numerical results for (K.2.5) for system sizes $mL = 50, 60$ and for various time instants. The kernel Ker was determined by numerical integration and we subtracted the mL residue term

$$\frac{g}{2}F_1 e^{-imt}\frac{g^4}{4}\frac{mLKer(\vartheta,t,0)''}{8} , \tag{K.2.7}$$

from (J.4.2) to check the resulted mL independence.

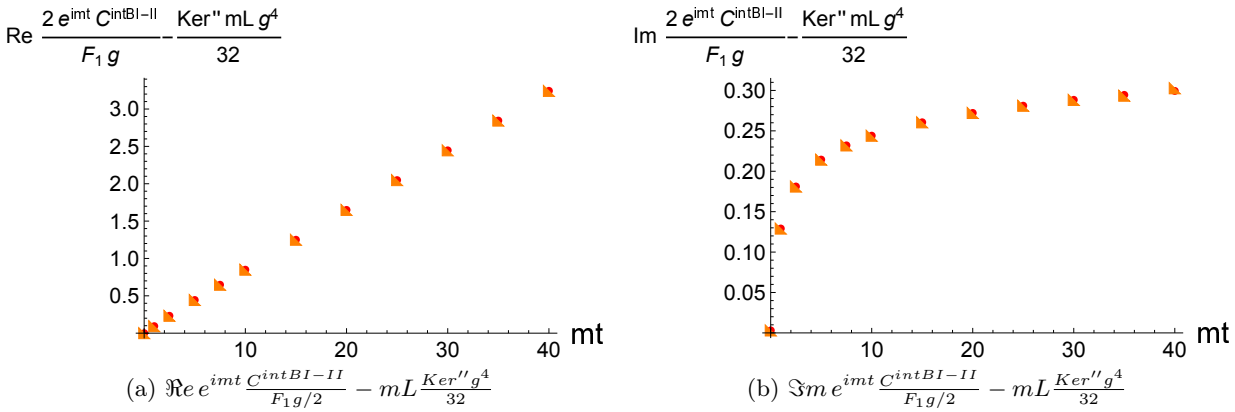

(a) $\Re e\, e^{imt}\frac{C^{intBI-II}}{F_1 g/2} - mL\frac{Ker'' g^4}{32}$ (b) $\Im m\, e^{imt}\frac{C^{intBI-II}}{F_1 g/2} - mL\frac{Ker'' g^4}{32}$

Figure K.2.1: Real and imaginary parts of $e^{imt}\frac{C^{intBI-II}}{F_1 g/2} - mL\frac{Ker'' g^4}{32}$ calculated with a discrete sum for time instants $mt = 0.1, 1, 2.5, 5, 7.5, 10, 15, 20, 25, 30, 35$ and 40 for a quench in the Ising model. The orange and red symbols correspond to system sizes $mL = 50$ and 60. $g = 1$.

Figure K.2.2 shows the real and imaginary factor multiplying the term $\frac{g}{2}F_1 e^{-imt}$ in $C^{intBI-II}$ calculated by a discrete summation (K.2.5) and by the integration (K.2.6). For the imaginary parts, we also keep the $F_S + F_C$ part from Ker_{stac} (J.0.7) but drop the $\sqrt{\sinh^2\vartheta}$ type function, f.

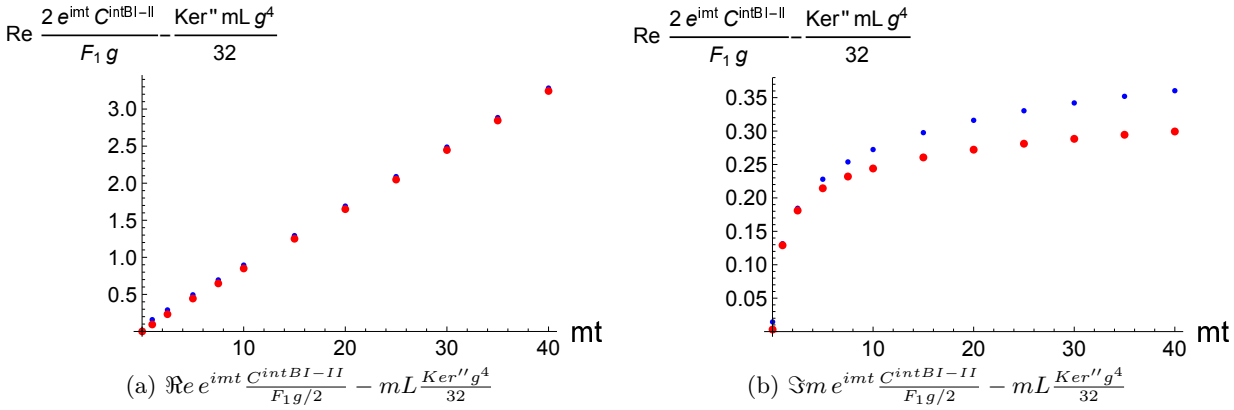

(a) $\Re e\, e^{imt\frac{C^{intBI-II}}{F_1 g/2}} - mL\frac{Ker'' g^4}{32}$ (b) $\Im m\, e^{imt\frac{C^{intBI-II}}{F_1 g/2}} - mL\frac{Ker'' g^4}{32}$

Figure K.2.2: Real and imaginary parts of $e^{imt\frac{C^{intBI-II}}{F_1 g/2}} - mL\frac{Ker'' g^4}{32}$ calculated by a discrete sum and a continuous integral using Ker_{stac} for time instants $mt = 0.1, 1, 2.5, 5, 7.5, 10, 15, 20, 25, 30, 35$ and 40 for a quench in the Ising model. The red dots correspond to system sizes $mL = 60$ and the blue dots to the analytic results. $g = 1$.

We can conclude that for the real part multiplying $\frac{g}{2}F_1 e^{-imt}$ using the real part of Ker_{stac} in (K.2.6) gives a correct result. For the imaginary part, however, the imaginary part without the singular f from Ker_{stac} alone is not able to reproduce the result of the discrete summation. On the other hand, the time dependence of the imaginary coefficient is only logarithmic, and therefore the calculation of this sub-leading time dependence is not addressed in this work. We also checked if the linear time dependence can be described by

$$\frac{g^4}{4}\frac{1}{\pi} mt\,,$$

as predicted in Appendix J and if the logarithmic time dependence for the imaginary part is a correct assumption. In Fig. K.2.3 we therefore fit the functions $a + b\, mt$ and $a + b\, \ln mt$ to the real and imaginary parts of

$$e^{imt\frac{C^{intBI-II}}{F_1 g/2}} - mL\frac{Ker'' g^4}{32}$$

calculated by the discrete summation with $mL = 60$ omitting the first 3 data points corresponding to the shortest times $mt = 0.01, 1, 2.5$.

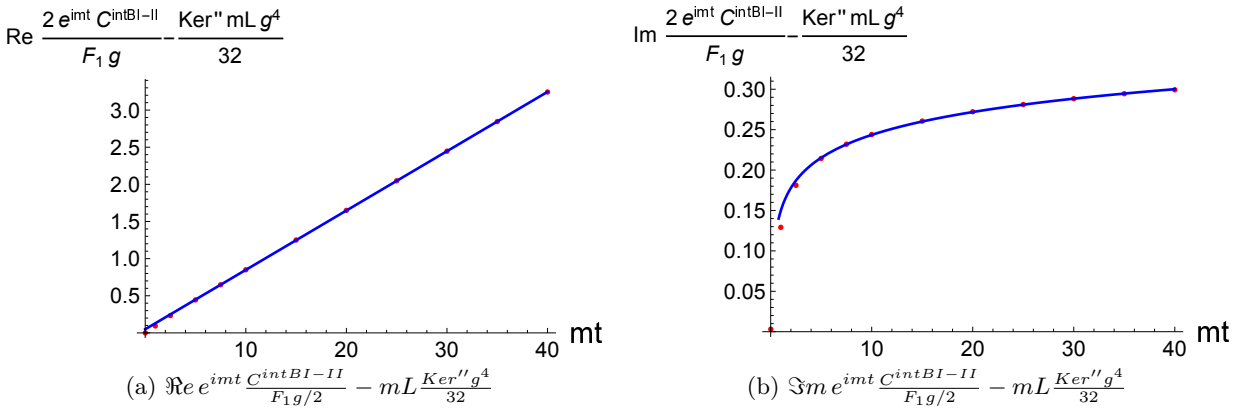

(a) $\Re e\, e^{imt\frac{C^{intBI-II}}{F_1 g/2}} - mL\frac{Ker'' g^4}{32}$ (b) $\Im m\, e^{imt\frac{C^{intBI-II}}{F_1 g/2}} - mL\frac{Ker'' g^4}{32}$

Figure K.2.3: Real and imaginary parts of $e^{imt\frac{C^{intBI-II}}{F_1 g/2}} - mL\frac{Ker'' g^4}{32}$ calculated by a discrete sum using Ker_{stac} for various time instants for a quench in the Ising model. The red dots correspond to system sizes $mL = 60$ and the blue line to the fitted curves of type $a + b\, mt$ and $a + b\, \ln mt$.

From the linear regression, the coefficient of the linearly time-dependent term is 0.0799167 which is to be compared with $\frac{1}{4\pi} = 0.0795775$ as $g = 1$. The agreement is excellent, and although the error of the fitted parameter is 7×10^{-5}, the match is convincing.

K.3 Comparing the time dependence of $\tilde{D}_{23}$ with the analytic results

In this subsection we study the time dependence of

$$e^{imt} \frac{\tilde{D}_{23}}{g/2}$$

for the Ising model with $K = -i\frac{g^2}{\sinh 2\vartheta}$ for $mL = 70$. We compute this quantity using discrete finite volume summation for various time instants, and fit its real and imaginary parts with the appropriate function dependences $a + b\sqrt{mt} + c\,mt + d\,mt \ln mt$ and $a + b\sqrt{mt} + c\,mt$ dictated by our analysis done in Appendix J, omitting the first 7 data points corresponding to short times.

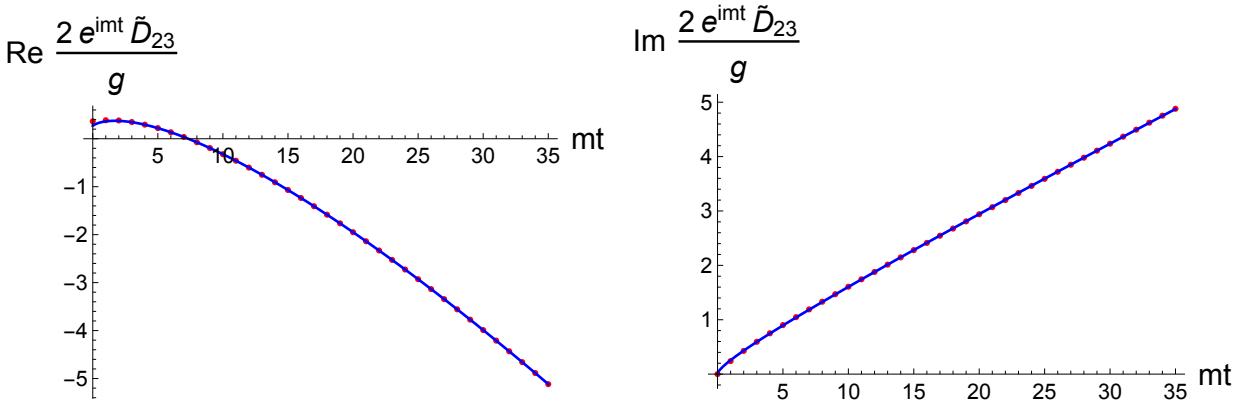

(a) $\Re e\, e^{imt} \frac{\tilde{D}_{23}}{g/2}$ (b) $\Im m\, e^{imt} \frac{\tilde{D}_{23}}{g/2}$

Figure K.3.1: Real and imaginary parts of $e^{imt} \frac{\tilde{D}_{23}}{g/2}$ for time instants $mt = 0, 1, 2..., 35$ for a quench in the Ising model. The red dots correspond to system sizes $mL = 70$ and the blue curve to to the fitted curves of type $a + b\sqrt{mt} + c\,mt + d\,mt \ln mt$ and $a + b\sqrt{mt} + c\,mt$. $g = 1$.

Concerning the real parts, the values obtained from the fit are $d = -0.0825821$ and $c = 0.149943$, which must be compared with $-\frac{1}{4\pi} = -0.0795775$ and $\mathcal{K} + \frac{3}{4\pi} = 0.131292$ resulting from (8.3.20) and (8.3.21) with $g = 1$ and $S = -1$. The accuracy of the fit itself is around $10^{-3} - 10^{-4}$. The difference between the fitted parameters and the analytic predictions is now a bit larger compared to the previous subsection. However, neglecting more data points for short times the fitted values move towards the analytic predictions. We note however, that omitting too many points leads to a deterioration of the fit quality, as for an accurate determination of a logarithmic term data points over several orders of magnitude should be used, which is not possible to extract due to the inaccuracy of the discrete sum for large times. As an additional test we also tried the fitting function $a + b\sqrt{mt} + c\,mt$ and noted that the fit residuals were two orders of magnitude larger than for the case including the term $mt \ln mt$, which is a confirmation of the presence of the term $mt \ln mt$ in the time dependence.

For the imaginary part the parameter c was found to be $c = 0.114809$ which must be compared with $\frac{1}{8} = 0.125$ for $g = 1$ according to (8.3.20) and (8.3.21). The total estimated error of the fitted value is of the order 10^{-3}. In principle we should have either included $\ln mt$ in the fitting function or subtracted the contribution of $\Im m\, e^{imt} \frac{C^{intBI-II}}{F_1 g/2} - mL\frac{Ker'' g^4}{32}$ discussed in the previous subsection from the data points, but since this correction is rather small it was simply discarded.